



UNIVERSITY OF CALCUTTA

DOCTORAL THESIS

Implications Of The Higgs Discovery On Physics Beyond The Standard Model

Author:

Dipankar DAS

Supervisor:

Prof. Gautam BHATTACHARYYA

Theory Division,
Saha Institute of Nuclear Physics,
1/AF Bidhan Nagar,
Kolkata 700 064, India

*A thesis submitted in fulfilment of the requirements
for the degree of Doctor of Philosophy*

in the

Theory Division
Department of Physics

November 2015

"What I have done is to show that it is possible for the way the universe began to be determined by the laws of science. In that case, it would not be necessary to appeal to God to decide how the universe began. This doesn't prove that there is no God, only that God is not necessary. "

Stephen Hawking

UNIVERSITY OF CALCUTTA

Abstract

Theory Division
Department of Physics

Doctor of Philosophy

Implications Of The Higgs Discovery On Physics Beyond The Standard Model

by Dipankar DAS

In this thesis, we investigate the implications of the LHC Higgs data on different BSM scenarios. Since the data seem to agree with the SM expectations, any nonstandard couplings will be strongly constrained. First we investigate, in a model independent way, the constraints on the nonstandard Higgs couplings with the fermions and the vector bosons in view of high energy unitarity and the measured value of the Higgs to diphoton signal strength. Then we concentrate on a particular BSM scenario, namely, the two Higgs-doublet models (2HDMs). Consistency of the Higgs data with the corresponding SM predictions strongly motivates us to work in the *alignment limit*. In this limit, including the informations of Higgs mass and its SM-like nature, we find many new constraints on the nonstandard masses and $\tan\beta$. We also study the constraints on the charged scalar mass arising from the $h \rightarrow \gamma\gamma$ signal strength measurements and observe that the charged scalar does not necessarily decouple from the diphoton decay width. We then move on to some particular variants of 2HDMs, known as BGL models, and study the flavor constraints on these models. Here we find that lighter than conventionally allowed nonstandard scalars can successfully negotiate the stringent bounds coming from flavor physics data and can leave unconventional decay signatures that can be used as distinctive features of these models. We also analyze the stability and unitarity constraints in a three Higgs-doublet model (3HDM) with S_3 symmetry and find that there must be many more nonstandard particles below 1 TeV. We also observe that the nondecoupling feature of the charged scalar in the context of $h \rightarrow \gamma\gamma$ is not unique to the 2HDMs only, instead it is a general property of the multi doublet extensions of the SM with an exact discrete symmetry.

Acknowledgements

First I thank my supervisor, Prof. Gautam Bhattacharyya, who has been the *guide* during my PhD career in the truest sense. It has been a pleasure to work with him and I learned a lot of things from him apart from physics. I am grateful to Prof. Palash B. Pal for his helps with the basics of physics as well as L^AT_EX. I am also thankful to my university professors, specially Anirban Kundu and Anindya Datta, for exposing me to the interesting and dynamic field of modern high energy physics.

But most of the time during the PhD, you don't talk or think about academics. That's when friends become important. I thank all my batchmates of the P.MSc year 2010 for a wonderful start of my PhD life. Due to the lack of my social skills, I did not have many acquaintances. Despite that I was very lucky to meet some great young people who could endure me and with time became close friends. Among them, Aminul interacted the most primarily because we shared the same office. In the first two years when my desk was beside him, he used to monitor my internet activities which, I must admit, has influenced my research in a positive way. He also tried to teach me how to maintain a balance between arrogance and modesty during social encounters. I don't know if I have learned anything or not but I thank him for his efforts. Next I thank Rajani for allowing me into his hostel room whenever I felt like going to Ruby and disturb him! Although he has a good strong heart, I apologize for any *joke* of mine that might have made him feel like I was actually testing that goodness and strength of his heart. I thank Amit (Dutta Banik) for being such a nice and supportive friend. I also thank Avik and Vijay for their friendships. I thoroughly enjoyed the companionship of Amit (Dey) and Debashis (Saha) during our many short P.MSc adventures. I thank KD for sharing his vast knowledge on different topics. I acknowledge the efforts of Arindam-da to educate me politically. I thank Mayukh and Kousik for the 'adda' sessions in their lab. I thank all members of G11, 363, MSA-I (Hostel) for many colorful memories.

My special thanks to Sadhan with whom I shared an apartment for four years. I fondly remember the weekends when I woke up at 11.30 in the morning (?) to find that he had already done all the hard works – bought the chicken, cleaned it and started cooking. Week after week with a toothbrush in my mouth I watched him cooking and wondered how he can live with the laziest possible flatmate and never complain! In fact, Sadhan is the reason why I had the good fortune of tasting some delicious dishes prepared by Indrani-di (now Sadhan's wife) on some lucky weekends. I express my sincere gratitude to Sadhan for keeping me alive during the weekends and holidays.

Next I thank Sir (Ujjal) for introducing me to many good movies. I also thank Ipsita for showing me how to 'act smart' at the airport and win a window seat. I am thankful to Amit-da (Chakraborty) for helps at different stages of my PhD.

Finally I thank my family for the constant support that has helped me to remain focused.

Dipankar Das
Kolkata, India

Contents

Abstract	ii
Acknowledgements	iii
List of Figures	vii
List of Tables	ix
Abbreviations	x
1 A bottom-up approach to the Standard Electroweak Theory	1
1.1 A quantum mechanical prelude	2
1.1.1 Calculation of differential cross section	3
1.1.2 Method of partial waves	4
1.1.3 Connection with Quantum Field Theory	8
1.2 Fermi Theory	9
1.3 Intermediate Vector Bosons	10
1.3.1 Electrodynamics of the W -bosons	11
1.3.2 Introducing the Z boson	14
1.4 Retrieving vector and axial-vector couplings	18
1.5 Vector boson quartic self couplings	21
1.6 Need for a neutral scalar	23
1.6.1 Trilinear couplings with vector bosons and fermions	24
1.6.2 Quartic couplings with the vector bosons	26
1.6.3 Scalar self couplings	27
1.7 ABJ anomaly and quarks	29
2 Modified Higgs couplings and unitarity violation	32
2.1 Modification of the Higgs couplings	33
2.2 Impact on high energy unitarity	34
2.3 Impact on diphoton signal strength	37
2.4 Correlation between E_{\max} and $\mu_{\gamma\gamma}$	39
2.5 Conclusions	39
3 Post Higgs overview of two Higgs-doublet models	41
3.1 The scalar potential	42
3.1.1 Physical eigenstates	44

3.1.2	The alignment limit	46
3.1.3	Bounded from below constraints	47
3.1.4	Constraints from unitarity	50
3.1.5	Numerical constraints on the scalar masses in the alignment limit	54
3.2	Yukawa part	59
3.2.1	The problem of FCNC	61
3.2.2	Natural flavor conservation (NFC)	61
	Flavor constraints on the NFC variants:	62
3.2.3	An alternative to NFC – BGL models	64
	Constraints from flavor data:	68
	Neutral meson mixing:	69
	$\mathbf{b} \rightarrow \mathbf{s}\gamma$:	69
	Other constraints:	71
3.3	Decay of the nonstandard Higgs bosons	72
3.4	Loop induced decays of the SM-like Higgs	74
3.5	Conclusions	77
4	Analysis of an extended scalar sector with S_3 symmetry	79
4.1	The scalar potential	80
4.2	Physical eigenstates	82
	4.2.1 Case-I ($\lambda_4 = 0$)	82
	4.2.2 Case-II ($v_1 = \sqrt{3}v_2$)	85
4.3	Constraints from unitarity	88
4.4	Impact on loop induced Higgs decays	90
4.5	Conclusions	91
5	The Higgs or a Higgs?	93
5.1	Two Higgs-doublet models	95
	5.1.1 Underlying dynamics behind decoupling	97
5.2	Three-Higgs-doublet models	98
5.3	Conclusions and outlook	100
6	Summary and conclusions	101
A	Calculation of the WW scattering amplitude	106
A.1	Calculation of the gauge part	107
	A.1.1 s -channel photon exchange	107
	A.1.2 s -channel Z -boson exchange	108
	A.1.3 t -channel photon exchange	109
	A.1.4 t -channel Z -boson exchange	110
	A.1.5 The quartic gauge vertex	111
A.2	Calculation of the Higgs part	112
	A.2.1 s -channel Higgs exchange	112
	A.2.2 t -channel Higgs exchange	112
A.3	Total amplitude and Lee-Quigg-Thacker limit	113

B	Calculation of the $e^-e^+ \rightarrow WW$ scattering amplitude	115
B.1	s -channel photon exchange	116
B.2	s -channel Z exchange	117
B.3	t -channel ν exchange	118
B.4	Amplitude without the Higgs	121
B.5	s -channel Higgs exchange	122
B.6	Explicit evaluation of the energy growths	123
B.6.1	The same helicity case	124
B.6.2	The opposite helicity case	125
C	Flavor observables and 2HDM	126
C.1	Neutral meson mixing	126
C.2	Expressions for $b \rightarrow s\gamma$	127
C.3	Leptonic and semileptonic B decays	131
C.4	$B_s \rightarrow \mu^+\mu^-$	133
C.5	Current experimental numbers	135
	Bibliography	136

List of Figures

1.1	Scattering in QM	2
1.2	Unitarity circle.	7
1.3	Feynman diagrams for the process $W^-(p_1) + W^+(p_2) \rightarrow \gamma(k_1) + \gamma(k_2)$	12
1.4	Feynman diagrams for the process $e^-e^+ \rightarrow WW$	14
1.5	Some Feynman diagrams to determine WWZ vertex	17
1.6	Feynman diagrams for the process $\nu\bar{\nu} \rightarrow WW$	18
1.7	Feynman diagrams for the process $e\bar{\nu} \rightarrow WZ$	19
1.8	$W_L^-W_L^-$ scattering	21
1.9	$W_L^-W_L^+ \rightarrow Z_LZ_L$ scattering	22
1.10	$W_L^-W_L^-$ scattering (Higgs diagrams)	24
1.11	$e^-e^+ \rightarrow Z_LZ_L$ scattering	25
1.12	$W^-W^+ \rightarrow hh$ scattering	26
1.13	$ZZ \rightarrow ZZh$ scattering	27
1.14	$ZZ \rightarrow hhh$ scattering	28
1.15	One-loop diagrams for the process $e^-e^+ \rightarrow \gamma\gamma$	29
2.1	Unitarity violation scale as a function of x	35
2.2	Allowed regions in the x - f plane	36
2.3	Correlation between E_{\max} and $\mu_{\gamma\gamma}$	38
3.1	Current fit for 2HDMs using the LHC data	47
3.2	Current values of the Higgs signal strengths	48
3.3	Unitarity and stability constraints for 2HDMs with exact Z_2 symmetry	55
3.4	Relaxation of the constraints on $\tan\beta$	56
3.5	Effect of soft breaking on the constraints on the nonstandard masses	57
3.6	Unitarity and stability constraints for 2HDMs with U(1) symmetry	58
3.7	Flavor constraints on Type-I and II 2HDMs	63
3.8	Flavor constraints on m_{1+} in BGL models	70
3.9	Neutral Higgs contributions to the $b \rightarrow s\gamma$ amplitude	70
3.10	Constraints from $B_s \rightarrow \mu^+\mu^-$	71
3.11	Nonstandard Higgs decays in conventional 2HDMs	72
3.12	Charged Higgs branching ratios in t-Type BGL	73
3.13	Neutral Higgs branching ratios in t-Type BGL	73
3.14	Impact on loop induced Higgs decays	76
4.1	Unitarity constrains on the nonstandard masses in S3HDM	88
4.2	Impact on diphoton signal strength	90
5.1	Allowed region for κ_1 in 2HDMs	96

A.1	Feynman diagrams for WW elastic scattering (gauge part)	107
A.2	Feynman diagrams for WW elastic scattering (Higgs part)	112
B.1	Feynman diagrams for $e^-(p_1) + e^+(p_2) \rightarrow W_L^-(k_1) + W_L^+(k_2)$	116
C.1	NP contributions to $b \rightarrow s\gamma$	128

List of Tables

4.1	Z_2 parity assignments to the physical mass eigenstates	87
5.1	Decoupling features of multi Higgs-doublet models	99

Abbreviations

SM	Standard Model
BSM	Beyond Standard Model
CM	Center of Momentum
LHC	Large Hadron Collider
IVB	Intermediate Vector Boson
QED	Quantum Electro-Dynamics
QCD	Quantum Chromo-Dynamics
LH	Left Handed
RH	Right Handed
2HDM	Two Higgs-Doublet Model
3HDM	Three Higgs-Doublet Model
VEV	Vacuum Expectation Value
BGL	Branco Grimus Lavoura
NFC	Natural Flavor Conservation

Dedicated to my Parents

*Two roads diverged in a wood, and I,
I took the one less traveled by ...*

Robert Frost in "The Road Not Taken"

1

A bottom-up approach to the Standard Electroweak Theory

The original theory was constructed fifty years ago from gauge theoretical point of view [1]. Here, however, we shall take a different route to reconstruct the essential virtues of the theory from the consideration of ‘tree-unitarity’ [2,3]. First of all, we need to note that every scattering amplitude can be expanded in terms of the partial waves [4]:

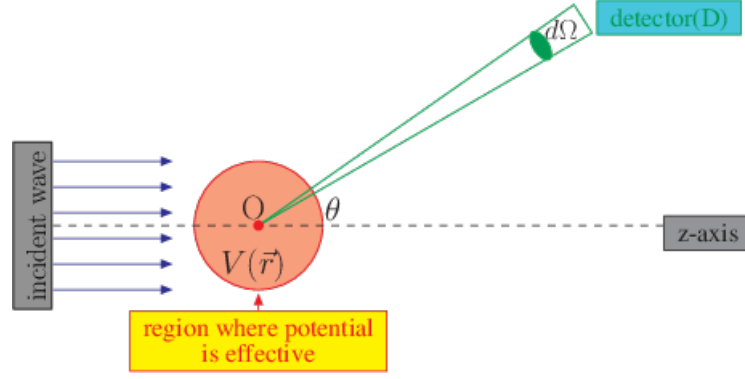
$$\mathcal{M}(\theta) = 16\pi \sum_{l=0}^{\infty} (2l+1) a_l P_l(\cos \theta), \quad (1.1)$$

where, θ is the angle of scattering. Every partial wave amplitude is bounded from the ‘unitarity’ condition:

$$|a_l| \leq 1. \quad (1.2)$$

If we trust in perturbative calculations then the unitarity condition must be satisfied order by order [5], *i.e.*, it must hold in tree level also. If the tree level amplitude grows with energy then unitarity is bound to be violated at large energies. In view of this, let us postulate the following:

Any remnant energy growth in a scattering amplitude must be canceled either by tuning the couplings suitably or, if the first option is unavailable, by introducing

FIGURE 1.1: Schematic diagram for scattering by a potential $V(\vec{r})$.

new particles.

In the following sections we shall see how this hypothesis along with the experimental facts and the requirement of ‘minimality’ lead us to the correct description of nature.

1.1 A quantum mechanical prelude

A good way to start will be to make a sense of Eqs. (1.1) and (1.2) from the lessons of quantum mechanical scattering. Let us consider a scattering experiment in which a steady incident beam is maintained for an indefinitely long time, i.e. the incident flux, F_{in} , is constant. Then, there will be a steady stream of scattered particles too. In Figure 1.1, the incident beam is parallel to the z -axis and is assumed to be much wider than the zone of influence of the potential, $V(\vec{r})$, centered at O . Far from this zone of influence a detector, D , measures the number, dn , of particles scattered per unit time into the solid angle $d\Omega$, centered around the direction defined by the polar angles θ and ϕ . The number, dn , is proportional to F_{in} and to $d\Omega$; the constant of proportionality, $d\sigma/d\Omega$, is defined to be the differential scattering cross-section in the direction (θ, ϕ) . Thus

$$dn = F_{\text{in}} \cdot d\Omega \cdot \frac{d\sigma}{d\Omega}. \quad (1.3)$$

In the quantum theory of scattering, we imagine that an incident plane wave, $\psi_{\text{in}} = Ae^{ikz}$, traveling along the z -axis, encounters a scattering potential producing an outgoing spherical wave. At large distances from the scattering center, the form of the wave function $\psi(\vec{r})$ must be such as to conform to the general pictures outlined below:

1. It must consist of a part of the incident wave corresponding to the parallel beam of incident particles which transmitted unmodified.
2. Another part ψ_{sc} representing the scattered particles, having same energy as the incident particles (because of *elastic* scattering) and moving radially outwards from the center.

Thus we may write,

$$\psi(\vec{r})_{r \rightarrow \infty} \approx e^{ikz} + \underbrace{f(\theta, \phi) \frac{e^{ikr}}{r}}_{\psi_{\text{sc}}} . \quad (1.4)$$

In this expression, only the function $f(\theta, \phi)$, which is called the scattering amplitude, depends on the potential $V(\vec{r})$. The ϕ dependence should be included in the general case, to account for the anisotropy of the potential. However, if the target is azimuthally symmetrical, the ϕ dependence would no longer be present. Note that, the spherical wave carries a factor of $1/r$, because this portion of $|\psi|^2$ is spherically diverging and must go like $1/r^2$ to conserve probability.

1.1.1 Calculation of differential cross section

We recall that the expression for the current density $J(\vec{r})$ associated with a wave function $\psi(\vec{r})$ is:

$$\vec{J}(\vec{r}) = \frac{\hbar}{2im} \left[\psi^*(\vec{\nabla}\psi) - (\vec{\nabla}\psi^*)\psi \right] = \frac{1}{m} \text{Re} \left[\psi^*(\vec{r}) \frac{\hbar}{i} \vec{\nabla}\psi(\vec{r}) \right] . \quad (1.5)$$

The incident and scattered fluxes are obviously proportional to the normal components of \vec{J}_{in} and \vec{J}_{sc} respectively. We will call the proportionality constant C . Since $\psi_{\text{in}} = e^{ikz}$, we obtain

$$(J_{\text{in}})_z = \frac{1}{m} \text{Re} \left[e^{-ikz} \frac{\hbar}{i} \frac{\partial}{\partial z} e^{ikz} \right] = \frac{\hbar k}{m} , \quad (1.6)$$

$$\Rightarrow F_{\text{in}} = C (J_{\text{in}})_z . \quad (1.7)$$

For radially diverging scattered wave, the number of particles crossing an area $d\vec{s} = ds\hat{r}$, subtending solid angle $d\Omega$ at the origin is

$$dn = \underbrace{C \vec{J}_{\text{sc}}}_{\vec{F}_{\text{sc}}} \cdot (ds\hat{r}) = C (J_{\text{sc}})_r ds . \quad (1.8)$$

Clearly, it is the r -th component of \vec{J}_{sc} which receives our attention. Remembering $\psi_{\text{sc}} = \frac{1}{r} f(\theta, \phi) e^{ikr}$ we may get,

$$(J_{\text{sc}})_r = \frac{1}{m} \text{Re} \left[f^*(\theta, \phi) \frac{e^{-ikr}}{r} \frac{\hbar}{i} \frac{\partial}{\partial r} \left\{ f(\theta, \phi) \frac{e^{ikr}}{r} \right\} \right] = \frac{1}{m} |f(\theta, \phi)|^2 \frac{\hbar k}{r^2} \quad (1.9)$$

Hence,

$$dn = \frac{C}{m} |f(\theta, \phi)|^2 \hbar k \frac{ds}{r^2} = F_{\text{in}} |f(\theta, \phi)|^2 d\Omega . \quad (1.10)$$

Comparing this with Eq. (1.3) we obtain,

$$\frac{d\sigma}{d\Omega} = |f(\theta, \phi)|^2 . \quad (1.11)$$

Thus problem of determining the scattering cross section reduces to finding the scattering amplitude, $f(\theta, \phi)$, in quantum mechanics. The quantity, $f(\theta, \phi)$, actually tells us about the ‘probability amplitude’ for scattering in a direction (θ, ϕ) , and hence is related to the differential cross-section which is the quantity of interest for the experimentalists. The scattering amplitude is obtained by solving the Schrödinger equation under the scattering potential. Depending on the mathematical form of the potential, there are several methods to find the scattering amplitude. The method of partial waves, in particular, comes in handy when the potential is central.

1.1.2 Method of partial waves

In the special case of a central potential $V(r)$, the orbital angular momentum \vec{L} of the particle is a constant of motion. Therefore, there exists stationary states with well defined angular momentum, *i.e.*, eigenstates common to H , L^2 and L_z . We shall call such wave functions ‘partial waves’ and denote them as $\psi_{klm}(\vec{r})$. Their angular dependence is always given by the spherical harmonics $Y_l^m(\theta, \phi)$ – the potential $V(r)$ influences their radial parts only.

We know that e^{ikz} is a solution of the Schrödinger equation with $V(r) = 0$ in the $\{H, p_x, p_y, p_z\}$ basis and may be denoted by $|0, 0, k\rangle$ where z-axis is chosen as the direction of motion. Now if we wish, we may translate our wave function in terms of $\psi_{klm}(\vec{r}) \equiv R_{kl}(r)Y_l^m(\theta, \phi)$ which are the eigenfunctions in the $\{H, L^2, L_z\}$ basis. For a free particle we know that $R_{kl}(r)$ is a linear combination of spherical Bessel and Neumann functions. But as Neumann function blows up at the origin it is dropped out. So we may write,

$$\psi_{klm}^{(0)}(r, \theta, \phi) = j_l(kr)Y_l^m(\theta, \phi), \quad (1.12)$$

where, the superscript ‘0’ denotes that these are ‘free’ (the potential is identically zero) spherical waves. Let us connect these two sets of bases as follows:

$$e^{ikz} = \sum_{l=0}^{\infty} \sum_{m=-l}^{+l} \mathcal{A}_l^m(k) j_l(kr) Y_l^m(\theta, \phi), \quad (1.13)$$

where $\mathcal{A}_l^m(k)$ are suitable expansion coefficients that can only be functions of the magnitude of the momentum. Since the LHS of above equation is independent of ϕ , we require that RHS should also be independent of ϕ , *i.e.* $m = 0$. Thus, we are left with,

$$e^{ikz} = \sum_{l=0}^{\infty} \mathcal{A}_l^0(k) j_l(kr) Y_l^0(\theta), \quad (1.14)$$

where $Y_l^0(\theta)$ is given by

$$Y_l^0(\theta) = \sqrt{\frac{(2l+1)}{4\pi}} P_l(\cos \theta). \quad (1.15)$$

In view of this, we introduce the following shorthand:

$$\mathcal{A}_l = \sqrt{\frac{(2l+1)}{4\pi}} \mathcal{A}_l^0. \quad (1.16)$$

Using this, one may rewrite Eq. (1.14) as

$$e^{ikz} = \sum_{l=0}^{\infty} \mathcal{A}_l(k) j_l(kr) P_l(\cos \theta). \quad (1.17)$$

To determine $\mathcal{A}_l(k)$, we need to use the following integral representation for the Bessel function:

$$j_l(kr) = \frac{1}{2i^l} \int_{-1}^{+1} P_l(\cos \theta) e^{ikr \cos \theta} d(\cos \theta). \quad (1.18)$$

To illustrate the use of the above formula, let us multiply Eq. (1.17) by $P_{l'}(\cos \theta) d(\cos \theta)$ and integrate between -1 to $+1$ to obtain

$$\begin{aligned} \int_{-1}^{+1} P_{l'}(\cos \theta) e^{ikr \cos \theta} d(\cos \theta) &= \frac{2}{(2l'+1)} \sum_{l=0}^{\infty} \mathcal{A}_l(k) j_l(kr) \delta_{ll'}, \\ \Rightarrow 2i^{l'} j_{l'}(kr) &= \frac{2}{(2l'+1)} \mathcal{A}_{l'}(k) j_{l'}(kr), \\ \Rightarrow \mathcal{A}_{l'}(k) &= i^{l'} (2l'+1). \end{aligned} \quad (1.19)$$

Plugging this into Eq. (1.17) we get the final expression as

$$e^{ikz} = \sum_{l=0}^{\infty} i^l (2l+1) j_l(kr) P_l(\cos \theta). \quad (1.20)$$

In view of the asymptotic form of the Bessel function,

$$j_l(kr) \xrightarrow{r \rightarrow \infty} \frac{\sin(kr - \frac{l\pi}{2})}{kr}, \quad (1.21)$$

we may rewrite Eq. (1.20) as

$$e^{ikz} \xrightarrow{r \rightarrow \infty} \frac{1}{2ikr} \sum_{l=0}^{\infty} (2l+1) \left[e^{ikr} - e^{-ikr} (-1)^l \right] P_l(\cos \theta). \quad (1.22)$$

Thus, at large distances, each $\psi_{klm}^{(0)}$ and so the ‘whole’ e^{ikz} results from the superposition of a converging spherical wave, e^{-ikr}/r , and a diverging spherical wave, e^{ikr}/r , whose amplitudes differ only by a phase. The fact that the squared amplitudes for both the incoming and outgoing spherical waves are same, simply reflects the conservation of probability. The presence of a scattering potential can only affect the amplitude of the outgoing spherical wave. Since probability conservation demands that the magnitude of the amplitude for the diverging wave should not

change, it can only pick up additional phases arising due to the presence of a scattering potential. We will see the details in the following subsection.

Presence of a central potential – asymptotic modification of the radial part

The previous subsection was devoted for $V(r) = 0$. Presence of a central potential simply modifies the wave function from the plane wave nature. But we know a special thing – whatever be the form of $V(r)$, it dies out at a finite distance and in the asymptotic limit we should get the wave function in the form of Eq. (1.4).

In the presence of $V(r)$ the radial part of Schrodinger equation reads:

$$\left[\frac{d^2}{dr^2} + \frac{2}{r} \frac{d}{dr} + \left\{ k^2 - \frac{2m}{\hbar^2} V(r) - \frac{l(l+1)}{r^2} \right\} \right] R_{kl}(r) = 0. \quad (1.23)$$

We assume that the potential is short ranged, *i.e.*, $V(r) \rightarrow 0$ as $r \rightarrow \infty$. Then, at large distances, Eq. (1.23) reduces to the free-particle equation. Therefore, the solution of Eq. (1.23) should asymptotically approach the general solution for free particle:

$$R_{kl}(r) \xrightarrow{r \rightarrow \infty} A_l j_l(kr) + B_l \eta_l(kr) = \frac{C_l}{kr} \sin(kr - \frac{l\pi}{2} + \delta_l), \quad (1.24)$$

where, the last step follows from the asymptotic forms of Bessel and Neumann functions:

$$j_l(kr) \xrightarrow{r \rightarrow \infty} \frac{\sin(kr - \frac{l\pi}{2})}{kr}, \quad \eta_l(kr) \xrightarrow{r \rightarrow \infty} -\frac{\cos(kr - \frac{l\pi}{2})}{kr}. \quad (1.25)$$

The quantities, C_l and δ_l are related to A_l and B_l as follows:

$$\tan \delta_l = -\frac{B_l}{A_l}, \quad \text{and, } C_l = \sqrt{A_l^2 + B_l^2}. \quad (1.26)$$

Note that, unlike the free-particle case, here we did not demand $B_l = 0$. This is due to the lack of information about the potential, we do not know the actual behavior of the wave function near the origin. Eq. (1.24) only represents the radial wave function at large distances where the potential is ineffective. Thus, the total wave function far away from the scatterer can be written as

$$\psi(\vec{r})_{r \rightarrow \infty} = \sum_{l=0}^{\infty} R_{kl}(r \rightarrow \infty) P_l(\cos \theta), \quad (1.27)$$

$$\Rightarrow \psi(\vec{r})_{r \rightarrow \infty} = \frac{1}{2ikr} \sum_{l=0}^{\infty} C_l e^{-i\delta_l} e^{-i\frac{l\pi}{2}} \left[e^{ikr} e^{2i\delta_l} - (-1)^l e^{-ikr} \right] P_l(\cos \theta). \quad (1.28)$$

Now, this equation should be equivalent to Eq. (1.4) with the expansion of e^{ikz} in terms of partial waves given by Eq. (1.22). So, we can rewrite eqn (1.4) as

$$\psi(\vec{r})_{r \rightarrow \infty} = \frac{1}{2ikr} \sum_{l=0}^{\infty} (2l+1) \left[e^{ikr} - (-1)^l e^{-ikr} \right] P_l(\cos \theta) + f_k(\theta) \frac{e^{ikr}}{r}. \quad (1.29)$$

Comparing the co-efficients of e^{-ikr}/r in Eqs. (1.28) and (1.29) one can easily get:

$$C_l = i^l (2l+1) e^{i\delta_l}. \quad (1.30)$$

Once the value of C_l is at hand, we can plug it into Eq. (1.28), and then proceed to compare the co-efficients of e^{ikr}/r to obtain the expression for $f_k(\theta)$. The final result is,

$$f_k(\theta) = \frac{1}{2ik} \sum_{l=0}^{\infty} (2l+1) (e^{2i\delta_l} - 1) P_l(\cos \theta). \quad (1.31)$$

Since $P_l(\cos \theta)$ serves as a complete set of basis vectors for any function of θ , one can expand the scattering amplitude as follows:

$$f_k(\theta) = \frac{1}{k} \sum_{l=0}^{\infty} (2l+1) f_l(k) P_l(\cos \theta). \quad (1.32)$$

Comparing Eqs. (1.31) and (1.32) one can easily get

$$f_l(k) = \frac{e^{2i\delta_l} - 1}{2i}, \quad (1.33)$$

$$\Rightarrow f_l(k) = e^{i\delta_l} \sin \delta_l. \quad (1.34)$$

From Eq. (1.34) it follows that

$$|f_l(k)| \leq 1 \quad \text{for all values of } l, \quad (1.35)$$

or, splitting $f_l(k)$ into its real and imaginary components, one can derive the equation of the *unitarity circle* (see Figure 1.2):

$$\left[\Re f_l(k) \right]^2 + \left[\Im f_l(k) - \frac{1}{2} \right]^2 = \frac{1}{4}. \quad (1.36)$$

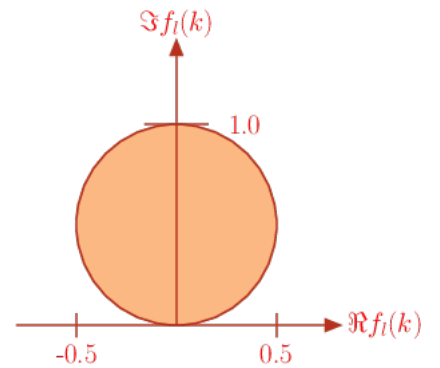


FIGURE 1.2: Unitarity circle.

Now we have learned that the expansion coefficients, $f_l(k)$, of the quantum mechanical scattering amplitude obey the unitarity conditions of Eq. (1.35). But, till now there is very little hint that these $f_l(k)$ -s are the same as the a_l -s of Eq. (1.1). Some intuitive arguments to make the connections will be presented shortly. Before that,

to make the discussion complete, we wish to present one important result that follows from Eq. (1.32).

Note that, using the value of $f_l(k)$ from Eq. (1.34), one can rewrite Eq. (1.32) as

$$f_k(\theta) = \frac{1}{k} \sum_{l=0}^{\infty} (2l+1) e^{i\delta_l} \sin \delta_l P_l(\cos \theta). \quad (1.37)$$

We can now find the expression for the total scattering cross-section as

$$\sigma = \int \frac{d\sigma}{d\Omega} d\Omega = \int |f_k(\theta)|^2 d\Omega. \quad (1.38)$$

Using the orthonormality of the Legendre polynomials, the final result becomes

$$\sigma = \frac{4\pi}{k^2} \sum_{l=0}^{\infty} (2l+1) \sin^2 \delta_l. \quad (1.39)$$

Looking at Eqs. (1.37) and (1.39) and keeping in mind that $P_l(1) = 1$ for any l , one can at once realize that

$$\sigma = \frac{4\pi}{k} \Im \{f_k(\theta = 0)\}, \quad (1.40)$$

where, $\Im \{f_k(\theta = 0)\}$ is the imaginary part of the forward scattering amplitude. Eq. (1.40) is known as the *optical theorem* in quantum mechanics.

1.1.3 Connection with Quantum Field Theory

We shall now give a hand waving argument on how the quantum mechanical scattering amplitude is related to the Feynman amplitude in Quantum Field Theory (QFT). We know the expression for differential scattering cross-section both in quantum mechanics and in QFT. This is given by

$$\frac{d\sigma}{d\Omega} = \frac{1}{64\pi^2 s} \underbrace{|\mathcal{M}(\theta)|^2}_{\text{QFT}} = \underbrace{|f_k(\theta)|^2}_{\text{QM}}, \quad (1.41)$$

where, $\mathcal{M}(\theta)$ is the Feynman amplitude for the process and $s = 4E^2$ is the CM energy squared. From Eq. (1.41) we can make a simple-minded connection:

$$\mathcal{M}(\theta) = 16\pi E f_k(\theta). \quad (1.42)$$

Now, plugging the expression of $f_k(\theta)$ from Eq. (1.32) into Eq. (1.42) and approximating $k \approx E$ at high energies, we may write

$$\mathcal{M}(\theta) = 16\pi \sum_{l=0}^{\infty} (2l+1) f_l(E) P_l(\cos \theta). \quad (1.43)$$

Thus, comparing Eqs. (1.1) and (1.43), one can see that a_l s of Eq. (1.1) are the same as $f_l(k)$ s of Eq. (1.32) and both of them must obey the unitarity condition of Eq. (1.35). Extraction of each partial wave amplitude from the Feynman amplitude will now be a straightforward task:

$$a_l = \frac{1}{32\pi} \int_{-1}^{+1} \mathcal{M}(\theta) P_l(\cos \theta) d(\cos \theta). \quad (1.44)$$

1.2 Fermi Theory

The Fermi lagrangian (for the leptonic sector) is given by,

$$\mathcal{L}_F = -\frac{G_F}{\sqrt{2}} J_{(\text{lep})}^\mu J_{\mu(\text{lep})}^\dagger. \quad (1.45)$$

We know from the experiments that only the left-handed fields take part in β -decay. So the leptonic current should be written as

$$J_{(\text{lep})}^\mu = \bar{\nu}_e \gamma^\mu (1 - \gamma^5) e. \quad (1.46)$$

The coupling constant G_F has mass dimension -2 . To explore the consequence of this negative mass dimension, let us consider the elastic scattering process $\nu_e e \rightarrow \nu_e e$. Neglecting the electron mass, the scattering amplitude will be non-zero for the following combination of helicities:

$$h_1 = h_2 = h_3 = h_4 = -\frac{1}{2}. \quad (1.47)$$

For these combination one has,

$$|\mathcal{M}(\theta)|_{\nu_e e \rightarrow \nu_e e} = 4\sqrt{2} G_F s. \quad (1.48)$$

Thus, only the partial wave with $l = 0$ contributes and that is given by,

$$|a_0|_{\nu_e e \rightarrow \nu_e e} = \frac{1}{2\sqrt{2}\pi} G_F s. \quad (1.49)$$

The unitarity condition (Eq. (1.2)) then sets an upper bound on the CM energy, beyond which Fermi theory ceases to be valid. In this case the limit is,

$$(E_{\text{CM}})_{\text{max}} = \left(\frac{2\pi\sqrt{2}}{G_F} \right)^{\frac{1}{2}} = 870 \text{ GeV}. \quad (1.50)$$

However, one must remember that the exact value of this cut-off is process dependent.

1.3 Intermediate Vector Bosons

We have just learned that the direct four fermion interaction causes the corresponding coupling constant (G_F) to have negative mass dimension which causes the scattering amplitude to grow as E^2 . A natural way out of this problem is to replace Eq. (1.45) with an interaction describe by ‘exchange’ of another particle (which must be a boson) in analogy with photon in QED. This means, instead of Eq. (1.45) we write the following interaction:¹

$$\mathcal{L}_{\text{int}}^W = \frac{g}{2\sqrt{2}} \left(J_{(\text{lep})}^\mu W_\mu^+ + J_{(\text{lep})}^{\mu\dagger} W_\mu^- \right), \quad (1.51)$$

where W_μ^\pm is a vector field corresponding to a ‘mediating’ particle (with spin-1) which is, therefore, usually called intermediate vector boson (IVB). The numerical factor of $(2\sqrt{2})^{-1}$ in front is purely conventional. One must remember that W^\pm must be massive so that it can describe a short range force and we should write the propagator as:

$$D^{\mu\nu}(q) = \frac{-g^{\mu\nu} + \frac{q^\mu q^\nu}{M_W^2}}{q^2 - M_W^2}. \quad (1.52)$$

The model of weak interactions defined by the Lagrangian of Eq. (1.51) must respect an experimentally established fact that the effective Fermi-type theory provides very good description of a considerable part of physical reality in the low energy region. Comparing low energy muon decay ($\mu^- \rightarrow e^- \nu_\mu \bar{\nu}_e$) amplitude for these two theories, we obtain,

$$\frac{G_F}{\sqrt{2}} = \frac{g^2}{8M_W^2}. \quad (1.53)$$

Note that, in the derivation of Eq. (1.53), the negative sign in the Fermi Lagrangian plays an important role. It is just this convention which guarantees that $G_F > 0$, if the Fermi theory

¹At this point, one might wonder why we are starting with the possibility of a charged vector current. We should begin with charged scalar current which would be a more minimalistic choice. Admittedly, we are implicitly using some experimental inputs – measurement of *Michel Parameters* [6] in polarized muon decay. These measurements confirm that the charged current processes are governed by $V - A$ type interactions and therefore, the possibility of a charged scalar as an intermediate boson is ruled out.

is viewed as an effective low-energy approximation of the theory with IVB. Remember, as a consequence of IVB, there will be no energy growths in $\nu_e e \rightarrow \nu_e e$ and $\bar{\nu}_e e \rightarrow \bar{\nu}_e e$ scattering amplitudes. We should now investigate whether W^\pm are sufficient for energy growth cancellation for all other possible processes.

1.3.1 Electrodynamics of the W -bosons

Since W -bosons carry electric charge, they must interact with the photon. The question is, how should we write the coupling. Let us motivate it in the following way:

The wave equation for a free particle with spin-1 and a non-zero mass,

$$\partial_\mu B^{\mu\nu} + m^2 B^\nu = 0, \quad (1.54)$$

can be obtained from the Proca Lagrangian,

$$\begin{aligned} \mathcal{L} &= -\frac{1}{4} B^{\mu\nu} B_{\mu\nu} + \frac{1}{2} m^2 B^\mu B_\mu \\ &= -\frac{1}{4} (\partial_\mu B_\nu - \partial_\nu B_\mu) (\partial^\mu B^\nu - \partial^\nu B^\mu) + \frac{1}{2} m^2 B^\mu B_\mu. \end{aligned} \quad (1.55)$$

For a complex (charged) spin-1 field, the generalization would be straightforward:

$$\begin{aligned} \mathcal{L} &= -\frac{1}{2} W^{\mu\nu} (W_{\mu\nu})^\dagger + M_W^2 W^{\mu+} W_\mu^- \\ &= -\frac{1}{2} (\partial_\mu W_\nu^- - \partial_\nu W_\mu^-) (\partial^\mu W^{\nu+} - \partial^\nu W^{\mu+}) + M_W^2 W^{\mu+} W_\mu^-. \end{aligned} \quad (1.56)$$

We want the above Lagrangian to be invariant under the following $U(1)$ transformation:

$$W_\mu^-(x) \rightarrow W_\mu^{-'}(x) = e^{-i\omega(x)} W_\mu^-(x), \quad (1.57a)$$

$$W_\mu^+(x) \rightarrow W_\mu^{+'}(x) = e^{+i\omega(x)} W_\mu^+(x). \quad (1.57b)$$

It would be accomplished if we replace the ordinary derivatives with the covariant derivatives:

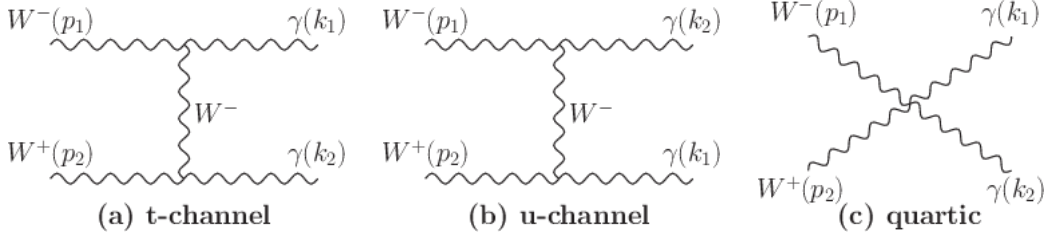
$$D_\mu = \partial_\mu + ieA_\mu, \quad (1.58)$$

with the $U(1)$ (electromagnetic) gauge field, $A_\mu(x)$, transforming as:

$$A'_\mu(x) = A_\mu(x) + \frac{1}{e} \partial_\mu \omega(x). \quad (1.59)$$

So our ‘minimal’ Lagrangian will be

$$\mathcal{L}^{\min} = -\frac{1}{2} (D_\mu W_\nu^- - D_\nu W_\mu^-) (D^{*\mu} W^{\nu+} - D^{*\nu} W^{\mu+}) + M_W^2 W^{\mu+} W_\mu^-. \quad (1.60)$$

FIGURE 1.3: Feynman diagrams for the process $W^-(p_1) + W^+(p_2) \rightarrow \gamma(k_1) + \gamma(k_2)$.

But there is more. One may add to the minimal Lagrangian of Eq. (1.60) another gauge invariant term:

$$\mathcal{L}' = -i\kappa e W_\mu^- W_\nu^+ F^{\mu\nu}, \quad (1.61)$$

$$\text{where, } F_{\mu\nu} = \partial_\mu A_\nu - \partial_\nu A_\mu. \quad (1.62)$$

So we write the total electromagnetic interaction as:

$$\mathcal{L}_W^{\text{e.m.}} = \mathcal{L}^{\text{min}} + \mathcal{L}' \quad (1.63)$$

Till now there is no good reason why we should keep \mathcal{L}' . The condition $\kappa = 0$ will correspond to the minimal case. But let us keep our minds open and see, using unitarity arguments, what value of κ should be chosen by nature. Assuming Eq. (1.63) to be our guiding Lagrangian, we may write the cubic and quartic couplings as:

$$\begin{aligned} \mathcal{L}_{WW\gamma} = & -ie \left[A^\mu \{ W^{\nu-} (\partial_\mu W_\nu^+) - (\partial_\mu W_\nu^+) W^{\nu+} \} + W^{\mu-} \{ \kappa W^{\nu+} (\partial_\mu A_\nu) \right. \\ & \left. - (\partial_\mu W_\nu^+) A^\nu \} + W^{\mu+} \{ A^\nu (\partial_\mu W_\nu^-) - \kappa (\partial_\mu A_\nu) W^{\nu-} \} \right] \end{aligned} \quad (1.64)$$

$$\mathcal{L}_{WW\gamma\gamma} = -e^2 (A_\mu A^\mu W_\nu^- W^{\nu+} - A^\mu A^\nu W_\mu^- W_\nu^-) \quad (1.65)$$

Determination of κ : Let us consider the following process:

$$W^-(p_1) + W^+(p_2) \rightarrow \gamma(k_1) + \gamma(k_2)$$

The Feynman diagrams for this process are shown in Figure 1.3. For diagrams (a) and (b) there will be a W propagator which contains a $g^{\mu\nu}$ term and a $q^\mu q^\nu$ term. From dimensional arguments one can understand that the leading order divergence comes from the $q^\mu q^\nu$ term. In view of this, we write the amplitude for diagram (a) as:

$$\mathcal{M}_a = \mathcal{M}_a^{(1)} + \mathcal{M}_a^{(2)}. \quad (1.66)$$

$\mathcal{M}_a^{(1)}$ contains the contribution from the $g^{\mu\nu}$ term and $\mathcal{M}_a^{(2)}$ contains that from the $q^\mu q^\nu$ term. Calculating explicitly we have, at the leading order,

$$\begin{aligned} \mathcal{M}_a^{(1)} = & -\frac{e^2}{M_W^2} \frac{1}{t - M_W^2} \left[(1 - \kappa)^2 \{ (p_1 \cdot k_1)(\epsilon_1 \cdot \epsilon'_1) - (p_1 \cdot \epsilon'_1)(k_1 \cdot \epsilon_1) \} \right. \\ & \left. \times \{ (p_2 \cdot k_2)(\epsilon_2 \cdot \epsilon'_2) - (p_2 \cdot \epsilon'_2)(k_2 \cdot \epsilon_2) \} + \dots \right] \end{aligned} \quad (1.67)$$

Diagram (b) will also have an analogous term, $\mathcal{M}_b^{(2)}$, with $t \leftrightarrow u$, $k_1 \leftrightarrow k_2$, $\epsilon'_1 \leftrightarrow \epsilon'_2$. Since $\mathcal{M}_b^{(2)}$ has $\frac{1}{u - M_W^2}$ as the prefactor, $\mathcal{M}_a^{(2)}$ and $\mathcal{M}_b^{(2)}$ will not cancel each other for any arbitrary set $\{p_1, p_2, k_1, k_2\}$ satisfying four-momentum conservation. So, $\mathcal{M}_a^{(2)}$ and $\mathcal{M}_b^{(2)}$ must vanish independently.

Observation: First of all, it should be noted that if at least one of the W bosons has longitudinal polarization, the leading growth of Eq. (1.67) (quartic or cubic) vanishes for any arbitrary value of κ . This statement can immediately be verified if we replace, in such a case, the polarization vector $\epsilon_1 \equiv \epsilon_L(p_1)$ or $\epsilon_2 \equiv \epsilon_L(p_2)$ in Eq. (1.67) by the corresponding leading term $\frac{p_1^\mu}{M_W}$ or, $\frac{p_2^\mu}{M_W}$ according to the formula:

$$\epsilon_L^\mu(p) = \frac{p^\mu}{M_W} + \mathcal{O}\left(\frac{M_W}{p^0}\right). \quad (1.68)$$

The corresponding expression within the curly brackets will be zero causing the leading energy growth in Eq. (1.67) to vanish. But, if both the W bosons have transverse polarizations, then the leading term in Eq. (1.67) will, in general, grow quadratically unless $\kappa = 1$.

Using this value of κ , Eq. (1.64) can be rewritten as:

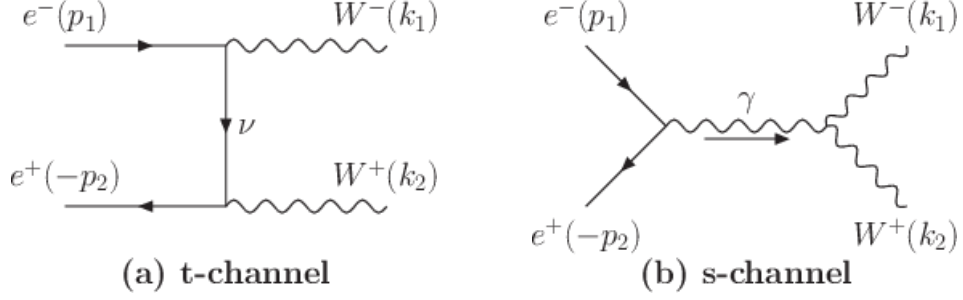
$$\mathcal{L}_{WW\gamma} = -ie \left[A^\mu (W^{\nu-} \overleftrightarrow{\partial}_\mu W_\nu^+) + W^{\mu-} (W^{\nu+} \overleftrightarrow{\partial}_\mu A_\nu) + W^{\mu+} (A^\nu \overleftrightarrow{\partial}_\mu W_\nu^-) \right]. \quad (1.69)$$

The symbol $\overleftrightarrow{\partial}$ in Eq. (1.69) is defined in the usual way as,

$$f \overleftrightarrow{\partial}_\mu g = f(\partial_\mu g) - (\partial_\mu f)g. \quad (1.70)$$

Therefore, we have arrived at the following important conclusion [3]:

Leading power growth arising in the high energy limit in tree level diagrams involving both external and internal lines of vector bosons, W^\pm , are eliminated for an arbitrary combination of the W^\pm polarizations if and only if the corresponding electromagnetic interaction is of the Yang-Mills type.

FIGURE 1.4: Feynman diagrams for the process $e^-(p_1) + e^+(p_2) \rightarrow W_L^-(k_1) + W_L^+(k_2)$.

1.3.2 Introducing the Z boson

Now consider the process [7]

$$e^-(p_1) + e^+(p_2) \rightarrow W_L^-(k_1) + W_L^+(k_2)$$

From what we have learned till now, there will be two possible diagrams for this process as shown in Figure 1.4. The corresponding amplitudes are written below (see Appendix B):

$$\mathcal{M}_a^\nu = -\frac{g^2}{4M_W^2} \underbrace{\bar{v}(p_2)\not{k}_1(1-\gamma_5)u(p_1)}_{\mathcal{O}(E^2)} + \mathcal{O}(E), \quad (1.71)$$

$$\mathcal{M}_b^\gamma = \frac{e^2}{M_W^2} \underbrace{\bar{v}(p_2)\not{k}_1 u(p_1)}_{\mathcal{O}(E^2)} + \mathcal{O}(1). \quad (1.72)$$

Remember that the u and v spinors contain a factor of \sqrt{E} in their normalization. So the leading terms grow as E^2 . Let us collect the quadratic growths in a single equation

$$\mathcal{M}^{\text{quadratic}} = -\frac{g^2}{4M_W^2} \bar{v}(p_2)\not{k}_1(1-\gamma_5)u(p_1) + \frac{e^2}{M_W^2} \bar{v}(p_2)\not{k}_1 u(p_1). \quad (1.73)$$

It is clear that one cannot arrange a mutual cancellation of quadratic energy growths between \mathcal{M}_a^ν and \mathcal{M}_b^γ by tuning the relative magnitudes of the coupling constants e and g . This is because the corresponding growth in Eq. (1.71) contains a factor of $(1-\gamma_5)$ but in Eq. (1.72) it does not. It is the consequence of the fact that the charged current interactions involve only the left handed (LH) fermions.

Thus we have no other choices than to introduce new particles which can compensate the residual growth of Eq. (1.73). We shall restrict ourselves to particles with lowest possible spin (*i.e.* 0, $\frac{1}{2}$, 1) and allow only those interaction terms which satisfy the condition $[\mathcal{L}_{\text{int}}] \leq 4$, so that renormalizability of the theory is not compromised.

Choice 1 (Spin 0)

Let us postulate the existence of spin 0 scalar (h) whose coupling with the fermions and W bosons can be written as:

$$\mathcal{L}_{WWh} = g_{WWh} W_\mu^- W^{\mu+} h \quad (1.74)$$

$$\mathcal{L}_{ffh} = g_{ffh} \bar{f} \Gamma f h. \quad (1.75)$$

Where Γ is, in general, a combination of the unit matrix and γ_5 and g_{WWh} , g_{ffh} are corresponding coupling strengths. Note that g_{ffh} is dimensionless but g_{WWh} is not. In fact, without any loss of generality, we may express g_{WWh} as

$$g_{WWh} = \alpha M_W, \quad (1.76)$$

where α is a dimensionless constant. As a result of these new couplings there will be a h -mediated s-channel diagram similar to Figure 1.4b. By simple dimension counting one can verify that this diagram can at best grow as $\mathcal{O}(E)$ for large CM energies when the external W bosons are longitudinally polarized. An exchange of a spin 0 particle is therefore not suitable for the desirable cancellation of the quadratic growths in Eq. (1.73). However, it is worth noting at this point that such a spin 0 particle can play a crucial role in suppressing linear energy growths in the $e^- e^+ \rightarrow WW$ amplitude. This will be used later in this chapter.

Choice 2 (Spin $\frac{1}{2}$)

In this case we shall assume the existence of a heavy neutrino-like fermion (E^0) which couples with the electron in the following way [8]:

$$\mathcal{L}_{\text{int}}^{(E^0)} = (b_L \bar{E}_L^0 \gamma^\mu e_L + b_R \bar{E}_R^0 \gamma^\mu e_R) + \text{h.c.} \quad (1.77)$$

We shall assume b_L and b_R to be real to respect CP invariance. This new interaction will lead to a new t-channel diagram similar to Figure 1.4a mediated by E^0 . Unlike the previous choice, the amplitude corresponding to this new diagram does contain terms which grow quadratically in the high-energy limit when the external W bosons are longitudinally polarized. The requirement of a cancellation of quadratic growths in Eq. (1.73) then yields the following conditions for the coupling constants b_L , b_R :

$$b_L^2 = e^2 - \frac{g^2}{2}, \quad (1.78)$$

$$b_R^2 = e^2. \quad (1.79)$$

Since b_L is real, the first relation leads to a constraint for relative strengths of weak and electromagnetic interactions, namely

$$g \leq \sqrt{2}e. \quad (1.80)$$

An interesting consequence of the above inequality and the general relation of Eq. (1.53) is an upper bound for the W^\pm mass:

$$M_W \leq \left(\frac{\sqrt{2}\pi\alpha}{G_F} \right)^{\frac{1}{2}} = 53 \text{ GeV}. \quad (1.81)$$

We now know that this is against the experimental facts. Therefore we shall not consider this scheme any further.

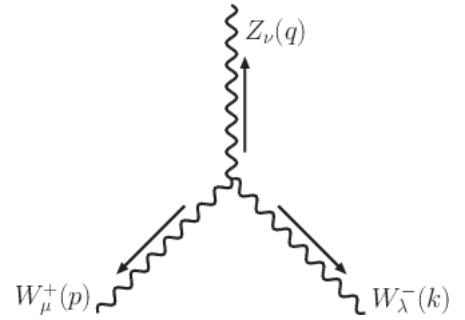
Choice 3 (Spin 1)

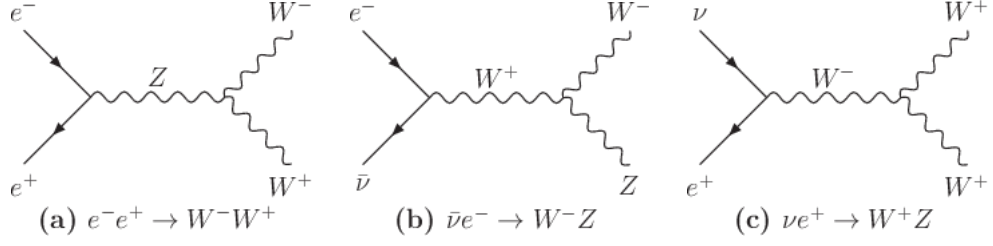
Now we shall consider the next alternative, *i.e.*, the case where the ‘‘compensation’’ diagram for $e^-e^+ \rightarrow W^-W^+$ corresponds to a s-channel exchange of a neutral spin 1 particle (Z) with non-zero mass. Note that a new massless neutral boson will imply the existence of a new kind of long range force (like electromagnetism) which is not observed in nature. But to calculate the amplitude we need to have some idea about the WWZ coupling. Here also we will concentrate on interactions which satisfy $[\mathcal{L}_{WWZ}] \leq 4$. We proceed as follows [9]:

It is obvious that a Lorentz invariant interaction involving three vector bosons and satisfying the above condition, must involve just one derivative of a vector boson field (the corresponding coupling constant is then of course dimensionless). In momentum space, this means that the interaction vertex shown in the adjacent picture can be represented by a linear polynomial in terms of the four momenta k , p and q . Among these only two are independent because of the four momentum conservation $k + p + q = 0$.

Choosing k and p to be independent variables, the most general linear polynomial representing the W^-W^+Z interaction vertex may be written as

$$\begin{aligned} V_{\lambda\mu\nu}(k, p, q) = & (Ak_\lambda + Bp_\lambda)g_{\mu\nu} + (Ck_\mu + Dp_\mu)g_{\lambda\nu} + (Ek_\nu + Fp_\nu)g_{\lambda\mu} \\ & + G\epsilon_{\lambda\mu\nu\rho}k^\rho + H\epsilon_{\lambda\mu\nu\rho}p^\rho. \end{aligned} \quad (1.82)$$



FIGURE 1.5: Some $2 \rightarrow 2$ scatterings to determine the WWZ vertex.

For comparison, let us write the Yang-Mills structure below

$$V_{\lambda\mu\nu}^{(\text{YM})}(k, p, q) = (k + 2p)_\lambda g_{\mu\nu} + (-2k - p)_\mu g_{\lambda\nu} + (k - p)_\nu g_{\lambda\mu} \quad (1.83)$$

The leading growth in the three processes shown in Figure 1.5 will come from the $\frac{q^\mu q^\nu}{M_{W,Z}^2}$ term in the intermediate vector boson propagator. If we demand the vanishing of this leading growth then we get the following relations involving A, B, \dots, G [3]:

$$B + C = 0, \quad (1.84a)$$

$$E + F = 0, \quad (1.84b)$$

$$B - E + F = 0, \quad (1.84c)$$

$$-C + 2D = 0, \quad (1.84d)$$

$$C + E - F = 0, \quad (1.84e)$$

$$2A - B = 0, \quad (1.84f)$$

$$G = H = 0. \quad (1.84g)$$

Solving the above set of equations we may rewrite Eq. (1.82) as

$$V_{\lambda\mu\nu}(k, p, q) = g_{WWZ} [(k + 2p)_\lambda g_{\mu\nu} + (-2k - p)_\mu g_{\lambda\nu} + (k - p)_\nu g_{\lambda\mu}], \quad (1.85)$$

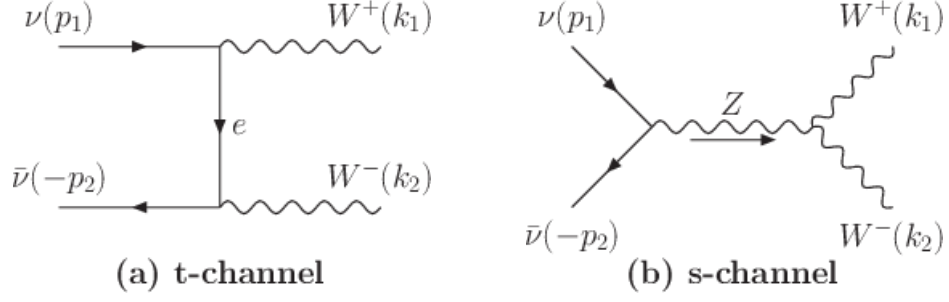
where, we have relabeled A as g_{WWZ} . Therefore, $V_{\lambda\mu\nu}$ has the exact Yang-Mills structure upto an overall multiplicative factor which, we hope, will be determined by the requirement of unitarity.

Now, as a consequence of this new particle, the process $e^-e^+ \rightarrow W^-W^+$ will have an extra s-channel diagram similar to Figure 1.4b mediated by the Z boson. If we express the eeZ coupling as

$$\mathcal{L}_{eeZ} = (g_L \bar{e}_L \gamma^\mu e_L + g_R \bar{e}_R \gamma^\mu e_R) Z_\mu, \quad (1.86)$$

Then the amplitude for the new diagram is found to be

$$\mathcal{M}_b^Z = -\frac{1}{2M_W^2} g_{WWZ} g_L \bar{v}(p_2) \not{k}_1 (1 - \gamma_5) u(p_1)$$

FIGURE 1.6: Feynman diagrams for the process $\nu(p_1) + \bar{\nu}(p_2) \rightarrow W_L^+(k_1) + W_L^-(k_2)$.

$$-\frac{1}{2M_W^2} g_{WWZ} g_R \bar{\nu}(p_2) \not{k}_1 (1 + \gamma_5) u(p_1) + \mathcal{O}(E) \quad (1.87)$$

Adding this with Eq. (1.73) we immediately get the conditions for cancellation of leading energy growths in $e^-e^+ \rightarrow WW$ at large values of CM energies:

$$-\frac{g^2}{2} + e^2 - g_L g_{WWZ} = 0, \quad (1.88)$$

$$e^2 - g_R g_{WWZ} = 0. \quad (1.89)$$

1.4 Retrieving vector and axial-vector couplings

For this purpose we need to consider a few more processes. The first of these will be

$$\nu(p_1) + \bar{\nu}(p_2) \rightarrow W_L^+(k_1) + W_L^-(k_2).$$

Taking into account the experimental fact that only left-handed neutrinos are observed in nature, we can express the $\nu\nu Z$ coupling as follows:

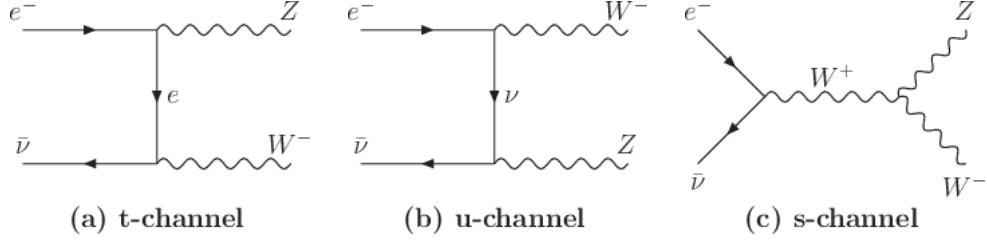
$$\mathcal{L}_{\nu\nu Z} = g_{\nu\nu Z} \bar{\nu} \gamma^\mu P_L \nu Z_\mu. \quad (1.90)$$

There are two possible Feynman diagrams as shown in Figure 1.6. The corresponding amplitudes are found to be

$$\mathcal{M}_a^e = -\frac{g^2}{4M_W^2} \underbrace{\bar{\nu}(p_2) \not{k}_1 (1 - \gamma_5) u(p_1)}_{\mathcal{O}(E^2)} + \mathcal{O}(1), \quad (1.91)$$

$$\mathcal{M}_b^Z = \frac{g_{\nu\nu Z} g_{WWZ}}{2M_W^2} \underbrace{\bar{\nu}(p_2) \not{k}_1 (1 - \gamma_5) u(p_1)}_{\mathcal{O}(E^2)} + \mathcal{O}(1). \quad (1.92)$$

Note that the absence of $\mathcal{O}(E)$ terms in the above amplitudes is a manifest of the assumption that neutrinos are massless. As we will see later, this absence of linear growth will lead us to conclude that neutrinos do not need to couple with the Higgs scalar. But one can see that there

FIGURE 1.7: Feynman diagrams for $e^-(p_1) + \bar{\nu}(p_2) \rightarrow Z_L(k_1) + W_L^-(k_2)$.

are quadratic growths present in the amplitude, cancellation of which would require

$$-\frac{g^2}{2} + g_{\nu\nu Z}g_{WWZ} = 0. \quad (1.93)$$

The next process we consider is

$$e^-(p_1) + \bar{\nu}(p_2) \rightarrow Z_L(k_1) + W_L^-(k_2)$$

The amplitudes corresponding to the diagrams shown in Figure 1.7 are given below:

$$\mathcal{M}_a = -\frac{gg_L}{2\sqrt{2}M_W M_Z} \underbrace{\bar{\nu}(p_2)\not{k}_1(1-\gamma_5)u(p_1)}_{\mathcal{O}(E^2)} + \mathcal{O}(E), \quad (1.94)$$

$$\mathcal{M}_b = -\frac{gg_{\nu\nu Z}}{2\sqrt{2}M_W M_Z} \underbrace{\bar{\nu}(p_2)\not{k}_1(1-\gamma_5)u(p_1)}_{\mathcal{O}(E^2)} + \mathcal{O}(E), \quad (1.95)$$

$$\mathcal{M}_c = -\frac{gg_{WWZ}}{2\sqrt{2}M_W M_Z} \underbrace{\bar{\nu}(p_2)\not{k}_1(1-\gamma_5)u(p_1)}_{\mathcal{O}(E^2)} + \mathcal{O}(E). \quad (1.96)$$

Clearly, the condition for cancellation of the quadratic growths reads:

$$-g_L + g_{\nu\nu Z} - g_{WWZ} = 0. \quad (1.97)$$

Till now we have obtained four equations (Eqs. (1.88), (1.89), (1.93) and (1.97)) involving four unknowns g_L , g_R , $g_{\nu\nu Z}$, and g_{WWZ} . Let us rewrite them below:

$$-\frac{g^2}{2} + e^2 - g_L g_{WWZ} = 0, \quad (1.98a)$$

$$e^2 - g_R g_{WWZ} = 0, \quad (1.98b)$$

$$-\frac{g^2}{2} + g_{\nu\nu Z} g_{WWZ} = 0, \quad (1.98c)$$

$$-g_L + g_{\nu\nu Z} - g_{WWZ} = 0. \quad (1.98d)$$

The solution of the above set of equations is unique up to an overall sign. Choosing $g_{WWZ} = \sqrt{g^2 - e^2}$ we have

$$g_{WWZ} = \sqrt{g^2 - e^2}, \quad (1.99a)$$

$$g_{\nu\nu Z} = \frac{g^2}{2\sqrt{g^2 - e^2}}, \quad (1.99b)$$

$$g_L = \frac{-\frac{g^2}{2} + e^2}{\sqrt{g^2 - e^2}}, \quad (1.99c)$$

$$g_R = \frac{e^2}{\sqrt{g^2 - e^2}}. \quad (1.99d)$$

The above solutions clearly demands $e < g$. Therefore we can use the parametrization,

$$\sin \theta_w = \frac{e}{g} \quad (1.100)$$

to cast the solutions in their familiar form,

$$g_{WWZ} = g \cos \theta_w, \quad (1.101a)$$

$$g_{\nu\nu Z} = \frac{g}{2 \cos \theta_w}, \quad (1.101b)$$

$$g_L = \frac{g}{2 \cos \theta_w} (-1 + 2 \sin^2 \theta_w), \quad (1.101c)$$

$$g_R = \frac{g}{\cos \theta_w} \sin^2 \theta_w. \quad (1.101d)$$

There is more! One should remember that a residual linear growth (not shown in Eq. (1.94)) is still present in the amplitude of the process $\bar{\nu}e^- \rightarrow W_L^- Z_L$. It can be easily shown that a cancellation of this growth can be arranged if we impose the following relation:

$$g_R - g_{\nu\nu Z} + g_{WWZ} \left(1 - \frac{M_Z^2}{2M_W^2}\right) = 0. \quad (1.102)$$

Using the solutions of Eq. (1.101) we can translate this into the following relation between the masses of the vector bosons:

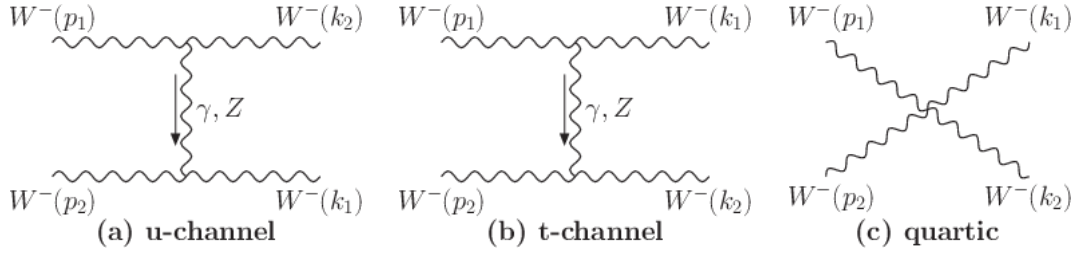
$$M_W = M_Z \cos \theta_w. \quad (1.103)$$

Using Eq. (1.53) together with this, we obtain the standard formulae for W and Z masses:

$$M_W = \left(\frac{\pi\alpha}{G_F\sqrt{2}}\right)^{\frac{1}{2}} \frac{1}{\sin \theta_w}, \quad (1.104a)$$

$$M_Z = \left(\frac{\pi\alpha}{G_F\sqrt{2}}\right)^{\frac{1}{2}} \frac{1}{\sin \theta_w \cos \theta_w}. \quad (1.104b)$$

Now comes the experiment. If this theoretical model is true then the scattering $\nu_\mu e^- \rightarrow \nu_\mu e^-$

FIGURE 1.8: Gauge diagrams for $W_L^- W_L^- \rightarrow W_L^- W_L^-$.

can only proceed via Z exchange. From these types of neutrino-fermion scatterings a preliminary value of $\sin^2 \theta_w$ (≈ 0.22) was obtained [10] and it was used in Eq. (1.104) to predict W and Z boson masses as

$$M_W \approx 79 \text{ GeV}, \quad M_Z \approx 90 \text{ GeV}. \quad (1.105)$$

Note that this is a robust prediction of the theory dictating not only what to look for but also where to look for! We now know that the experimental values are very close to these predictions vindicating the theory.

1.5 Vector boson quartic self couplings

Let us first investigate the process

$$W_L^-(p_1) + W_L^-(p_2) \rightarrow W_L^-(k_1) + W_L^-(k_2).$$

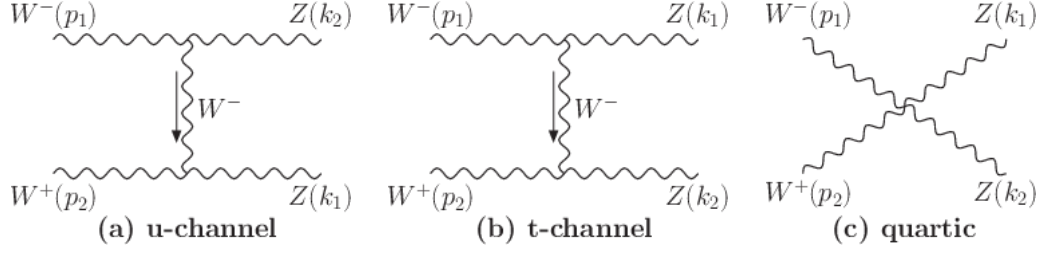
From what we have gathered till now, only (a) and (b) of Figure 1.8 exist. We can calculate their total amplitude as

$$\mathcal{M}_{a+b}^{\gamma+Z} = \frac{g^2}{4M_W^4} (t^2 + u^2 - 2s^2) + \mathcal{O}(E^2) + \mathcal{O}(1) \quad (1.106)$$

Clearly, the quartic growth cannot be canceled by a scalar (spin 0) mediated diagram as it can give $\mathcal{O}(E^2)$ growth at best. The next possible choice would be to introduce another neutral vector boson (Z' say). But that will add same kind of quartic growth as already present in Eq. (1.106). So these will not help.

It appears that the simplest possibility is to introduce a direct self interaction between the W bosons. Since $[\mathcal{L}_{\text{int}}] \leq 4$, it is clear that terms involving derivative of vector fields are not allowed. The most general interaction of this type can be written as

$$\mathcal{L}_{WWW} = a(W^- \cdot W^+)(W^- \cdot W^+) + b(W^- \cdot W^-)(W^+ \cdot W^+). \quad (1.107)$$

FIGURE 1.9: Gauge diagrams for $W_L^- W_L^+ \rightarrow Z_L Z_L$.

This new interaction will add one more diagram shown in Figure 1.8c. The amplitude for this diagram can be found to be

$$\mathcal{M}_c = a \frac{1}{2M_W^4} (t^2 + u^2) + b \frac{1}{M_W^4} s^2 + \mathcal{O}(E^2). \quad (1.108)$$

It is obvious that the leading growths of Eqs. (1.106) and (1.108) will cancel each other if

$$a = -b = -\frac{g^2}{2}, \quad (1.109)$$

$$\Rightarrow \mathcal{L}_{WWWW} = \frac{g^2}{2} [(W^- \cdot W^-)(W^+ \cdot W^+) - (W^- \cdot W^+)(W^- \cdot W^+)]. \quad (1.110)$$

The quadratic residual growth for WW scattering is given by:

$$\mathcal{M}^{\text{gauge}} = -\frac{g^2}{4M_W^2} s + \mathcal{O}(1). \quad (1.111)$$

Similarly, for the process

$$W_L^-(p_1) + W_L^+(p_2) \rightarrow Z_L(k_1) + Z_L(k_2),$$

we have (see Figure 1.9),

$$\mathcal{M}_{a+b} = -\frac{g_{WWZ}^2}{4M_W^2 M_Z^2} (t^2 + u^2 - 2s^2) + \mathcal{O}(E^2) + \mathcal{O}(1), \quad (1.112)$$

which will invite us to introduce the following quartic interaction:

$$\mathcal{L}_{WWZZ} = c(W^- \cdot Z)(W^+ \cdot Z) + d(W^- \cdot W^+)(Z \cdot Z). \quad (1.113)$$

The amplitude of the corresponding diagram is found to be

$$\mathcal{M}_c = \frac{1}{4M_W^2 M_Z^2} [c(t^2 + u^2) + 2ds^2] + \mathcal{O}(E^2) + \mathcal{O}(1). \quad (1.114)$$

Cancellation of the $\mathcal{O}(E^4)$ growth would require

$$c = g_{WWZ}^2; \quad d = -g_{WWZ}^2, \quad (1.115)$$

which means

$$\mathcal{L}_{WWZZ} = g_{WWZ}^2 [(W^- \cdot Z)(W^+ \cdot Z) - (W^- \cdot W^+)(Z \cdot Z)]. \quad (1.116)$$

Similar considerations for $W_L^- W_L^+ \rightarrow Z_L \gamma$ leads to

$$\begin{aligned} \mathcal{L}_{WWZ\gamma} &= g_{WWZ} g_{WW\gamma} [(W^- \cdot Z)(W^+ \cdot A) + (W^- \cdot A)(W^+ \cdot Z) \\ &\quad - 2(W^- \cdot W^+)(Z \cdot A)]. \end{aligned} \quad (1.117)$$

Thus collecting Eqs. (1.65), (1.110), (1.116) and (1.117) and defining

$$W_\mu^3 = \cos \theta_w Z_\mu + \sin \theta_w A_\mu, \quad (1.118)$$

we can write the quartic vector boson self couplings in the following compact form:

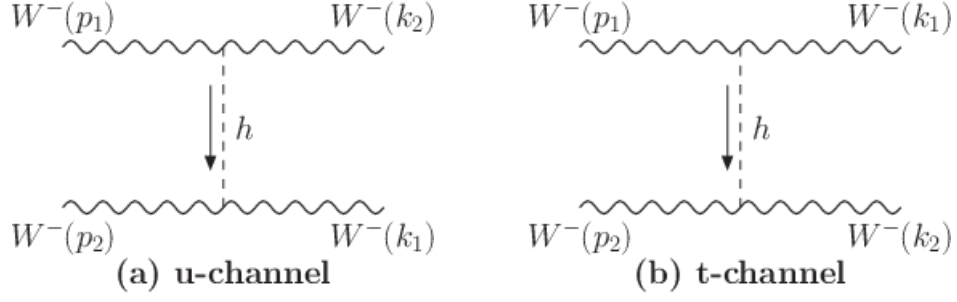
$$\begin{aligned} \mathcal{L}_{VVVV} &= \mathcal{L}_{WWWW} + \mathcal{L}_{WW\gamma\gamma} + \mathcal{L}_{WWZZ} + \mathcal{L}_{WWZ\gamma} \\ &= -g^2 \left\{ \frac{1}{2} (W^- \cdot W^+)^2 - \frac{1}{2} (W^-)^2 (W^+)^2 \right. \\ &\quad \left. + (W^3)^2 (W^- \cdot W^+) - (W^- \cdot W^3)(W^+ \cdot W^3) \right\}, \end{aligned} \quad (1.119)$$

where, we have used the solution of Eq. (1.101). The same thing can be done with the cubic self couplings of Eqs. (1.69) and (1.85)

$$\begin{aligned} \mathcal{L}_{VVV} &= \mathcal{L}_{WW\gamma} + \mathcal{L}_{WWZ} \\ &= -ig \left[W^{3\mu} (W^{\nu-} \overleftrightarrow{\partial}_\mu W_\nu^+) + W^{\mu-} (W^{\nu+} \overleftrightarrow{\partial}_\mu W_\nu^3) \right. \\ &\quad \left. + W^{\mu+} (W^{3\nu} \overleftrightarrow{\partial}_\mu W_\nu^-) \right]. \end{aligned} \quad (1.120)$$

1.6 Need for a neutral scalar

As already mentioned in the preceding sections, some processes do contain some remnant energy growths even after the introduction of the quartic gauge self couplings. With no other couplings to tune freely, we must now extend the particle content of the theory to eliminate those residual energy growths. In doing this, we shall stick to the minimal choice, *i.e.*, we shall start from spin 0 particles and we shall not include any interaction with $[\mathcal{L}]_{\text{int}} > 4$ for they will come with

FIGURE 1.10: Higgs diagrams for $W_L^- W_L^- \rightarrow W_L^- W_L^-$.

coupling constants having negative mass dimensions which is bad for the high energy behavior of the theory.

1.6.1 Trilinear couplings with vector bosons and fermions

- Let us now go back to $W_L^- W_L^- \rightarrow W_L^- W_L^-$ scattering again. For this process, there is a remaining quadratic growth even after the introduction of the quartic self couplings (see Eq. (1.111)). We shall now try to eliminate this growth by introducing a new interaction of the W 's with a neutral scalar field which will be denoted by h . It is not difficult to realize that the only possible choice satisfying $[\mathcal{L}_{\text{int}}] \leq 4$ is represented by the interaction Lagrangian

$$\mathcal{L}_{WWh} = g_{WWh} W_\mu^- W^{\mu+} h \quad (1.121)$$

Tree diagrams for the process $W^- W^- \rightarrow W^- W^-$ corresponding to the interaction of Eq. (1.121), have been shown in Figure 1.10. One can calculate:

$$\mathcal{M}^{(h)} = \mathcal{M}_a^{(h)} + \mathcal{M}_a^{(h)} = g_{WWh}^2 \frac{s}{M_W^4} + \mathcal{O}(1). \quad (1.122)$$

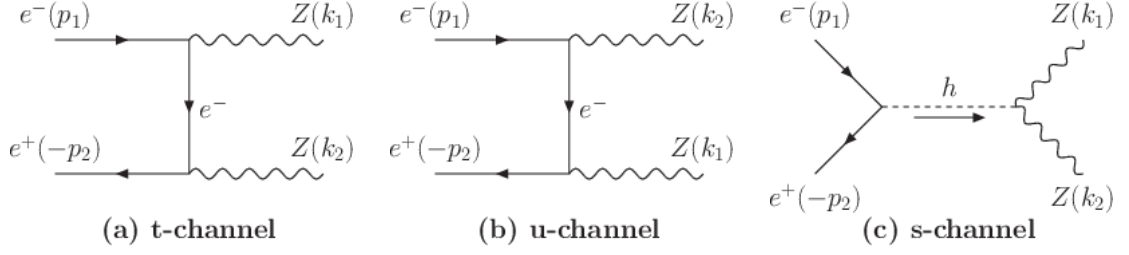
So, the desired cancellation would require:

$$g_{WWh} = g M_W. \quad (1.123)$$

- To have an idea of the coupling of this new scalar with massive fermions, let us consider the process

$$e^-(p_1) + e^+(p_2) \rightarrow W_L^-(k_1) + W_L^+(k_2).$$

Without this new scalar, there will be three Feynman diagrams as shown in Figure 1.4 (don't forget to include the Z mediated s-channel diagram similar to Figure 1.4b). The

FIGURE 1.11: Feynman diagrams for $e^- e^+ \rightarrow Z_L Z_L$.

total amplitude can be calculated as:

$$\mathcal{M}_{\text{without scalar}} = \mathcal{M}_a^\nu + \mathcal{M}_b^{\gamma, Z} = -\frac{g^2}{4M_W^2} m_e \underbrace{\bar{v}(p_2)u(p_1)}_{\mathcal{O}(E)} + \mathcal{O}(1). \quad (1.124)$$

To eliminate this linear energy growth, we introduce the following interaction:

$$\mathcal{L}_{eeh} = g_{eeh} \bar{e} e h. \quad (1.125)$$

Note that as there is no γ_5 in the residual growth of Eq. (1.124), we do not introduce any pseudoscalar interaction with h . This new interaction will lead to a h mediated s-channel diagram whose amplitude is found to be:

$$\mathcal{M}^h = -\frac{g_{eeh} g_{WW} h}{2M_W^2} \bar{v}(p_2)u(p_1) + \mathcal{O}(1), \quad (1.126)$$

where, $g_{WW} h$ is given by Eq. (1.123). So the linear growth can be canceled by tuning g_{eeh} as:

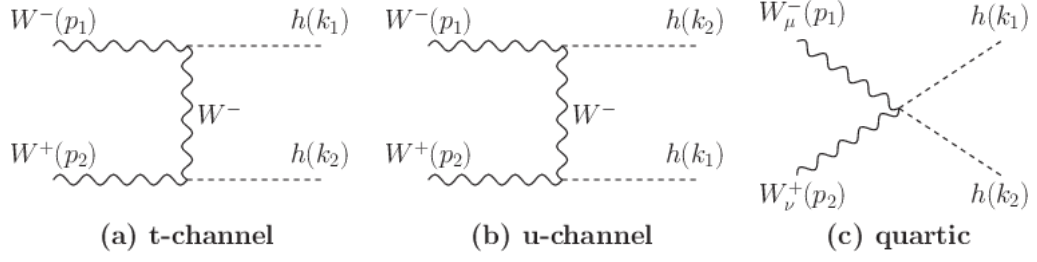
$$g_{eeh} = -\frac{g m_e}{2M_W}. \quad (1.127)$$

- To get an idea of ZZh coupling, we consider the process

$$e^-(p_1) + e^+(p_2) \rightarrow Z_L(k_1) + Z_L(k_2).$$

The Feynman diagrams for this process have been displayed in Figure 1.11. Without the scalar mediated s-channel diagram, the total amplitude linearly grows with energy as follows:

$$\mathcal{M}_{\text{without scalar}} = \mathcal{M}_a + \mathcal{M}_b = -\frac{g^2 m_e}{4M_Z^2 \cos^2 \theta_w} \underbrace{\bar{v}(p_2)u(p_1)}_{\mathcal{O}(E)} + \mathcal{O}(1). \quad (1.128)$$

FIGURE 1.12: Feynman diagrams for $W_L^- W_L^+ \rightarrow hh$.

To eliminate this growth we introduce the ZZh interaction

$$\mathcal{L}_{ZZh} = g_{ZZh} Z_\mu Z^\mu h \quad (1.129)$$

which brings in Diagram 1.11c with the following amplitude:

$$\mathcal{M}_c = -\frac{g_{eeh} g_{ZZh}}{M_Z^2} \bar{v}(p_2) u(p_1). \quad (1.130)$$

Using the value of g_{eeh} from Eq. (1.127), one can find the condition for the cancellation of the $\mathcal{O}(E)$ growth in Eq. (1.128) to be

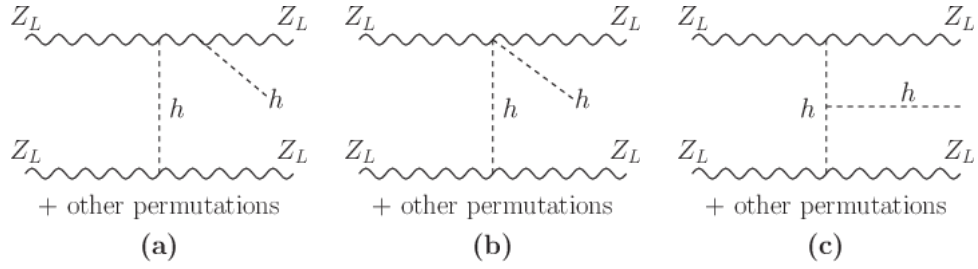
$$g_{ZZh} = \frac{g M_Z}{2 \cos \theta_w}. \quad (1.131)$$

From Eqs. (1.124) and (1.128) it is interesting to note that the amplitudes for the processes $\ell^+ \ell^- \rightarrow V_L V_L$ (ℓ stands for leptons and $V = W, Z$) without the scalar contain energy growths which are proportional to the mass (m_ℓ) of the lepton involved. Clearly, there will be no such energy growths even without this new scalar for $\nu_\ell \bar{\nu}_\ell \rightarrow VV$ as long as neutrinos are considered to be massless. Therefore, this new scalar need not couple to a pair of neutrinos. Thus, we have learned one remarkable feature of the trilinear interactions of this new scalar field, h , that a corresponding coupling constant is always proportional to the mass of the particle interacting with h .

1.6.2 Quartic couplings with the vector bosons

Since we already have concluded the existence of $WW h$ interaction the process $W_L^- W_L^+ \rightarrow hh$ is possible. From what we have gathered till now, only diagrams 1.12a and 1.12b exist. Quadratic energy growths will appear from the $k^\mu k^\nu$ term in the intermediate W propagator as follows:

$$\mathcal{M}_a + \mathcal{M}_b = -\frac{g^2 s}{4M_W^2} + \mathcal{O}(1). \quad (1.132)$$

FIGURE 1.13: Feynman diagrams for $Z_L Z_L \rightarrow Z_L Z_L h$.

To remove this growth we propose the existence of a quartic interaction of the form

$$\mathcal{L}_{WWhh} = g_{WWhh} W_\mu^- W^{+\mu} h h \quad (1.133)$$

which will introduce diagram 1.12c with the following amplitude

$$\mathcal{M}_c = g_{WWhh} \frac{s}{M_W^2} + \mathcal{O}(1) . \quad (1.134)$$

Clearly, the cancellation of the quadratic growth requires

$$g_{WWhh} = \frac{g^2}{4} . \quad (1.135)$$

Similar consideration of $Z_L Z_L \rightarrow hh$ scattering will lead to the existence of a $ZZhh$ quartic interaction of the form

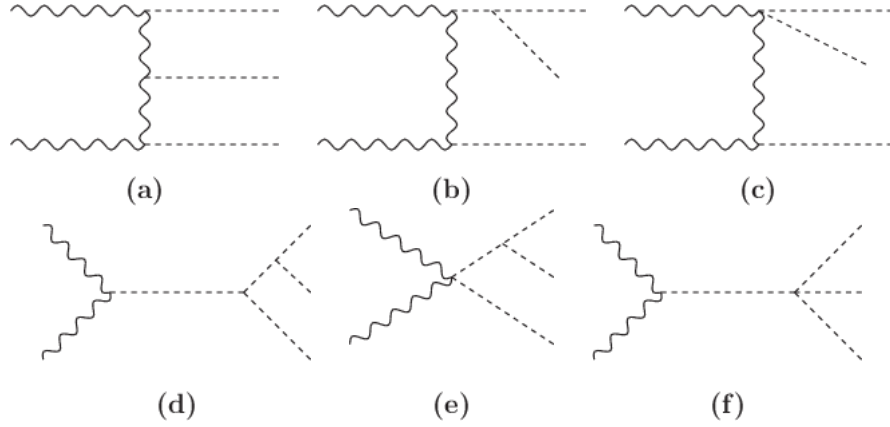
$$\mathcal{L}_{ZZhh} = \frac{g^2}{8 \cos^2 \theta_w} Z_\mu Z^\mu h h . \quad (1.136)$$

1.6.3 Scalar self couplings

Scalar self couplings do not follow from the requirement of tree unitarity alone. For this, we need a stronger condition of renormalizability. For a renormalizable theory, it has been shown [11] that the k -th loop amplitude of a scattering involving n particles ($1 + 2 \rightarrow 3 + 4 + \dots + n$) behaves at very high energies as follows:

$$\mathcal{M}^{(n)}|_{E \rightarrow \infty} = \mathcal{O} \left(E^{4-n} \ln^k E \right) . \quad (1.137)$$

Clearly, the tree level amplitude ($k = 0$) of a process $1 + 2 \rightarrow 3 + 4 + 5$ should go as $\mathcal{O}(1/E)$. As an example, consider the process $Z_L Z_L \rightarrow Z_L Z_L h$ which can proceed at the tree level due to the existence of interactions in the form of Eqs. (1.131) and (1.136). The Feynman diagrams stemming from these interactions have been displayed in Figures 1.13a and 1.13b. But the total amplitude from these two types of diagrams behaves at $E \rightarrow \infty$ as a constant independent of

FIGURE 1.14: Feynman diagrams for $Z_L Z_L \rightarrow h h h$.

the CM energy. An explicit calculation leads to the conclusion that the desired cancellation of the unwanted constant term occurs if we put in a self coupling of the form

$$\mathcal{L}_{hhh} = -\frac{gm_h^2}{4M_W} h^3 \quad (1.138)$$

leading to the diagram 1.13c. In this connection it is interesting to note that it is the first time when a non-zero mass (m_h) of the scalar h became explicitly necessary.

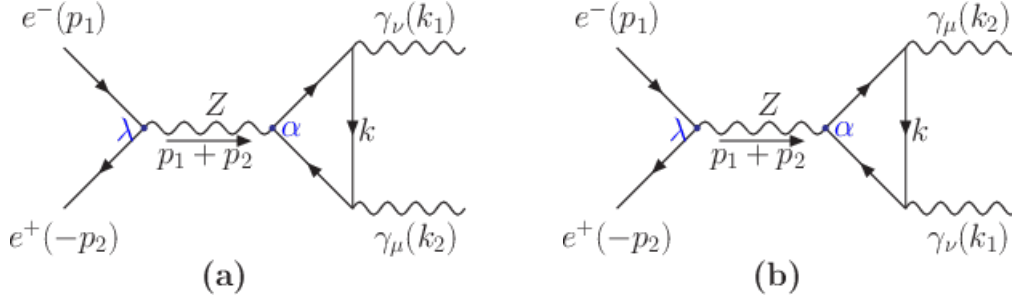
Now let us turn our attention to another five particle scattering, $Z_L Z_L \rightarrow h h h$. Tree level Feynman graphs have been shown in Figure 1.14. Note that, without diagram 1.14f the total amplitude would go as $\mathcal{O}(1)$ instead of $\mathcal{O}(1/E)$ at high energies. The requirement of cancellation of this constant term fixes the quartic coupling involved in diagram 1.14f. The resulting interaction Lagrangian is

$$\mathcal{L}_{hhhh} = -\frac{g^2 m_h^2}{32M_W^2} h^4. \quad (1.139)$$

This was the final piece. We now have the complete but minimal theory that is needed to describe all the electroweak phenomena involving electrons. We have obtained this by a systematic cancellation of energy growths appearing in different scattering amplitude and therefore this theory is “ultraviolet safe”, *i.e.*, valid upto arbitrarily high energies. The different pieces of interactions now can be collected into a master Lagrangian,

$$\begin{aligned} \mathcal{L}_{\text{int}} = & \mathcal{L}_{ee\gamma} + \mathcal{L}_{\text{int}}^W + \mathcal{L}_{eeZ} + \mathcal{L}_{\nu\nu Z} + \mathcal{L}_{VVV} + \mathcal{L}_{VVVV} + \mathcal{L}_{WW h} \\ & + \mathcal{L}_{ZZ h} + \mathcal{L}_{eeh} + \mathcal{L}_{WW hh} + \mathcal{L}_{ZZ hh} + \mathcal{L}_{hhh} + \mathcal{L}_{hhhh}. \end{aligned} \quad (1.140)$$

Amazingly, Eq. (1.140) is what we get from the well known $SU(2) \times U(1)$ gauge theoretic construction of the Standard Model (SM) which has been tested experimentally with fantastic accuracy. Thus, the principle of tree unitarity which started off as an ‘educated guess’ is now

FIGURE 1.15: One-loop diagrams for the process $e^-(p_1) + e^+(p_2) \rightarrow \gamma(k_1) + \gamma(k_2)$.

qualified enough to be declared as a rule which must be obeyed by all the future theories that promise to address the questions left unanswered by the SM. In the upcoming chapters, we will show how several new physics models can be constrained theoretically by employing the prescription of tree unitarity. In passing, we should keep in mind that as in the case of the SM, consideration of tree unitarity does not predict the number of lepton generations. But, given the number of lepton generations, one can show that the number of quark generations cannot be arbitrary. Historically it happened in the reverse order: from the observation of CP violation in kaon decay it was inferred that there must be at least three generations of quarks and three generations of quarks will require three generation of leptons. How this can be done using unitarity is the subject matter of the next section.

1.7 ABJ anomaly and quarks

Some processes are completely innocuous at the tree level but contain bad energy growths at the loop level. For example, consider the process

$$e^-(p_1) + e^+(p_2) \rightarrow \gamma(k_1) + \gamma(k_2).$$

Figure 1.15 shows the one-loop diagrams in which an effect of the Adler-Bell-Jackiw (ABJ) axial anomaly is manifested. Denoting $p_1 + p_2$ by p , the total amplitude of these triangle graphs can be written as

$$\begin{aligned} \mathcal{M}_\Delta = \mathcal{M}_a + \mathcal{M}_b &= i \frac{g^2 a_e Q_e^2 e^2}{\cos^2 \theta_w} \bar{v}(p_2) \gamma_\lambda (v_e - a_e \gamma_5) u(p_1) \\ &\quad \times \frac{-g^{\lambda\alpha} + \frac{p^\lambda p^\alpha}{M_Z^2}}{p^2 - M_Z^2} T_{\alpha\mu\nu}(k_1, k_2) \epsilon^\nu(k_1) \epsilon^\mu(k_2), \end{aligned} \quad (1.141)$$

where,

$$v_e = -\frac{1}{4} + \sin^2 \theta_w, \quad (1.142)$$

$$a_e = -\frac{1}{4}, \quad (1.143)$$

$$T_{\alpha\mu\nu}(k_1, k_2) = \int \frac{d^4k}{(2\pi)^4} \text{Tr} \left(\frac{1}{\not{k} - \not{k}_2 - m_e} \gamma^\mu \frac{1}{\not{k} - m_e} \gamma^\nu \frac{1}{\not{k} + \not{k}_1 - m_e} \gamma^\alpha \gamma^5 \right) + (k_1, \nu) \leftrightarrow (k_2, \mu). \quad (1.144)$$

A simple power counting reveals that $T_{\alpha\mu\nu}(k_1, k_2) \sim \mathcal{O}(E)$ as $E \rightarrow \infty$. Consequently \mathcal{M}_Δ should go as $\mathcal{O}(E^2)$ due to the presence of the $p^\lambda p^\alpha$ term in the Z propagator. But multiplying p^λ with γ_λ in the first neutral current vertex and using Dirac equation the electron mass (m_e) can be factored out. This compensates one factor of energy growth *i.e.*, \mathcal{M}_Δ now grows linearly with energy.

Let us now investigate whether another factor of electron mass can be factorized or not. Rigorous calculation shows

$$p^\alpha T_{\alpha\mu\nu}(k_1, k_2) = 2m_e T_{\mu\nu}(k_1, k_2) + \frac{1}{2\pi^2} \epsilon_{\mu\nu\rho\sigma} k_2^\rho k_1^\sigma, \quad (1.145)$$

where $T_{\mu\nu}$ is given by Eq. (1.144) with $\gamma_\alpha \gamma_5$ replaced by γ_5 . The second term in Eq. (1.145) is just the celebrated ABJ axial anomaly. Since the fermion mass does not get factored out in this anomalous term, there remains an uncompensated factor of energy growth and therefore \mathcal{M}_Δ continues to grow as $\mathcal{O}(E)$. It should be noted that the coefficient of the linearly growing term depends solely on the properties of the fermion which occurs in the loop. For a general fermion this coefficient can be calculated to be

$$C_{\text{anomaly}}^{(f)} = a_f Q_f^2, \quad (1.146)$$

where a_f is the axial vector coupling and Q_f is the electric charge of the fermion in units of the electronic charge. It is clear that adding more and more *electron-like* fermions will only worsen things because they will go on adding to the coefficient. A neutrino loop, of course, does not contribute. Therefore, we need some *other* kinds of fermions to cancel this. But first we note that the contribution to C_{anomaly} due to a single lepton generation is

$$C_{\text{anomaly}}^{(\ell)} = -\frac{1}{4}. \quad (1.147)$$

Now, if we assume that the quarks, with similar axial vector couplings as the leptons, are the possible candidates to cancel the anomaly then we can determine the number of colors of the quarks. Suppose, a single generation of quarks contains an up-type and a down-type quark with $Q_u = +2/3$, $a_u = 1/4$ and $Q_d = -1/3$, $a_d = -1/4$ respectively. If this generation has N_c replicas, then

$$C_{\text{anomaly}}^{(q)} = \frac{N_c}{4} (Q_u^2 - Q_d^2). \quad (1.148)$$

The condition for the anomaly cancellation then requires $N_c = 3$, *i.e.*, each quark generation should come with three varieties which, with hindsight, we can connect with the *color* quantum number. Using similar unitarity arguments in association with simple phenomenology, it is also possible to obtain the couplings and spectrum for the quarks [3].

It is a capital mistake to theorize before one has data. Insensibly one begins to twist facts to suit theories, instead of theories to suit facts.

Sherlock Holmes in "A Scandal In Bohemia"

2

Modified Higgs couplings and unitarity violation

One of the crucial arguments for the existence of the Higgs boson in the Standard Model (SM) is that, without it, the longitudinal vector boson (V_L , where $V = W, Z$) scattering amplitudes at the tree level would uncontrollably grow with the center of mass energy (E). This will result in the violation of ‘unitarity’, thus implying breakdown of quantum mechanical sense of probability conservation in scattering amplitudes. In the SM, the Higgs boson possesses appropriate gauge couplings to ensure exact cancellation of the residual E^2 growth in the $V_L V_L \rightarrow V_L V_L$ scattering amplitude that survives after adding the gauge boson contributions. It has been explicitly shown in [12] how, for $E \gg M_V$, the E^2 dependence is traded in favor of the unknown m_h^2 , where m_h is the Higgs boson mass. From this it was concluded that m_h should be less than about a TeV for unitarity not to be violated. An intimate relationship between unitarity and renormalizability adds a special relevance to this issue. For a renormalizable theory the tree level amplitude for $2 \rightarrow 2$ scattering should not contain any term which grows with energy [11]. In perturbative expansion of scattering amplitudes these energy growths must be canceled order by order [5]. It has been shown that the energy dependent terms in tree level amplitudes get exactly canceled if the couplings satisfy certain sets of ‘unitarity sum rules’ [13]. It has also been realized that the presence of the Higgs boson is not the only option to satisfy these sum rules [14, 15].

Meanwhile, a Higgs-like particle has been observed with a mass of around 125 GeV by the ATLAS and CMS collaborations of the LHC [16, 17]. This is much below the upper limit coming from unitarity violation mentioned above. If this particle indeed turns out to be the SM Higgs,

then the scattering amplitudes involving not only the longitudinal vector bosons but any other SM particles as external states would be well behaved for arbitrarily high energies. However, the recent observation of some excess events in the $h \rightarrow \gamma\gamma$ channel¹, as well as large errors associated with other decay channels, has fuelled speculation that Higgs couplings to fermions and/or gauge bosons might not be exactly as predicted by the SM [19]. There are more than one ways to modify the Higgs couplings. One way is to hypothesize that the WWh and the ZZh couplings are modified; more specifically, enhanced with respect to their SM values. This would result not only in an increase in the Higgs production cross section via vector boson fusion and associated production, but also in an enhancement of the W -loop contribution to $h \rightarrow \gamma\gamma$ decay. But this would at the same time lead to excess events in the $h \rightarrow WW^*$ and $h \rightarrow ZZ^*$ channels, something which is not obvious from data. It would also result in the violation of unitarity in longitudinal gauge boson scattering channels. This was indeed explored long back [20], however, in the absence of the LHC data there was no motivation to study the correlation between unitarity violation and the Higgs decay branching ratios at that time. If we refrain from adding any extra particle to the SM and yet attempt to account for the excess in the diphoton channel, the next natural choice would be to modify the Yukawa coupling of the top quark. As is already known, if we put the sign of the top Yukawa coupling opposite to what it is in the SM, the $h \rightarrow \gamma\gamma$ rate gets enhanced due to a constructive interference between the W -loop diagram and the top-loop diagram [19]. One of the fall-outs of this sign flip is that $t\bar{t} \rightarrow V_L V_L$ scattering no longer remains unitary. In fact, as we shall show, any non-trivial admixture of CP-even and CP-odd states in the composition of the scalar particle jeopardizes the good high energy behavior of the $t\bar{t} \rightarrow V_L V_L$ amplitude even if we keep the moduli of the top Yukawa coupling and the Higgs gauge coupling to their SM values. The purpose of this chapter is to explicitly demonstrate how the scales of unitarity violation in $W_L W_L \rightarrow W_L W_L$ and $t\bar{t} \rightarrow W_L W_L$ scattering processes depend on the modification parameters of the gauge and the top Yukawa couplings of the Higgs. We demonstrate what an enhanced diphoton rate may imply in this context.

2.1 Modification of the Higgs couplings

In our analysis, we modify only the top Yukawa coupling, since the other Yukawa couplings are numerically much less relevant. We take

$$g_{tth} = (1 - f)(\cos \delta - i \sin \delta \gamma_5) g_{tth}^{\text{SM}} = (1 - f) e^{-i\delta \gamma_5} g_{tth}^{\text{SM}}. \quad (2.1a)$$

¹This chapter is based on our paper [18] which was written in view of the excess events observed at that time in the $h \rightarrow \gamma\gamma$ channel. Now, after an upgraded analysis of the data both by CMS and ATLAS, the excess seems to have gone away.

The parameter f is a measure of the overall coupling of the Higgs boson to the top quark, whereas δ is a parameter that quantifies the mixture of CP-even and CP-odd components in the Higgs boson. We also modify the gauge couplings of the Higgs boson as

$$g_{VVh} = (1 - x)g_{VVh}^{\text{SM}}, \quad (2.1b)$$

where V can be W or Z , as said before. We maintain equality between the WWh and ZZh couplings to respect custodial symmetry. The parameters x , f and δ are all real, and they all vanish in the SM.

We now comment on the existing experimental constraints on these modification parameters. First, it has been shown in [21] that precision electroweak measurements imply $-0.2 \leq x \leq 0.1$ at 95% C.L. for $m_h = 125$ GeV and $m_t = 173$ GeV, while from the recent LHC Higgs data analysis the 95% C.L. range has been estimated to be $-0.4 \leq x \leq 0.4$ [22, 23]. Second, the allowed range of f can be extracted from recent fits of modified Higgs couplings against the LHC data. For example, for $x = 0$, the range is $-0.1 < f < 0.6$ for values of δ fixed at 0 and π [23, 24]. Note that similar bounds have been obtained by the authors of Ref. [25], who considered a phase in the effective coupling due to an absorptive part in the amplitude. In this chapter, we take a more conservative approach and consider a hermitian Yukawa Lagrangian.

2.2 Impact on high energy unitarity

With the modifications prescribed in Eq. (2.1), one should examine unitarity constraints on scattering processes involving the top quark and the W -boson. Note that we will talk about the longitudinally polarized component of the W -boson only, dropping the polarization subscript L which is implicitly assumed. We have looked at the energy dependence of the elastic scattering $WW \rightarrow WW$ and the inelastic scattering $t\bar{t} \rightarrow WW$. The scattering amplitudes that we find are as follows (see Appendices A and B for details):

$$\mathcal{A}^{WW \rightarrow WW} = 2\sqrt{2}G_F E^2(2x - x^2)(1 + \cos\theta) + \dots, \quad (2.2a)$$

$$\mathcal{A}^{t\bar{t} \rightarrow WW} = 2\sqrt{2}G_F E m_t Y(x, f, \delta) + \dots, \quad (2.2b)$$

where the dots indicate sub-leading terms in energy which do not concern us, θ is the scattering angle, and

$$Y(x, f, \delta) = \mp \left[1 - (1 - x)(1 - f)e^{\mp i\delta} \right], \quad (2.3)$$

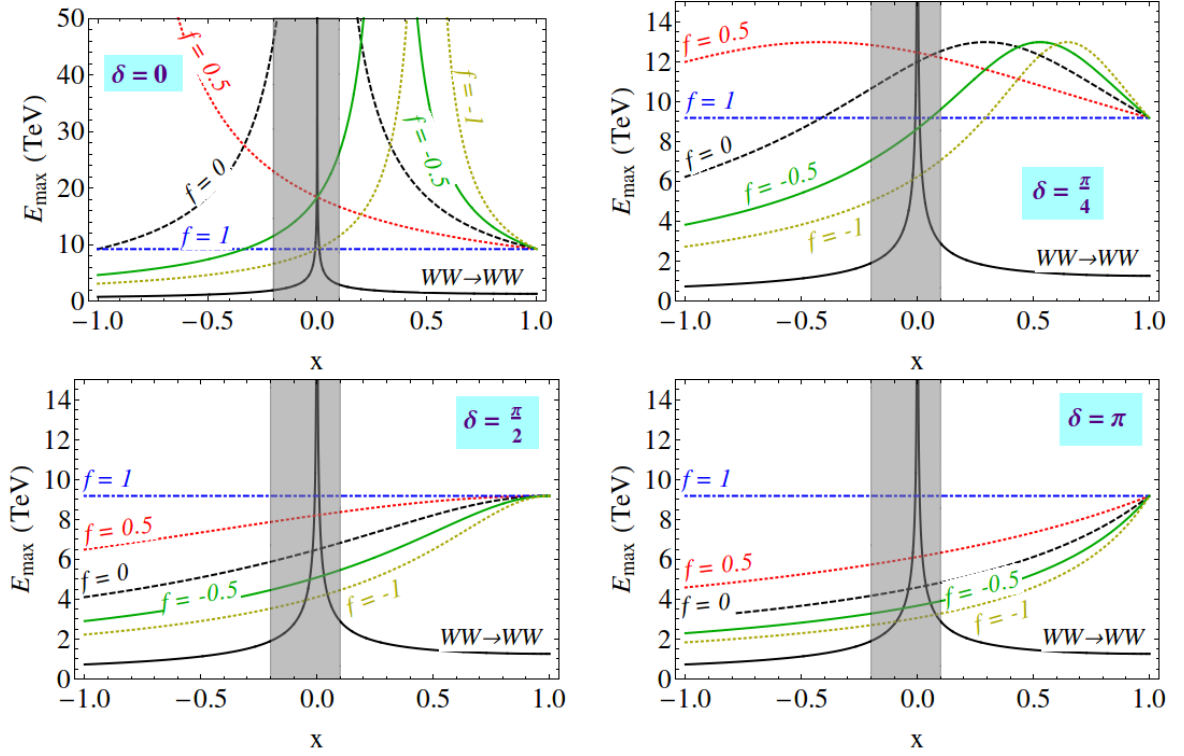


FIGURE 2.1: Unitarity violation scale as a function of x , for specific values of f and δ . For each panel, the scale coming from the elastic $WW \rightarrow WW$ scattering has been marked. The other lines come from $t\bar{t} \rightarrow WW$ scattering for various values of f . The vertical shaded region represents the range of x consistent with electroweak precision data. Note the different scale on the vertical axis for the plot with $\delta = 0$.

where different signs correspond to different combinations of helicities [26]. The scattering amplitude can be expanded in terms of partial waves [12]:

$$\mathcal{A}(\theta) = 16\pi \sum_{l=0}^{\infty} (2l+1) a_l P_l(\cos \theta). \quad (2.4)$$

The unitarity condition $|a_0| \leq 1$ puts upper limits on the center of mass energy in each of these processes. These limits are as follows:

$$E \leq E_{\max}^{WW} = \left(\frac{4\sqrt{2}\pi}{G_F} \frac{1}{|2x - x^2|} \right)^{\frac{1}{2}} \quad [\text{from } WW \rightarrow WW]; \quad (2.5a)$$

$$E \leq E_{\max}^{t\bar{t}} = \frac{4\sqrt{2}\pi}{G_F m_t} \frac{1}{|Y(x, f, \delta)|} \quad [\text{from } t\bar{t} \rightarrow WW]. \quad (2.5b)$$

Because only $\cos \delta$ appears in $|Y|$, we can take δ in the range $[0, \pi]$. Without any loss of generality, we can take $1 - f \geq 0$ to cover the entire parameter space. In passing, let us add that the constraints from $t\bar{t} \rightarrow ZZ$ is the same in the leading order in E as that given in Eq. (2.5b).

We now discuss the numerical dependence of the unitarity violation scale on the nonstandard

parameters expressed through our master equations given in Eq. (2.5). Our results are displayed in Fig. 2.1. The different panels correspond to different choices of δ , as indicated in the figure. For the $WW \rightarrow WW$ scattering amplitude which grows as E^2 , there is contribution coming from Higgs mediated diagram and therefore it depends on x , but there is no dependence on f and δ since the top-Higgs coupling is not involved. The latter coupling is of course relevant for the $t\bar{t} \rightarrow WW$ scattering, and the Higgs mediated graph is sensitive to all the three nonstandard parameters, i.e. x , f and δ . In all the panels the lines titled $WW \rightarrow WW$, obtained by plotting Eq. (2.5a), show the scale of unitarity violation as the WW_h coupling departs from its SM value. The other lines mark the unitarity violation scale arising from $t\bar{t} \rightarrow WW$, and are obtained from Eq. (2.5b). In the limit $x = 1$, i.e. when the Higgs either does not exist or does not couple to W , unitarity is violated at a pretty low scale, $E_{\max}^{WW} \approx 1.3$ TeV. As x approaches zero, E_{\max}^{WW} goes up. On the other hand, the limit $f = 1$ implies that the Higgs does not couple to the top quark, so in this limit the Higgs mediated graph for $t\bar{t} \rightarrow WW$ would not exist, and hence, the unitarity violation scale arising from the above scattering would be independent of x and δ . Similar things happen in the limit $x = 1$, causing the unitarity violation scale from $t\bar{t} \rightarrow WW$ to be independent of f and δ . This is precisely the reason as to why the horizontal $f = 1$ line in all the panels meet the curvy lines for other values of f at one single point which is at $x = 1$ corresponding to $E_{\max}^{tt} \approx 9$ TeV.

An important observation at this stage is the following: for $\delta \neq 0$ and $\delta \neq \pi$, the process $t\bar{t} \rightarrow WW$ is not unitary regardless of the choice of x and f . The vertical shades in the four panels restrict the values of x within the zone allowed by precision tests. One thing is quite clear that if x happens to take a value near the edge of the shade in any panel, the unitarity violation would set in for $WW \rightarrow WW$ at a scale much lower than where it would happen for $t\bar{t} \rightarrow WW$, which is easily understood from the E^2 versus E growth in the two amplitudes. But if x settles at a much smaller value, as one can see from the different panels, the unitarity violation scales from these two amplitudes get closer and at some point the hierarchy mentioned earlier is reversed.

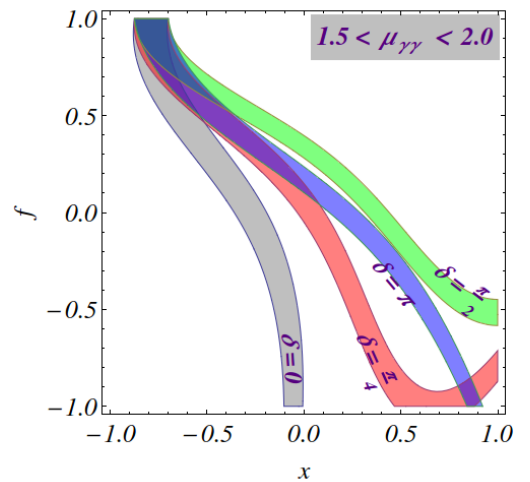


FIGURE 2.2: Allowed regions in the x - f plane that correspond to the diphoton enhancement ratio $\mu_{\gamma\gamma}$ lying between 1.5 and 2, for different values of δ .

2.3 Impact on diphoton signal strength

We now consider the decay of the 125 GeV particle into two photons. Two-photon final states have a definite CP property, more specifically, a definite parity. As a result, if the initial spin-zero state is not an eigenstate of parity, the parity-even and parity-odd components will contribute incoherently, *i.e.*, their loop contributions can be added together separately in the amplitude squared level.

The decay $h \rightarrow \gamma\gamma$ proceeds dominantly through a W boson loop and a top loop diagram. For a CP-mixed h whose couplings are given by Eqs. (2.1b) and (2.1a), the decay width is given by [27]:

$$\Gamma(h \rightarrow \gamma\gamma) = \frac{\alpha^2 g^2}{2^{10} \pi^3} \frac{m_h^3}{M_W^2} \left[\left| (1-x)F_W + \frac{4}{3}(1-f)\cos\delta F_t \right|^2 + \left| \frac{4}{3}(1-f)\sin\delta P_t \right|^2 \right], \quad (2.6)$$

where, the values of F_W , F_t and P_t are given by

$$F_W = 2 + 3\tau_W + 3\tau_W(2 - \tau_W)f(\tau_W), \quad (2.7a)$$

$$F_t = -2\tau_t [1 + (1 - \tau_t)f(\tau_t)], \quad (2.7b)$$

$$P_t = 2\tau_t f(\tau_t), \quad (2.7c)$$

$$\text{with } \tau_x \equiv (2m_x/m_h)^2. \quad (2.7d)$$

In the above equations, F_t and P_t represent the top-loop contributions from the scalar and pseudoscalar parts respectively. For $m_h \approx 125$ GeV, $\tau_x > 1$ for both $x = W, t$. In this situation,

$$f(\tau) = \left[\sin^{-1} \left(\sqrt{1/\tau} \right) \right]^2. \quad (2.8)$$

The SM expression for the Higgs to diphoton decay width is obtained by putting $x, f, \delta = 0$ in Eq. (2.6). In view of this, the modification factor for the partial decay width can be expressed as:

$$R_{\gamma\gamma} = \frac{\Gamma(h \rightarrow \gamma\gamma)}{\Gamma^{\text{SM}}(h \rightarrow \gamma\gamma)} = \frac{|(1-x)F_W + \frac{4}{3}(1-f)\cos\delta F_t|^2 + |\frac{4}{3}(1-f)\sin\delta P_t|^2}{|F_W + \frac{4}{3}F_t|^2}. \quad (2.9)$$

It should also be noted that due to the modification of the tth Yukawa coupling, the ggh effective vertex will also be modified. Denoting the modification factor for $h \rightarrow gg$ decay width by \mathcal{G} , one can easily find

$$\mathcal{G} = \frac{\Gamma^{\text{SM}}(h \rightarrow gg)}{\Gamma(h \rightarrow gg)} = (1-f)^2 \frac{|\cos\delta F_t|^2 + |\sin\delta P_t|^2}{|F_t|^2}. \quad (2.10)$$

We should also remember that the same factor, \mathcal{G} , also controls the modification of the production cross-section through the $gg \rightarrow h$ channel.

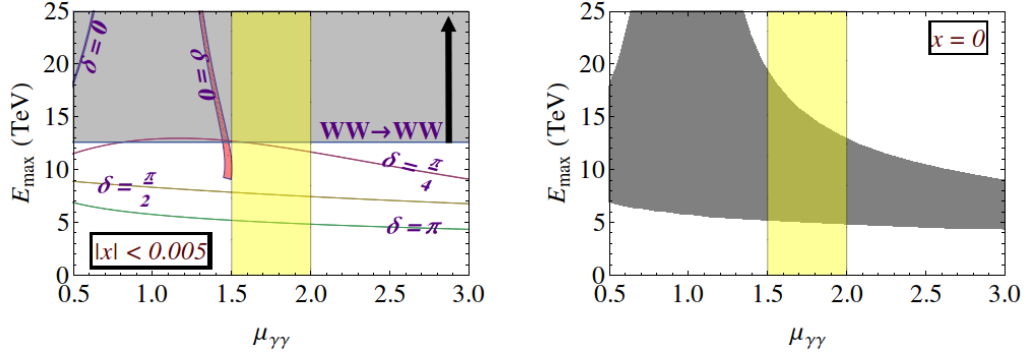


FIGURE 2.3: Unitarity violation scale plotted against diphoton enhancement. The vertical shaded region (in yellow) corresponds to $1.5 < \mu_{\gamma\gamma} < 2.0$. In the left panel we vary x in a very narrow range: $[-0.005, +0.005]$. In the right panel, we set $x = 0$ so that WW scattering remain always unitary and vary f and δ within $[-1, +1]$ and $[0, \pi]$ respectively to see the correlation between E_{\max} for $t\bar{t} \rightarrow WW$ and $\mu_{\gamma\gamma}$.

We now estimate how the Higgs production cross section would be modified. For 7(8)-TeV LHC, the top loop driven gluon-gluon fusion channel contributes around 85% of the total cross section, while the associated production and the vector boson fusion together almost account for the remaining 15% [27]. The production cross section would then be modified roughly by the factor

$$\frac{\sigma(pp \rightarrow h)}{\sigma^{\text{SM}}(pp \rightarrow h)} = \frac{\mathcal{G} \cdot \sigma_G + (1-x)^2 \sigma_V}{\sigma_G + \sigma_V} \approx \mathcal{G} \cdot 85\% + (1-x)^2 15\%. \quad (2.11)$$

As far as the different decay channels of the Higgs are concerned, for $m_h \approx 125$ GeV, branching ratios of the SM Higgs boson are roughly as follows: 58% to $b\bar{b}$, 7% to $\tau^+\tau^-$, 3% to $c\bar{c}$, 24% to VV^* and 8% to gg [27]. We then express the modification of the total decay width by the ratio:

$$\frac{\Gamma_h}{\Gamma_h^{\text{SM}}} = (58\% + 7\% + 3\%) + (1-x)^2 24\% + \mathcal{G} \cdot 8\%. \quad (2.12)$$

The above expressions lead us to define

$$\mu_{\gamma\gamma} = \frac{\sigma(pp \rightarrow h)}{\sigma^{\text{SM}}(pp \rightarrow h)} \times \frac{\Gamma(h \rightarrow \gamma\gamma)}{\Gamma^{\text{SM}}(h \rightarrow \gamma\gamma)} \times \frac{\Gamma_h^{\text{SM}}}{\Gamma_h}. \quad (2.13)$$

In Fig. 2.2 we have shaded different regions in the x - f plane, for different choices of δ , which can account for the apparent excess of the diphoton events. Motivated by the recent LHC data, we choose $\mu_{\gamma\gamma}$ in the range 1.5 to 2 for the sake of illustration. For $x \approx 0$ and $\delta = \pi$, we observe that

$$0.1 < f < 0.25 \quad (2.14)$$

which is roughly consistent with the limit quoted earlier in connection with global fits. Thus a *top-phobic Higgs*, which corresponds to $f \rightarrow 1$, is highly unlikely. We must admit though that

this comparison is not entirely fair as we have modified only the top Yukawa coupling, while in the global fits all the Yukawa couplings were modified. We also admit that for the simplicity of illustration we have not taken into account the efficiency factors in the estimation of $\mu_{\gamma\gamma}$.

2.4 Correlation between E_{\max} and $\mu_{\gamma\gamma}$

In the left panel of Fig. 2.3, we have exhibited the correlation between the unitarity violation scale and the diphoton enhancement ratio $\mu_{\gamma\gamma}$. For drawing this plot, we have varied f between -1 and $+1$. Keeping in mind the relative sensitivity of the two scattering processes, we restrict x in a rather narrow range: $-0.005 < x < 0.005$ in the left panel. The lower horizontal boundary of the (gray) shaded region around $E_{\max} = 13$ TeV, appropriately labeled, corresponds to the unitarity violation scale in $WW \rightarrow WW$ scattering with $|x| = 0.005$. For smaller values of x , this line will appear at higher energy. The other curvy lines come from $t\bar{t} \rightarrow WW$ and they correspond to four different choices of δ , viz., 0 , $\pi/4$, $\pi/2$ and π . The thickness of these lines for different values of δ come from the range of x just mentioned. For $\delta = 0$, it is hard to achieve a value of $\mu_{\gamma\gamma}$ as large as 1.5. For $\delta = \pi$, it is possible to obtain a value of $\mu_{\gamma\gamma}$ in the range 1.5 to 2, as can be seen by the corresponding line going through the vertical shade. The corresponding range of f , which can be read from Fig. 2.2, has been mentioned in Eq. (2.14). It is worth noting from this figure that for $\delta = \pi$, which facilitates diphoton rate enhancement, the unitarity violation scale comes down to around 5 TeV. This is true even when $x = 0$, i.e., when the gauge coupling of the Higgs boson matches the SM value and therefore the $WW \rightarrow WW$ scattering is perfectly unitary. For visual clarification, we have set $x = 0$ in the right panel of Fig. 2.3 so that WW -scattering remains unitary up to arbitrary high energies. Here we can see (from the overlap between vertical yellow band and gray shaded region) that if the value of $\mu_{\gamma\gamma}$ eventually settles somewhere within 1.5 to 2, then high scale unitarity of the process $t\bar{t} \rightarrow WW$ is bound to be violated somewhere between 5 and 19 TeV.

2.5 Conclusions

To summarize, even though the existence of a Higgs-like particle has been announced, precise measurements of its couplings to gauge bosons and fermions would take quite a while. If the measured couplings eventually match their SM values, the theory is unitary, i.e. well-behaved up to arbitrarily high energies. Otherwise, the extent of departure of the measured values of the couplings from their SM predictions would mark the scale where unknown dynamics would set in (see e.g. [28]). We have carried out a quantitative study of this scale as a function of the deviation of the Higgs couplings from their SM values through studies of the $WW \rightarrow WW$ and $t\bar{t} \rightarrow WW$ scattering processes. We have specifically focused on nonstandard effects on the

gauge coupling of the Higgs and the top Yukawa coupling, as these two couplings play a crucial rôle in the stability of the electroweak vacuum and the perturbative unitarity of the theory. If future measurements favor Higgs couplings closer to its SM values, the expected scale of unitarity saturation would go up.

‘That’s a rather broad idea’, I remarked.

‘One’s ideas must be as broad as Nature if they are to interpret Nature’, he answered.

Watson and Holmes in “A study in scarlet”

3

Post Higgs overview of two Higgs-doublet models

The discovery of a new boson in July of 2012 at the LHC [16, 17] is undoubtedly the greatest achievement of this decade in the field of Particle Physics. This might be the final missing piece of the SM. But at the same time, SM does not account for observations like neutrino oscillations, dark matter. Phenomena like these constitute the primary motivation to look for other avenues beyond the SM (BSM). The SM relies on the minimal choice of a single $SU(2)$ scalar doublet giving masses to all the massive particles contained in the SM. Extension of the SM scalar sector is a common practice in constructing BSM models. While extending the scalar sector, one runs into the risk of altering the tree level value of the electroweak ρ -parameter. If we construct an $SU(2) \times U(1)$ gauge theory with n scalar multiplets, then the general expression for the tree level ρ -parameter reads

$$\rho^{\text{tree}} = \frac{\sum_{i=1}^n \left\{ T_i(T_i + 1) - \frac{Y_i^2}{4} \right\} v_i}{\frac{1}{2} \sum_{i=1}^n Y_i^2 v_i}, \quad (3.1)$$

where, T_i and Y_i denote the weak isospin and hypercharge of the i -th scalar multiplet respectively and v_i refers to the vacuum expectation value (vev) picked up by the neutral component of the i -th multiplet. One can easily verify that if the scalar sector contains only $SU(2)$ singlets ($T_i = 0$) and doublets ($T_i = 1/2$) with hypercharges 0 and ± 1 respectively, the $\rho^{\text{tree}} = 1$ is automatically recovered without requiring any fine tuning among the vevs. In this article we restrict ourselves to

the doublet extensions only. This simplest extension of this type is the case of two Higgs-doublet model (2HDM) [29] which receives a lot of attention because minimal supersymmetry relies on it. In a general 2HDM both the doublets can couple to each type of fermions. Consequently, there will be two Yukawa matrices which, in general, are not diagonalizable simultaneously. This will introduce new flavor changing neutral current (FCNC) couplings mediated by neutral Higgses. It was shown by Glashow and Weinberg [30] and independently by Paschos [31] that Higgs mediated FCNC can be avoided altogether if fermions of a particular charge get their masses from a single scalar doublet. This prescription was realized by employing a Z_2 symmetry under which one of the doublet is odd. Then there are four different possibilities for assigning Z_2 parities to the fermions so that Glashow-Weinberg-Paschos theorem is satisfied. This leads to the following four types of 2HDMs:

- Type I: all quarks and leptons couple to only one scalar doublet Φ_2 ;
- Type II: Φ_2 couples to up-type quarks, while Φ_1 couples to down-type quarks and charged leptons (minimal supersymmetry conforms to this category);
- Type X or lepton specific: Φ_2 couples to all quarks, while Φ_1 couples to all leptons;
- Type Y or flipped: Φ_2 couples to up-type quarks and leptons, while Φ_1 couples to down-type quarks.

There is also the option for preventing tree level FCNC by assuming the two Yukawa matrices proportional to each other. This gives rise to the so called aligned 2HDM. However Branco, Grimus and Lavoura (BGL) employed a global $U(1)$ symmetry which textures both Yukawa matrices in a certain way [32]. As a result of this the tree level Higgs FCNC couplings get related to the off diagonal elements of the CKM matrix and thereby are naturally suppressed. In this chapter, I intend to highlight some major phenomenological aspects of these different types of 2HDMs with special emphasis on the BGL models. We will also discuss how the recent LHC Higgs data constrain these models.

3.1 The scalar potential

There are two equivalent notations that are used in the literature to write the 2HDM scalar potential invariant under a Z_2 symmetry ($\Phi_2 \rightarrow -\Phi_2$) :

■ Notation 1

$$V(\Phi_1, \Phi_2) = m_{11}^2 \Phi_1^\dagger \Phi_1 + m_{22}^2 \Phi_2^\dagger \Phi_2 - \left(m_{12}^2 \Phi_1^\dagger \Phi_2 + \text{h.c.} \right) + \frac{\beta_1}{2} \left(\Phi_1^\dagger \Phi_1 \right)^2 + \frac{\beta_2}{2} \left(\Phi_2^\dagger \Phi_2 \right)^2$$

$$+\beta_3 \left(\Phi_1^\dagger \Phi_1 \right) \left(\Phi_2^\dagger \Phi_2 \right) + \beta_4 \left(\Phi_1^\dagger \Phi_2 \right) \left(\Phi_2^\dagger \Phi_1 \right) + \left\{ \frac{\beta_5}{2} \left(\Phi_1^\dagger \Phi_2 \right)^2 + \text{h.c.} \right\} \quad (3.2)$$

■ **Notation 2**

$$\begin{aligned} V = & \lambda_1 \left(\Phi_1^\dagger \Phi_1 - \frac{v_1^2}{2} \right)^2 + \lambda_2 \left(\Phi_2^\dagger \Phi_2 - \frac{v_2^2}{2} \right)^2 + \lambda_3 \left(\Phi_1^\dagger \Phi_1 + \Phi_2^\dagger \Phi_2 - \frac{v_1^2 + v_2^2}{2} \right)^2 \\ & + \lambda_4 \left((\Phi_1^\dagger \Phi_1)(\Phi_2^\dagger \Phi_2) - (\Phi_1^\dagger \Phi_2)(\Phi_2^\dagger \Phi_1) \right) + \lambda_5 \left(\text{Re } \Phi_1^\dagger \Phi_2 - \frac{v_1 v_2}{2} \right)^2 + \lambda_6 \left(\text{Im } \Phi_1^\dagger \Phi_2 \right)^2 \end{aligned} \quad (3.3)$$

The bilinear terms proportional to m_{12}^2 in Eq. (3.2) and λ_5 in Eq. (3.3) break the Z_2 symmetry softly. The significance of these types of soft breaking term will be discussed later. We assume all the potential parameters to be real so that CP symmetry is conserved in the scalar sector. Note that, when we minimize the potential of Eq. (3.2), the two minimization conditions can be used to trade m_{11}^2 and m_{22}^2 for v_1 and v_2 and the potential can be cast in the form of Eq. (3.3). Note that, unlike Eq. (3.2), Eq. (3.3) implicitly assumes that the Z_2 symmetry is also broken spontaneously, *i.e.*, both the doublets receive vevs. In this chapter, we shall only consider 2HDMs where the value of $\tan \beta$ ($\equiv v_2/v_1$) is nonzero and finite. The connections between the parameters of Eq. (3.2) and Eq. (3.3) are given below:

$$\begin{aligned} m_{11}^2 &= -(\lambda_1 v_1^2 + \lambda_3 v^2) ; m_{22}^2 = -(\lambda_2 v_2^2 + \lambda_3 v^2) ; m_{12}^2 = \frac{\lambda_5}{2} v_1 v_2 ; \beta_1 = 2(\lambda_1 + \lambda_3) ; \\ \beta_2 &= 2(\lambda_2 + \lambda_3) ; \beta_3 = 2\lambda_3 + \lambda_4 ; \beta_4 = \frac{\lambda_5 + \lambda_6}{2} - \lambda_4 ; \beta_5 = \frac{\lambda_5 - \lambda_6}{2} . \end{aligned} \quad (3.4)$$

In Eq. (3.4) $v = \sqrt{v_1^2 + v_2^2} = 246$ GeV, where v_1 and v_2 are the vevs of the two doublets Φ_1 and Φ_2 respectively. We also remember that it is the combination $m_{12}^2/(\sin \beta \cos \beta)$, not m_{12}^2 itself, which controls the nonstandard masses [33]. In view of these facts, λ_5 , rather than m_{12}^2 , constitutes a convenient parameter that can track down the effect of soft breaking. Therefore, for most part of this chapter, we choose to work with the notation of Eq. (3.3).

Before we move on, it should be reemphasized that the parametrization of Eq. (3.3) is less general than that of Eq. (3.2). Any connection between the two sets of parameters can be established only when both the scalars receive vevs. The inert doublet scenario can be very easily realized in the parametrization of Eq. (3.2), while just setting $v_2 = 0$ in the parametrization of Eq. (3.3) does not lead us to the same limit. To appreciate this salient aspect, we consider a simpler scenario when we have only one Higgs doublet. Then the potential can be written in two equivalent ways: $V \sim \mu^2 |\phi|^2 + \lambda |\phi|^4$, and $V' \sim \lambda (|\phi|^2 - v^2/2)^2$. They become truly equivalent when $\mu^2 < 0$, and consequently, the scalar receives a vev. But when $\mu^2 > 0$, the scalar remains inert. In that case, putting $v = 0$ in V' does not take us to the physical situation given by V , as the latter still contains, in addition to λ , an independent dimensionful parameter μ^2 . Our Eqs. (3.3) and (3.2) are 2HDM generalizations of V' and V , respectively.

3.1.1 Physical eigenstates

Expressing the scalar doublets as

$$\Phi_i = \frac{1}{\sqrt{2}} \begin{pmatrix} \sqrt{2}w_i^+ \\ (h_i + v_i) + iz_i \end{pmatrix}, \quad (3.5)$$

we will be able to construct the mass matrices using Eq. (3.3). Since we have assumed all the potential parameters to be real, there will be no bilinear mixing term of the form $h_i z_j$. As a result, the neutral mass eigenstates will also be the eigenstates of CP. For the charged sector we get the following mass matrix :

$$V_{\text{mass}}^{\text{charged}} = \begin{pmatrix} w_1^+ & w_2^+ \end{pmatrix} M_C^2 \begin{pmatrix} w_1^- \\ w_2^- \end{pmatrix} \quad \text{with, } M_C^2 = \frac{\lambda_4}{2} \begin{pmatrix} v_2^2 & -v_1 v_2 \\ -v_1 v_2 & v_1^2 \end{pmatrix}. \quad (3.6)$$

M_C^2 can be diagonalized to obtain a physical charged Higgs pair (H_1^\pm) and a pair of charged Goldstones as follows :

$$\begin{pmatrix} \omega^\pm \\ H_1^\pm \end{pmatrix} = \begin{pmatrix} \cos \beta & \sin \beta \\ -\sin \beta & \cos \beta \end{pmatrix} \begin{pmatrix} w_1^\pm \\ w_2^\pm \end{pmatrix}, \quad (3.7)$$

where, the rotation angle, β , is defined through the relation $\tan \beta = v_2/v_1$. The mass of the charged Higgs pair (H_1^\pm) is found to be

$$m_{1+}^2 = \frac{\lambda_4}{2} v^2. \quad (3.8)$$

Similarly for the pseudoscalar part one can easily find

$$V_{\text{mass}}^{\text{CP odd}} = \begin{pmatrix} z_1 & z_2 \end{pmatrix} \frac{1}{2} M_P^2 \begin{pmatrix} z_1 \\ z_2 \end{pmatrix} \quad \text{with, } M_P^2 = \frac{\lambda_6}{2} \begin{pmatrix} v_2^2 & -v_1 v_2 \\ -v_1 v_2 & v_1^2 \end{pmatrix}. \quad (3.9)$$

The diagonalization is similar to that in the charged sector. Here we shall get a physical pseudoscalar (A) and a neutral Goldstone (ζ) as follows :

$$\begin{pmatrix} \zeta \\ A \end{pmatrix} = \begin{pmatrix} \cos \beta & \sin \beta \\ -\sin \beta & \cos \beta \end{pmatrix} \begin{pmatrix} z_1 \\ z_2 \end{pmatrix}. \quad (3.10)$$

The mass of the pseudoscalar is given by

$$m_A^2 = \frac{\lambda_6}{2} v^2. \quad (3.11)$$

For the scalar part we find

$$V_{\text{mass}}^{\text{CP even}} = \begin{pmatrix} h_1 & h_2 \end{pmatrix} \frac{1}{2} M_S^2 \begin{pmatrix} h_1 \\ h_2 \end{pmatrix} \quad \text{with, } M_S^2 = \begin{pmatrix} A_S & B_S \\ B_S & C_S \end{pmatrix}, \quad (3.12a)$$

$$\text{where, } A_S = 2(\lambda_1 + \lambda_3)v_1^2 + \frac{\lambda_5}{2}v_2^2, \quad (3.12b)$$

$$B_S = 2\left(\lambda_3 + \frac{\lambda_5}{4}\right)v_1v_2, \quad (3.12c)$$

$$C_S = 2(\lambda_2 + \lambda_3)v_2^2 + \frac{\lambda_5}{2}v_1^2. \quad (3.12d)$$

The masses of the physical eigenstates, H and h , can be readily found as

$$m_H^2 = \frac{1}{2} \left[(A_S + C_S) + \sqrt{(A_S - C_S)^2 + B_S^2} \right], \quad (3.13a)$$

$$m_h^2 = \frac{1}{2} \left[(A_S + C_S) - \sqrt{(A_S - C_S)^2 + B_S^2} \right]. \quad (3.13b)$$

The physical scalars are obtained by rotating the original basis by an angle α :

$$\begin{pmatrix} H \\ h \end{pmatrix} = \begin{pmatrix} \cos \alpha & \sin \alpha \\ -\sin \alpha & \cos \alpha \end{pmatrix} \begin{pmatrix} h_1 \\ h_2 \end{pmatrix}. \quad (3.14)$$

This rotation angle is defined through the following relation

$$\tan 2\alpha = \frac{2B_S}{A_S - C_S} = \frac{2\left(\lambda_3 + \frac{\lambda_5}{4}\right)v_1v_2}{\lambda_1v_1^2 - \lambda_2v_2^2 + \left(\lambda_3 + \frac{\lambda_5}{4}\right)(v_1^2 - v_2^2)}. \quad (3.15)$$

Note that there were eight parameters to start with: v_1 , v_2 and 6 lambdas. We trade v_1 and v_2 for v and $\tan \beta$. All the lambdas except λ_5 can be traded for 4 physical Higgs masses and α . The relations between these two equivalent sets of parameters are given below :

$$\lambda_1 = \frac{1}{2v^2 \cos^2 \beta} \left[m_H^2 \cos^2 \alpha + m_h^2 \sin^2 \alpha - \frac{\sin \alpha \cos \alpha}{\tan \beta} (m_H^2 - m_h^2) \right] - \frac{\lambda_5}{4} (\tan^2 \beta - 1), \quad (3.16a)$$

$$\lambda_2 = \frac{1}{2v^2 \sin^2 \beta} \left[m_h^2 \cos^2 \alpha + m_H^2 \sin^2 \alpha - \sin \alpha \cos \alpha \tan \beta (m_H^2 - m_h^2) \right] - \frac{\lambda_5}{4} (\cot^2 \beta - 1), \quad (3.16b)$$

$$\lambda_3 = \frac{1}{2v^2} \frac{\sin \alpha \cos \alpha}{\sin \beta \cos \beta} (m_H^2 - m_h^2) - \frac{\lambda_5}{4}, \quad (3.16c)$$

$$\lambda_4 = \frac{2}{v^2} m_{1+}^2, \quad (3.16d)$$

$$\lambda_6 = \frac{2}{v^2} m_A^2. \quad (3.16e)$$

Among these, v is already known and if we assume that the lightest CP-even Higgs is what has been observed at the LHC, then m_h is also known. The rest of the parameters need to be constrained from theoretical as well as experimental considerations.

3.1.2 The alignment limit

The *alignment limit* addresses the possibility of recovering a CP-even mass eigenstate with exactly same couplings as the SM Higgs with the SM particles. To start with, it is instructive to look at the trilinear gauge-Higgs couplings which stem from the Higgs kinetic terms. As an example, consider the case of a 2HDM :

$$\mathcal{L}_{\text{kin}}^{\text{scalar}} = |D_\mu \Phi_1|^2 + |D_\mu \Phi_2|^2 \ni \frac{g^2}{2} W_\mu^+ W^{\mu-} (v_1 h_1 + v_2 h_2). \quad (3.17)$$

Clearly the combination

$$H^0 = \frac{1}{v} (v_1 h_1 + v_2 h_2) \quad (3.18)$$

will carry away the exact SM-like gauge couplings and its orthogonal combination (R say) will not have any trilinear couplings with the gauge bosons. Obviously, for n Higgs-doublet case, the definition of H^0 will be

$$H^0 = \frac{1}{v} (v_1 h_1 + v_2 h_2 + \cdots + v_n h_n). \quad (3.19)$$

As we will illustrate later, this H^0 will mimic the SM Higgs in its Yukawa couplings also. For the case of 2HDM this combination can be obtained by applying the same rotation as in the charged and pseudoscalar cases:

$$\begin{pmatrix} H^0 \\ R \end{pmatrix} = \begin{pmatrix} \cos \beta & \sin \beta \\ -\sin \beta & \cos \beta \end{pmatrix} \begin{pmatrix} h_1 \\ h_2 \end{pmatrix}. \quad (3.20)$$

Now, this SM-like state, H^0 , is not guaranteed to be a mass eigenstate in general. The alignment limit specifically points towards the condition under which H^0 coincides with one of the CP-even physical eigenstates. For the 2HDM case, the relationships are :

$$H = \cos(\beta - \alpha) H^0 - \sin(\beta - \alpha) R, \quad (3.21a)$$

$$h = \sin(\beta - \alpha) H^0 + \cos(\beta - \alpha) R. \quad (3.21b)$$

Clearly, if we want the lightest CP-even scalar, h , to possess SM-like couplings, we must set

$$\sin(\beta - \alpha) = 1 \quad (3.22)$$

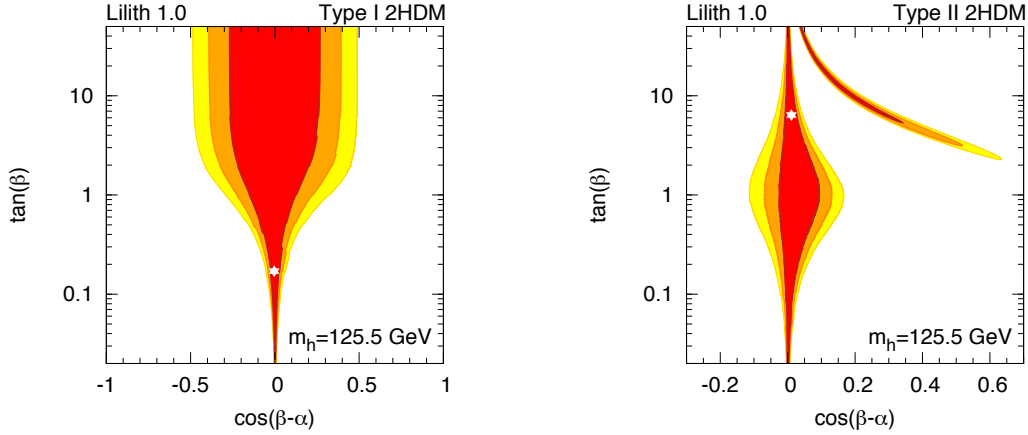


FIGURE 3.1: The red, orange and yellow regions represent the 68%, 95% and 99% CL allowed regions respectively coming from the Higgs signal strength measurement at the LHC. The left panel shows the situation for Type I model, whereas, the right panel shows that of Type II model. The figures have been taken from [34].

which is the definition of the alignment limit in the 2HDM context. So, going to the alignment limit reduces one more parameter from the theory.

Now we come to the important question of how crucial this limit is in the context of current LHC Higgs data. Many global fit results in view of the recent data can be found in the literature [34–39]. In Fig. 3.1 we choose to display the result of a recent analysis [34]. The orange regions represent the 95% CL allowed region from measurements of the Higgs signal strengths in various channels (See Fig. 3.2). Since the data is compatible with the SM prediction, one can easily see that the alignment limit is preferred. The horizontal widths of the allowed regions reflect the present accuracy of measurements. In ref [39], it has also been projected how this region will shrink if future measurement continues to agree with the SM predictions with greater amount of accuracy. We can easily guess that if this is the case, we will continuously be pushed closer and closer to the alignment limit. Thus finding an alignment limit might be crucial for survival of the different BSM scenarios.

3.1.3 Bounded from below constraints

For this particular part, it might be convenient to work with the notation of Eq. (3.2). Here we try to derive the constraints on parameters β_i such that the scalar potential, V , is bounded from below in any direction in the field space. It is sufficient to examine the quartic terms of the scalar potential (which we denote by V_4) because only this part of the potential will be dominant for large values of the field components of Φ_1 and Φ_2 . We define $a = \Phi_1^\dagger \Phi_1$, $b = \Phi_2^\dagger \Phi_2$, $c = \text{Re } \Phi_1^\dagger \Phi_2$, $d = \text{Im } \Phi_1^\dagger \Phi_2$ and note that

$$ab \geq c^2 + d^2. \quad (3.23)$$

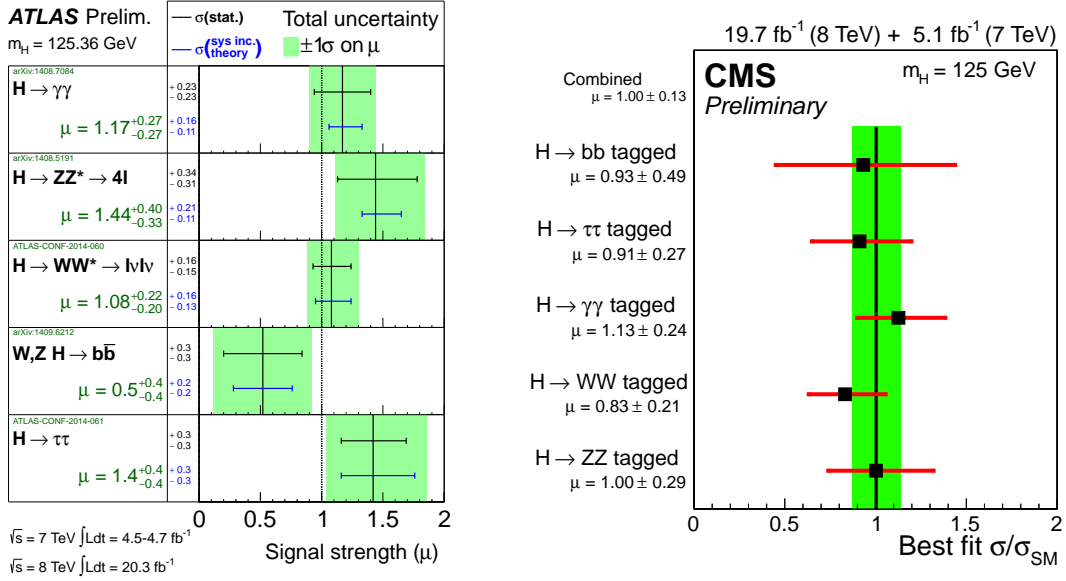


FIGURE 3.2: Current measurements of the Higgs signal strengths into different channels by ATLAS [40] and CMS [41].

Using these definitions we can rewrite the quartic part of the scalar potential as follows [33]:

$$\begin{aligned}
 V_4 = & \frac{1}{2} \left(\sqrt{\beta_1} a - \sqrt{\beta_2} b \right)^2 + \left(\beta_3 + \sqrt{\beta_1 \beta_2} \right) (ab - c^2 - d^2) + 2 \left(\beta_3 + \beta_4 + \sqrt{\beta_1 \beta_2} \right) c^2 \\
 & + \left(\text{Re } \beta_5 - \beta_3 - \beta_4 - \sqrt{\beta_1 \beta_2} \right) (c^2 - d^2) - 2cd \text{Im } \beta_5. \quad (3.24)
 \end{aligned}$$

Although we shall assume all the potential parameters to be real for our phenomenological studies, here we wish to keep things general because our arguments in this subsection do not depend on the reality of β_5 . We have to ensure that V_4 never becomes infinitely negative in any direction of the field space, *i.e.*, for any choice of 8 independent field parameters (4 of Φ_1 and 4 of Φ_2). Note that, since Φ_1 and Φ_2 are two component column matrices, it is possible to choose arbitrary nonzero values for a and b even when we make $c = d = 0$. But if a and/or b becomes zero, then $c = d = 0$ for sure. Keeping these facts in mind, we now proceed to find the constraints for the potential to be bounded from below.

- Consider the field direction $b = 0$ (and therefore $c = d = 0$) and $a \rightarrow \infty$; then $V_4 = \beta_1/2a^2$. So, V_4 is not largely negative requires

$$\beta_1 \geq 0. \quad (3.25)$$

- Consider the field direction $a = 0$ (and therefore $c = d = 0$) and $b \rightarrow \infty$; then $V_4 = \beta_2/2b^2$. So, V_4 is not largely negative requires

$$\beta_2 \geq 0. \quad (3.26)$$

- Consider the field direction along which $a = \sqrt{\beta_2/\beta_1}b$ (so that the first term in Eq. (3.24) vanishes) and $c = d = 0$. In addition to this we go to large field values in that direction, *i.e.*, $a, b \rightarrow \infty$. Then, $V_4 = (\beta_3 + \sqrt{\beta_1\beta_2})ab$. Now, as $a, b > 0$ by definition, the condition for the potential not to hit $-\infty$ becomes

$$\beta_3 + \sqrt{\beta_1\beta_2} \geq 0. \quad (3.27)$$

- Again consider the field direction in which $a = \sqrt{\beta_2/\beta_1}b$ along with $ab = c^2 + d^2$. Along this direction, V_4 is of the form

$$V_4 = Pc^2 + 2Qcd + Rd^2, \quad (3.28a)$$

$$\text{where, } P = \text{Re } \beta_5 + \Lambda, \quad (3.28b)$$

$$Q = -\text{Im } \beta_5, \quad (3.28c)$$

$$R = -\text{Re } \beta_5 + \Lambda, \quad (3.28d)$$

$$\text{with, } \Lambda = \beta_3 + \beta_4 + \sqrt{\beta_1\beta_2}. \quad (3.28e)$$

Since c and d are still arbitrary, by choosing $d = 0, c \rightarrow \infty$ and $c = 0, d \rightarrow \infty$ successively, we require

$$P = \text{Re } \beta_5 + \Lambda \geq 0, \quad (3.29a)$$

$$R = -\text{Re } \beta_5 + \Lambda \geq 0, \quad (3.29b)$$

$$\text{and hence, } \Lambda \geq 0. \quad (3.29c)$$

To have another condition, let us recast Eq. (3.28a) into the following form :

$$V_4 = P \left(c + \frac{Q}{P}d \right)^2 + \left(R - \frac{Q^2}{P} \right) d^2. \quad (3.30)$$

We can now choose a direction along which $c = -Q/P d$ with $d \rightarrow \infty$ so that we have the following condition :

$$R - \frac{Q^2}{P} > 0 \Rightarrow PR > Q^2. \quad (3.31)$$

For the last step, remember that $P > 0$ (Eq. (3.29a)) so that we can multiply both sides by P without flipping the inequality sign. After substituting for P, Q and R we get from Eq. (3.31) :

$$\Lambda^2 - (\text{Re } \beta_5)^2 > (\text{Im } \beta_5)^2 \Rightarrow \Lambda^2 > |\beta_5|^2, \quad (3.32a)$$

$$\Lambda > |\beta_5|, \quad (3.32b)$$

where, in the last step we have used the fact that $\Lambda > 0$ (Eq. (3.29c)). Since $|\beta_5| > \pm\beta_5$, 0, Eq. (3.32b) puts a stronger constrain on Λ than Eq. (3.29). Therefore, substituting for Λ , Eq. (3.32b) becomes

$$\beta_3 + \beta_4 + \sqrt{\beta_1\beta_2} > |\beta_5|. \quad (3.33)$$

We now collect Eqs. (3.25), (3.26), (3.27) and (3.33) together and, using Eq. (3.4), express them in terms of lambdas for later use :

$$\lambda_1 + \lambda_3 > 0, \quad (3.34a)$$

$$\lambda_2 + \lambda_3 > 0, \quad (3.34b)$$

$$(2\lambda_3 + \lambda_4) + 2\sqrt{(\lambda_1 + \lambda_3)(\lambda_2 + \lambda_3)} > 0, \quad (3.34c)$$

$$2\lambda_3 + \frac{\lambda_5 + \lambda_6}{2} - \frac{|\lambda_5 - \lambda_6|}{2} + 2\sqrt{(\lambda_1 + \lambda_3)(\lambda_2 + \lambda_3)} > 0. \quad (3.34d)$$

The way we have presented the derivation, it appears that these are only the *necessary* conditions for the potential to be bounded from below. But rigorous analysis [42, 43] shows that these are indeed the sufficient conditions also.

3.1.4 Constraints from unitarity

As mentioned in Chapter 1, any scattering amplitude can be expanded in terms of the partial waves as follows:

$$\mathcal{M}(\theta) = 16\pi \sum_{\ell=0}^{\infty} a_{\ell}(2\ell + 1)P_{\ell}(\cos \theta), \quad (3.35)$$

where, θ is the scattering angle and $P_{\ell}(x)$ is the Legendre polynomial of order ℓ . The prescription is simple : once we calculate the Feynman amplitude of a certain $2 \rightarrow 2$ scattering process, each of the partial wave amplitude (a_{ℓ}), in Eq. (3.35), can be extracted by using the orthonormality of the Legendre polynomials. In the context of SM, the pioneering work has been done by Lee, Quigg and Thacker (LQT) [12]. They have analyzed several two body scatterings involving longitudinal gauge bosons and physical Higgs in the SM. All such scattering amplitudes are proportional to Higgs quartic coupling in the high energy limit. The $\ell = 0$ partial wave amplitude (a_0) is then extracted from these amplitudes and cast in the form of an S-matrix having different two-body states as rows and columns. The largest eigenvalue of this matrix is bounded by the unitarity constraint, $|a_0| < 1$. This restricts the quartic Higgs self coupling and therefore the Higgs mass to a maximum value.

The procedure has been extended to the case of a 2HDM scalar potential [44–47]. Here also same types of two body scattering channels are considered. Thanks to the equivalence theorem [48, 49], we can use unphysical Higgses instead of actual longitudinal components of the gauge bosons

when considering the high energy limit. So, we can use the Goldstone-Higgs potential of Eq. (3.3) for this analysis. Still it will be a much involved calculation. But we notice that the diagrams containing trilinear vertices will be suppressed by a factor of E^2 coming from the intermediate propagator. Thus they do not contribute at high energies, – only the quartic couplings contribute. Clearly the physical Higgs masses that could come from the propagators, do not enter this analysis. Since we are interested only in the eigenvalues of the S-matrix, this allows us to work with the original fields of Eq. (3.3) instead of the physical mass eigenstates.

As already argued, only the dimensionless quartic couplings will contribute to the amplitudes under consideration at high energies. As a result, only $\ell = 0$ partial amplitude (a_0) will receive nonzero contribution from the leading order term in the scattering amplitude. It is our purpose, then, to find the expressions of a_0 for every possible $2 \rightarrow 2$ scattering process and cast them in the form of an S-matrix which is constructed by taking the different two-body channels as rows and columns. Unitarity will restrict the magnitude of each of the eigenvalues of this S-matrix to lie below unity.

First important part of the calculation is to identify all the possible two-particle channels. These two-particle states are made of the fields w_k^\pm , h_k and z_k corresponding to the parametrization of Eq. (3.5). For our calculation, we consider neutral two-particle states (e.g., $w_i^+ w_j^-$, $h_i h_j$, $z_i z_j$, $h_i z_j$) and singly charged two-particle states (e.g., $w_i^+ h_j$, $w_i^+ z_j$). In general, if we have n -number of doublets ϕ_k ($k = 1, \dots, n$) there will be $(3n^2 + n)$ -number of neutral and $2n^2$ -number of charged two-particle states. Clearly, the dimensions of S-matrices formed out of these two-particle states will be a $(3n^2 + n) \times (3n^2 + n)$ and $2n^2 \times 2n^2$ for the neutral and charged cases respectively. The eigenvalues of these matrices should be bounded by the unitarity constraint.

We will exemplify these by considering the case of a 2HDM. In this case, the neutral channel S-matrix will be a 14×14 matrix with the following two-particle states as rows and columns :

$$\begin{aligned} &w_1^+ w_1^-, w_2^+ w_2^-, w_1^+ w_2^-, w_2^+ w_1^-, \frac{h_1 h_1}{\sqrt{2}}, \frac{z_1 z_1}{\sqrt{2}}, \\ &\frac{h_2 h_2}{\sqrt{2}}, \frac{z_2 z_2}{\sqrt{2}}, h_1 z_2, h_2 z_1, z_1 z_2, h_1 h_2, h_1 z_1, h_2 z_2. \end{aligned}$$

The factor of $1/\sqrt{2}$ associated with the identical particle states arises due to Bose symmetry. In the most general case, finding the eigenvalues of the 14×14 matrix would be a tedious job. But the potential of Eq. (3.3) contains some obvious symmetries in its quartic terms. These symmetries will allow us to decompose the full matrix in smaller blocks. One must note that the quartic part of the potential always contain even number of indices, 1 or 2. Consequently a state $x_1 y_1$ or $x_2 y_2$ will always go into $x_1 y_1$ or $x_2 y_2$ but not into $x_1 y_2$ or $x_2 y_1$ and vice versa. Furthermore, CP symmetry is conserved. This implies, a neutral state with combination $h_i h_j$ or $z_i z_j$ will never go into $h_i z_j$. Keeping these facts in mind we can now decompose the S-matrix

in the neutral sector into smaller blocks as follows :

$$\mathcal{M}_N = \begin{pmatrix} (\mathcal{M}_N^{11})_{6 \times 6} & 0 & 0 \\ 0 & (\mathcal{M}_N^{11})_{2 \times 2} & 0 \\ 0 & 0 & (\mathcal{M}_N^{12})_{6 \times 6} \end{pmatrix}. \quad (3.36)$$

The submatrices are given below :

$$(\mathcal{M}_N^{11})_{6 \times 6} = \begin{pmatrix} (\mathcal{A}_N^{11})_{3 \times 3} & (\mathcal{B}_N^{11})_{3 \times 3} \\ (\mathcal{B}_N^{11})_{3 \times 3}^\dagger & (\mathcal{C}_N^{11})_{3 \times 3} \end{pmatrix}, \quad (3.37a)$$

where,

$$(\mathcal{A}_N^{11})_{3 \times 3} = \begin{matrix} & w_1^+ w_1^- & w_2^+ w_2^- & \frac{z_1 z_1}{\sqrt{2}} \\ w_1^+ w_1^- & \begin{pmatrix} 4(\lambda_1 + \lambda_3) & 2\lambda_3 + \frac{\lambda_5 + \lambda_6}{2} & \sqrt{2}(\lambda_1 + \lambda_3) \\ 2\lambda_3 + \frac{\lambda_5 + \lambda_6}{2} & 4(\lambda_2 + \lambda_3) & \sqrt{2}\left(\lambda_3 + \frac{\lambda_4}{2}\right) \\ \sqrt{2}(\lambda_1 + \lambda_3) & \sqrt{2}\left(\lambda_3 + \frac{\lambda_4}{2}\right) & 3(\lambda_1 + \lambda_3) \end{pmatrix} \\ w_2^+ w_2^- & & & \\ \frac{z_1 z_1}{\sqrt{2}} & & & \end{matrix}, \quad (3.37b)$$

$$(\mathcal{B}_N^{11})_{3 \times 3} = \begin{matrix} & \frac{h_1 h_1}{\sqrt{2}} & \frac{z_2 z_2}{\sqrt{2}} & \frac{h_2 h_2}{\sqrt{2}} \\ w_1^+ w_1^- & \begin{pmatrix} \sqrt{2}(\lambda_1 + \lambda_3) & \sqrt{2}\left(\lambda_3 + \frac{\lambda_4}{2}\right) & \sqrt{2}\left(\lambda_3 + \frac{\lambda_4}{2}\right) \\ \sqrt{2}\left(\lambda_3 + \frac{\lambda_4}{2}\right) & \sqrt{2}(\lambda_2 + \lambda_3) & \sqrt{2}(\lambda_2 + \lambda_3) \\ (\lambda_1 + \lambda_3) & \lambda_3 + \frac{\lambda_5}{2} & \lambda_3 + \frac{\lambda_6}{2} \end{pmatrix} \\ w_2^+ w_2^- & & & \\ \frac{z_1 z_1}{\sqrt{2}} & & & \end{matrix}, \quad (3.37c)$$

$$(\mathcal{C}_N^{11})_{3 \times 3} = \begin{matrix} & \frac{h_1 h_1}{\sqrt{2}} & \frac{z_2 z_2}{\sqrt{2}} & \frac{h_2 h_2}{\sqrt{2}} \\ \frac{h_1 h_1}{\sqrt{2}} & \begin{pmatrix} 3(\lambda_1 + \lambda_3) & \lambda_3 + \frac{\lambda_6}{2} & \lambda_3 + \frac{\lambda_5}{2} \\ \lambda_3 + \frac{\lambda_6}{2} & 3(\lambda_2 + \lambda_3) & (\lambda_2 + \lambda_3) \\ \lambda_3 + \frac{\lambda_5}{2} & (\lambda_2 + \lambda_3) & 3(\lambda_2 + \lambda_3) \end{pmatrix} \\ \frac{z_2 z_2}{\sqrt{2}} & & & \\ \frac{h_2 h_2}{\sqrt{2}} & & & \end{matrix}. \quad (3.37d)$$

$$(\mathcal{M}_N^{11})_{2 \times 2} = \begin{matrix} & h_1 z_1 & h_2 z_2 \\ h_1 z_1 & \begin{pmatrix} 2(\lambda_1 + \lambda_3) & \frac{\lambda_5 - \lambda_6}{2} \\ \frac{\lambda_5 - \lambda_6}{2} & 2(\lambda_2 + \lambda_3) \end{pmatrix} \\ h_2 z_2 & & \end{matrix}, \quad (3.37e)$$

$$(\mathcal{M}_N^{12})_{6 \times 6} = \begin{pmatrix} (\mathcal{A}_N^{12})_{3 \times 3} & (\mathcal{B}_N^{12})_{3 \times 3} \\ (\mathcal{B}_N^{12})_{3 \times 3}^\dagger & (\mathcal{C}_N^{12})_{3 \times 3} \end{pmatrix}, \quad (3.37f)$$

where,

$$(\mathcal{A}_N^{12})_{3 \times 3} = \begin{array}{c} w_1^+ w_2^- \quad w_2^+ w_1^- \quad h_1 z_2 \\ w_1^+ w_2^- \left(\begin{array}{ccc} 2\lambda_3 + \frac{\lambda_5 + \lambda_6}{2} & \lambda_5 - \lambda_6 & -\frac{i}{2}(\lambda_4 - \lambda_6) \\ \lambda_5 - \lambda_6 & 2\lambda_3 + \frac{\lambda_5 + \lambda_6}{2} & \frac{i}{2}(\lambda_4 - \lambda_6) \\ \frac{i}{2}(\lambda_4 - \lambda_6) & -\frac{i}{2}(\lambda_4 - \lambda_6) & 2\lambda_3 + \lambda_6 \end{array} \right), \end{array} \quad (3.37g)$$

$$(\mathcal{B}_N^{12})_{3 \times 3} = \begin{array}{c} h_2 z_1 \quad z_1 z_2 \quad h_1 h_2 \\ w_1^+ w_2^- \left(\begin{array}{ccc} \frac{i}{2}(\lambda_4 - \lambda_6) & \frac{\lambda_5 - \lambda_4}{2} & \frac{\lambda_5 - \lambda_4}{2} \\ -\frac{i}{2}(\lambda_4 - \lambda_6) & \frac{\lambda_5 - \lambda_4}{2} & \frac{\lambda_5 - \lambda_4}{2} \\ \frac{\lambda_5 - \lambda_6}{2} & 0 & 0 \end{array} \right), \end{array} \quad (3.37h)$$

$$(\mathcal{C}_N^{12})_{3 \times 3} = \begin{array}{c} h_2 z_1 \quad z_1 z_2 \quad h_1 h_2 \\ z_1 z_2 \left(\begin{array}{ccc} 2\lambda_3 + \lambda_6 & 0 & 0 \\ 0 & 2\lambda_3 + \lambda_5 & \frac{\lambda_5 - \lambda_6}{2} \\ 0 & \frac{\lambda_5 - \lambda_6}{2} & 2\lambda_3 + \lambda_5 \end{array} \right). \end{array} \quad (3.37i)$$

The same exercise can be repeated for the charged two-particle states. For the singly charged sector, it will be a 8×8 matrix which will take the following block diagonal form :

$$\mathcal{M}_C = \begin{pmatrix} (\mathcal{M}_C^{11})_{4 \times 4} & 0 \\ 0 & (\mathcal{M}_C^{12})_{4 \times 4} \end{pmatrix}. \quad (3.38)$$

The submatrices are given below :

$$(\mathcal{M}_C^{11})_{4 \times 4} = \begin{array}{c} h_1 w_1^+ \quad h_2 w_2^+ \quad z_1 w_1^+ \quad z_2 w_2^+ \\ h_1 w_1^+ \left(\begin{array}{ccc} 2(\lambda_1 + \lambda_3) & \frac{\lambda_5 - \lambda_4}{2} & 0 \\ \frac{\lambda_5 - \lambda_4}{2} & 2(\lambda_2 + \lambda_3) & -\frac{i}{2}(\lambda_4 - \lambda_6) \\ 0 & \frac{i}{2}(\lambda_4 - \lambda_6) & 2(\lambda_1 + \lambda_3) \\ \frac{i}{2}(\lambda_4 - \lambda_6) & 0 & \frac{\lambda_5 - \lambda_4}{2} \end{array} \right), \end{array} \quad (3.39a)$$

$$(\mathcal{M}_C^{12})_{4 \times 4} = \begin{array}{c} h_1 w_2^+ \quad h_2 w_1^+ \quad z_1 w_2^+ \quad z_2 w_1^+ \\ h_1 w_2^+ \left(\begin{array}{ccc} 2\lambda_3 + \lambda_4 & \frac{\lambda_5 - \lambda_4}{2} & 0 \\ \frac{\lambda_5 - \lambda_4}{2} & 2\lambda_3 + \lambda_4 & \frac{i}{2}(\lambda_4 - \lambda_6) \\ 0 & -\frac{i}{2}(\lambda_4 - \lambda_6) & 2\lambda_3 + \lambda_4 \\ -\frac{i}{2}(\lambda_4 - \lambda_6) & 0 & \frac{\lambda_5 - \lambda_4}{2} \end{array} \right). \end{array} \quad (3.39b)$$

The eigenvalues for these matrices are listed below :

- $(\mathcal{M}_N^{11})_{6 \times 6}$: $a_1^\pm, a_2^\pm, a_3^\pm$.
- $(\mathcal{M}_N^{11})_{2 \times 2}$: a_3^\pm .
- $(\mathcal{M}_N^{12})_{6 \times 6}$: b_1, b_2, b_3, b_4, b_5 with b_5 twofold degenerate.

- $(\mathcal{M}_C^{11})_{4 \times 4} : a_2^\pm, a_3^\pm.$
- $(\mathcal{M}_C^{12})_{4 \times 4} : b_2, b_4, b_5, b_6.$

We also enlist below the explicit expressions for these eigenvalues:

$$a_1^\pm = 3(\lambda_1 + \lambda_2 + 2\lambda_3) \pm \sqrt{9(\lambda_1 - \lambda_2)^2 + \left(4\lambda_3 + \lambda_4 + \frac{\lambda_5 + \lambda_6}{2}\right)^2}, \quad (3.40a)$$

$$a_2^\pm = (\lambda_1 + \lambda_2 + 2\lambda_3) \pm \sqrt{(\lambda_1 - \lambda_2)^2 + \frac{1}{4}(2\lambda_4 - \lambda_5 - \lambda_6)^2}, \quad (3.40b)$$

$$a_3^\pm = (\lambda_1 + \lambda_2 + 2\lambda_3) \pm \sqrt{(\lambda_1 - \lambda_2)^2 + \frac{1}{4}(\lambda_5 - \lambda_6)^2}, \quad (3.40c)$$

$$b_1 = 2\lambda_3 - \lambda_4 - \frac{1}{2}\lambda_5 + \frac{5}{2}\lambda_6, \quad (3.40d)$$

$$b_2 = 2\lambda_3 + \lambda_4 - \frac{1}{2}\lambda_5 + \frac{1}{2}\lambda_6, \quad (3.40e)$$

$$b_3 = 2\lambda_3 - \lambda_4 + \frac{5}{2}\lambda_5 - \frac{1}{2}\lambda_6, \quad (3.40f)$$

$$b_4 = 2\lambda_3 + \lambda_4 + \frac{1}{2}\lambda_5 - \frac{1}{2}\lambda_6, \quad (3.40g)$$

$$b_5 = 2\lambda_3 + \frac{1}{2}\lambda_5 + \frac{1}{2}\lambda_6, \quad (3.40h)$$

$$b_6 = 2(\lambda_3 + \lambda_4) - \frac{1}{2}\lambda_5 - \frac{1}{2}\lambda_6. \quad (3.40i)$$

Each of the above eigenvalues should be bounded from the unitarity constraint as

$$|a_i^\pm|, |b_i| \leq 16\pi. \quad (3.41)$$

3.1.5 Numerical constraints on the scalar masses in the alignment limit

Next important thing is to investigate the implications of these conditions on the physical scalar masses especially the nonstandard ones. Fig. 3.3 shows the region allowed by the combined constraints coming from unitarity and boundedness of the potential for the case $\lambda_5 = 0$, *i.e.*, exact Z_2 symmetry. Noteworthy features are listed below :

- From the left panel, we can read the limit on $\tan \beta$, $1/8 < \tan \beta < 8$.
- Limits on the masses are, $m_H, m_A, m_{1+} < 1$ TeV.

The reason for the above mentioned bounds can be traced back to the eigenvalues of Eq. (3.40). First two constraints for boundedness in Eq. (3.34) can be combined into

$$\lambda_1 + \lambda_2 + 2\lambda_3 > 0. \quad (3.42)$$

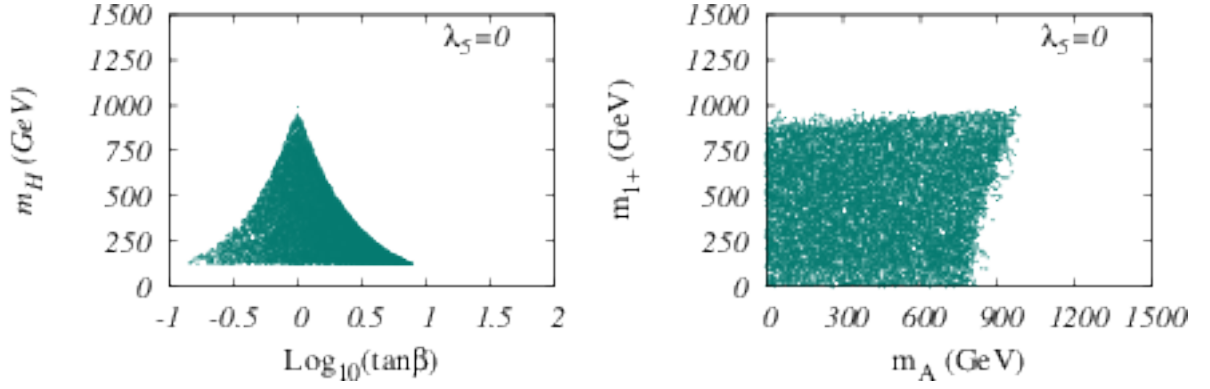


FIGURE 3.3: Allowed region from unitarity and stability for exact Z_2 symmetry. The figures have been taken from [50].

This, then together with the condition $|a_1^\pm| < 16\pi$, implies

$$0 < \lambda_1 + \lambda_2 + 2\lambda_3 < \frac{16\pi}{3}, \quad (3.43)$$

$$\Rightarrow 0 < \left(m_H^2 - \frac{1}{2}\lambda_5 v^2 \right) (\tan^2 \beta + \cot^2 \beta) + 2m_h^2 < \frac{32\pi v^2}{3}, \quad (3.44)$$

where the last expression is obtained from the previous one by using Eq. (3.16) in the alignment limit. Since $m_H > 125$ GeV, this will put a limit on $\tan \beta$ (as well as $\cot \beta$) when $\lambda_5 = 0$. Since the minimum value of $(\tan^2 \beta + \cot^2 \beta)$ is 2 when $\tan \beta = 1$, the maximum possible value of m_H occurs at $\tan \beta = 1$. In summary, Eq. (3.44) explains the $\tan \beta$ dependent bound on m_H as depicted in the left panel of Fig. 3.3.

Eq. (3.44) also implies that the restriction on $\tan \beta$ will be lifted for $1/2\lambda_5 v^2 > (m_H^2)_{\min} = (125 \text{ GeV})^2$. Once this condition is satisfied, m_H^2 will have the chance to saturate to $1/2\lambda_5 v^2$ making the difference between them to vanish in Eq. (3.44). In fact, to a very good approximation, one can use

$$m_H^2 \approx 1/2\lambda_5 v^2 \quad (3.45)$$

for $\tan \beta > 5$.

To understand the restrictions on m_A and m_{1+} , we use the triangle inequality to note the following:

$$|b_1 - b_3| \equiv 3|\lambda_6 - \lambda_5| < 32\pi, \quad \Rightarrow \left| m_A^2 - \frac{1}{2}\lambda_5 v^2 \right| < \frac{16\pi v^2}{3}, \quad (3.46a)$$

$$|b_6 - b_3| \equiv 3|\lambda_4 - \lambda_5| < 32\pi, \quad \Rightarrow \left| m_{1+}^2 - \frac{1}{2}\lambda_5 v^2 \right| < \frac{16\pi v^2}{3}. \quad (3.46b)$$

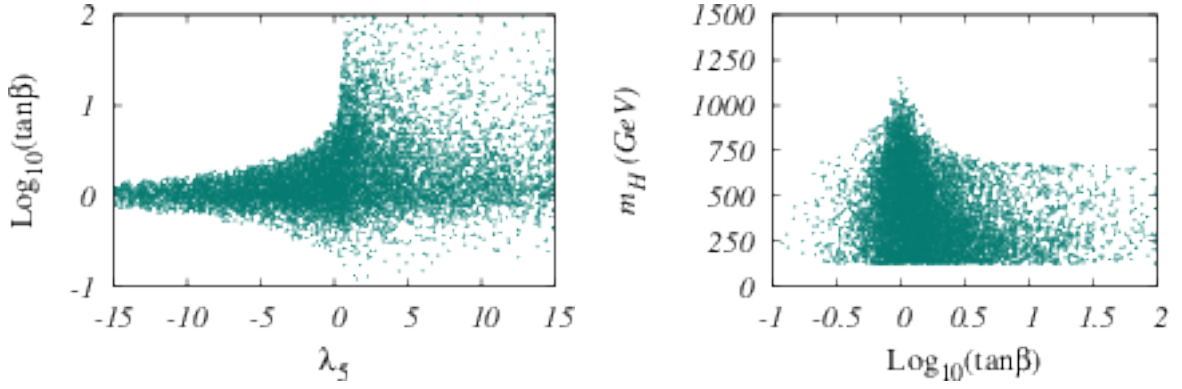


FIGURE 3.4: Relaxation of the unitarity and stability constraints on $\tan\beta$ in the presence of soft breaking. In the right panel, the vertical width of the tail in the region where $\tan\beta$ is much away from unity is caused by the variation of λ_5 in the range $[-15, 15]$. The figures have been taken from [50].

Because of Eqs. (3.46a) and (3.46b) we expect to put limits on m_A and m_{1+} respectively, when $\lambda_5 = 0$. Additionally, note that due to the inequality

$$|b_1 - b_6| \equiv 3|\lambda_6 - \lambda_4| < 32\pi, \quad \Rightarrow |m_A^2 - m_{1+}^2| < \frac{16\pi v^2}{3}, \quad (3.47)$$

we expect the splitting between m_A and m_{1+} to be *always* restricted in a 2HDM. It is also interesting to note that the conclusions obtained from Eqs. (3.46a), (3.46b) and (3.47) *do not* depend on the imposition of the alignment condition.

Next we shall investigate the implications of the soft breaking parameter on these constraints. We have varied λ_5 in the range $[-15, 15]$ for this purpose. From Eq. (3.44) one can observe that the space for $\tan\beta$ is squeezed further if $\lambda_5 < 0$ but the bound is relaxed if $\lambda_5 > 0$. This feature emerges from the left panel of Fig. 3.4. One can also see from Eq. (3.44) that m_H^2 must follow $1/2\lambda_5 v^2$ if $\tan\beta$ moderately deviates from unity. This feature is reflected by the horizontal tail in the right panel of Fig. 3.4 on both sides of the peak. The vertical width of the tail is caused by the variation of λ_5 in the range $[-15, 15]$. On the other hand, from Eqs. (3.46a), (3.46b) and (3.44), it should be noted that the upper bounds on the nonstandard scalar masses will be relaxed for $\lambda_5 > 0$ but will get tighter for $\lambda_5 < 0$. Fig. 3.5 reflects these features where one can see that this dependence is rather weak.

It is also important to note that the production as well as the tree-level decay widths of h remain unaltered from the corresponding SM expectations due to the imposition of alignment limit of Eq. (3.22). But the loop induced decay modes of h , such as $h \rightarrow \gamma\gamma$ and $h \rightarrow Z\gamma$, will pick up additional contributions due the presence of the charged scalar in loops. For example, the diphoton signal strength ($\mu_{\gamma\gamma}$), in general, depends on both λ_5 and m_{1+} [51]. The current measurement by CMS gives $\mu_{\gamma\gamma} = 1.14_{-0.23}^{+0.26}$ [52], whereas ATLAS measures $\mu_{\gamma\gamma}$ to be 1.17 ± 0.27 [53]. In addition to this, the direct search limit of $m_{1+} > 80$ GeV [54] should also be taken into account. Considering all of these experimental constraints, the allowed region at 95% C.L. has

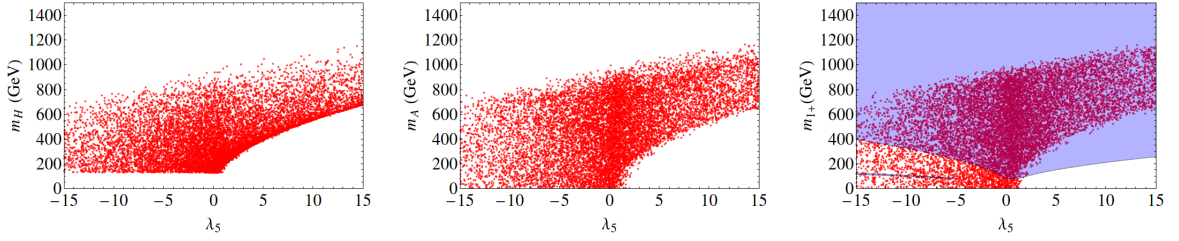


FIGURE 3.5: *Effect of soft breaking on the constraints on the nonstandard masses. The (light blue) shaded region in the rightmost panel represents the combined allowed region from direct search and the diphoton signal strength at 95% C.L. The figures have been taken from [50].*

been shaded (in light blue) in the rightmost panel of Fig. 3.5. Only those points that lie within the shaded region survive both the theoretical and experimental constraints.

An interesting alternative arises if, instead of Z_2 , one imposes an $U(1)$ symmetry under which $\Phi_2 \rightarrow e^{i\alpha}\Phi_2$. This $U(1)$ symmetry needs to be broken softly to forbid the appearance of a massless pseudoscalar. This symmetry will imply $\beta_6 = 0$ in Eq. (3.2) or $\lambda_5 = \lambda_6$ in Eq. (3.3). Thus, the soft breaking parameter now gets related to the pseudoscalar mass as $m_A^2 = 1/2\lambda_5 v^2$. Consequently, the correlation between m_H and λ_5 in the leftmost panel of Fig. 3.5 transforms into the degeneracy between m_H and m_A [55]. The constraints on the scalar masses imposed by the stability and unitarity conditions in Eqs. (3.34) and (3.40) have been plotted in Fig. 3.6 for $\tan\beta = 1, 5$ and 10 by performing random scan over all non-standard scalar masses. The following salient features emerge from the plots.

- There is a correlation between m_A and m_H which gets stronger for larger values of $\tan\beta$, to the extent that they become nearly degenerate once $\tan\beta$ crosses 10 . To understand this, we note that for $\lambda_5 = \lambda_6$, Eq. (3.44) reduces to the following form

$$0 \leq (m_H^2 - m_A^2)(\tan^2\beta + \cot^2\beta) + 2m_h^2 \leq \frac{32\pi v^2}{3}. \quad (3.48)$$

Clearly, for $\tan\beta$ away from unity, H and A are almost degenerate.

- There is a similar correlation between m_H and m_{1+} , but this time without any dependence on $\tan\beta$. This can again be seen from the inequalities of Eqs. (3.46a) and (3.46b) keeping in mind that now $m_A^2 = 1/2\lambda_5 v^2$.
- As regards the non-standard scalars, the unitarity conditions essentially apply on the difference of their squared masses. Thus, any individual mass can be arbitrarily large without affecting the unitarity conditions. This conclusion crucially depends on the existence of a $U(1)$ symmetry of the potential. When the symmetry of the potential is only a discrete Z_2 , considerations of unitarity do restrict the individual non-standard masses as has already been demonstrated.

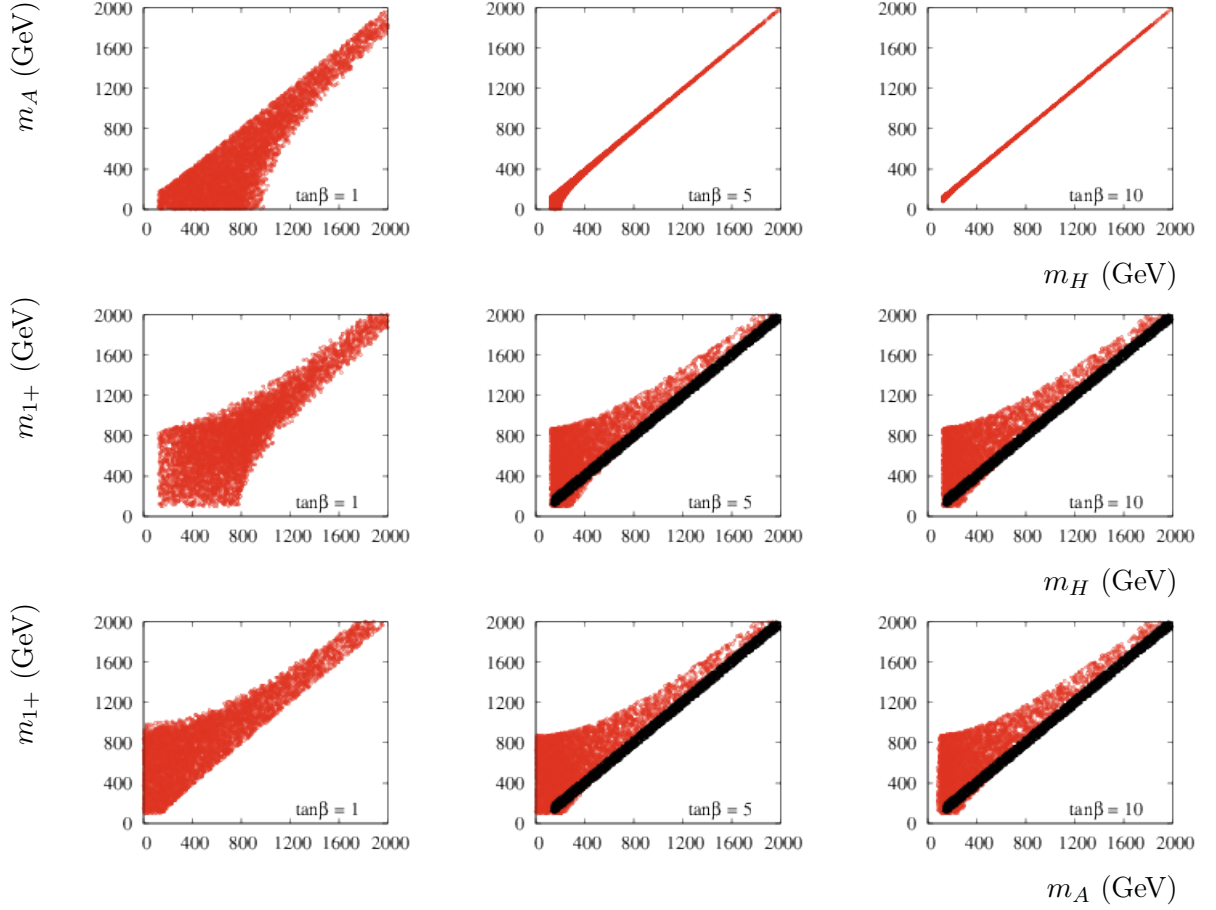


FIGURE 3.6: $2HDM$ potential with softly broken $U(1)$ symmetry: regions allowed in m_H - m_A , m_H - m_{1+} and m_A - m_{1+} planes from unitarity and stability (red points), and from T -parameter (black points), for three choices of $\tan\beta$. The plots have been taken from [55] where $m_{1+} > 100$ GeV was assumed to respect LEP direct search bound [54].

- We note at this point that the splitting between the heavy scalar masses is also constrained by the oblique electroweak T -parameter. In the present case, the expression of the T -parameter in the alignment limit is given by [56, 57]

$$T = \frac{1}{16\pi \sin^2 \theta_w M_W^2} \left[F(m_{1+}^2, m_H^2) + F(m_{1+}^2, m_A^2) - F(m_H^2, m_A^2) \right], \quad (3.49)$$

with

$$F(x, y) = \frac{x+y}{2} - \frac{xy}{x-y} \ln(x/y). \quad (3.50)$$

The new physics contribution to the T -parameter can be found to be [58]

$$T = 0.05 \pm 0.12. \quad (3.51)$$

To provide an intuitive feel on the constraints from the T -parameter, we assume $m_H = m_A$,

which is anyway dictated by the unitarity constraints for $\tan\beta$ somewhat away from unity. It then follows from Eq. (3.49) that the splitting between m_{1+} and m_H is approximately 50 GeV, for $|m_{1+} - m_H| \ll m_{1+}, m_H$. It turns out from Fig. 3.6 that the constraints from the T -parameter are stronger than that from unitarity and stability.

For $\tan\beta = 1$, unitarity and stability do not compel m_H and m_A to be very close. In this case, the T -parameter cannot give any definitive constraints in the planes of the heavy scalar masses, unlike the unitarity and stability constraints. For this reason, we have shown only the latter constraints in Fig. 3.6 for $\tan\beta = 1$.

- Thus, for moderate or large $\tan\beta$, the unitarity and stability constraints, together with the constraints coming from the T -parameter, imply that all three heavy scalar states are nearly degenerate in the alignment limit.

3.2 Yukawa part

We shall start by proving the assertion made below Eq. (3.19) that H^0 carries SM-like Yukawa couplings too. The most general Yukawa interaction for n Higgs-doublet model can be written as:

$$\mathcal{L}_Y = - \sum_{j=1}^n \left[\bar{Q}_L \Gamma_j \Phi_j n_R + \bar{Q}_L \Delta_j \tilde{\Phi}_j n_R \right] + \text{h.c.} \quad (3.52)$$

Here $Q_L = (p_L \ n_L)^T$ is the left-handed quark doublet and, p_R and n_R are up- and down-type singlets respectively. In writing the Yukawa Lagrangian, we have suppressed the flavor indices. Γ_j and Δ_j are actually 3×3 Yukawa matrices in the down- and up-sectors respectively. After spontaneous symmetry breaking

$$\Phi_j = \frac{1}{\sqrt{2}} \begin{pmatrix} \sqrt{2}w_j^+ \\ (h_j + v_j) + iz_j \end{pmatrix}, \quad \tilde{\Phi}_j = i\sigma_2 \Phi_j^* = \frac{1}{\sqrt{2}} \begin{pmatrix} (h_j + v_j) - iz_j \\ -\sqrt{2}w_j^- \end{pmatrix}. \quad (3.53)$$

Hence the mass-matrices take the following form in the gauge basis:

$$M_n = \frac{1}{\sqrt{2}} \sum_{j=1}^n v_j \Gamma_j, \quad (3.54a)$$

$$M_p = \frac{1}{\sqrt{2}} \sum_{j=1}^n v_j \Delta_j. \quad (3.54b)$$

The diagonal mass matrices can be obtained via the following biunitary transformations:

$$D_d = U_L^\dagger \cdot M_n \cdot U_R = \text{diag}(m_d, m_s, m_b), \quad (3.55a)$$

$$D_u = V_L^\dagger \cdot M_p \cdot V_R = \text{diag}(m_u, m_c, m_t). \quad (3.55b)$$

The matrices, U and V relates the quark fields in the gauge basis to those in the mass basis:

$$n_L = U_L d_L, \quad n_R = U_R d_R; \quad (3.56a)$$

$$p_L = V_L u_L, \quad p_R = V_R u_R. \quad (3.56b)$$

Clearly, the CP-even Yukawa interaction arising from Eq. (3.52) becomes

$$\mathcal{L}_Y^{\text{CPeven}} = -\frac{1}{\sqrt{2}} \bar{n}_L \left(\sum_{j=1}^n \Gamma_j h_j \right) n_R - \frac{1}{\sqrt{2}} \bar{p}_L \left(\sum_{j=1}^n \Delta_j h_j \right) p_R + \text{h.c.} \quad (3.57)$$

Let us now rotate the $\{h_1, h_2, \dots, h_n\}$ basis, via an orthogonal transformation, to a new basis containing the state H^0 which has been defined in Eq. (3.19). The transformation will look like

$$\begin{pmatrix} H^0 \\ \checkmark \\ \checkmark \\ \vdots \end{pmatrix} = \frac{1}{v} \begin{pmatrix} v_1 & v_2 & \dots & v_n \\ \checkmark & \checkmark & \dots & \checkmark \\ \checkmark & \checkmark & \dots & \checkmark \\ \vdots & \vdots & \vdots & \vdots \end{pmatrix} \begin{pmatrix} h_1 \\ h_2 \\ \vdots \\ h_n \end{pmatrix}, \quad (3.58)$$

$$\Rightarrow \begin{pmatrix} h_1 \\ h_2 \\ \vdots \\ h_n \end{pmatrix} = \frac{1}{v} \begin{pmatrix} v_1 & \checkmark & \checkmark & \dots \\ v_2 & \checkmark & \checkmark & \dots \\ \vdots & \vdots & \vdots & \vdots \\ v_n & \checkmark & \checkmark & \dots \end{pmatrix} \begin{pmatrix} H^0 \\ \checkmark \\ \checkmark \\ \vdots \end{pmatrix} \quad (3.59)$$

Using Eq. (3.59), we can extract the Yukawa coupling of H^0 from Eq. (3.57) as follows :

$$\mathcal{L}_Y^{H^0} = \frac{H^0}{v} \left[-\frac{1}{\sqrt{2}} \bar{n}_L \left(\sum_{j=1}^n \Gamma_j v_j \right) n_R - \frac{1}{\sqrt{2}} \bar{p}_L \left(\sum_{j=1}^n \Delta_j v_j \right) p_R \right] + \text{h.c.} \quad (3.60)$$

$$= -\frac{H^0}{v} [\bar{n}_L M_n n_R + \bar{p}_L M_p p_R] + \text{h.c.} \quad (3.61)$$

Using Eqs. (3.55) and (3.56) we can rewrite the coupling of Eq. (3.61) in the mass basis as

$$\mathcal{L}_Y^{H^0} = -\frac{H^0}{v} [\bar{d}_L D_d d_R + \bar{u}_L D_u u_R] + \text{h.c.} \equiv -\frac{H^0}{v} [\bar{d} D_d d + \bar{u} D_u u], \quad (3.62)$$

where, the last step follows from the fact that $D_{u,d}$ are diagonal. Eq. (3.62) shows that H^0 , by construction, possesses SM-like Yukawa couplings with the SM fermions.

3.2.1 The problem of FCNC

The general Yukawa Lagrangian for the 2HDM case is given by Eq. (3.52) with $n = 2$. Following the definitions of Eqs. (3.20) and (3.53) we can take out the Yukawa coupling for the CP even part :

$$\begin{aligned} \mathcal{L}_{2\text{HDM}}^{\text{CP even}} &= -\frac{H^0}{v} \left\{ \bar{n}_L \left[\frac{1}{\sqrt{2}} (\Gamma_1 v_1 + \Gamma_2 v_2) \right] n_R + \bar{p}_L \left[\frac{1}{\sqrt{2}} (\Delta_1 v_1 + \Delta_2 v_2) \right] p_R \right\} \\ &\quad + \frac{R}{v} \left\{ \bar{n}_L \left[\frac{1}{\sqrt{2}} (\Gamma_1 v_2 - \Gamma_2 v_1) \right] n_R + \bar{p}_L \left[\frac{1}{\sqrt{2}} (\Delta_1 v_2 - \Delta_2 v_1) \right] p_R \right\} \end{aligned} \quad (3.63)$$

$$\begin{aligned} &= -\frac{H^0}{v} (\bar{d} D_d d + \bar{u} D_u u) \\ &\quad + \frac{R}{v} \left\{ \bar{d} (N_d P_R + N_d^\dagger P_L) d + \bar{u} (N_u P_R + N_u^\dagger P_L) u \right\}. \end{aligned} \quad (3.64)$$

In Eq. (3.64), $N_{u,d}$ are defined as follows :

$$N_d = \frac{1}{\sqrt{2}} U_L^\dagger (\Gamma_1 v_2 - \Gamma_2 v_1) U_R = \frac{v_2}{v_1} D_d - \frac{v_2}{\sqrt{2}} \left(\frac{v_2}{v_1} + \frac{v_1}{v_2} \right) U_L^\dagger \Gamma_2 U_R, \quad (3.65a)$$

$$N_u = \frac{1}{\sqrt{2}} V_L^\dagger (\Delta_1 v_2 - \Delta_2 v_1) V_R = \frac{v_2}{v_1} D_u - \frac{v_2}{\sqrt{2}} \left(\frac{v_2}{v_1} + \frac{v_1}{v_2} \right) V_L^\dagger \Delta_2 V_R. \quad (3.65b)$$

In writing Eq. (3.65) we have made use of Eqs. (3.54) and (3.55) with $n = 2$. Clearly, $N_{u,d}$ are non-diagonal in general and consequently, the state R in Eq. (3.64) carries tree-level flavor changing couplings which are very much constrained from the experiments. Following the definition of Eq. (3.10), it can be shown that the pseudoscalar (A) also mediates tree-level flavor changing processes :

$$\mathcal{L}_{2\text{HDM}}^{\text{CP odd}} = -\frac{iA}{v} \left\{ \bar{u} (N_u P_R - N_u^\dagger P_L) u - \bar{d} (N_d P_R - N_d^\dagger P_L) d \right\}. \quad (3.66)$$

For completeness, we record the general charged Higgs Yukawa interaction as follows :

$$\mathcal{L}_{2\text{HDM}}^{\text{charged}} = \frac{\sqrt{2} H_1^+}{v} \bar{u} \left[V N_d P_R - N_u^\dagger V P_L \right] d + \text{h.c.}, \quad (3.67)$$

where, $V = V_L^\dagger U_L$ is the CKM matrix.

3.2.2 Natural flavor conservation (NFC)

As prescribed by Glashow, Weinberg and Pascos, the tree-level Higgs mediated FCNC can be avoided altogether if all the fermions of a particular charge get their masses from a single scalar doublet. As the easiest example, if all the fermions couple to only Φ_1 (say) then $\Gamma_2 = \Delta_2 = 0$. Consequently, from Eq. (3.65) one can easily see that $N_{u,d}$ are diagonal and so there will be no Higgs mediated FCNC. These arrangements are generally made by employing a Z_2 symmetry

under which $\Phi_2 \rightarrow -\Phi_2$. Proper assignments of Z_2 charges to the different fermions then dictate which fermion couples to which doublet. To fix our convention, we shall always call Φ_2 the doublet which couples to the up-type quarks. Then, there are only two possibilities for the quark sector – either Φ_1 or Φ_2 gives masses to the down-type quarks. For each possibility in the quark sector, either Φ_1 or Φ_2 can give masses to the charged leptons making a total of four variants of 2HDMs as mentioned in Sec. 1. However, in this review, we shall primarily concentrate only on the phenomenology of the quark sector. In the following, we spell out the relevant Yukawa interaction in the *alignment limit* for the two possibilities in the quark sector.

- **Type-I and Lepton specific or X:** In these cases $\Gamma_1 = \Delta_1 = 0$. Consequently, the Yukawa Lagrangian becomes

$$\begin{aligned} \mathcal{L}_Y^I &= -\frac{h}{v} (\bar{u}D_u u + \bar{d}D_d d) + \frac{H}{v} \cot \beta (\bar{u}D_u u + \bar{d}D_d d) \\ &\quad + \frac{iA}{v} \cot \beta (\bar{u}D_u \gamma_5 u - \bar{d}D_d \gamma_5 d) \\ &\quad + \left[\frac{\sqrt{2}H_1^+}{v} \cot \beta \{ \bar{u}_R (D_u V) d_L - \bar{u}_L (V D_d) d_R \} + \text{h.c.} \right] \end{aligned} \quad (3.68)$$

- **Type-II and Flipped or Y:** In these cases $\Gamma_2 = \Delta_1 = 0$. Consequently, the Yukawa Lagrangian becomes

$$\begin{aligned} \mathcal{L}_Y^{II} &= -\frac{h}{v} (\bar{u}D_u u + \bar{d}D_d d) + \frac{H}{v} (\cot \beta \bar{u}D_u u - \tan \beta \bar{d}D_d d) \\ &\quad + \frac{iA}{v} (\cot \beta \bar{u}D_u \gamma_5 u + \tan \beta \bar{d}D_d \gamma_5 d) \\ &\quad + \left[\frac{\sqrt{2}H_1^+}{v} \{ \cot \beta \bar{u}_R (D_u V) d_L + \tan \beta \bar{u}_L (V D_d) d_R \} + \text{h.c.} \right] \end{aligned} \quad (3.69)$$

Flavor constraints on the NFC variants: Now we shall concentrate on the constraints on the charged scalar mass (m_{1+}), imposed by the measured values of $b \rightarrow s\gamma$ branching ratio [59] and neutral meson mass differences (ΔM) [60]. Since we are concerned with the quark sector only, the constraints will be the same for Type I and Type X models. The same is true for Type II and Type Y models.

For the process $b \rightarrow s\gamma$, the major new physics contributions come from charged scalar loops. We have added the new physics contribution to the SM one at the amplitude level and therefore have taken the interference into account. The branching ratio is then compared with the experimental value, $(3.55 \pm 0.26) \times 10^{-4}$ [59], to obtain the allowed region at 95% C.L. in Fig. 3.7. As can be seen from Eq. (3.69), for Type II and Y models, in the charged Higgs Yukawa interaction, the up-type Yukawa coupling is multiplied by $\cot \beta$ while the down-type Yukawa is multiplied by $\tan \beta$. Their product is responsible for setting $\tan \beta$ -independent limit $m_{1+} > 320$ GeV for

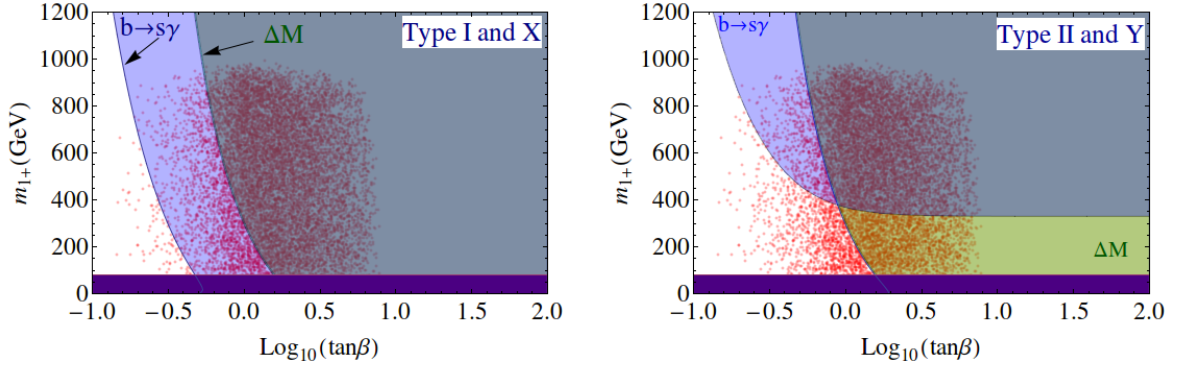


FIGURE 3.7: Constraints on $\tan\beta$ and the charged Higgs mass from unitarity and flavor physics. The left panel corresponds to Type I and X and the right panel to Type II and Y scenarios. The lower horizontal dark (purple) strip in both the panels corresponds to the direct search limit of 80 GeV [54]. The lighter shades represent allowed regions from individual flavor observables. The scattered points are allowed from unitarity and stability for 2HDMs with exact Z_2 symmetry. The figures have been taken from [50].

$\tan\beta > 1$ [61, 62]. This feature has been depicted in the right panel of Fig. 3.7. In Type I and X models, on the other hand, each of these couplings picks up a $\cot\beta$ factor. This is why there is essentially no bound on m_{1+} for $\tan\beta > 1$ in these models [61]. This character of Type I and X models emerges from the left panel of Fig. 3.7.

The dominant new physics contributions to neutral meson mass differences come from the charged scalar box diagrams. In Fig. 3.7, allowed regions have been shaded assuming that the new physics contributions saturate the experimental values of ΔM [60]. Since the amplitudes for the new box diagrams receive prevailing contributions from the up-type quark masses which, for all four variants of 2HDMs, comes with a $\cot\beta$ prefactor, the overall charged scalar contribution to the amplitude goes as $\cot^4\beta$ due to the presence of four charged scalar vertices in the box diagram. Not surprisingly, ΔM offers a stronger constraint than $b \rightarrow s\gamma$ for $\tan\beta < 1$ because, in this region, the new physics amplitude for the latter goes as $\cot^2\beta$.

Things become more interesting when the above flavor constraints are superimposed on top of the constraints from unitarity and stability. Most stringent constraints are obtained when Z_2 symmetry is exact in the scalar potential, *i.e.*, $\lambda_5 = 0$. In Fig. 3.7, the scattered points span the region allowed by the combined constraints of unitarity and stability for the case of exact Z_2 symmetry. Only those points which lie within the common shaded region survive when all the constraints are imposed. For 2HDMs of all four types, one can read the bound on $\tan\beta$ as

$$0.5 < \tan\beta < 8. \quad (3.70)$$

However, in order to allow a lighter charged scalar in the ballpark of 400 GeV or below, one must require $1 < \tan\beta < 8$. It should be remembered that, the lower bound on $\tan\beta$ mainly comes from the flavor data, whereas the upper limit, for the case of exact Z_2 symmetry, is dictated by

unitarity and stability. In the presence of a soft breaking parameter, the upper bound will be lifted allowing $\tan\beta$ to take much larger values at the expense of a strong correlation between the soft breaking parameter and m_H as depicted by Eq. (3.45).

3.2.3 An alternative to NFC – BGL models

In this subsection, we shall study a special category of 2HDM formulated by Branco, Grimus and Lavoura [32], where tree level FCNC exists with appropriate suppression arising from the elements of the Cabibbo-Kobayashi-Maskawa (CKM) matrix. Unlike the general 2HDM with tree level FCNC [63, 64], the BGL models introduce no new parameters in the Yukawa sector, and therefore, are more predictive. In this scenario, instead of the discrete Z_2 symmetry a global $U(1)$ symmetry acts on a particular generation i at a time, as follows:

$$\mathcal{S}: \quad Q_{Li} \rightarrow e^{i\theta} Q_{Li}, \quad p_{Ri} \rightarrow e^{2i\theta} p_{Ri}, \quad \Phi_2 \rightarrow e^{i\theta} \Phi_2. \quad (3.71)$$

Here $Q_{Li} = (p_{Li}, n_{Li})^T$ is the left-handed quark doublet for the i -th generation ($i = 1, 2, 3$), while p_R denotes the up-type right-handed quark singlets, all in the weak basis. The scalar doublet Φ_1 and the other quark fields remain unaffected by this transformation. For this particular choice of the symmetry, there will be no FCNC in the up sector and the FCNC in the down sector will be controlled by the i -th row of the CKM matrix. This will lead to three variants which will be called u-, c- and t-type models according to $i = 1, 2$, and 3 respectively. The other three variants can be obtained by replacing p_R in Eq. (3.71) with n_R (down-type singlet), as a result of which there will be no FCNC in the down sector and the FCNC in the up sector will be controlled by the i -th column of the CKM matrix. We will not consider the later scenario here primarily because the FCNC in the up sector is less restrictive.

To understand the details of the BGL models, let us consider, as an example, the case when $i = 3$ in Eq. (3.71). As has been already asserted in the previous paragraph, the FCNC couplings, in this particular example, will be controlled by the third row of the CKM matrix. To begin with, one should realize that certain terms in the Yukawa Lagrangian of Eq. (3.52) (with $n = 2$) will be forbidden when the BGL symmetry is imposed. In our case with $i = 3$, the following terms will not remain invariant under the symmetry \mathcal{S} :

$$\overline{Q}_{L3}(\Gamma_1)_{3A}\Phi_1(n_R)_A, \quad \overline{Q}_{L1}(\Gamma_2)_{1A}\Phi_2(n_R)_A, \quad \overline{Q}_{L2}(\Gamma_2)_{2A}\Phi_2(n_R)_A, \quad (3.72)$$

where, ‘ A ’ represents the generation index and can take values 1, 2, 3. Consequently, the third row of Γ_1 and the first and second rows of Γ_2 will be zero:

$$\Gamma_1 = \begin{pmatrix} \checkmark & \checkmark & \checkmark \\ \checkmark & \checkmark & \checkmark \\ 0 & 0 & 0 \end{pmatrix}, \quad \Gamma_2 = \begin{pmatrix} 0 & 0 & 0 \\ 0 & 0 & 0 \\ \checkmark & \checkmark & \checkmark \end{pmatrix}. \quad (3.73)$$

In a similar way, one can easily verify that the matrices Δ_1 and Δ_2 will assume the following textures:

$$\Delta_1 = \begin{pmatrix} \checkmark & \checkmark & 0 \\ \checkmark & \checkmark & 0 \\ 0 & 0 & 0 \end{pmatrix}, \quad \Delta_2 = \begin{pmatrix} 0 & 0 & 0 \\ 0 & 0 & 0 \\ 0 & 0 & \checkmark \end{pmatrix}. \quad (3.74)$$

Due to Eq. (3.74), the mass matrix, M_p (see Eq. (3.54)), in the up sector will be block diagonal as follows:

$$M_p = \begin{pmatrix} \checkmark & \checkmark & 0 \\ \checkmark & \checkmark & 0 \\ 0 & 0 & \checkmark \end{pmatrix}. \quad (3.75)$$

Consequently, the matrices which bi-diagonalize M_p will have the same block diagonal structure as M_p :

$$V_L = \begin{pmatrix} \checkmark & \checkmark & 0 \\ \checkmark & \checkmark & 0 \\ 0 & 0 & \checkmark \end{pmatrix}, \quad V_R = \begin{pmatrix} \checkmark & \checkmark & 0 \\ \checkmark & \checkmark & 0 \\ 0 & 0 & \checkmark \end{pmatrix}. \quad (3.76)$$

At this point, it is important to realize that we are at liberty to choose

$$V_L = \begin{pmatrix} \checkmark & \checkmark & 0 \\ \checkmark & \checkmark & 0 \\ 0 & 0 & 1 \end{pmatrix}, \quad (3.77)$$

with the understanding that the phase of $(M_p)_{33}$ can always be dumped into $(V_R)_{33}$. Denoting the bi-diagonalizing matrices in the down sector by $U_{L,R}$, we can see that the particular form of V_L , given by Eq. (3.77), has the following consequence on the CKM matrix:

$$V = V_L^\dagger U_L = \begin{pmatrix} \checkmark & \checkmark & 0 \\ \checkmark & \checkmark & 0 \\ 0 & 0 & 1 \end{pmatrix} \begin{pmatrix} \checkmark & \checkmark & \checkmark \\ \checkmark & \checkmark & \checkmark \\ (U_L)_{31} & (U_L)_{32} & (U_L)_{33} \end{pmatrix} \quad (3.78a)$$

$$\Rightarrow \begin{pmatrix} \checkmark & \checkmark & \checkmark \\ \checkmark & \checkmark & \checkmark \\ V_{td} & V_{ts} & V_{tb} \end{pmatrix} = \begin{pmatrix} \checkmark & \checkmark & \checkmark \\ \checkmark & \checkmark & \checkmark \\ (U_L)_{31} & (U_L)_{32} & (U_L)_{33} \end{pmatrix}. \quad (3.78b)$$

This implies that the third row of the CKM matrix is identical to the third row of U_L :

$$(U_L)_{3A} = V_{tA} \equiv V_{3A}, \quad (3.79a)$$

$$\Rightarrow (U_L^\dagger)_{A3} = (U_L)_{3A}^* = V_{3A}^*. \quad (3.79b)$$

Note that, Eq. (3.79) is a direct consequence of our choice $i = 3$ in Eq. (3.71). In general, for FCNC in the down sector, the i -th row of U_L should be identical with the i -th row of the CKM matrix. To proceed further with our choice of $i = 3$, it is useful to define the following projection matrix:

$$P = \begin{pmatrix} 0 & 0 & 0 \\ 0 & 0 & 0 \\ 0 & 0 & 1 \end{pmatrix}. \quad (3.80)$$

Using Eq. (3.54) in conjunction with Eq. (3.73), we see that it is only Γ_2 that contributes to the third row of M_n , *i.e.*,

$$\frac{v_2}{\sqrt{2}}\Gamma_2 = P \cdot M_n. \quad (3.81)$$

We also note the following:

$$P \cdot \Gamma_1 = 0, \quad P \cdot \Gamma_2 = \Gamma_2, \quad P \cdot \Delta_1 = 0, \quad P \cdot \Delta_2 = \Delta_2. \quad (3.82)$$

From Eq. (3.65) we recall that the matrices $N_{u,d}$ actually control the FCNC couplings. The non-diagonal part of N_d is given by

$$X = U_L^\dagger \cdot \frac{v_2}{\sqrt{2}}\Gamma_2 \cdot U_R \quad (3.83a)$$

$$= U_L^\dagger \cdot (P \cdot M_n) \cdot U_R \quad [\text{Using Eq. (3.81)}] \quad (3.83b)$$

$$= U_L^\dagger P U_L \cdot U_L^\dagger M_n U_R \quad (3.83c)$$

$$= U_L^\dagger P U_L \cdot D_d. \quad (3.83d)$$

Thus,

$$X_{AB} = \sum_C \left(U_L^\dagger P U_L \right)_{AC} (D_d)_{CB} \quad (3.84a)$$

$$= \sum_C \left(U_L^\dagger P U_L \right)_{AC} m_B^d \delta_{CB} = m_B^d \left(U_L^\dagger P U_L \right)_{AB}. \quad (3.84b)$$

But note that

$$U_L^\dagger = \begin{pmatrix} \checkmark & \checkmark & (U_L)_{31}^* \\ \checkmark & \checkmark & (U_L)_{32}^* \\ \checkmark & \checkmark & (U_L)_{33}^* \end{pmatrix}, \quad \text{and,} \quad PU_L = \begin{pmatrix} 0 & 0 & 0 \\ 0 & 0 & 0 \\ (U_L)_{31} & (U_L)_{32} & (U_L)_{33} \end{pmatrix}. \quad (3.85)$$

Thus,

$$\left(U_L^\dagger PU_L \right)_{AB} = (U_L)_{3A}^* (U_L)_{3B} \equiv V_{3A}^* V_{3B}, \quad (3.86)$$

where, in the last step, we have used Eq. (3.79). Hence, we obtain

$$X_{AB} = m_B^d V_{3A}^* V_{3B}. \quad (3.87)$$

Substituting this into Eq. (3.65b) we get

$$\begin{aligned} (N_d)_{AB}^t &= \tan \beta (D_d)_{AB} - (\tan \beta + \cot \beta) X_{AB} \\ &= \tan \beta m_A^d \delta_{AB} - (\tan \beta + \cot \beta) V_{3A}^* V_{3B} m_B^d. \end{aligned} \quad (3.88)$$

To obtain a simplified form for N_u^t , we note, similar to Eq. (3.81), that

$$\frac{v_2}{\sqrt{2}} \Delta_2 = P \cdot M_p. \quad (3.89)$$

In a similar way, we can write the following for the non-diagonal part of N_u^t :

$$Y = V_L^\dagger \cdot \frac{v_2}{\sqrt{2}} \Delta_2 \cdot V_R = V_L^\dagger PV_L \cdot D_u. \quad (3.90)$$

Because of the special form of V_L in Eq. (3.77), we have

$$PV_L = \begin{pmatrix} 0 & 0 & 0 \\ 0 & 0 & 0 \\ 0 & 0 & 1 \end{pmatrix} \Rightarrow V_L^\dagger PV_L = \begin{pmatrix} 0 & 0 & 0 \\ 0 & 0 & 0 \\ 0 & 0 & 1 \end{pmatrix}. \quad (3.91)$$

Substituting this into Eq. (3.90), one can easily verify

$$Y = \text{diag}\{0, 0, m_t\}. \quad (3.92)$$

Plugging this into Eq. (3.65b) we get the final expression for N_u^t :

$$\begin{aligned} N_u^t &= \tan \beta D_u - (\tan \beta + \cot \beta) Y \\ &= \tan \beta \text{diag}\{m_u, m_c, 0\} - \cot \beta \text{diag}\{0, 0, m_t\}. \end{aligned} \quad (3.93)$$

Since N_u^t is diagonal, there will be no Higgs mediated tree-level FCNC in the up sector and from Eq. (3.88) one can see that the tree-level FCNC in the down sector is controlled by the off-diagonal elements of the third row of the CKM matrix. Had we considered u- or c-type models, the tree-level FCNC in the down sector would be controlled by the first or second row of the CKM matrix respectively.

Constraints from flavor data: Here we will only consider the u-, c- and t-type BGL scenarios where the tree-level FCNC exists in the down sector. To begin with, it might be useful to rewrite the explicit expressions for the matrices that control the tree-level FCNC couplings for these models. The matrices N_u and N_d , for the u-, c- and t-type models, have the following form (the (i, j) indices in N_d refer to (d, s, b) quarks and the superscripts in bold font refer to the model type):

$$N_u^{\mathbf{u}} = \text{diag}\{-m_u \cot \beta, m_c \tan \beta, m_t \tan \beta\}, \quad (3.94a)$$

$$(N_d)_{ij}^{\mathbf{u}} = \tan \beta m_i \delta_{ij} - (\tan \beta + \cot \beta) V_{ui}^* V_{uj} m_j, \quad (3.94b)$$

$$N_u^{\mathbf{c}} = \text{diag}\{m_u \tan \beta, -m_c \cot \beta, m_t \tan \beta\}, \quad (3.94c)$$

$$(N_d)_{ij}^{\mathbf{c}} = \tan \beta m_i \delta_{ij} - (\tan \beta + \cot \beta) V_{ci}^* V_{cj} m_j, \quad (3.94d)$$

$$N_u^{\mathbf{t}} = \text{diag}\{m_u \tan \beta, m_c \tan \beta, -m_t \cot \beta\}, \quad (3.94e)$$

$$(N_d)_{ij}^{\mathbf{t}} = \tan \beta m_i \delta_{ij} - (\tan \beta + \cot \beta) V_{ti}^* V_{tj} m_j. \quad (3.94f)$$

In the leptonic sector (with only left-handed neutrinos), the Yukawa couplings of Eqs. (3.66) and (3.67) should be read with the replacement $(N_u, D_u) \rightarrow 0$, $V = 1$, and $N_d(D_d) \rightarrow N_e(D_e)$, with N_e resembling the diagonal N_u matrices in Eq. (3.94) with appropriate replacement of quark masses by the charged lepton masses. This means that there is no FCNC in the leptonic sector when the neutrinos are considered to be massless. But if we assume the neutrinos to be massive, then the tree-level FCNC in the leptonic sector will be controlled by the rows and columns of the PMNS matrix.

The CP-odd scalar mass eigenstate A would be massless if the symmetry of Eq. (3.71) is exact in the Higgs potential. Thus, in the 't Hooft sense, a light pseudoscalar will be natural in these models. While there are five free parameters in any BGL model, namely, α , β , m_{1+} , m_H , and m_A , we can make some reasonable simplifications. Considerations of perturbativity and stability of scalar potential ensure that $m_A \sim m_H$ if $\tan \beta \geq 10$ [55]. If m_A and m_H are large, we can even bring down the $\tan \beta$ limit further, say up to $\tan \beta = 5$. However, for the sake of simplicity and economy of parameters, we will assume $m_H = m_A$ for the remainder of this chapter unless explicitly mentioned otherwise. Thus, in the alignment limit, i.e. $\sin(\beta - \alpha) = 1$, we are left with only three unknown parameters: $\tan \beta$, m_{1+} and $m_{H/A}$. It should be noted though that consistency with the oblique T -parameter requires $m_{1+} \sim m_H$ once we assume $m_H = m_A$ [55].

Neutral meson mixing: Neutral meson mass differences offer important constraints. The tree-level scalar exchange contribution to the off-diagonal element of the 2×2 Hamiltonian matrix is given by [32]

$$(M_{12}^K)^{\text{BGL}} \approx \frac{5}{24} \frac{f_K^2 m_K^3}{v^2} (V_{id}^* V_{is})^2 \frac{1}{\mathcal{A}^2}, \quad (3.95)$$

where m_K is the neutral kaon mass and f_K is the decay constant. Similar expressions exist for B_d and B_s systems. The mass difference is given by $\Delta M_K \approx 2|M_{12}^K|$. The contributions of three neutral scalars are contained in

$$\begin{aligned} \frac{1}{\mathcal{A}^2} &= (\tan \beta + \cot \beta)^2 \left(\frac{\cos^2(\beta - \alpha)}{m_h^2} + \frac{\sin^2(\beta - \alpha)}{m_H^2} - \frac{1}{m_A^2} \right) \\ &= (\tan \beta + \cot \beta)^2 \left(\frac{1}{m_H^2} - \frac{1}{m_A^2} \right). \end{aligned} \quad (3.96)$$

The last equality in Eq. (3.96) holds in the alignment limit. The size of the prefactors in Eq. (3.95) tells us that $m_A = m_H$ is very well motivated from the neutral kaon mass difference for the u- and c-type models. For the t-type model, however, this degeneracy is more of an assumption than a requirement especially for $\tan \beta \sim 1$.

With the assumption $m_H = m_A$, the dominant contributions to neutral meson mass differences come from the charged Higgs box diagrams. The expressions for the loop-induced amplitudes are given explicitly in Appendix C. In Fig. 3.8, constraints have been placed assuming that the new physics contributions saturate the experimental values of ΔM [65]. For $\tan \beta > 1$, ΔM_d and ΔM_s severely restrict the u- and c-type models, whereas the t-type model can admit a light charged Higgs, at least for $m_H = m_A$. For large $\tan \beta$, ΔM_K offers a stronger constraint than $b \rightarrow s\gamma$ (discussed later) in the t-type model due to the dominance of the charm-induced box graph.

$b \rightarrow s\gamma$: The process $b \rightarrow s\gamma$ offers severe constraint on the charged Higgs mass [67, 68]. For Type II and Y models, in the charged Higgs Yukawa interaction, the up-type Yukawa coupling is multiplied by $\cot \beta$ while the down-type Yukawa is multiplied by $\tan \beta$. Their product is responsible for setting $\tan \beta$ -independent limit $m_{1+} > 300$ GeV for $\tan \beta > 1$ [61, 62, 69]. In Type I and X models, each of these couplings picks up a $\cot \beta$ factor, which is why there is essentially no bound on charged Higgs mass for $\tan \beta > 1$ in these models [61].

In the BGL class of models, the constraint on m_{1+} is different from that in Type I or Type X 2HDM (detailed expressions are displayed in Appendix C). This is because the BGL symmetry of Eq. (3.71) does not respect family universality. For the i -type BGL model, the relevant Yukawa couplings contain an overall factor of $(-\cot \beta)$ for vertices involving the i -th generation up-type fermion and a factor of $\tan \beta$ for the others. Consequently, the top loop contribution to the $b \rightarrow s\gamma$ amplitude will grow as $\tan^2 \beta$ for u- and c-type models resulting in very tight constraints

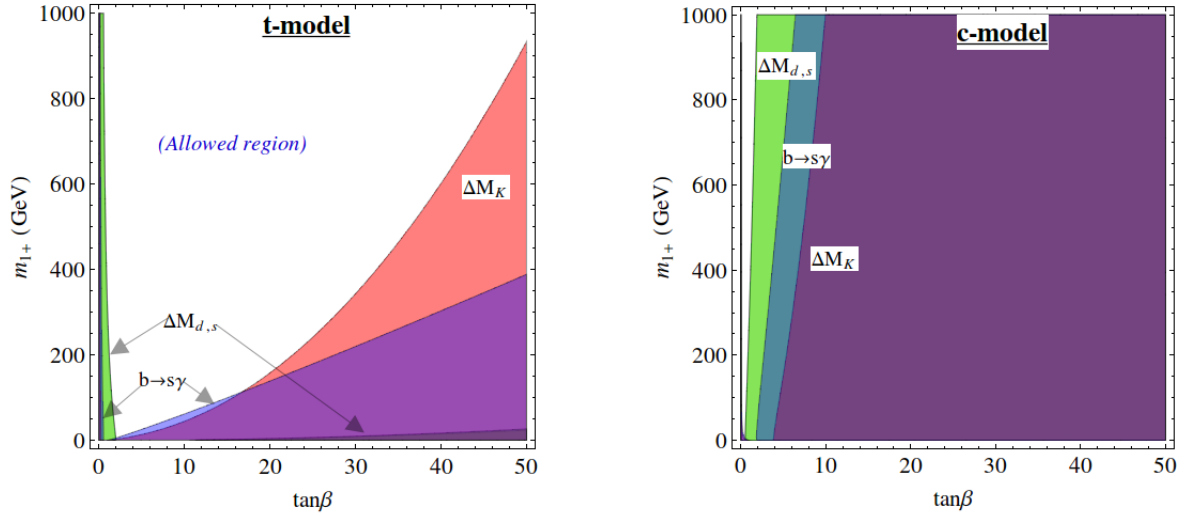


FIGURE 3.8: Constraints from various observables for t - and c -(u -) type BGL models. In the left panel (t -type), for large $\tan\beta$, ΔM_K offers a stronger constraint than $b \rightarrow s\gamma$. The vertical spiked shaded region in the extreme left also correspond to the entire disallowed region in Type I and X models. In the right panel (c - or u -types), ΔM_d and ΔM_s provide the most stringent constraints. Note that an assumption $m_H = m_A$ has been made to switch off the tree level contribution to the neutral meson mass differences. The figures have been taken from [66].

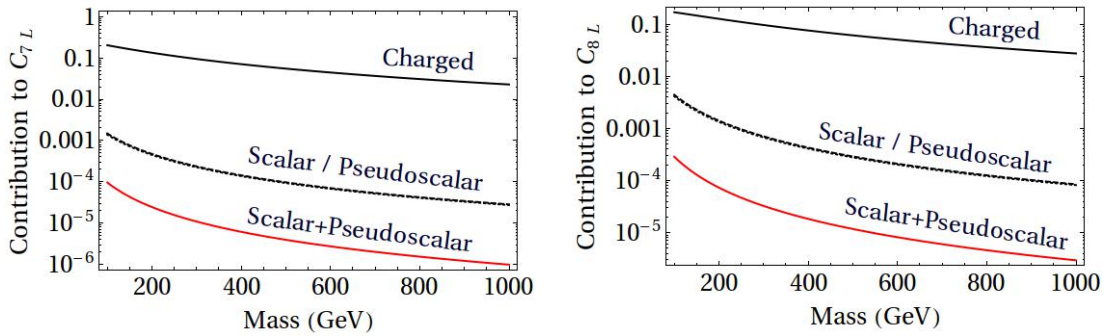


FIGURE 3.9: Magnitude of the contributions to the effective Wilson coefficients C_{7L} and C_{8L} for $b \rightarrow s\gamma$, coming from H_1^+ , H , and A , plotted against the corresponding masses. The middle curve in each panel shows the magnitude of the individual scalar and pseudoscalar contributions; they are too close to be differentiated in the shown scale. The lowest curve in each panel shows the sum of H and A contributions for the case $m_H = m_A$, which shows that the scalar and pseudoscalar contributions interfere destructively. C_{7R} and C_{8R} are suppressed by m_s/m_b and are not shown here. The figures have been taken from [66].

on m_{1+} for $\tan\beta > 1$. On the contrary, for t-type models, the top-loop contribution will decrease with increasing $\tan\beta$ and will hardly leave any effect for $\tan\beta > 1$, similar to what happens in the Type I and X models. But unlike in the latter scenarios, the charm loop amplitude in t-type BGL grows as $\tan^2\beta$. It becomes numerically important for large $\tan\beta$ and does not allow H_1^+ to be very light.

Taking the branching ratio $\text{Br}(b \rightarrow s\gamma)_{\text{SM}} = (3.15 \pm 0.23) \times 10^{-4}$ [70–72] and $\text{Br}(b \rightarrow s\gamma)_{\text{exp}} = (3.55 \pm 0.26) \times 10^{-4}$ [59], these features of the BGL models have been displayed in Fig. 3.8. The regions excluded at 95% CL from $b \rightarrow s\gamma$ have been shaded and appropriately marked. Note that we have considered not only the contributions from (H_1^+, u_i) loops, but also from $(H/A, d_i)$ loops (due to tree level FCNC couplings of H and A). The numerical effects of the latter are found to be small; we refer the reader to Fig. 3.9, where separate contributions from the charged and the neutral scalars to C_{7L} and C_{8L} are shown. The behavior can also be intuitively understood from the following comparison of the dominant contributions from the charged and neutral scalar induced loops to the $b \rightarrow s\gamma$ amplitude. The ratio of H_1^+ and (H/A) -induced loop contributions roughly goes like $(m_c^2 \tan^2\beta / m_b m_s)$ for large $\tan\beta$, and $(m_t^2 \cot^2\beta / m_b m_s)$ for $\tan\beta$ of the order of one. This justifies that the constraint from $b \rightarrow s\gamma$ essentially applies on the charged Higgs mass. In other words, that H_1^+ can be really light does not crucially depend on the values of m_H and m_A . From now on, we stick only to the t-type model to promote light charged Higgs phenomenology.

Other constraints: For t-type model, the branching ratios $\text{Br}(B \rightarrow D^{(*)}\tau\nu)$ and $\text{Br}(B^+ \rightarrow \tau\nu)$ do not receive any appreciable contributions unless the charged Higgs mass is unnaturally small defying the LEP2 direct search limit of 80 GeV [54]. The process $B_s \rightarrow \ell^+\ell^-$ proceeds at the tree level mediated by H/A providing important constraints. The amplitudes are proportional to $(\tan^2\beta + 1)/m_{H/A}^2$ for $\ell = e, \mu$, and $(\cot^2\beta + 1)/m_{H/A}^2$ for $\ell = \tau$. In Fig. 3.10 we have shaded the region excluded at 95% CL, obtained by comparing the SM expectation of $\text{Br}(B_s \rightarrow \mu^+\mu^-) = (3.65 \pm 0.23) \times 10^{-9}$ [73] with its experimental value $(3.2 \pm 1.0) \times 10^{-9}$ [74]. The details are provided in Appendix C. In the same plot we display different contours for $\text{Br}(B_s \rightarrow \tau^+\tau^-)/\text{Br}(B_s \rightarrow \tau^+\tau^-)_{\text{SM}}$, where we observe slight enhancement over the SM expectation.

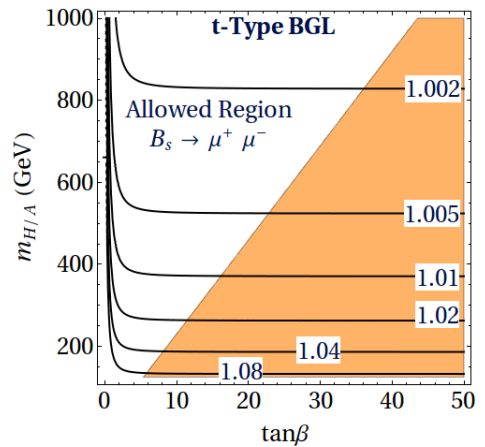


FIGURE 3.10: The shaded region is disallowed by $B_s \rightarrow \mu^+\mu^-$ at 95% CL. Contours of enhancements in $B_s \rightarrow \tau^+\tau^-$ over the SM estimate are also shown.

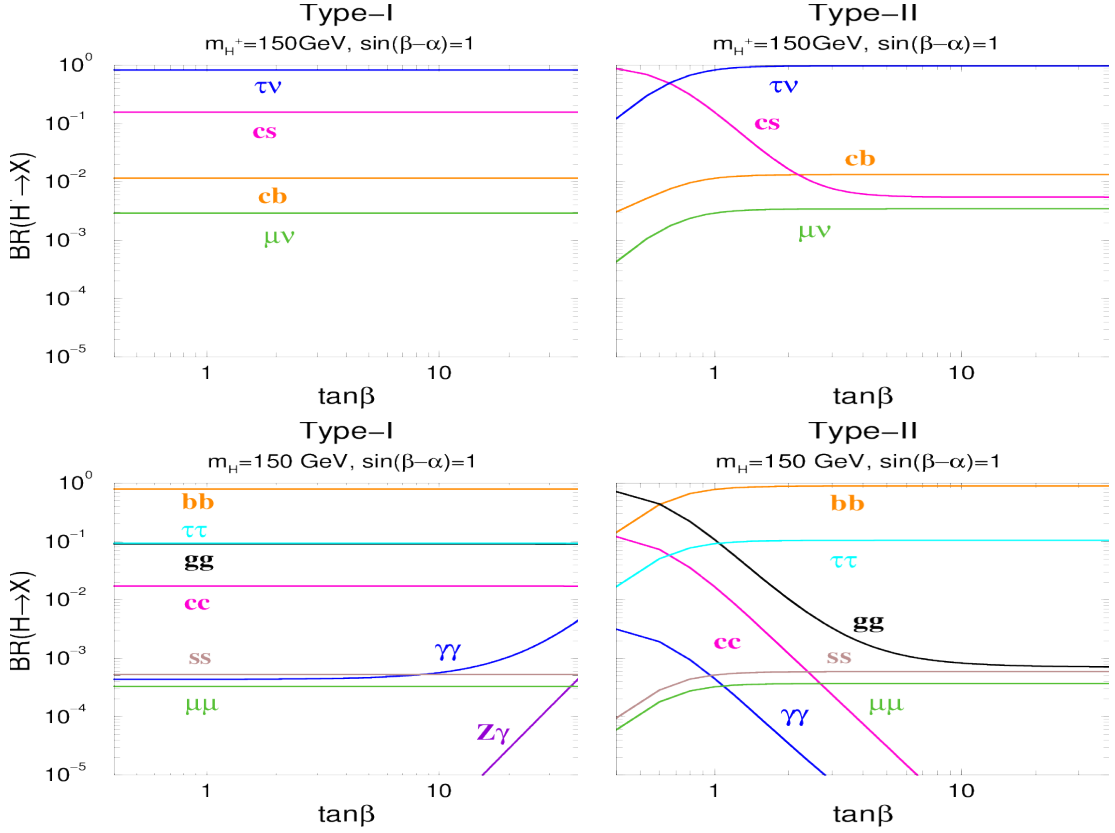


FIGURE 3.11: Branching ratios of H and H_1^+ in Type I and Type II models as a function of $\tan\beta$ for $m_H = m_{1+} = 150$ GeV in the alignment limit. The plots have been taken from [75].

3.3 Decay of the nonstandard Higgs bosons

In Type I model, the light charged Higgs goes to $\tau\nu$ and cs (below the tb threshold), and the branching ratios are independent of $\tan\beta$ (see Fig. 3.11), because both the leptonic and the quark couplings have the same $\cot\beta$ prefactor [75, 76]. In Type X model, the leptonic part has an overall $\tan\beta$ multiplicative factor, so the charged Higgs preferentially decays into third generation leptonic channels for large $\tan\beta$ (e.g. almost entirely so for $\tan\beta \geq 2.5$). In the t-type BGL scenario, the charged Higgs branching ratios into two-body fermionic final states have been plotted in Fig. 3.12. We have considered two benchmark values for m_{1+} , one below the tb threshold and the other well above it. To a good approximation it is enough to consider fermionic final states, because in the alignment limit the $W^\pm h H_1^\mp$ coupling vanishes and if we consider near degeneracy of m_{1+} and $m_{H/A}$ to satisfy the T -parameter constraint, then H_1^+ cannot decay into $W^+ S^0$ ($S^0 = H, A$) channel. Two noteworthy features which distinguish the t-type BGL model from others are: (i) the $\mu\nu$ final state dominates over $\tau\nu$ for $\tan\beta > 5$, which is a distinctive characteristic of t-type BGL model unlike any of the Type I, II, X or Y models (due to family nonuniversal BGL Yukawa couplings); (ii) for $\tan\beta > 10$, the branching ratio into cs significantly dominates over other channels including tb , again a unique feature of t-type

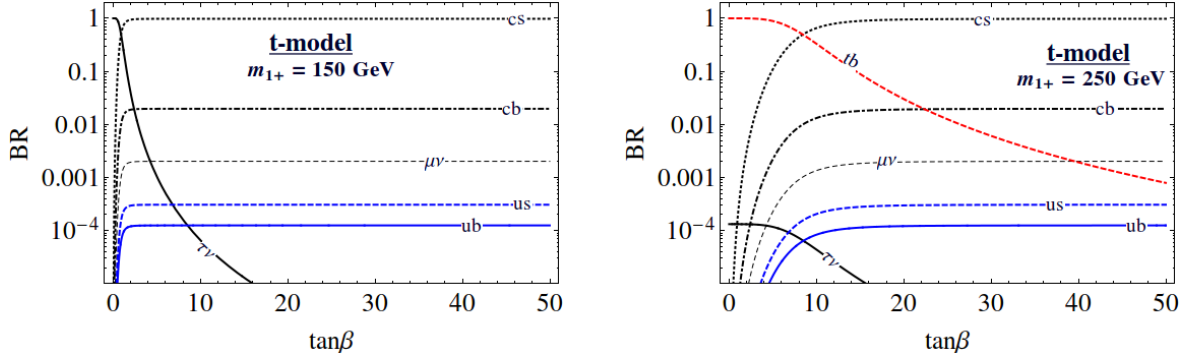


FIGURE 3.12: The charged Higgs branching ratios to two-body final states for two benchmark choices of m_{1+} . The figures have been taken from [66].

BGL. The reason for the latter can be traced to the relative size of the top and charm quark masses *vis-à-vis* the $\tan\beta$ or $\cot\beta$ prefactor. This will result in a dijet final state at the LHC, without any b -jet, and hence the signal will be extremely difficult to be deciphered over the standard QCD background.

We now discuss the decay branching ratios of the neutral scalar H . In the alignment limit HVV ($V = W, Z$) coupling vanishes. Hence we discuss flavor diagonal ff final states (flavor violating modes are CKM suppressed), together with $\gamma\gamma$ and gg final states. In conventional types of 2HDM, the bb and $\tau\tau$ final states dominate over cc and $\mu\mu$ channels, respectively [75]. Here, the hierarchy is reversed, which transpires from the expressions of N_d and N_u in Eq. (3.94). To provide an intuitive estimate of the signal strength, we define the following variable:

$$R_X = \frac{\sigma(pp \rightarrow H \rightarrow X)}{\sigma(pp \rightarrow h \rightarrow \gamma\gamma)}, \quad (3.97)$$

where the normalization has been done with respect to the SM Higgs production and its diphoton

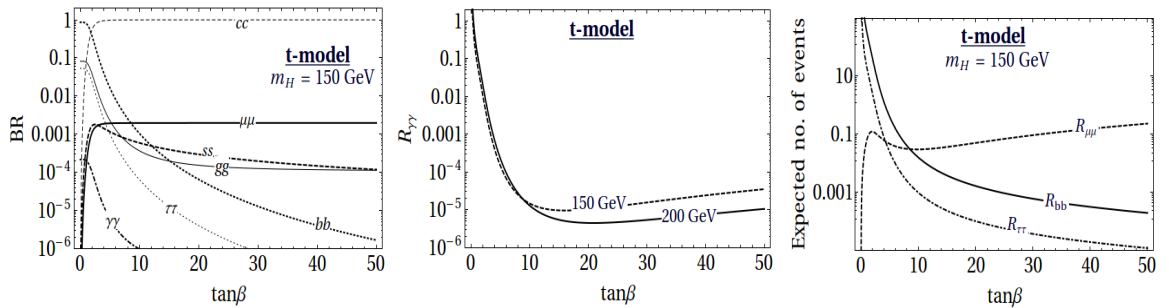


FIGURE 3.13: For various two-body final states, the R values, and the branching ratios of H . The figures have been taken from [66].

decay branching ratio. We recall that the loop contributions of charged scalars to $h \rightarrow \gamma\gamma$ is tiny as long as $m_{H/A} \simeq m_{1+}$ [55]. The relative merits of various channels have been plotted in Fig. 3.13. The crucial thing to observe is that although for $\tan\beta > 5$, H decays entirely into dijet (cc), the $\mu^+\mu^-$ mode may serve as a viable detection channel for H in future. With 20 fb^{-1}

luminosity at LHC8, the expected number of diphoton events from the SM Higgs decay is about 400. Fig. 3.13 shows that $R_{\mu\mu} \sim 0.1$, i.e. about 40 dimuon events from H decay should have been observed. However, they are going to be swamped by huge background (mainly Drell-Yan, also QCD jets faking dimuon) [77, 78]. At LHC14 with an integrated luminosity of 300 fb^{-1} , we expect about 39000 $h \rightarrow \gamma\gamma$ events [79], which means about 3900 $H \rightarrow \mu\mu$ events for $m_H = 150 \text{ GeV}$. Dimuon background studies at 14 TeV are not yet publicly available. A rough conservative extrapolation of the existing 7 and 8 TeV studies of the dimuon background [77, 78] gives us hope that the signal can be deciphered over the background. Note that these are all crude estimates, made mainly to get our experimental colleagues interested in probing such exotic decay modes. A more careful study including, e.g. detection efficiencies and detailed background estimates, is beyond the scope of this chapter. We emphasize that our scenario does not say that H , A or H_1^+ have to be necessarily light. If they are heavy as they are forced to be in many other 2HDMs ($\sim 500 \text{ GeV}$ or more), their direct detection in early LHC14 would be that much difficult. The feature that makes our scenario unique is the *possibility* of their relative lightness as well as unconventional decay signatures.

3.4 Loop induced decays of the SM-like Higgs

Since we are working in the alignment limit, the couplings of h with the fermions and gauge bosons will be exactly like in the SM. The production cross section of h will therefore be as expected in the SM. All the tree level decay widths of h will also have the SM values for the same reason. Loop induced decays like $h \rightarrow \gamma\gamma$ and $h \rightarrow Z\gamma$ will however have additional contributions from virtual charged scalars (H_1^\pm). Since the branching fractions of such decays are tiny, the total decay width is hardly modified.

The contribution of the W -boson loop and the top loop diagrams to $h \rightarrow \gamma\gamma$ and $h \rightarrow Z\gamma$ are same as in the SM. As regards the charged scalar induced loop, we first parametrize the cubic coupling $g_{hH_1^+H_1^-}$ in the following way:

$$g_{hH_1^+H_1^-} = \kappa_1 \frac{gm_{1+}^2}{M_W}, \quad (3.98)$$

where κ_1 is dimensionless. The diphoton decay width is then given by [27, 80]:

$$\Gamma(h \rightarrow \gamma\gamma) = \frac{\alpha^2 g^2}{2^{10} \pi^3} \frac{m_h^3}{M_W^2} \left| F_W + \frac{4}{3} F_t + \kappa_1 F_{1+} \right|^2, \quad (3.99)$$

where, introducing the notation

$$\tau_x \equiv (2m_x/m_h)^2, \quad (3.100)$$

the values of F_W , F_t and F_{i+} are given by

$$F_W = 2 + 3\tau_W + 3\tau_W(2 - \tau_W)f(\tau_W), \quad (3.101a)$$

$$F_t = -2\tau_t[1 + (1 - \tau_t)f(\tau_t)], \quad (3.101b)$$

$$F_{i+} = -\tau_{i+}[1 - \tau_{i+}f(\tau_{i+})]. \quad (3.101c)$$

If we assume $m_{1+} > 80$ GeV to respect the direct search bound [54], then $\tau_x > 1$ for $x = W, t, H_1^\pm$. In this limit

$$f(\tau) = \left[\sin^{-1} \left(\sqrt{1/\tau} \right) \right]^2. \quad (3.102)$$

The decay width for $h \rightarrow Z\gamma$ can analogously be written as:

$$\Gamma(h \rightarrow Z\gamma) = \frac{\alpha^2 g^2}{2^9 \pi^3} \frac{m_h^3}{M_W^2} \left| A_W + A_t + \kappa_1 A_{i+} \right|^2 \left(1 - \frac{M_Z^2}{m_h^2} \right)^3, \quad (3.103)$$

where, introducing

$$\eta_x = (2m_x/M_Z)^2, \quad (3.104)$$

the values of A_W , A_t and A_{i+} are given by [81]

$$A_W = \cot \theta_w \left[4(\tan^2 \theta_w - 3)I_2(\tau_W, \eta_W) + \left\{ \left(5 + \frac{2}{\tau_W} \right) - \left(1 + \frac{2}{\tau_W} \right) \tan^2 \theta_w \right\} I_1(\tau_W, \eta_W) \right], \quad (3.105a)$$

$$A_t = \frac{4 \left(\frac{1}{2} - \frac{4}{3} \sin^2 \theta_w \right)}{\sin \theta_w \cos \theta_w} \left[I_2(\tau_t, \eta_t) - I_1(\tau_t, \eta_t) \right], \quad (3.105b)$$

$$A_{i+} = \frac{(2 \sin^2 \theta_w - 1)}{\sin \theta_w \cos \theta_w} I_1(\tau_{i+}, \eta_{i+}). \quad (3.105c)$$

The functions I_1 and I_2 are given by

$$I_1(\tau, \eta) = \frac{\tau\eta}{2(\tau - \eta)} + \frac{\tau^2\eta^2}{2(\tau - \eta)^2} \left[f(\tau) - f(\eta) \right] + \frac{\tau^2\eta}{(\tau - \eta)^2} \left[g(\tau) - g(\eta) \right], \quad (3.106a)$$

$$I_2(\tau, \eta) = -\frac{\tau\eta}{2(\tau - \eta)} \left[f(\tau) - f(\eta) \right], \quad (3.106b)$$

where the function f has been defined in Eq. (3.102). Since $\tau_x, \eta_x > 1$ for $x = W, t, H_1^\pm$, the function g assumes the following form:

$$g(a) = \sqrt{a-1} \sin^{-1} \left(\sqrt{1/a} \right). \quad (3.107)$$

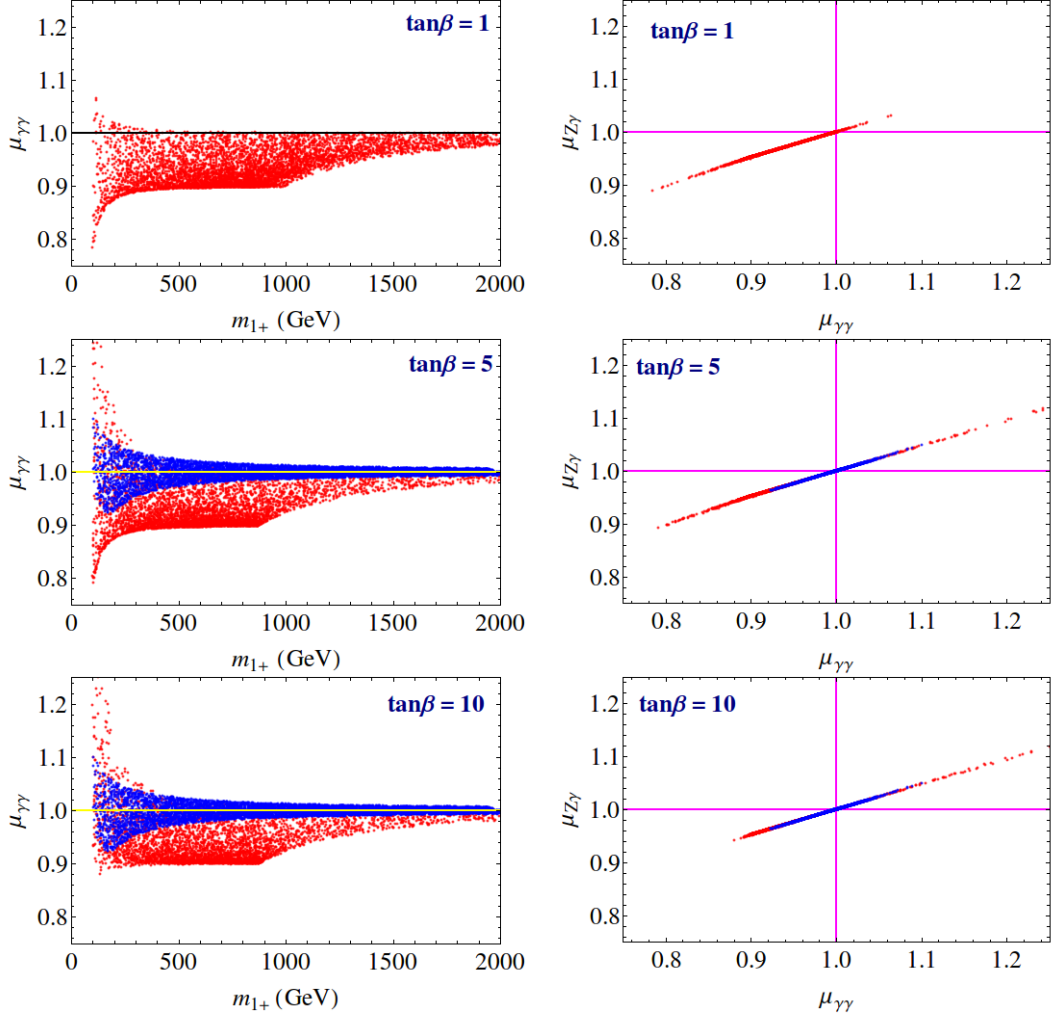


FIGURE 3.14: (*2HDMs with softly broken $U(1)$ symmetry in the scalar potential.*) The left panels show allowed regions in m_{1+} - $\mu_{\gamma\gamma}$ plane for three values of $\tan\beta$, while the right panels show correlation between $\mu_{\gamma\gamma}$ and $\mu_{Z\gamma}$ for the same choices of $\tan\beta$. The regions shown in red are allowed by unitarity and stability, while the blue regions additionally pass the T-parameter test. We put $m_{1+} > 100$ GeV and $m_H > m_h$. These figures have been taken from [55].

In the alignment limit with softly broken $U(1)$ symmetry, the parameter κ_1 which appears in Eqs. (3.98), (3.99) and (3.103) is given by

$$\kappa_1 = \frac{1}{m_{1+}^2} (m_A^2 - m_{1+}^2 - \frac{1}{2}m_h^2). \quad (3.108)$$

The appearance of m_A in Eq. (3.108) is merely an artefact of the $U(1)$ symmetry in the scalar potential which enforces $\lambda_5 = \lambda_6$. In the more general potential of Eq. (3.3), the expression for κ_1 involves λ_5 , which has nothing to do with m_A . The decoupling behavior of κ_1 for large m_{1+} is not then guaranteed, as noted in Refs. [66, 82]. Later we will see that such nondecoupling of charged scalars are not unique to the 2HDMs. In fact, whenever we have a scalar potential invariant under an exact discrete symmetry with multiple Higgs doublets, this kind of nondecoupling phenomena are expected. However, in the present scenario, unitarity conditions bound the splitting between

heavy scalar masses [55], ensuring smooth decoupling of κ_1 with increasing m_{1+} . As we have noticed, this splitting is also controlled by the T -parameter.

In our case, the quantities $\mu_{\gamma\gamma}$ and $\mu_{Z\gamma}$, defined through the equations

$$\mu_{\gamma\gamma} = \frac{\sigma(pp \rightarrow h)}{\sigma^{\text{SM}}(pp \rightarrow h)} \cdot \frac{\text{BR}(h \rightarrow \gamma\gamma)}{\text{BR}^{\text{SM}}(h \rightarrow \gamma\gamma)}, \quad (3.109)$$

$$\mu_{Z\gamma} = \frac{\sigma(pp \rightarrow h)}{\sigma^{\text{SM}}(pp \rightarrow h)} \cdot \frac{\text{BR}(h \rightarrow Z\gamma)}{\text{BR}^{\text{SM}}(h \rightarrow Z\gamma)}, \quad (3.110)$$

assume the following forms:

$$\mu_{\gamma\gamma} = \frac{\Gamma(h \rightarrow \gamma\gamma)}{\Gamma^{\text{SM}}(h \rightarrow \gamma\gamma)} = \frac{\left|F_W + \frac{4}{3}F_t + \kappa_1 F_{1+}\right|^2}{\left|F_W + \frac{4}{3}F_t\right|^2}, \quad (3.111)$$

$$\mu_{Z\gamma} = \frac{\Gamma(h \rightarrow Z\gamma)}{\Gamma^{\text{SM}}(h \rightarrow Z\gamma)} = \frac{\left|A_W + A_t + \kappa_1 A_{1+}\right|^2}{\left|A_W + A_t\right|^2}. \quad (3.112)$$

In Fig. 3.14, we show the variation of $\mu_{\gamma\gamma}$ against m_{1+} and the correlation between $\mu_{\gamma\gamma}$ and $\mu_{Z\gamma}$ for $\tan\beta = 1, 5, 10$. When we show the variation of $\mu_{\gamma\gamma}$ with m_{1+} , we take into consideration all values of m_H and m_A which are allowed in Fig. 3.6. In case of Fig. 3.14, the red points are those which are allowed by unitarity and stability constraints, while the superimposed blue points are allowed by the T -parameter. The points allowed by unitarity prefer suppression in $\mu_{\gamma\gamma}$ compared to the SM expectation. The correlation between $\mu_{\gamma\gamma}$ and $\mu_{Z\gamma}$ can in principle be used for discriminating new physics models with increased sensitivity in the future course of the LHC run.

3.5 Conclusions

In the first part of this chapter, we have revisited the constraints from tree-unitarity and stability in the context of 2HDMs. The observed scalar at LHC has been identified with the lightest CP-even scalar of the model. The *alignment limit* has been imposed in view of the conformity of the LHC Higgs data with the SM predictions. These are the *new* informations that became available only after the Higgs discovery. If the Z_2 symmetry is exact in the potential, it is found that all the nonstandard masses are restricted below 1 TeV from unitarity with the upper limit on m_H being highly correlated to $\tan\beta$. The value of $\tan\beta$ is also confined within the range $1/8 < \tan\beta < 8$ from unitarity and stability. The constraints from flavor data severely restrict the region with $\tan\beta < 1$. Therefore, for an exact Z_2 symmetry, $\tan\beta$ is bounded within a very narrow range of $1 < \tan\beta < 8$ when a light charged scalar with mass around 400 GeV is looked for.

In the presence of an appropriate soft breaking parameter the bounds on $\tan\beta$ will be diluted. However, for large values of $\tan\beta$, the unitarity and stability conditions will render a strong correlation between the soft breaking parameter and m_H as appears in Eq. (3.45). It is also worth noting that the value of $\mu_{\gamma\gamma}$ can play a crucial role in the presence of soft breaking. For example, if $\mu_{\gamma\gamma}$ is measured to be consistent with the SM expectation with 5% accuracy then one can conclude $m_{H^+}^2 \approx 1/2\lambda_5 v^2$ [51] for any value of $\tan\beta$. Thus, for large values of $\tan\beta$ one may expect $m_H^2 \approx m_{H^+}^2 \approx 1/2\lambda_5 v^2$. We have also studied quantitative correlation among the non-standard scalar masses in a class of 2HDM with a global $U(1)$ symmetry in the potential. In this context, we have observed that for values of $\tan\beta \sim 5$ or larger, all the three non-standard scalar masses are roughly degenerate. More specifically, in this limit unitarity dictates m_H and m_A to be almost equal and $|m_{1^+}^2 - m_H^2|$ to be small, while the T -parameter restricts $|m_{1^+} - m_H|$ to be very small. It is also important to note that, due to the global $U(1)$ symmetry, unitarity restricts mass-squared differences and not the individual masses of the non-standard scalars.

Later in this chapter, we have shown that BGL class of two-Higgs-doublet model admits charged and additional neutral scalars which can be as light as ~ 150 GeV. They successfully negotiate the stringent constraints from radiative b -decay, neutral meson mass differences, and dimuon decays of B mesons. Special features of Yukawa couplings in this model lead to characteristic decay signatures of the nonstandard scalars, which are different from the signatures of similar scalars in other 2HDM variants. Preferential decays of both the charged and additional neutral scalars into *second*, rather than the *third*, generation fermions for $\tan\beta > 5$ constitute the trademark distinguishing feature of this scenario, which can be tested in the high luminosity option of the LHC or at the ILC.

Symmetry is what we see at a glance; based on the fact that there is no reason for any difference . . .

Blaise Pascal

4

Analysis of an extended scalar sector with S_3 symmetry

The newly observed boson at the Large Hadron Collider (LHC) [16, 17] fits very well to the description of the Higgs scalar in the Standard Model (SM). The SM relies on the minimal choice that a single Higgs doublet provides masses to all particles. But unexplained phenomena like neutrino masses and existence dark matter motivate us to contemplate other avenues beyond the SM (BSM). Majority of these BSM scenarios extend the SM Higgs sector predicting a richer scalar spectrum. One of them – the S_3 flavor model – stems from an effort to answer the aesthetic question as to why there are precisely three fermion generations [83]. Keeping the fermions in appropriate S_3 -multiplets, it is possible to reproduce all the measured parameters of the CKM and PMNS matrices as well as make testable predictions for the unknown parameters of the PMNS matrix [84–104]. But one needs at least three Higgs doublets to achieve this goal [86]. However, the S_3 invariant scalar potential contains some new parameters which are difficult to constrain phenomenologically. Although some lower bounds on the additional scalar masses can be placed from the Higgs mediated flavor changing neutral current (FCNC) processes [105], these bounds rely heavily on the Yukawa structure of the model. In this article we will present some new bounds on the physical scalar masses which do not depend on the parameters of the Yukawa sector. To achieve this, we will employ the prescription of tree unitarity which is known to be able to set upper limits on different scalar masses [12]. Although various aspects of the S_3 scalar potential have been discussed in the literature [106, 107], to the best of our knowledge, this

is the first attempt to derive the exact unitarity constraints on the quartic couplings in the S_3 invariant three-Higgs-doublet model (S3HDM) scalar potential. We also identify an *alignment limit* in the context of S3HDM where a CP-even Higgs with SM-like properties can be obtained. Since the recent LHC Higgs data seem to increasingly lean towards the SM expectations, our numerical analysis will be restricted to this limit.

The chapter is organized as follows: in Section 4.1 we discuss the scalar potential and derive necessary conditions for the potential to be bounded from below. In Section 4.2 we minimize the potential and calculate the physical scalar masses. In this section we also figure out an alignment limit in which one neutral CP-even physical scalar behaves exactly like the SM Higgs. In Section 4.3 we derive the exact constraints arising from the considerations of tree level unitarity and use them to constrain the nonstandard scalar masses. In Section 4.4 we quantitatively investigate the effect of the charged scalar induced loops on $h \rightarrow \gamma\gamma$ and $h \rightarrow Z\gamma$ signal strengths. Finally, we summarize our findings in Section 4.5.

4.1 The scalar potential

S_3 is the permutation group involving three objects, $\{\Phi_a, \Phi_b, \Phi_c\}$. The three dimensional representation of S_3 is not an irreducible one simply because we can easily construct a linear combination of the elements, $\Phi_a + \Phi_b + \Phi_c$, which remains unaltered under the permutation of the indices. We choose to decompose the three dimensional representation into a singlet and doublet as follows:

$$\mathbf{1} : \quad \Phi_3 = \frac{1}{\sqrt{3}}(\Phi_a + \Phi_b + \Phi_c), \quad (4.1a)$$

$$\mathbf{2} : \quad \begin{pmatrix} \Phi_1 \\ \Phi_2 \end{pmatrix} = \begin{pmatrix} \frac{1}{\sqrt{2}}(\Phi_a - \Phi_b) \\ \frac{1}{\sqrt{6}}(\Phi_a + \Phi_b - 2\Phi_c) \end{pmatrix}. \quad (4.1b)$$

The elements of S_3 for this particular doublet representation are given by:

$$\begin{pmatrix} \cos \theta & \sin \theta \\ -\sin \theta & \cos \theta \end{pmatrix}, \quad \begin{pmatrix} \cos \theta & \sin \theta \\ \sin \theta & -\cos \theta \end{pmatrix}, \quad \text{for } \left(\theta = 0, \pm \frac{2\pi}{3} \right). \quad (4.2)$$

The most general renormalizable potential invariant under S_3 can be written in terms of Φ_3 , Φ_1 and Φ_2 as follows [106–110]:

$$V(\Phi) = V_2(\Phi) + V_4(\Phi), \quad (4.3a)$$

$$\text{where, } V_2(\Phi) = \mu_1^2(\Phi_1^\dagger\Phi_1 + \Phi_2^\dagger\Phi_2) + \mu_3^2\Phi_3^\dagger\Phi_3, \quad (4.3b)$$

$$V_4(\Phi) = \lambda_1(\Phi_1^\dagger\Phi_1 + \Phi_2^\dagger\Phi_2)^2 + \lambda_2(\Phi_1^\dagger\Phi_2 - \Phi_2^\dagger\Phi_1)^2 \\ + \lambda_3 \left\{ (\Phi_1^\dagger\Phi_2 + \Phi_2^\dagger\Phi_1)^2 + (\Phi_1^\dagger\Phi_1 - \Phi_2^\dagger\Phi_2)^2 \right\}$$

$$\begin{aligned}
& +\lambda_4 \left\{ (\Phi_3^\dagger \Phi_1)(\Phi_1^\dagger \Phi_2 + \Phi_2^\dagger \Phi_1) + (\Phi_3^\dagger \Phi_2)(\Phi_1^\dagger \Phi_1 - \Phi_2^\dagger \Phi_2) + \text{h.c.} \right\} \\
& +\lambda_5 (\Phi_3^\dagger \Phi_3)(\Phi_1^\dagger \Phi_1 + \Phi_2^\dagger \Phi_2) + \lambda_6 \left\{ (\Phi_3^\dagger \Phi_1)(\Phi_1^\dagger \Phi_3) + (\Phi_3^\dagger \Phi_2)(\Phi_2^\dagger \Phi_3) \right\} \\
& +\lambda_7 \left\{ (\Phi_3^\dagger \Phi_1)(\Phi_3^\dagger \Phi_1) + (\Phi_3^\dagger \Phi_2)(\Phi_3^\dagger \Phi_2) + \text{h.c.} \right\} + \lambda_8 (\Phi_3^\dagger \Phi_3)^2. \quad (4.3c)
\end{aligned}$$

In general λ_4 and λ_7 can be complex, but we assume them to be real so that CP symmetry is not broken explicitly. For the stability of the vacuum in the asymptotic limit we impose the requirement that there should be no direction in the field space along which the potential becomes infinitely negative. The necessary and sufficient conditions for this is well known in the context of two Higgs-doublet models (2HDMs) [33]. For the potential of Eq. (4.3), a 2HDM equivalent situation arise if one of the doublets is made identically zero. Then it is quite straightforward to find the following *necessary* conditions for the global stability in the asymptotic limit:

$$\lambda_1 > 0, \quad (4.4a)$$

$$\lambda_8 > 0, \quad (4.4b)$$

$$\lambda_1 + \lambda_3 > 0, \quad (4.4c)$$

$$2\lambda_1 + (\lambda_3 - \lambda_2) > |\lambda_2 + \lambda_3|, \quad (4.4d)$$

$$\lambda_5 + 2\sqrt{\lambda_8(\lambda_1 + \lambda_3)} > 0, \quad (4.4e)$$

$$\lambda_5 + \lambda_6 + 2\sqrt{\lambda_8(\lambda_1 + \lambda_3)} > 2|\lambda_7|, \quad (4.4f)$$

$$\lambda_1 + \lambda_3 + \lambda_5 + \lambda_6 + 2\lambda_7 + \lambda_8 > 2|\lambda_4|. \quad (4.4g)$$

To avoid confusion, we wish to mention that an equivalent doublet representation,

$$\begin{pmatrix} \chi_1 \\ \chi_2 \end{pmatrix} = \frac{1}{\sqrt{2}} \begin{pmatrix} i & 1 \\ -i & 1 \end{pmatrix} \begin{pmatrix} \Phi_1 \\ \Phi_2 \end{pmatrix}, \quad (4.5)$$

has also been used in the literature. In terms of this new doublet, the quartic part of the scalar potential is written as [111–113]:

$$\begin{aligned}
V_4 = & \frac{\beta_1}{2} (\chi_1^\dagger \chi_1 + \chi_2^\dagger \chi_2)^2 + \frac{\beta_2}{2} (\chi_1^\dagger \chi_1 - \chi_2^\dagger \chi_2)^2 + \beta_3 (\chi_1^\dagger \chi_2)(\chi_2^\dagger \chi_1) + \frac{\beta_4}{2} (\Phi_3^\dagger \Phi_3)^2 \\
& +\beta_5 (\Phi_3^\dagger \Phi_3)(\chi_1^\dagger \chi_1 + \chi_2^\dagger \chi_2) + \beta_6 \Phi_3^\dagger (\chi_1 \chi_1^\dagger + \chi_2 \chi_2^\dagger) \Phi_3 + \beta_7 \left\{ (\Phi_3^\dagger \chi_1)(\Phi_3^\dagger \chi_2) + \text{h.c.} \right\} \\
& +\beta_8 \left\{ \Phi_3^\dagger (\chi_1 \chi_2^\dagger \chi_1 + \chi_2 \chi_1^\dagger \chi_2) + \text{h.c.} \right\}. \quad (4.6)
\end{aligned}$$

It is easy to verify that the parameters of Eq. (4.6) are related to the parameters of Eq. (4.3c) in the following way:

$$\begin{aligned}
\beta_1 &= 2\lambda_1; \quad \beta_2 = -2\lambda_2; \quad \beta_3 = 4\lambda_3; \quad \beta_4 = 2\lambda_8; \\
\beta_5 &= \lambda_5; \quad \beta_6 = \lambda_6; \quad \beta_7 = 2\lambda_7; \quad \beta_8 = -\sqrt{2}\lambda_4. \quad (4.7)
\end{aligned}$$

This mapping can be used to translate the constraints on λ s into constraints on β s. In this chapter we choose to work with the parametrization of Eq. (4.3).

4.2 Physical eigenstates

We represent the scalar doublets in the following way:

$$\Phi_k = \begin{pmatrix} w_k^+ \\ \frac{1}{\sqrt{2}}(v_k + h_k + iz_k) \end{pmatrix} \quad \text{for } k = 1, 2, 3. \quad (4.8)$$

We shall assume that CP symmetry is not spontaneously broken and so the vacuum expectation values (vevs) are taken to be real. They also satisfy the usual vev relation: $v = \sqrt{v_1^2 + v_2^2 + v_3^2} = 246$ GeV. The minimization conditions for the scalar potential of Eq. (4.3) reads:

$$2\mu_1^2 = -2\lambda_1(v_1^2 + v_2^2) - 2\lambda_3(v_1^2 + v_2^2) - v_3\{6\lambda_4 v_2 + (\lambda_5 + \lambda_6 + 2\lambda_7)v_3\}, \quad (4.9a)$$

$$2\mu_1^2 = -2\lambda_1(v_1^2 + v_2^2) - 2\lambda_3(v_1^2 + v_2^2) - \frac{3v_3}{v_2}\lambda_4(v_1^2 - v_2^2) - (\lambda_5 + \lambda_6 + 2\lambda_7)v_3^2, \quad (4.9b)$$

$$2\mu_3^2 = \lambda_4 \frac{v_2}{v_3}(v_2^2 - 3v_1^2) - (\lambda_5 + \lambda_6 + 2\lambda_7)(v_1^2 + v_2^2) - 2\lambda_8 v_3^2. \quad (4.9c)$$

For the self-consistency of Eqs. (4.9a) and (4.9b), two possible scenarios arise¹:

$$\lambda_4 = 0, \quad (4.10a)$$

$$\text{or, } v_1 = \sqrt{3}v_2. \quad (4.10b)$$

In the following subsections we shall discuss each of the above scenarios separately.

4.2.1 Case-I ($\lambda_4 = 0$)

Since CP symmetry is assumed to be exact in the scalar potential, the neutral physical states will be eigenstates of CP too. We find that the mass-squared matrices in the scalar(M_S^2), pseudoscalar(M_P^2) and charged(M_C^2) sectors are simultaneously block diagonalizable by the following matrix:

$$X = \begin{pmatrix} \cos \gamma & -\sin \gamma & 0 \\ \sin \gamma & \cos \gamma & 0 \\ 0 & 0 & 1 \end{pmatrix} \quad \text{with } \tan \gamma = \frac{v_1}{v_2}. \quad (4.11)$$

¹Another possibility, $v_3 = 0$, while mathematically consistent, is unattractive. This is because, in some S_3 structure of the Yukawa sector, the S_3 -singlet fermion generation will remain massless.

For the charged mass matrix, we obtain:

$$XM_C^2 X^T = \begin{pmatrix} m_{1+}^2 & 0 & 0 \\ 0 & -\frac{1}{2}v_3^2(\lambda_6 + 2\lambda_7) & \frac{1}{2}v_3\sqrt{v_1^2 + v_2^2}(\lambda_6 + 2\lambda_7) \\ 0 & \frac{1}{2}v_3\sqrt{v_1^2 + v_2^2}(\lambda_6 + 2\lambda_7) & -\frac{1}{2}(v_1^2 + v_2^2)(\lambda_6 + 2\lambda_7) \end{pmatrix}, \quad (4.12)$$

where, one of the charged Higgs (H_1^+) with mass m_{1+} is defined as:

$$H_1^+ = \cos \gamma w_1^+ - \sin \gamma w_2^+, \quad (4.13a)$$

$$m_{1+}^2 = -\left\{2\lambda_3 \sin^2 \beta + \frac{1}{2}(\lambda_6 + 2\lambda_7) \cos^2 \beta\right\} v^2, \quad (4.13b)$$

$$\text{with, } \tan \beta = \frac{\sqrt{v_1^2 + v_2^2}}{v_3}. \quad (4.13c)$$

The second charged Higgs (H_2^+) along with the massless Goldstone (ω^+), which will appear as the longitudinal component of the W -boson, can be obtained by diagonalizing the remaining 2×2 block:

$$\begin{pmatrix} H_2^+ \\ \omega^+ \end{pmatrix} = \begin{pmatrix} \cos \beta & -\sin \beta \\ \sin \beta & \cos \beta \end{pmatrix} \begin{pmatrix} w_2'^+ \\ w_3^+ \end{pmatrix} \quad \text{with, } w_2'^+ = \sin \gamma w_1^+ + \cos \gamma w_2^+. \quad (4.14)$$

The mass of the second charged Higgs is given by:

$$m_{2+}^2 = -\frac{1}{2}(\lambda_6 + 2\lambda_7)v^2. \quad (4.15)$$

Similar considerations for the pseudoscalar part gives:

$$XM_P^2 X^T = \begin{pmatrix} \frac{1}{2}m_{A1}^2 & 0 & 0 \\ 0 & -v_3^2\lambda_7 & v_3\sqrt{v_1^2 + v_2^2}\lambda_7 \\ 0 & v_3\sqrt{v_1^2 + v_2^2}\lambda_7 & -(v_1^2 + v_2^2)\lambda_7 \end{pmatrix}, \quad (4.16)$$

where, the pseudoscalar state (A_1) with mass eigenvalue m_{A1} is defined as:

$$A_1 = \cos \gamma z_1 - \sin \gamma z_2, \quad (4.17a)$$

$$m_{A1}^2 = -2\{(\lambda_2 + \lambda_3) \sin^2 \beta + \lambda_7 \cos^2 \beta\} v^2, \quad (4.17b)$$

where, $\tan \beta$ has already been defined in Eq. (4.13c). Similar to the charged part, here also the second pseudoscalar (A_2) along with the massless Goldstone (ζ) can be obtained as follows:

$$\begin{pmatrix} A_2 \\ \zeta \end{pmatrix} = \begin{pmatrix} \cos \beta & -\sin \beta \\ \sin \beta & \cos \beta \end{pmatrix} \begin{pmatrix} z_2' \\ z_3 \end{pmatrix} \quad \text{with, } z_2' = \sin \gamma z_1 + \cos \gamma z_2, \quad (4.18a)$$

$$\text{and, } m_{A2}^2 = -2\lambda_7 v^2. \quad (4.18b)$$

Finally, for the CP-even part we have:

$$XM_S^2 X^T = \begin{pmatrix} 0 & 0 & 0 \\ 0 & A'_S & -B'_S \\ 0 & -B'_S & C'_S \end{pmatrix}, \quad (4.19a)$$

$$\text{where, } A'_S = (\lambda_1 + \lambda_3)(v_1^2 + v_2^2), \quad (4.19b)$$

$$B'_S = -\frac{1}{2}v_3\sqrt{v_1^2 + v_2^2}(\lambda_5 + \lambda_6 + 2\lambda_7), \quad (4.19c)$$

$$C'_S = \lambda_8 v_3^2. \quad (4.19d)$$

The massless state (h^0), as also noted in [114], is given by:

$$h^0 = \cos \gamma h_1 - \sin \gamma h_2. \quad (4.20)$$

But we wish to add here that the appearance of a massless scalar is not surprising. One can easily verify that the potential of Eq. (4.3) has the following $SO(2)$ symmetry for $\lambda_4 = 0$:

$$\begin{pmatrix} \Phi'_1 \\ \Phi'_2 \end{pmatrix} = \begin{pmatrix} \cos \theta & -\sin \theta \\ \sin \theta & \cos \theta \end{pmatrix} \begin{pmatrix} \Phi_1 \\ \Phi_2 \end{pmatrix} \quad (4.21)$$

Since $SO(2)$ is a continuous symmetry isomorphic to $U(1)$, a massless physical state is expected. Other two physical scalars are obtained as follows:

$$\begin{pmatrix} h \\ H \end{pmatrix} = \begin{pmatrix} \cos \alpha & -\sin \alpha \\ \sin \alpha & \cos \alpha \end{pmatrix} \begin{pmatrix} h'_2 \\ h_3 \end{pmatrix} \quad \text{with, } h'_2 = \sin \gamma h_1 + \cos \gamma h_2, \quad (4.22a)$$

$$\text{and, } \tan 2\alpha = \frac{2B'_S}{A'_S - C'_S}. \quad (4.22b)$$

We assume H and h to be the heavier and lighter CP-even mass eigenstates respectively, with the following eigenvalues:

$$m_H^2 = (A'_S + C'_S) + \sqrt{(A'_S - C'_S)^2 + 4B_S'^2}, \quad (4.23a)$$

$$m_h^2 = (A'_S + C'_S) - \sqrt{(A'_S - C'_S)^2 + 4B_S'^2}. \quad (4.23b)$$

At this stage, it is worth noting that we can define two intermediate scalar states, H^0 and R , as

$$\begin{pmatrix} R \\ H^0 \end{pmatrix} = \begin{pmatrix} \cos \beta & -\sin \beta \\ \sin \beta & \cos \beta \end{pmatrix} \begin{pmatrix} h'_2 \\ h_3 \end{pmatrix}, \quad (4.24)$$

with the property that H^0 has the exact SM couplings with the vector boson pairs and fermions. H^0 does not take part in the flavor changing processes as well. Of course, H^0 and R are not the

physical eigenstates in general but are related to them in the following way:

$$h = \cos(\beta - \alpha)R + \sin(\beta - \alpha)H^0, \quad (4.25a)$$

$$H = -\sin(\beta - \alpha)R + \cos(\beta - \alpha)H^0. \quad (4.25b)$$

In view of the fact that a 125 GeV scalar with SM-like properties has already been observed at the LHC, we wish the lighter CP-even mass eigenstate (h) to coincide with H^0 . Then we must require:

$$\cos(\beta - \alpha) \approx 0. \quad (4.26)$$

In analogy with the 2HDM case [33], this limit can be taken as the *alignment limit* in the context of a 3HDM with an S_3 symmetry. We must emphasize though, the term ‘alignment limit’ does not necessarily imply the heaviness of the additional scalars. Considering Eqs. (4.20) and (4.24), it is also interesting to note that the state h^0 , being orthogonal to H^0 , does not have any trilinear h^0VV ($V = W, Z$) coupling. But, in general, it will have flavor changing coupling in the Yukawa sector. This type of neutral massless state with flavor changing fermionic coupling will be ruled out from the well measured values of neutral meson mass differences. This means that the choice $\lambda_4 = 0$ is phenomenologically unacceptable and we shall not pursue this scenario any further.

4.2.2 Case-II ($v_1 = \sqrt{3}v_2$)

This situation has recently been analyzed in [115]. We, however, use a convenient parametrization that can provide intuitive insight into the scenario and additionally, we also discuss the possibility of a *alignment limit* in the same way as done in the previous subsection.

The definitions for the angles, γ and β , and the diagonalizing matrix, X , remain the same as before. Only difference is that, due to the vev alignment ($v_1 = \sqrt{3}v_2$), $\tan \gamma (= \sqrt{3})$ and hence X is determined completely. Now only two of the vevs, v_2 and v_3 (say), can be considered independent and $\tan \beta$ is given in terms of them as follows :

$$\tan \beta = \frac{2v_2}{v_3}. \quad (4.27)$$

The charged and pseudoscalar mass eigenstates have the same form as before; only the mass eigenvalues get modified due to the presence of λ_4 :

$$m_{1+}^2 = - \left\{ 2\lambda_3 \sin^2 \beta + \frac{5}{2}\lambda_4 \sin \beta \cos \beta + \frac{1}{2}(\lambda_6 + 2\lambda_7) \cos^2 \beta \right\} v^2, \quad (4.28a)$$

$$m_{2+}^2 = -\frac{1}{2} \{ \lambda_4 \tan \beta + (\lambda_6 + 2\lambda_7) \} v^2, \quad (4.28b)$$

$$m_{A1}^2 = - \left\{ 2(\lambda_2 + \lambda_3) \sin^2 \beta + \frac{5}{2}\lambda_4 \sin \beta \cos \beta + 2\lambda_7 \cos^2 \beta \right\} v^2, \quad (4.28c)$$

$$m_{A_2}^2 = - \left(\frac{1}{2} \lambda_4 \tan \beta + 2\lambda_7 \right) v^2. \quad (4.28d)$$

In the presence of λ_4 , analysis of the scalar part will be slightly different :

$$XM_S^2 X^T = \begin{pmatrix} \frac{1}{2} m_{h_0}^2 & 0 & 0 \\ 0 & A_S & -B_S \\ 0 & -B_S & C_S \end{pmatrix}, \quad (4.29a)$$

$$\text{where, } A_S = (\lambda_1 + \lambda_3) v^2 \sin^2 \beta + \frac{3}{4} \lambda_4 v^2 \sin \beta \cos \beta, \quad (4.29b)$$

$$B_S = -\frac{1}{2} \left\{ \frac{3}{2} \lambda_4 \sin^2 \beta + (\lambda_5 + \lambda_6 + 2\lambda_7) \sin \beta \cos \beta \right\} v^2, \quad (4.29c)$$

$$C_S = -\frac{\lambda_4}{4} v^2 \sin^2 \beta \tan \beta + \lambda_8 v^2 \cos^2 \beta. \quad (4.29d)$$

The state, h^0 , will no longer be massless, in fact,

$$m_{h_0}^2 = -\frac{9}{2} \lambda_4 v^2 \sin \beta \cos \beta. \quad (4.30)$$

The angle α , which was used to rotate from (h'_2, h_3) basis to the physical (H, h) basis, should be redefined as :

$$\tan 2\alpha = \frac{2B_S}{A_S - C_S}, \quad (4.31)$$

and corresponding mass eigenvalues should have the following expressions :

$$m_H^2 = (A_S + C_S) + \sqrt{(A_S - C_S)^2 + 4B_S^2}, \quad (4.32a)$$

$$m_h^2 = (A_S + C_S) - \sqrt{(A_S - C_S)^2 + 4B_S^2}. \quad (4.32b)$$

The conclusion of the previous subsection that in the alignment limit, $\cos(\beta - \alpha) = 0$, h possesses SM-like gauge and Yukawa couplings, still holds. It should be emphasized that the Yukawa couplings of h in this limit, resembles that of the SM, do not depend on the transformation properties of the fermions under S_3 . Also, the self couplings of h coincides with the corresponding SM expressions in the alignment limit :

$$\mathcal{L}_h^{\text{self}} = -\frac{m_h^2}{2v} h^3 - \frac{m_h^2}{8v^2} h^4. \quad (4.33)$$

Similar to the case described in the previous subsection, h^0 will not have any $h^0 V V$ ($V = W, Z$) couplings, but in the present scenario, we may identify a symmetry which forbids such couplings. Note that, when the specified relation between v_1 and v_2 is taken, there exists a two dimensional

Physical States	Transformation under Z_2
h^0, H_1^\pm, A_1	Odd
H^0, R, H_2^\pm, A_2	Even

TABLE 4.1: Z_2 parity assignments to the physical mass eigenstates.

representation of Z_2 :

$$\begin{pmatrix} 1 & 0 \\ 0 & 1 \end{pmatrix}, \quad \frac{1}{2} \begin{pmatrix} 1 & \sqrt{3} \\ \sqrt{3} & -1 \end{pmatrix}, \quad (4.34)$$

which was initially a subgroup of the original S_3 symmetry, remains intact even after the spontaneous symmetry breaking, *i.e.*, the vacuum is invariant under this Z_2 symmetry. This allows us to assign a Z_2 parity for different physical states and this should be conserved in the theory. The state h^0 is odd under this Z_2 and this is what forbids it to couple with the VV pair. In fact, using the assignments of Table 4.1, together with CP symmetry, many of the scalar self couplings can be inferred to be zero.

In connection with the number of independent parameters in the Higgs potential, we note that there were ten to start with ($\mu_{1,3}$ and $\lambda_{1,2,\dots,8}$). μ_1 and μ_3 can be traded for v_2 and v_3 or, equivalently for v and $\tan\beta$. The remaining eight λ s can be traded for seven physical Higgs masses and α . The connections are given below :

$$\lambda_1 = \frac{1}{2v^2 \sin^2 \beta} \left\{ (m_h^2 \cos^2 \alpha + m_H^2 \sin^2 \alpha) + \left(m_{1+}^2 - m_{2+}^2 \cos^2 \beta - \frac{1}{9} m_{h0}^2 \right) \right\}, \quad (4.35a)$$

$$\lambda_2 = \frac{1}{2v^2 \sin^2 \beta} \left\{ (m_{1+}^2 - m_{A1}^2) - (m_{2+}^2 - m_{A2}^2) \cos^2 \beta \right\}, \quad (4.35b)$$

$$\lambda_3 = \frac{1}{2v^2 \sin^2 \beta} \left(\frac{4}{9} m_{h0}^2 + m_{2+}^2 \cos^2 \beta - m_{1+}^2 \right), \quad (4.35c)$$

$$\lambda_4 = -\frac{2 m_{h0}^2}{9} \frac{1}{v^2 \sin \beta \cos \beta}, \quad (4.35d)$$

$$\lambda_5 = \frac{1}{v^2} \left\{ \frac{\sin \alpha \cos \alpha}{\sin \beta \cos \beta} (m_H^2 - m_h^2) + 2m_{2+}^2 + \frac{1}{9} \frac{m_{h0}^2}{\cos^2 \beta} \right\}, \quad (4.35e)$$

$$\lambda_6 = \frac{1}{v^2} \left(\frac{1}{9} \frac{m_{h0}^2}{\cos^2 \beta} + m_{A2}^2 - 2m_{2+}^2 \right), \quad (4.35f)$$

$$\lambda_7 = \frac{1}{2v^2} \left(\frac{1}{9} \frac{m_{h0}^2}{\cos^2 \beta} - m_{A2}^2 \right), \quad (4.35g)$$

$$\lambda_8 = \frac{1}{2v^2 \cos^2 \beta} \left\{ (m_h^2 \sin^2 \alpha + m_H^2 \cos^2 \alpha) - \frac{1}{9} m_{h0}^2 \tan^2 \beta \right\}. \quad (4.35h)$$

In passing, we wish to state that for the analysis purpose we will always be working in the alignment limit with $v_1 = \sqrt{3}v_2$.

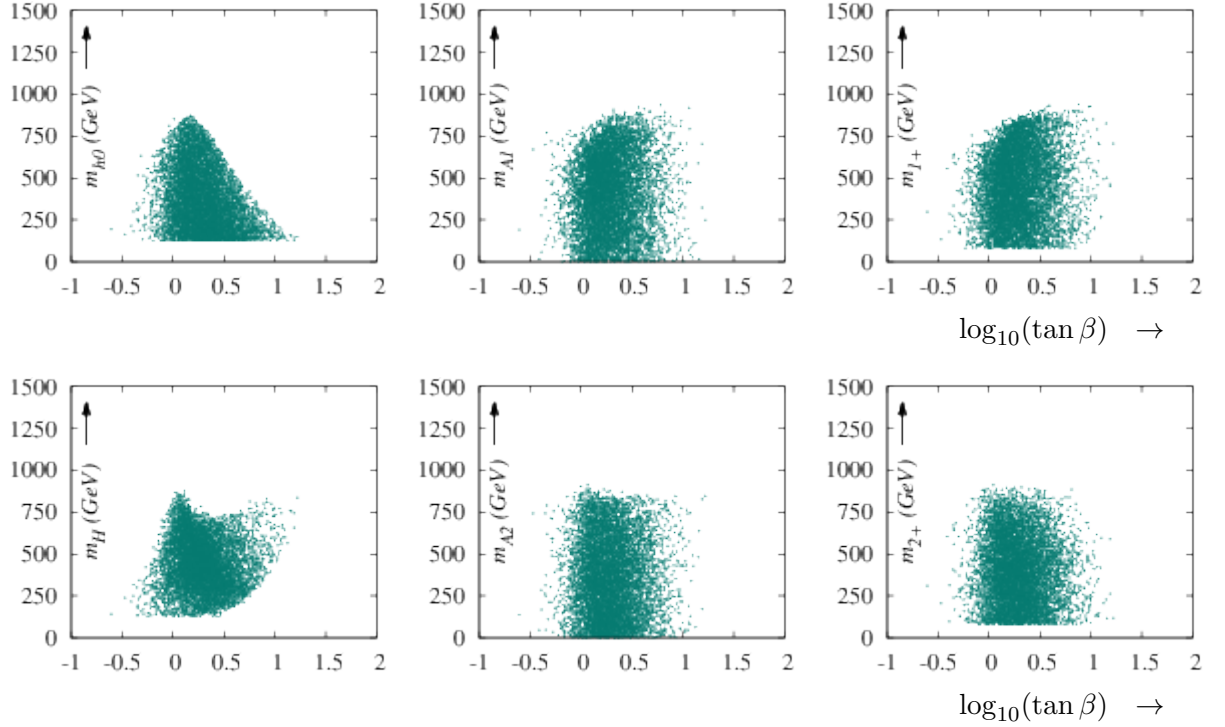


FIGURE 4.1: (Case-II) Regions allowed from unitarity and stability. We have fixed m_h at 125 GeV and taken $m_{1+}, m_{2+} > 80$ GeV and $m_H, m_{h0} > m_h$.

4.3 Constraints from unitarity

In this context, the pioneering work has been done by Lee, Quigg and Thacker (LQT) [12]. They have analyzed several two body scatterings involving longitudinal gauge bosons and physical Higgs in the SM. All such scattering amplitudes are proportional to Higgs quartic coupling in the high energy limit. The $\ell = 0$ partial wave amplitude (a_0) is then extracted from these amplitudes and cast in the form of an S-matrix having different two-body states as rows and columns. The largest eigenvalue of this matrix is bounded by the unitarity constraint, $|a_0| < 1$. This restricts the quartic Higgs self coupling and therefore the Higgs mass to a maximum value.

The procedure has been extended to the case of a 2HDM scalar potential [44–47]. We take it one step further and apply it in the context of 3HDMs. Here also same types of two body scattering channels are considered. Thanks to the equivalence theorem [48, 49], we can use unphysical Higgses instead of actual longitudinal components of the gauge bosons when considering the high energy limit. So, we can use the Goldstone-Higgs potential of Eq. (4.3) for this analysis. Still it will be a much involved calculation. But we notice that the diagrams containing trilinear vertices will be suppressed by a factor of E^2 coming from the intermediate propagator. Thus they do not contribute at high energies, – only the quartic couplings contribute. Clearly the physical Higgs masses that could come from the propagators, do not enter this analysis. Since we are interested only in the eigenvalues of the S-matrix, this allows us to work with the original fields of Eq. (4.3c) instead of the physical mass eigenstates. After an inspection of all the neutral

and charged two-body channels, we find the following eigenvalues to be bounded from unitarity:

$$|a_i^\pm|, |b_i| \leq 16\pi, \text{ for } i = 1, 2, \dots, 6. \quad (4.36)$$

The expressions for the individual eigenvalues in terms of λ s are given below:

$$a_1^\pm = \left(\lambda_1 - \lambda_2 + \frac{\lambda_5 + \lambda_6}{2} \right) \pm \sqrt{\left(\lambda_1 - \lambda_2 + \frac{\lambda_5 + \lambda_6}{2} \right)^2 - 4 \left\{ (\lambda_1 - \lambda_2) \left(\frac{\lambda_5 + \lambda_6}{2} \right) - \lambda_4^2 \right\}}, \quad (4.37a)$$

$$a_2^\pm = (\lambda_1 + \lambda_2 + 2\lambda_3 + \lambda_8) \pm \sqrt{(\lambda_1 + \lambda_2 + 2\lambda_3 + \lambda_8)^2 - 4 \{ \lambda_8(\lambda_1 + \lambda_2 + 2\lambda_3) - 2\lambda_7^2 \}}, \quad (4.37b)$$

$$a_3^\pm = (\lambda_1 - \lambda_2 + 2\lambda_3 + \lambda_8) \pm \sqrt{(\lambda_1 - \lambda_2 + 2\lambda_3 + \lambda_8)^2 - 4 \left\{ \lambda_8(\lambda_1 - \lambda_2 + 2\lambda_3) - \frac{\lambda_6^2}{2} \right\}}, \quad (4.37c)$$

$$a_4^\pm = \left(\lambda_1 + \lambda_2 + \frac{\lambda_5}{2} + \lambda_7 \right) \pm \sqrt{\left(\lambda_1 + \lambda_2 + \frac{\lambda_5}{2} + \lambda_7 \right)^2 - 4 \left\{ (\lambda_1 + \lambda_2) \left(\frac{\lambda_5}{2} + \lambda_7 \right) - \lambda_4^2 \right\}}, \quad (4.37d)$$

$$a_5^\pm = (5\lambda_1 - \lambda_2 + 2\lambda_3 + 3\lambda_8) \pm \sqrt{(5\lambda_1 - \lambda_2 + 2\lambda_3 + 3\lambda_8)^2 - 4 \left\{ 3\lambda_8(5\lambda_1 - \lambda_2 + 2\lambda_3) - \frac{1}{2}(2\lambda_5 + \lambda_6)^2 \right\}}, \quad (4.37e)$$

$$a_6^\pm = \left(\lambda_1 + \lambda_2 + 4\lambda_3 + \frac{\lambda_5}{2} + \lambda_6 + 3\lambda_7 \right) \pm \sqrt{\left(\lambda_1 + \lambda_2 + 4\lambda_3 + \frac{\lambda_5}{2} + \lambda_6 + 3\lambda_7 \right)^2 - 4 \left\{ (\lambda_1 + \lambda_2 + 4\lambda_3) \left(\frac{\lambda_5}{2} + \lambda_6 + 3\lambda_7 \right) - 9\lambda_4^2 \right\}}, \quad (4.37f)$$

$$b_1 = \lambda_5 + 2\lambda_6 - 6\lambda_7, \quad (4.37g)$$

$$b_2 = \lambda_5 - 2\lambda_7, \quad (4.37h)$$

$$b_3 = 2(\lambda_1 - 5\lambda_2 - 2\lambda_3), \quad (4.37i)$$

$$b_4 = 2(\lambda_1 - \lambda_2 - 2\lambda_3), \quad (4.37j)$$

$$b_5 = 2(\lambda_1 + \lambda_2 - 2\lambda_3), \quad (4.37k)$$

$$b_6 = \lambda_5 - \lambda_6. \quad (4.37l)$$

In passing, we remark that the perturbativity criteria, $|\lambda_i| < 4\pi$, coming from the requirement that the leading order contribution to the physical amplitude must have higher magnitude than the subleading order, may have some ambiguity in this context. This is due to the fact the individual λ s do not appear in the quartic couplings involving the physical scalars. Hence the combination of λ s, that constitute the physical couplings, should be used for this purpose and it does not necessarily imply that the individual λ s should be bounded. We have presented here the exact constraints on λ s which should be satisfied for unitarity not to be violated.

Eqs. (4.4) and (4.37) can be used to put limits on the physical Higgs masses. For this purpose, we work in the alignment limit taking the lightest scalar (h) to be the SM-like Higgs that has been found at the LHC and we set its mass at 125 GeV. We also assume the charged scalars (m_{1+} and m_{2+}) to be heavier than 80 GeV to respect the direct search bound from LEP2 [54]. To collect sufficient number of data points we have generated fifty million random

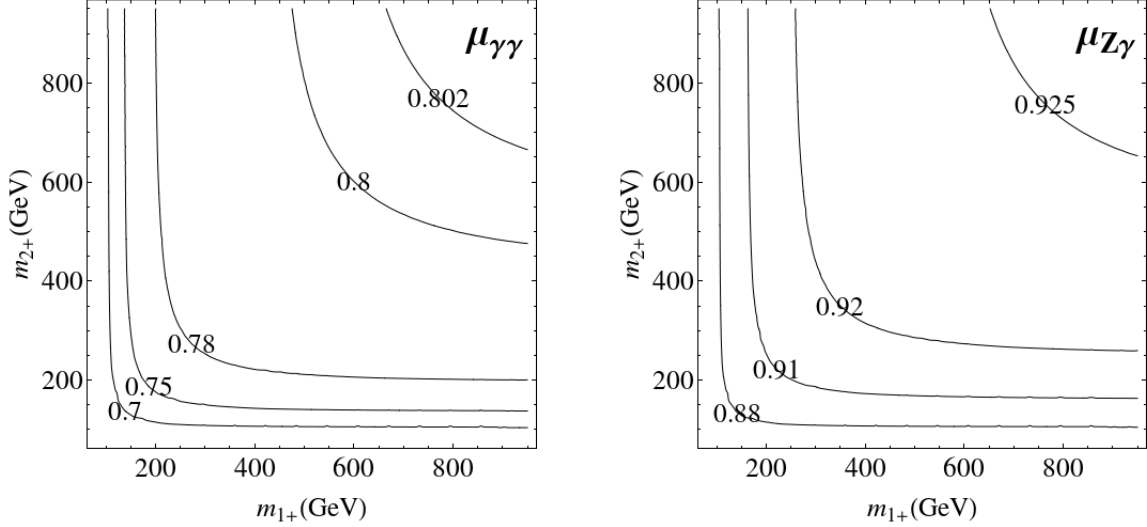


FIGURE 4.2: Signal strengths for diphoton and Z -photon decay modes within the allowed range for charged Higgs masses.

sets of $\{\tan \beta, m_{h0}, m_H, m_{A1}, m_{A2}, m_{1+}, m_{2+}\}$ by varying $\tan \beta$ from 0.1 to 100 and filter them through the combined constraints from unitarity and stability. The sets that survive the filtering are plotted in Figure 4.1. The bounds that follow from these figures are listed below:

- $\tan \beta \in [0.3, 17]$,
- $m_{h0} < 870$ GeV, $m_H < 880$ GeV, $m_{A1} < 940$ GeV, $m_{A2} < 910$ GeV, $m_{1+} < 940$, $m_{2+} < 910$ GeV.

It is interesting to note that if the observed scalar at the LHC has its root in the S3HDM, then there must be several other nonstandard scalars with masses below 1 TeV.

4.4 Impact on loop induced Higgs decays

Similar to the 2HDM case, to display the contribution of the charged scalar loops to the decay amplitudes in a convenient form, we define dimensionless parameters, κ_i ($i = 1, 2$), in the following way:

$$g_{hH_i^+H_i^-} = \kappa_i \frac{gm_{i+}^2}{M_W}. \quad (4.38)$$

Following this definition in analogy with the 2HDM case, we can write the diphoton and Z -photon signal strengths in the alignment limit as follows:

$$\mu_{\gamma\gamma} = \frac{\Gamma(h \rightarrow \gamma\gamma)}{\Gamma^{\text{SM}}(h \rightarrow \gamma\gamma)} = \frac{\left| F_W + \frac{4}{3}F_t + \sum_{i=1}^2 \kappa_i F_{i+} \right|^2}{\left| F_W + \frac{4}{3}F_t \right|^2}, \quad (4.39)$$

$$\mu_{Z\gamma} = \frac{\Gamma(h \rightarrow Z\gamma)}{\Gamma^{\text{SM}}(h \rightarrow Z\gamma)} = \frac{\left| A_W + A_t + \sum_{i=1}^2 \kappa_i A_{i+} \right|^2}{\left| A_W + A_t \right|^2}, \quad (4.40)$$

where the expressions for the quantities F_x and A_x already appear in Eqs. (3.101) and (3.105). In the alignment limit, the parameters κ_i ($i = 1, 2$), which appear in Eq. (4.38) are given by,

$$\kappa_i = - \left(1 + \frac{m_h^2}{2m_{i+}^2} \right). \quad (4.41)$$

As the charged Higgs becomes heavy, the quantity F_{i+} , for example, saturates to $\frac{1}{3}$. So the decoupling of charged Higgs from loop induced Higgs decay depends on how κ_i behaves with increasing m_{i+} . It follows from Eq. (4.41) that $\kappa_i \rightarrow -1$ if $m_{i+} \gg m_h$. Consequently, the charged Higgs never decouples from the diphoton or Z -photon decay amplitudes. In fact, it reduces the decay widths from their corresponding SM expectations. These features have been displayed in Figure 4.2 where we have made a contour plot by varying the charged Higgs masses within the allowed ranges coming from unitarity and vacuum stability. We find that $\mu_{\gamma\gamma}$ and $\mu_{Z\gamma}$ should lie within $[0.42, 0.80]$ and $[0.73, 0.93]$ for $m_{1+} \in [80, 950]$ and $m_{2+} \in [80, 950]$. We must admit though, this nondecoupling of charged scalar is not a unique feature of a S3HDM as it is also known to be present in the context of a 2HDMs [55, 82, 116, 117]. Currently both the ATLAS and CMS data shows agreement with the SM expectations [40, 41]. Thus a precise measurement of the diphoton and Z -photon signal strengths can pin down the difference between the SM Higgs and a SM-like Higgs arising from an extended scalar sector.

4.5 Conclusions

In this chapter the scalar sector of an S3HDM has been analyzed in detail. The major findings are listed below:

- The minimization of the scalar potential leads to a specific relation between the vevs of the first two doublets, $v_1 = \sqrt{3}v_2$ in particular.
- In this limit we find a Z_2 subgroup of S_3 that remains unbroken even after the spontaneous symmetry breaking. The different scalar mass eigenstates can then be assigned with appropriate Z_2 parity which can help us understand why certain couplings do not appear in the theory.
- Additionally, we have identified an alignment limit for this model where the lightest CP-even scalar has the exact same coupling as the SM Higgs with the other SM particles.

- We have also derived the exact tree unitarity constraints and exploited them, in the decoupling limit, to put new bounds on the physical nonstandard Higgs masses, which we consider to be an important development in the multi-Higgs context.
- From unitarity and stability $\tan\beta$ is likely to be in the range $[0.3,17]$ and all the nonstandard Higgs masses lie below 1 TeV.
- Regarding the decay of the SM-like S_3 Higgs, we have observed that the charged Higgs never decouples from the diphoton or Z -photon decay modes. The additional contributions from the charged Higgs loops to the decay amplitudes actually reduces the signal strengths of these modes. Although this depletion may not be a unique property of this scenario, but any statistically significant enhancement in $h \rightarrow \gamma\gamma$ and/or $h \rightarrow Z\gamma$ modes will certainly disfavor the possibility of an SM-like Higgs arising from an S3HDM.

5

The Higgs or a Higgs? Will the LHC be able to decipher?

The behavior of the scalar boson observed at the CERN LHC is tantalizingly close to that of the SM Higgs boson. A very timely and relevant question is whether this scalar is the only one of its type as predicted by the SM, or it is the first to have been discovered in a family of more such species arising from an underlying extended scalar sector. A natural extension of the SM scalar structure is realized by adding more $SU(2)$ scalar doublets, which we consider in this chapter. There are two advantages for choosing doublets. First, the ρ -parameter remains unity at tree level. Second, it is straightforward to find a combination, namely,

$$h = \frac{1}{v} \sum_{i=1}^n v_i h_i, \quad \text{with } v^2 = \sum_{i=1}^n v_i^2 = (246 \text{ GeV})^2, \quad (5.1)$$

(v_i is the vev of the i -th doublet and h_i is the corresponding real scalar field), which has SM-like couplings with fermions and gauge bosons. This is not in general a mass eigenstate. But when we demand that this is indeed the physical state observed at the LHC with a mass $m_h \approx 125$ GeV, we are automatically led to the so called *alignment limit*. This limit is motivated by the LHC data on the Higgs boson signal strengths in different channels which are showing increasing affinity towards the SM predictions. In this chapter we pay specific attention to the $h \rightarrow \gamma\gamma$ process. Though this process is loop driven and has a small branching ratio, it played

an important role in the Higgs discovery. Importantly, this branching ratio is expected to be measured in LHC-14 with much greater accuracy. Now, additional $SU(2)$ scalar doublets would bring in additional states, both charged and neutral, in the spectrum. Here our primary concern is how those charged scalars couple to h and how much they contribute to the $h \rightarrow \gamma\gamma$ rate as virtual states in loops. This leads to the observation that even when the masses of the charged scalars floating in the loop are taken to very large values, they do not *necessarily* decouple from this process. Deciphering the underlying reasons behind this constitutes the motive of this chapter. Although this has been noted in the past in the context of 2HDMs, only some cursory remarks were made on it without exploring its full implications [55, 82, 116–119]. We investigate the rôle of symmetries which are imposed on the scalar potential in figuring out under what conditions the decoupling of heavy charged scalars in the $h \rightarrow \gamma\gamma$ loop takes place. The upshot is that if the potential has an exact Z_2 symmetry *and* both the scalars receive vevs, which is the case for a large class of 2HDM scenarios [29], the contribution of the charged scalar does not decouple. If Z_2 is softly broken by a term in the potential then decoupling can be achieved at the expense of tuning of parameters. On the other hand, a global $U(1)$ symmetry followed by its soft breaking can ensure decoupling. For simplicity, we first demonstrate this behavior in the context of 2HDM. We then address the same question, for the first time, in the context of 3HDMs. It is not difficult to foresee what happens if we add more doublets, which leads us to draw an important conclusion: unless decoupling is ensured, e.g. as we did by imposing a global $U(1)$ symmetry in the 2HDM potential, precision measurements of $h \rightarrow \gamma\gamma$ branching ratio can put constraints on the number of additional non-inert scalar doublets regardless of how heavy the charged scalars are. It should be recalled that only lower bounds on charged scalar masses have been placed from processes like $b \rightarrow s\gamma$, as the effects decouple when their masses are heavy for all such flavor observables. Thus, precision measurements of $h \rightarrow \gamma\gamma$ would provide complementary information. Incidentally, whatever we comment on $h \rightarrow \gamma\gamma$ applies for $h \rightarrow Z\gamma$ as well at least on a qualitative level.

It has already been emphasized in the preceding chapters that in multi doublet scalar models, the production cross section as well as the tree-level decay widths of the Higgs boson remain unaltered from their respective SM expectations in the alignment limit. Only the loop induced decay modes like $h \rightarrow \gamma\gamma$ and $h \rightarrow Z\gamma$ will pick up additional contributions induced by virtual charged scalars. However, the branching ratios into these channels are too tiny compared to other dominant modes. As a result, the total Higgs decay width will be hardly modified. Considering all these, the expression for the diphoton signal strength is simplified to

$$\mu_{\gamma\gamma} \equiv \frac{\sigma(pp \rightarrow h)}{\sigma^{\text{SM}}(pp \rightarrow h)} \cdot \frac{\text{BR}(h \rightarrow \gamma\gamma)}{\text{BR}^{\text{SM}}(h \rightarrow \gamma\gamma)} = \frac{\Gamma(h \rightarrow \gamma\gamma)}{\Gamma^{\text{SM}}(h \rightarrow \gamma\gamma)}. \quad (5.2)$$

For convenience, we parametrize again the coupling of h to the charged scalars in the following generic way:

$$g_{hH_i^+H_i^-} = \kappa_i \frac{gm_{i+}^2}{M_W}, \quad (5.3)$$

where m_{i+} is the mass of the i -th charged scalar (H_i^\pm). As we will see later, the decoupling or nondecoupling behavior of the i -th charged scalar from $\mu_{\gamma\gamma}$ is encoded in κ_i . The expression of the Higgs to diphoton signal strength will be given by

$$\mu_{\gamma\gamma} = \frac{\left|F_W + \frac{4}{3}F_t + \sum_i \kappa_i F_{i+}\right|^2}{\left|F_W + \frac{4}{3}F_t\right|^2}, \quad (5.4)$$

where the expressions for F_x appear in Eq. (3.101). In the limit the charged scalar is very heavy, the quantity F_{i+} saturates to $1/3$. If κ_i also saturates to some finite value in that limit then the charged scalar would not decouple from the $h \rightarrow \gamma\gamma$ loop. Then no matter how heavy the charged scalar is, $\mu_{\gamma\gamma}$ will differ from its SM value. If the experimental value of $\mu_{\gamma\gamma}$ eventually settles on very close to the SM prediction then such nondecoupling scenarios will be disfavored. The decoupling would happen only if κ_i falls with increasing charged scalar mass. In what follows, we will illustrate these features by considering some popular doublet extensions of the SM scalar sector.

5.1 Two Higgs-doublet models

The 2HDM potential has been discussed in detail in Chapter 3. Here we will briefly highlight the main conclusions in the context of $h \rightarrow \gamma\gamma$. First, it is important to note that the charged scalar contribution to $\mu_{\gamma\gamma}$ is controlled by (putting $i = 1$ in κ_i) [55, 82, 116, 117, 120]

$$\kappa_1 = -\frac{1}{m_{1+}^2} \left(m_{1+}^2 + \frac{m_h^2}{2} - \frac{\lambda_5 v^2}{2} \right). \quad (5.5)$$

Clearly, κ_1 saturates to -1 as the charged scalar becomes excessively heavy. Decoupling can be achieved by tuning $m_{1+}^2 \simeq \lambda_5 v^2/2$ [33]. Recalling our counting of independent parameters, any adjustment between the charged scalar mass and λ_5 is nothing short of fine-tuning. On the other hand, if the Z_2 symmetry in the scalar potential is exact, *i.e.* $\lambda_5 = 0$, then the charged scalar will never decouple and will cause $\mu_{\gamma\gamma}$ to settle below its SM prediction. In Fig. 5.1 we have plotted the allowed range of κ_1 in 2HDM from the present LHC data as well as from an anticipation of future sensitivity.

An interesting possibility arises when we employ a $U(1)$ symmetry, instead of the usual Z_2 symmetry, in the potential. The choice $\lambda_5 = \lambda_6$ will ensure $U(1)$ symmetry in the quartic terms.

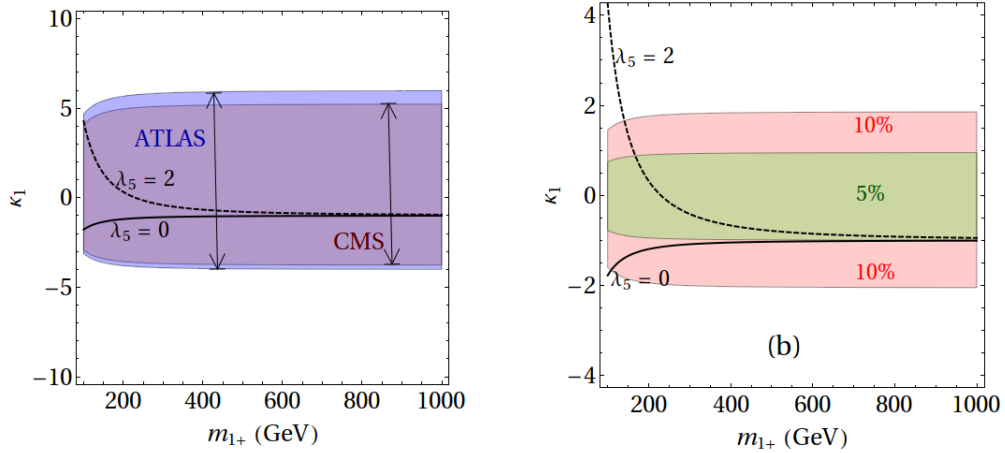


FIGURE 5.1: In the left panel (a) we display the constraints on κ_1 in 2HDM coming from the measured values of $\mu_{\gamma\gamma}$ at 95% C.L. by the CMS ($1.14^{+0.26}_{-0.23}$ [52]) and ATLAS (1.17 ± 0.27 [53]) Collaborations. In the right panel (b) we show what would be the 95% C.L. allowed range of κ_1 if $\mu_{\gamma\gamma}$ is hypothetically measured to be as $1 \pm 0.1(0.05)$ in future colliders. In both panels we have plotted Eq. (5.5) for two different values of λ_5 . The figures have been taken from [51].

The bilinear term involving λ_5 still breaks the $U(1)$ symmetry softly. Then the mass of the pseudoscalar gets related to the soft breaking parameter λ_5 as $m_A^2 = \lambda_5 v^2/2$. In this case, the expression for κ_1 reads [55]:

$$\kappa_1 = -\frac{1}{m_{1+}^2} \left(m_{1+}^2 - m_A^2 + \frac{m_h^2}{2} \right). \quad (5.6)$$

In the paper [55], a detailed analysis on the unitarity and stability constraints on various combination of λ_i couplings when the 2HDM scalar potential has a softly broken $U(1)$ symmetry has been provided. We cite some of them here to demonstrate ‘decoupling’ for large individual quartic couplings, as what is constrained from unitarity is only their differences in certain combinations. For example, $(2\lambda_3 + \lambda_4) \leq 16\pi$ implies $(2m_{1+}^2 - m_H^2 - m_A^2 + m_h^2) \leq 16\pi v^2$. Also, $(\lambda_1 + \lambda_2 + 2\lambda_3) \leq 16\pi/3$ implies $(m_H^2 - m_A^2)(\tan^2 \beta + \cot^2 \beta) + 2m_h^2 \leq 32\pi v^2/3$. These relations, together with $|m_{1+} - m_H| \ll (m_{1+}, m_H)$ arising from the electroweak T parameter, restrict the splitting between the charged scalar and the pseudoscalar mass ($|m_{1+}^2 - m_A^2|$). As displayed through more such relations among quartic couplings and the associated plots in the plane of non-SM scalar masses in [55], the individual scalar masses can become very large without violating unitarity as long as their mass-square differences are within certain limits. Consequently, the numerator in Eq. (5.6) cannot grow indefinitely with increasing m_{1+} . Thus κ_1 becomes very small in that limit and $\mu_{\gamma\gamma}$ reaches the SM predicted value. The key issue is that the Z_2 symmetry breaking λ_5 term was not related to the mass of any particle in the spectrum, and hence its adjustment *vis-à-vis* the charged scalar mass was nothing short of fine-tuning. Now, the global $U(1)$ breaking λ_5 is related to the pseudoscalar mass whose splitting with the charged scalar mass is restricted from unitarity.

5.1.1 Underlying dynamics behind decoupling

We now discuss the underlying reason behind decoupling or nondecoupling of nonstandard scalars from physical processes in the 2HDM context. The conclusion is equally applicable for n HDM where $n > 2$. We first recall the 2HDM potential in Eqs. (3.2) and (3.3). The parametrization of Eq. (3.2) does not *a priori* assume, unlike the one in Eq. (3.3), that Φ_1 or Φ_2 necessarily acquires any vev. In this parametrization, in the limit when the dimensionless couplings $\beta_2 = \beta_3 = \beta_4 = \beta_5 = 0$, the mass mixing parameter $m_{12}^2 = 0$ the second Higgs doublet Φ_2 does not acquire any vev, and the SM scalar potential is recovered with the relation $v^2 = v_1^2 = -m_{11}^2/\beta_1$. This is one special case of the more general *inert doublet* scenario with a perfectly Z_2 symmetric potential, in which all the nonstandard scalars decouple from physical processes when the parameter m_{22}^2 controlling their masses is taken to infinitely large value. Note that m_{22}^2 , in this case, does not have its origin in spontaneous symmetry breaking (SSB), and this is why its large value could ensure decoupling. But when both the doublets receive vevs, one can trade the two parameters m_{11}^2 and m_{22}^2 in favor of v_1 and v_2 . Then the magnitude of the third parameter m_{12}^2 , or equivalently λ_5 , has nothing to do with SSB, and this parameter provides the regulator whose large value ensures decoupling of all nonstandard scalars from physical processes. However, while employing m_{12}^2 (or equivalently λ_5 in our parametrization) for decoupling, one cannot escape from some tuning of parameters for softly broken Z_2 as explained around Eq. (5.5), but no such tuning is required for softly broken $U(1)$ (discussed before). Nondecoupling would result when the symmetry of the potential is exact ($m_{12}^2 = 0$), *and at the same time*, both the scalars receive vevs (which implies $\lambda_5 = 0$). In this case all the non-SM physical scalar masses would be proportional to the electroweak vev, and there is no independent mass-dimensional parameter which has non-SSB origin. As illustrated in the inert doublet case, even with exactly symmetric potential, decoupling is achieved in 2HDM.

To provide further intuition into the argument of decoupling and its close connection to the existence of some non-SSB origin parameter, let us consider the following analogy. It is well known that the top quark in the SM does not decouple from $h \rightarrow \gamma\gamma$. This is because the top quark receives all its mass from SSB and increasing its mass will invariably imply enhancing the Yukawa coupling (h_t). Now suppose that the top quark receives part of its mass (M) from some non-SSB origin, i.e. $m_t = h_tv + M$. Then the top-loop contribution will yield a prefactor $h_tv/(h_tv + M)$. In this case, by taking $M \rightarrow \infty$, the top quark contribution can be made to decouple from the diphoton decay width of the Higgs boson.

5.2 Three-Higgs-doublet models

S_3 or A_4 symmetric flavor models are typical examples which employ three Higgs doublets. With Φ_1 , Φ_2 and Φ_3 as the three scalar $SU(2)$ doublets, the scalar potential for the S_3 symmetric has been already written in Eq. (4.3) (see e.g. [115, 121], and also references therein for flavor physics discussions both when the S_3 symmetry is exact as well as when it is softly broken). Assuming the lambdas to be real, potential minimization conditions attribute a relation between two of the three vevs ($v_1 = \sqrt{3}v_2$). Using this relation, an alignment limit can be obtained for this model also [121].

Now we write the potential satisfying A_4 symmetry (see e.g. [122]),

$$\begin{aligned}
 V_{3\text{HDM}}^{A_4} = & -\mu^2 \left(\Phi_1^\dagger \Phi_1 + \Phi_2^\dagger \Phi_2 + \Phi_3^\dagger \Phi_3 \right) + \lambda_1 \left(\Phi_1^\dagger \Phi_1 + \Phi_2^\dagger \Phi_2 + \Phi_3^\dagger \Phi_3 \right)^2 \\
 & + \lambda_2 \left(\Phi_1^\dagger \Phi_1 \Phi_2^\dagger \Phi_2 + \Phi_2^\dagger \Phi_2 \Phi_3^\dagger \Phi_3 + \Phi_3^\dagger \Phi_3 \Phi_1^\dagger \Phi_1 \right) \\
 & + \lambda_3 \left(\Phi_1^\dagger \Phi_2 \Phi_2^\dagger \Phi_1 + \Phi_2^\dagger \Phi_3 \Phi_3^\dagger \Phi_2 + \Phi_3^\dagger \Phi_1 \Phi_1^\dagger \Phi_3 \right) \\
 & + \lambda_4 \left[e^{i\epsilon} \left\{ \left(\Phi_1^\dagger \Phi_2 \right)^2 + \left(\Phi_2^\dagger \Phi_3 \right)^2 + \left(\Phi_3^\dagger \Phi_1 \right)^2 \right\} + \text{h.c.} \right]. \quad (5.7)
 \end{aligned}$$

In one plausible scenario, the minimization conditions require that all the three vevs are equal [123]. This particular choice automatically yields a SM-like Higgs as well as two pairs of complex neutral states with mixed CP properties. Note that for $\epsilon = 0$ in Eq. (5.7), the symmetry of the potential is enhanced to S_4 . However, our conclusions do not depend on the value of ϵ .

Thus, a 3HDM can provide an SM-like Higgs along with two pairs of charged scalars, as exemplified with S_3 and A_4 scenarios. After expressing the lambdas in terms of the physical masses, we obtain the following expressions for κ_i ($i = 1, 2$) in the alignment limit, which are the same for both S_3 and A_4 :

$$\kappa_i = - \left(1 + \frac{m_h^2}{2m_{i+}^2} \right) \quad \text{for } i = 1, 2. \quad (5.8)$$

Clearly, the charged scalars do not decouple from the diphoton decay width, since κ_i settles to -1 when m_{i+} is very large compared to m_h . Note, both the charged scalars contribute in the same direction to reduce $\mu_{\gamma\gamma}$.

Now we turn our attention to the case of a global continuous symmetry in 3HDM potential. For illustration, we consider that the symmetry is $SO(2)$ under which Φ_1 and Φ_2 form a doublet. The expression for the scalar potential is similar to Eq. (4.3), only that now $\lambda_4 = 0$ and the potential contains an additional bilinear term ($-\mu_{12}^2 \Phi_1^\dagger \Phi_2 + \text{h.c.}$). The real part of μ_{12}^2 softly breaks the $SO(2)$ symmetry and prevents the occurrence of any massless scalar in the theory. In any case, we assume μ_{12}^2 to be real just like any other parameters in the potential. The relevant

Model		Expression for κ_i	prediction $\mu_{\gamma\gamma}$	prediction $\mu_{Z\gamma}$	Decoupling?
2HDM	Softly broken Z_2	$-\left(1 + \frac{m_h^2}{2m_{1+}^2} - \frac{\lambda_5 v^2}{2m_{1+}^2}\right)$	Depends on λ_5	Depends on λ_5	Possible
	Exact Z_2	$-\left(1 + \frac{m_h^2}{2m_{1+}^2}\right)$	≤ 0.9	≤ 0.96	No
	Softly broken $U(1)$	$-\left(1 + \frac{m_h^2}{2m_{1+}^2} - \frac{m_A^2}{m_{1+}^2}\right)$	Depends on m_A	Depends on m_A	Yes
3HDM	Exact S_3	$-\left(1 + \frac{m_h^2}{2m_{i+}^2}\right)$ for $i = 1, 2$	≤ 0.8	≤ 0.93	No
	Exact A_4	$-\left(1 + \frac{m_h^2}{2m_{i+}^2}\right)$ for $i = 1, 2$	≤ 0.8	≤ 0.93	No
	Softly broken $SO(2)$	$\kappa_1 = -\left(1 + \frac{m_h^2}{2m_{1+}^2} - \frac{m_{h'}^2}{m_{1+}^2}\right)$ $\kappa_2 = -\left(1 + \frac{m_h^2}{2m_{2+}^2}\right)$	Depends on $m_{h'}$	Depends on $m_{h'}$	Partial

TABLE 5.1: *Behavior of 2HDM and 3HDM scenarios in the alignment limit strictly when all the doublets receive vevs. In the case of exact discrete symmetries, every charged scalar pair reduces $\mu_{\gamma\gamma}$ approximately by 0.1. Although explicit expression for $\mu_{Z\gamma}$ is not shown in text, its predictions in different scenarios are displayed. In the last column where we say ‘Possible’, we mean that decoupling can be achieved with some tuning, while in the last row ‘Partial’ implies that only the first charged scalar decouples.*

minimization conditions are given by

$$v_1\mu_1^2 + v_2\mu_{12}^2 = v_1(v_1^2 + v_2^2)(\lambda_1 + \lambda_3) + \frac{1}{2}v_1v_3^2(\lambda_5 + \lambda_6 + 2\lambda_7), \quad (5.9a)$$

$$v_2\mu_1^2 + v_1\mu_{12}^2 = v_2(v_1^2 + v_2^2)(\lambda_1 + \lambda_3) + \frac{1}{2}v_2v_3^2(\lambda_5 + \lambda_6 + 2\lambda_7). \quad (5.9b)$$

Note that nonzero μ_{12}^2 will require $v_1 = v_2$. An interchange symmetry ($1 \leftrightarrow 2$) is accidentally preserved even after spontaneous symmetry breaking. We will have three CP even scalars (h' , H , h), two pseudoscalars (A_1 , A_2) and two pairs of charged scalars (H_1^\pm , H_2^\pm). Among these, h' , A_1 and H_1^\pm are odd under the interchange symmetry and the rest are even under it. Being odd under this interchange symmetry, h' does *not* couple to gauge bosons as $h'VV$ ($V = W, Z$). Appearance of such an exotic scalar was noted earlier in the context of an S_3 symmetric 3HDM [111, 112, 121]. The soft breaking parameter (μ_{12}^2) gets related to the mass of h' as

$$m_{h'}^2 = 2\mu_{12}^2. \quad (5.10)$$

It is straightforward to express the lambdas in terms of the physical masses. We then obtain

$$\kappa_1 = -\frac{1}{m_{1+}^2} \left(m_{1+}^2 - m_{h'}^2 + \frac{m_h^2}{2} \right), \quad (5.11a)$$

$$\kappa_2 = -\left(1 + \frac{m_h^2}{2m_{2+}^2} \right). \quad (5.11b)$$

The similarity between Eq. (5.11a) and Eq. (5.6) is striking. Note that ($|m_{1+}^2 - m_{h'}^2|$) is constrained from unitarity. Therefore, when the first charged Higgs mass m_{1+} is very large, κ_1 becomes vanishingly small. However, this decoupling does not occur in κ_2 which contains the

second charged Higgs mass m_{2+} . It is not difficult to intuitively argue that with an extended global symmetry $SO(2) \times U(1)$, together with an extra soft breaking parameter which is related to m_{A2} , decoupling in κ_2 can be ensured. Starting from the softly broken $SO(2)$ symmetric potential, this additional $U(1)$ extension ($\phi_3 \rightarrow e^{i\alpha}\phi_3$) and its soft breaking can be realized by putting $\lambda_7 = 0$ in Eq. (4.3) and introducing a term that softly breaks this $U(1)$. A crucial observation we make in this chapter is that the masses m_A in the 2HDM context and $m_{h'}$ in the 3HDM context enter into the expressions of κ_i – e.g. see Eqs. (5.6) and (5.11a) – only when they are related to *soft* global symmetry breaking parameters.

5.3 Conclusions and outlook

In this chapter we have made an attempt to establish a connection between decoupling or nondecoupling of charged scalars from the diphoton decay of the Higgs with the symmetries of the scalar potential. We have argued that charged scalars in multi doublet scalar extensions of the SM do not necessarily decouple from physical processes, e.g. $\mu_{\gamma\gamma}$ in the context of this chapter, specifically when the potential has an exact symmetry and all the scalars receive vevs. In such scenarios, a precisely measured $\mu_{\gamma\gamma}$ can smell the presence of nonstandard scalars even if they are super-heavy. In fact, $\mu_{\gamma\gamma}$ can constrain the *number* of such doublets. Table 5.1 shows that each additional pair of charged scalars (H_i^\pm) reduces $\mu_{\gamma\gamma}$ approximately by 0.1 when the potential has an exact discrete symmetry. Our illustrations are based on two- and three-Higgs-doublet models which are motivated by flavor symmetries. We have explicitly demonstrated how soft breaking of a global $U(1)$ symmetry can ensure decoupling in 2HDM in the alignment limit. In the case of 3HDM, with a softly broken global $SO(2)$ symmetry in the potential, decoupling can be ensured for one pair of charged scalars (H_1^\pm), while the second pair (H_2^\pm) still do not decouple. Employing the soft breaking terms of an extended global continuous symmetry, namely, $SO(2) \times U(1)$, the nondecoupling effects of H_2^\pm can be tamed. If we have more pairs of charged scalars in the theory stemming from additional scalar doublets, even more enhanced or extended global continuous symmetries – only softly broken – would be required to ensure decoupling of all charged scalars from $\mu_{\gamma\gamma}$. Keeping in mind the expected accuracy in the measurement of the hhh vertex in the high luminosity option of LHC or in the future linear collider, whose tree level expression in the alignment limit remains the same as in SM even for multi doublet Higgs structure, $\mu_{\gamma\gamma}$ may offer a better bet for diagnosing the underlying layers of the Higgs dynamics.

*Look at the end of work, contrast
The petty done, the undone vast ...*

Robert Browning in “The Last Ride Together”

6

Summary and conclusions

The discovery of a new boson in the July of 2012 at the LHC is undoubtedly the greatest achievement of this decade in the field of Particle Physics. Precise measurements of the properties of this new boson will be the major objective of the future high energy collider experiments. Although the signal strengths of this new boson into various decay channels have been found to be compatible with what is expected from the SM Higgs scalar, unambiguous determination of the couplings of this new boson is necessary to make any conclusive remark on its *standardness*.

But, besides these fantastic agreements, preliminary data from both CMS and ATLAS showed larger than 2σ excess over the SM expectation in the diphoton signal strengths. It is well known that Higgs to diphoton decay, in the SM, proceeds at the leading order through W and top quark (largest among the fermions) loops. It is also known that the amplitudes from these two types of loop diagrams interfere destructively with W -loop contribution dominating over the top-loop. Naturally if the sign of the top-Higgs Yukawa coupling is reversed the interference will be constructive and an enhancement, as was seen in the experiments, can be obtained. This led many people to speculate that the SM might have been wrong in predicting the sign of the top quark Yukawa (or, every Yukawa) coupling. But we must remember that in absence of the SM Higgs, the amplitude of $f\bar{f} \rightarrow W_L^+ W_L^-$ scattering will grow linearly with the CM energy and the co-efficient of this linear growth is proportional to the fermion mass, m_f (see Appendix B). In fact, the requirement of the cancellation of this growth uniquely fixes the $\bar{f}fh$ Yukawa coupling. Thus, tormenting the Yukawa couplings in the SM by hand will lead to an imperfect cancellation

of the energy growths spoiling the high energy unitarity of the $f\bar{f} \rightarrow W_L^+ W_L^-$ scattering and this effect will be most prominent in the case of $t\bar{t} \rightarrow W_L^+ W_L^-$ scattering because of the large mass of the top quark. In Chapter 2, it has been showed that any departure from the SM couplings will inevitably introduce a new energy scale at which unitarity will be violated and therefore, some new physics must set in before this energy scale to restore it. A quantitative analysis of how this energy scale depends on the amount of nonstandard deviation of the couplings has been demonstrated in this chapter.

However after an updated analysis of the data by ATLAS and CMS, the excess in the diphoton channel seems to have gone away and all the signal strengths are in agreement with the SM. We have not found any direct evidence for new physics so far. Even if this new boson turns out to be the SM Higgs particle, there are still some issues, not addressed in the SM, which invite us to take a closer look at the BSM physics. The major shortcomings of the SM are as follows:

- Neutrinos are massless in the SM. But oscillation experiments with solar and atmospheric neutrinos have established that neutrinos have small but finite mass. The neutrino oscillation experiments have raised new puzzles as the mixing among the neutrinos are very different from that among the quarks.
- Different cosmological and astrophysical observations have confirmed the existence of *dark matter* in the universe. The fact that we cannot *see* it suggests that this must be some new kind of particle without strong and electromagnetic interactions. On the other hand, the fact that it occurs with a certain abundance requires that it must have some other kind of interactions which allow this to happen. In the SM there is no dark matter candidate and one should, therefore, look beyond.
- All observations in the large as well as the small scale universe have found no evidence of antimatter. There is only matter in the universe, and the density of matter is only a billionth of the photon density at the present epoch. There is no way to understand this matter-antimatter asymmetry within the framework of the SM.

Speaking of BSM scenarios, Chapter 3 is dedicated to the phenomenology of CP conserving 2HDMs – one of the simplest BSM constructions. The first part of this chapter concentrates on the scalar potential only and the conclusions obtained in this part are independent of the Yukawa structure of the 2HDM. Our motivation here was to explore the scalar potential in view of the observation of a 125 GeV Higgs boson (h) at the LHC, using constraints from unitarity of scalar scattering cross-sections, stability of the potential and electroweak precision tests. These considerations restrict the spectrum of the non-standard scalars. Since the LHC Higgs data seem to be compatible with the SM expectations, we restricted ourselves to the alignment limit when the lightest CP even scalar (h) resembles the SM Higgs particle in its

gauge and Yukawa couplings. In addition to h , a 2HDM contains one heavy CP even scalar (H), one pseudoscalar (A) and a pair of charged scalars (H_1^\pm). We found that when the potential has an exact Z_2 symmetry, unitarity and stability put severe constraints on $\tan\beta$. This bound, however, is diluted in the presence of a soft breaking parameter. In the case of a softly broken $U(1)$ symmetry, we find that unitarity constraints essentially applies to the difference between the nonstandard scalar masses but not on the individual masses. This means any individual nonstandard mass can be arbitrarily large without violating unitarity provided the other masses are close by. In particular, it has been shown that unitarity and stability restricts the quantity $|(m_H^2 - m_A^2)(\tan^2\beta + \cot^2\beta)|$. Consequently the difference between m_H and m_A is squeezed with increasing $\tan\beta$ and, for practical purposes, becomes degenerate for $\tan\beta \gtrsim 5$. On top of this, when we imposed the constraint coming from the T -parameter, it is found that all three nonstandard masses should be degenerate for $\tan\beta \gtrsim 5$.

Later in Chapter 3 some key features of the BGL models were explored. Note that the BGL models use a softly broken $U(1)$ symmetry to tame the FCNC couplings by relating them to the off diagonal elements of the CKM matrix and so all the conclusions of the previous paragraph, in the context of $U(1)$ symmetry, hold for these models too. The crucial motivation of this chapter was to look for a lighter than conventionally allowed charged scalar which can found in the next run of the LHC. It should be remembered that the charged scalar mass in the conventional 2HDMs like Type II 2HDM faces stringent constraints mainly from the well measured value of the $b \rightarrow s\gamma$ decay width. From this observable alone the value of m_{1+} in Type II 2HDM is forced to be more than 350 GeV. On the contrary, it has been found in this chapter that in certain variants of the BGL models a charged scalar in the ballpark of 150-200 GeV can successfully negotiate the major experimental constraints coming from the flavor data. In fact, all the three nonstandard masses (m_H , m_A and m_{1+}) can be taken in the same 150-200 GeV range without upsetting any major theoretical or experimental constraints whatsoever. What's more interesting is to note that since the BGL models break the fermionic family universality explicitly, these light nonstandard scalars can have unconventional decay hierarchies which can be observed at LHC and this might be the hallmark signature of the BGL models.

Multi doublet extensions of the SM scalar sector have been further investigated in Chapter 4 where an S_3 symmetric 3HDM has been analyzed. Again an alignment limit for this model has been found when one of the CP even scalars mimics the SM gauge and Yukawa coupling. In addition to this SM-like scalar (h) a 3HDM contains two heavier scalars (h^0 and H), two pseudoscalars (A_1 and A_2) and two pairs of charged scalars (H_1^\pm and H_2^\pm). Theoretical constraints coming from the tree-level unitarity of the scattering amplitudes were derived and the consequences of these constraints on the nonstandard masses have been explored. It is found that all the nonstandard masses are constrained to lie below 1 TeV. Then the effect of two pairs of charged scalars on the loop induced Higgs decays has been analyzed. Similar to the case of Z_2 symmetric 2HDM, here again we find that none of the charged scalars decouples from

diphoton decay and an enhancement in the diphoton signal strengths is impossible to obtain in the alignment limit. In fact, a sharp prediction that the diphoton signal strength in this model cannot be more than 80% of the SM expectation has been made in this chapter.

In Chapter 5 it has been shown that decoupling of the charged scalar in the loop induced Higgs decays like $h \rightarrow \gamma\gamma$ is not guaranteed. The role played by symmetries in this context has been emphasized. It is found that this nondecoupling is a typical characteristic of non-inert multi Higgs-doublet models with an exact discrete symmetry. It has been suggested that decoupling can be achieved by invoking a soft symmetry breaking term in the scalar potential.

Details are not just details, collectively they make the design.

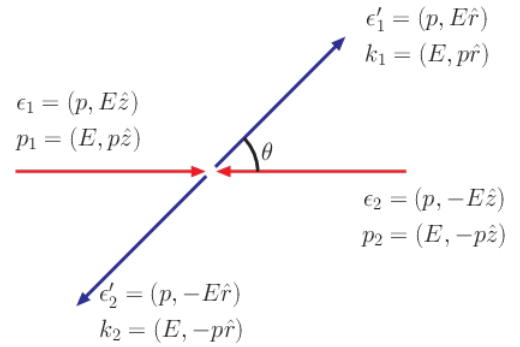


Calculation of the WW scattering amplitude

Consider the following elastic scattering process in the CM frame:

$$W_L^+(p_1) + W_L^-(p_2) \rightarrow W_L^+(k_1) + W_L^-(k_2).$$

We abbreviate $\epsilon_L(p_1) = \epsilon_1/M_W$ etc. Since $p \cdot \epsilon_L(p) = 0$ and $\epsilon_L(p) \cdot \epsilon_L(p) = -1$, we may take, in the CM frame, the momentum and polarization vectors as shown in the adjacent figure. For our



calculation, we shall need the following expressions which follow from the kinematics in the CM frame:

$$p_1 \cdot \epsilon_2 = p_2 \cdot \epsilon_1 = k_1 \cdot \epsilon'_2 = k_2 \cdot \epsilon'_1 = 2Ep, \quad (\text{A.1a})$$

$$p_1 \cdot \epsilon'_1 = p_2 \cdot \epsilon'_2 = k_1 \cdot \epsilon_1 = k_2 \cdot \epsilon_2 = Ep(1 - \cos \theta), \quad (\text{A.1b})$$

$$p_1 \cdot \epsilon'_2 = p_2 \cdot \epsilon'_1 = k_1 \cdot \epsilon_2 = k_2 \cdot \epsilon_1 = Ep(1 + \cos \theta), \quad (\text{A.1c})$$

$$\epsilon_1 \cdot \epsilon_2 = \epsilon'_1 \cdot \epsilon'_2 = p^2 + E^2, \quad (\text{A.1d})$$

$$\epsilon'_1 \cdot \epsilon_2 = \epsilon_1 \cdot \epsilon'_2 = p^2 + E^2 \cos \theta, \quad (\text{A.1e})$$

$$\epsilon_1 \cdot \epsilon'_1 = \epsilon_2 \cdot \epsilon'_2 = p^2 - E^2 \cos \theta, \quad (\text{A.1f})$$

$$p_1 \cdot p_2 = k_1 \cdot k_2 = \left(\frac{s}{2} - M_W^2 \right), \quad (\text{A.1g})$$

$$\begin{aligned} t &= (p_1 - k_1)^2 = 2M_W^2 - 2p_1 \cdot k_1 \\ &= 2M_W^2 - 2(E^2 - p^2 \cos \theta), \end{aligned} \quad (\text{A.1h})$$

$$\Rightarrow \frac{t}{2} = -p^2(1 - \cos \theta), \quad (\text{A.1i})$$

$$\Rightarrow p_1 \cdot k_1 = p_2 \cdot k_2 = -\left(\frac{t}{2} - M_W^2\right), \quad (\text{A.1j})$$

$$\text{Similarly, } \frac{u}{2} = -p^2(1 + \cos \theta), \quad (\text{A.1k})$$

$$\Rightarrow p_1 \cdot k_2 = p_2 \cdot k_1 = -\left(\frac{u}{2} - M_W^2\right). \quad (\text{A.1l})$$

A.1 Calculation of the gauge part

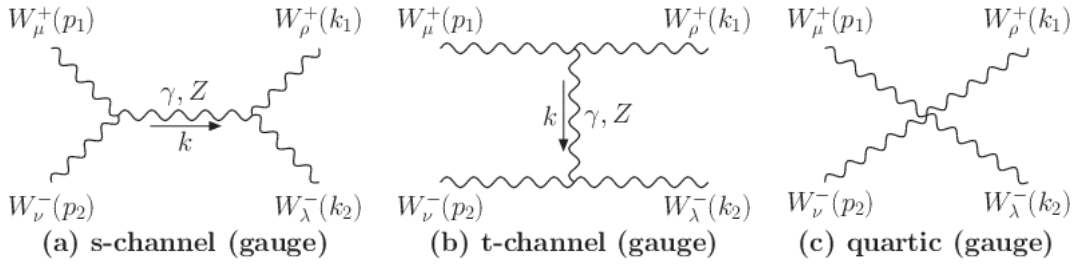


FIGURE A.1: Gauge diagrams for $W_L^+(p_1) + W_L^-(p_2) \rightarrow W_L^+(k_1) + W_L^-(k_2)$.

A.1.1 s-channel photon exchange

The Feynman amplitude can be written as

$$\begin{aligned} i\mathcal{M}_a^\gamma &= -g^2 \sin^2 \theta_w \left[(p_2 - p_1)_\alpha g_{\mu\nu} + (p_1 + k)_\nu g_{\mu\alpha} - (k + p_2)_\mu g_{\nu\alpha} \right] \times \left(-\frac{ig^{\alpha\beta}}{s} \right) \\ &\times \left[(k_2 - k_1)_\beta g_{\lambda\rho} + (k_1 + k)_\lambda g_{\rho\beta} - (k + k_2)_\rho g_{\lambda\beta} \right] \times \frac{\epsilon_1^\mu \epsilon_2^\nu \epsilon_1'^\rho \epsilon_2'^\lambda}{M_W^4}. \end{aligned} \quad (\text{A.2})$$

Remembering $k = (p_1 + p_2) = (k_1 + k_2)$ and $p_1 \cdot \epsilon_1 = p_2 \cdot \epsilon_2 = k_1 \cdot \epsilon_1' = k_2 \cdot \epsilon_2' = 0$ we may simplify the above equation as

$$\begin{aligned} \mathcal{M}_a^\gamma &= \frac{g^2 \sin^2 \theta_w}{M_W^4 s} \left[(p_2 - p_1)_\alpha (\epsilon_1 \cdot \epsilon_2) + 2(p_1 \cdot \epsilon_2) \epsilon_{1\alpha} - 2(p_2 \cdot \epsilon_1) \epsilon_{2\alpha} \right] \times g^{\alpha\beta} \\ &\times \left[(k_2 - k_1)_\beta (\epsilon_2' \cdot \epsilon_1') - 2(k_1 \cdot \epsilon_2') \epsilon_{1\beta}' + 2(k_2 \cdot \epsilon_1') \epsilon_{2\beta}' \right]. \end{aligned} \quad (\text{A.3})$$

Using the scalar products of Eq. (A.1l) we may write

$$\mathcal{M}_a^\gamma = \frac{g^2 \sin^2 \theta_w}{M_W^4 s} \left\{ (p_2 - p_1)_\alpha (E^2 + p^2) + 4Ep(\epsilon_1 - \epsilon_2)_\alpha \right\}$$

$$\times \left\{ (k_2 - k_1)^\alpha (E^2 + p^2) + 4Ep(\epsilon'_1 - \epsilon'_2)^\alpha \right\} \quad (\text{A.4})$$

$$= \frac{g^2 \sin^2 \theta_w}{M_W^4 s} \times T_s \quad (\text{say}). \quad (\text{A.5})$$

■ Terms inside the square bracket:

$$\begin{aligned} T_s &= \left[(p_2 \cdot k_2 - p_2 \cdot k_1 - p_1 \cdot k_2 + p_1 \cdot k_1)(E^2 + p^2)^2 + 4Ep(E^2 + p^2) \times \right. \\ &\quad \left. (p_2 \cdot \epsilon'_1 - p_2 \cdot \epsilon'_2 - p_1 \cdot \epsilon'_1 + p_1 \cdot \epsilon'_2 + k_2 \cdot \epsilon_1 - k_2 \cdot \epsilon_2 - k_1 \cdot \epsilon_1 + k_1 \cdot \epsilon_2) \right. \\ &\quad \left. + 16E^2 p^2 (\epsilon_1 \cdot \epsilon'_1 - \epsilon_1 \cdot \epsilon'_2 - \epsilon_2 \cdot \epsilon'_1 + \epsilon_2 \cdot \epsilon'_2) \right] \\ &= \left[2(-2p^2 \cos \theta)(E^2 + p^2)^2 + 32E^2 p^2 \cos \theta (E^2 + p^2) + 32E^2 p^2 (-2E^2 \cos \theta) \right] \\ &= \left[-4p^2 \cos \theta (E^2 + p^2)^2 + 32E^2 p^2 \cos \theta (E^2 + p^2 - 2E^2) \right] \\ &= -4p^2 \cos \theta \left(\frac{s}{2} - M_W^2 \right)^2 - 32E^2 p^2 M_W^2 \cos \theta \\ &= -4E^4 s \cos \theta + \mathcal{O}(M_W^4). \end{aligned} \quad (\text{A.6})$$

Therefore,

$$\begin{aligned} \mathcal{M}_a^\gamma &= \frac{g^2 \sin^2 \theta_w}{M_W^4 s} [-4E^4 s \cos \theta] + \mathcal{O}(1) \\ &= -\frac{g^2 E^4 \sin^2 \theta_w}{M_W^4} (4 \cos \theta) + \mathcal{O}(1). \end{aligned} \quad (\text{A.7})$$

A.1.2 s-channel Z -boson exchange

Firstly, the photon propagator of Eq. (A.2) should be replaced by the massive Z -boson propagator:

$$\frac{-g^{\alpha\beta} + k^\alpha k^\beta}{(s - M_Z^2)}. \quad (\text{A.8})$$

But it should be noted that the $k^\alpha k^\beta$ term does not contribute to the amplitude because of the following identity:

$$\begin{aligned} &\left[(p_2 - p_1)_\alpha g_{\mu\nu} + (p_1 + k)_\nu g_{\mu\alpha} - (k + p_2)_\mu g_{\nu\alpha} \right] \times k^\alpha k^\beta \\ &\times \left[(k_2 - k_1)_\beta g_{\lambda\rho} + (k_1 + k)_\lambda g_{\rho\beta} - (k + k_2)_\rho g_{\lambda\beta} \right] = 0. \end{aligned} \quad (\text{A.9})$$

Another modification is that $WW\gamma$ coupling will be replaced by WWZ coupling, *i.e.*, $\sin \theta_w$ should be replaced by $\cos \theta_w$. Keeping this in mind, we can rewrite Eq. (A.5) for s-channel

Z-boson mediation as

$$\mathcal{M}_a^Z = \frac{g^2 \cos^2 \theta_w}{M_W^4 (s - M_Z^2)} \times T_s \simeq \frac{g^2 \cos^2 \theta_w}{M_W^4 (s - M_Z^2)} [- (4E^4 s) \cos \theta] \quad (\text{A.10})$$

$$\begin{aligned} &= \frac{g^2 E^2 \cos^2 \theta_w s}{M_W^4} \left(1 - \frac{M_Z^2}{s}\right)^{-1} \cos \theta \\ &= -\frac{g^2 E^4 \cos^2 \theta_w}{M_W^4} (4 \cos \theta) - \frac{g^2 E^2}{M_W^2} \cos \theta + \mathcal{O}(1). \end{aligned} \quad (\text{A.11})$$

In the last step, we have used $M_W = M_Z \cos \theta_w$. We now get the total amplitude for the s-channel process as

$$\mathcal{M}_a = \mathcal{M}_a^\gamma + \mathcal{M}_a^Z = -\frac{g^2 E^4}{M_W^4} (4 \cos \theta) - \frac{g^2 E^2}{M_W^2} (\cos \theta). \quad (\text{A.12})$$

A.1.3 t-channel photon exchange

The Feynman amplitude for this diagram reads

$$\begin{aligned} i\mathcal{M}_b^\gamma &= (-g^2 \sin^2 \theta_w) [-(p_1 + k_1)_\alpha g_{\mu\nu} + (p_1 + k)_\nu g_{\mu\alpha} + (-k + k_1)_\mu g_{\nu\alpha}] \times \left(-\frac{ig^{\alpha\beta}}{t}\right) \\ &\quad \times [(p_2 + k_2)_\beta g_{\lambda\rho} - (k_2 + k)_\rho g_{\lambda\beta} + (k - p_2)_\lambda g_{\rho\beta}] \times \frac{\epsilon_1^\mu \epsilon_1^\nu \epsilon_2^\rho \epsilon_2^\lambda}{M_W^4}. \end{aligned} \quad (\text{A.13})$$

Again remembering $k = p_1 - k_1 = k_2 - p_2$, and using the gauge condition $p \cdot \epsilon(p) = 0$ we may simplify the above expression as:

$$\begin{aligned} \mathcal{M}_b^\gamma &= \frac{g^2 \sin^2 \theta_w}{M_W^4 t} [-(p_1 + k_1)_\alpha (\epsilon_1 \cdot \epsilon'_1) + 2(p_1 \cdot \epsilon'_1) \epsilon_{1\alpha} + 2(k_1 \cdot \epsilon_1) \epsilon'_{1\alpha}] \\ &\quad \times [(p_2 + k_2)_\beta (\epsilon_2 \cdot \epsilon'_2) - 2(k_2 \cdot \epsilon_2) \epsilon'_{2\beta} - 2(p_2 \cdot \epsilon'_2) \epsilon_{2\beta}] \times g^{\alpha\beta} \\ &= \frac{g^2 \sin^2 \theta_w}{M_W^4 t} [-(p_1 + k_1)_\alpha (p^2 - E^2 \cos \theta) + 2Ep(1 - \cos \theta)(\epsilon_1 + \epsilon'_1)_\alpha] \\ &\quad \times [(p_2 + k_2)_\alpha (p^2 - E^2 \cos \theta) - 2Ep(1 - \cos \theta)(\epsilon_2 + \epsilon'_2)_\alpha] \end{aligned} \quad (\text{A.14})$$

$$= \frac{g^2 \sin^2 \theta_w}{M_W^4 t} \times T_t \quad (\text{say}). \quad (\text{A.15})$$

■ Terms inside the square bracket:

$$\begin{aligned} T_t &= +2Ep(1 - \cos \theta)(p^2 - E^2 \cos \theta) \{ (p_2 + k_2) \cdot (\epsilon_1 + \epsilon'_1) + (p_1 + k_1) \cdot (\epsilon_2 + \epsilon'_2) \} \\ &\quad - (p_1 + k_1) \cdot (p_2 + k_2) (p^2 - E^2 \cos \theta)^2 \\ &\quad - 4E^2 p^2 (1 - \cos \theta)^2 (\epsilon_1 + \epsilon'_1) \cdot (\epsilon_2 + \epsilon'_2) \\ &= -2(p^2 - E^2 \cos \theta)^2 (2E^2 + p^2 + p^2 \cos \theta) \end{aligned}$$

$$\begin{aligned}
& +8E^2p^2(1-\cos\theta)(p^2-E^2\cos\theta)(3+\cos\theta) \\
& -8E^2p^2(1-\cos\theta)^2\{2p^2+E^2(1+\cos\theta)\} \\
= & +8E^2p^2(1-\cos\theta)\{(p^2-E^2\cos\theta)(3+\cos\theta)-2p^2(1-\cos\theta)-E^2(1-\cos^2\theta)\} \\
& -2\{p^2(1-\cos\theta)-M_W^2\cos\theta\}^2(3E^2+E^2\cos\theta-M_W^2-M_W^2\cos\theta). \quad (\text{A.16})
\end{aligned}$$

After some algebraic manipulation, the terms inside the curly bracket in the first part of Eq. (A.16) can be evaluated to be equal to $-M_W^2(1+3\cos\theta)$. Using this in conjunction with Eq. (A.1i), the terms inside the square bracket becomes:

$$\begin{aligned}
T_t & = -2\left(\frac{t}{2}+M_W^2\cos\theta\right)^2\{E^2(3+\cos\theta)-M_W^2(1+\cos\theta)\} \\
& \quad +4E^2tM_W^2(1+3\cos\theta), \quad (\text{A.17})
\end{aligned}$$

$$\begin{aligned}
& \approx -\frac{t^2}{2}E^2(3+\cos\theta)+\frac{t^2}{2}M_W^2(1+\cos\theta) \\
& \quad -2M_W^2tE^2\cos\theta(3+\cos\theta)+4E^2tM_W^2(1+3\cos\theta)+\mathcal{O}(M_W^4), \quad (\text{A.18})
\end{aligned}$$

$$= -\frac{t^2}{2}E^2(3+\cos\theta)+M_W^2tE^2(3+6\cos\theta-\cos^2\theta)+\mathcal{O}(M_W^4). \quad (\text{A.19})$$

Plugging this into Eq. (A.15), we obtain

$$\mathcal{M}_b^\gamma \approx \frac{g^2\sin^2\theta_w}{M_W^4t}\left[-\frac{t^2}{2}E^2(3+\cos\theta)+M_W^2tE^2(3+6\cos\theta-\cos^2\theta)\right] \quad (\text{A.20})$$

$$\begin{aligned}
& \approx \frac{g^2E^2p^2\sin^2\theta_w}{M_W^4}(1-\cos\theta)(3+\cos\theta) \\
& \quad +\frac{g^2E^2\sin^2\theta_w}{M_W^2}(3+6\cos\theta-\cos^2\theta) \quad (\text{A.21})
\end{aligned}$$

$$= \frac{g^2E^4\sin^2\theta_w}{M_W^4}(3-2\cos\theta-\cos^2\theta)+\frac{g^2E^2\sin^2\theta_w}{M_W^2}(8\cos\theta)+\mathcal{O}(1). \quad (\text{A.22})$$

A.1.4 t-channel Z -boson exchange

Similar to the s-channel calculation, for t-channel Z -boson mediation we may write:

$$\begin{aligned}
\mathcal{M}_b^Z & = \frac{g^2\cos^2\theta_w}{M_W^4(t-M_Z^2)}\times T_t \\
& \approx \frac{g^2\cos^2\theta_w}{M_W^4t}\left(1+\frac{M_Z^2}{t}\right)\times T_t \\
& = \left(\frac{g^2\cos^2\theta_w}{M_W^4t}+\frac{g^2}{M_W^2t^2}\right)\times T_t \\
& \approx \frac{g^2E^4\cos^2\theta_w}{M_W^4}(3-2\cos\theta-\cos^2\theta)+\frac{g^2E^2\cos^2\theta_w}{M_W^2}(8\cos\theta)
\end{aligned}$$

$$+ \frac{g^2}{M_W^2 t^2} \left[-\frac{t^2}{2} E^2 (3 + \cos \theta) \right] \quad (\text{A.23})$$

$$= \frac{g^2 E^4 \cos^2 \theta_w}{M_W^4} (3 - 2 \cos \theta - \cos^2 \theta) + \frac{g^2 E^2 \cos^2 \theta_w}{M_W^2} (8 \cos \theta) - \frac{g^2 E^2}{M_W^2} \left(\frac{3}{2} + \frac{1}{2} \cos \theta \right) + \mathcal{O}(1) . \quad (\text{A.24})$$

Therefore, the total amplitude for the t-channel process becomes:

$$\begin{aligned} \mathcal{M}_b &= \mathcal{M}_b^\gamma + \mathcal{M}_b^Z \\ &= \frac{g^2 E^4}{M_W^4} (3 - 2 \cos \theta - \cos^2 \theta) + \frac{g^2 E^2}{M_W^2} \left(\frac{15}{2} \cos \theta - \frac{3}{2} \right) + \mathcal{O}(1) . \end{aligned} \quad (\text{A.25})$$

A.1.5 The quartic gauge vertex

The Feynman amplitude is given by

$$i\mathcal{M}_c = ig^2 (2g_{\mu\rho}g_{\nu\lambda} - g_{\mu\nu}g_{\rho\lambda} - g_{\mu\lambda}g_{\nu\rho}) \times \frac{\epsilon_1^\mu \epsilon_2^\nu \epsilon_1^{\prime\lambda} \epsilon_2^{\prime\rho}}{M_W^4} \quad (\text{A.26})$$

$$\Rightarrow \mathcal{M}_c = \frac{g^2}{M_W^4} [2(\epsilon_1 \cdot \epsilon_2)(\epsilon_2 \cdot \epsilon_1') - (\epsilon_1 \cdot \epsilon_2)(\epsilon_1' \cdot \epsilon_2') - (\epsilon_1 \cdot \epsilon_1')(\epsilon_2 \cdot \epsilon_2')] \quad (\text{A.27})$$

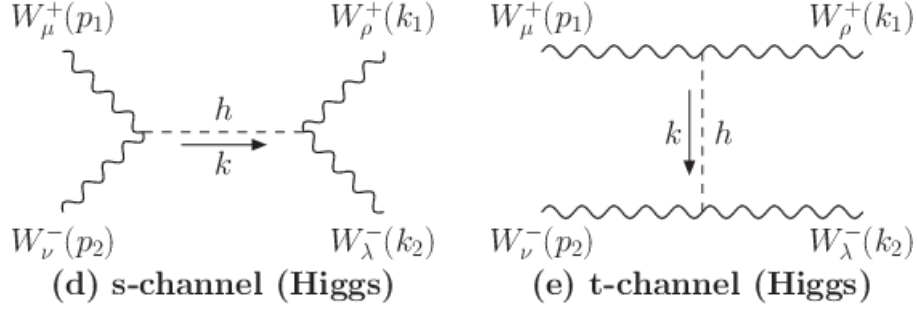
$$\Rightarrow \mathcal{M}_c = \frac{g^2}{M_W^4} [2(p^2 + E^2 \cos \theta)^2 - (p^2 + E^2)^2 - (p^2 - E^2 \cos \theta)^2] \quad (\text{A.28})$$

$$\Rightarrow \mathcal{M}_c = \frac{g^2 E^4}{M_W^4} (6 \cos \theta - 2 - \sin^2 \theta) + \frac{g^2 E^2}{M_W^2} (2 - 6 \cos \theta) + \mathcal{O}(1) . \quad (\text{A.29})$$

Adding Eqs. (A.12), (A.25) and (A.29) together one can see that the quartic growth is already canceled. The remaining quadratic growth in the total gauge part of the amplitude is given below:

$$\begin{aligned} \mathcal{M}^{\gamma+Z} &= \mathcal{M}_a + \mathcal{M}_b + \mathcal{M}_c , \\ &= \frac{g^2 E^2}{2M_W^2} (1 + \cos \theta) + \mathcal{O}(1) , \end{aligned} \quad (\text{A.30})$$

$$= \frac{g^2 s}{8M_W^2} (1 + \cos \theta) + \mathcal{O}(1) \equiv \frac{G_F s}{\sqrt{2}} (1 + \cos \theta) + \mathcal{O}(1) . \quad (\text{A.31})$$

FIGURE A.2: *Higgs mediated diagrams for $W_L^+(p_1) + W_L^-(p_2) \rightarrow W_L^+(k_1) + W_L^-(k_2)$.*

A.2 Calculation of the Higgs part

A.2.1 s-channel Higgs exchange

The Feynman amplitude for diagram A.2d can be written as follows:

$$\begin{aligned}
 i\mathcal{M}_d &= (igM_W g_{\mu\nu}) \frac{i}{(s - m_h^2)} (igM_W g_{\alpha\beta}) \frac{\epsilon_1^\mu \epsilon_2^\nu \epsilon_1'^\alpha \epsilon_2'^\beta}{M_W^4} \\
 \Rightarrow \mathcal{M}_d &= -\frac{g^2}{M_W^2 (s - m_h^2)} p_1^\mu p_2^\nu k_1^\alpha k_2^\beta g_{\mu\nu} g_{\alpha\beta}.
 \end{aligned} \tag{A.32}$$

Note that unlike in the gauge part of the calculation, here we already have M_W^2 in the denominator. Therefore, any modification of the $\mathcal{O}(M_W^2/E^2)$ in the numerator will lead to a constant term independent of the CM energy. For this reason, here we can approximate

$$\epsilon_L^\mu(p) \approx \frac{p^\mu}{M_W}. \tag{A.33}$$

Using this, we may rewrite Eq. (A.32) as

$$\begin{aligned}
 \mathcal{M}_d &= -\frac{g^2 (p_1 \cdot p_2) (k_1 \cdot k_2)}{M_W^2 (s - m_h^2)} \\
 &= -\frac{g^2 s^2}{4M_W^2 (s - m_h^2)} \\
 &= -\frac{g^2}{4M_W^2} \left[s + \frac{m_h^2 s}{(s - m_h^2)} \right].
 \end{aligned} \tag{A.34}$$

A.2.2 t-channel Higgs exchange

Similar to the s-channel calculation, for diagram A.2e we can write

$$\mathcal{M}_e = -\frac{g^2}{4M_W^2} \left[t + \frac{m_h^2 t}{(t - m_h^2)} \right]. \tag{A.35}$$

Thus, the total amplitude for the Higgs part becomes

$$\mathcal{M}^h = \mathcal{M}_d + \mathcal{M}_e = -\frac{g^2}{4M_W^2}(s+t) - \frac{g^2 m_h^2}{4M_W^2} \left(\frac{s}{s-m_h^2} + \frac{t}{t-m_h^2} \right) \quad (\text{A.36})$$

$$\Rightarrow \mathcal{M}^h \approx -\frac{g^2 s}{8M_W^2}(1+\cos\theta) - \frac{g^2 m_h^2}{4M_W^2} \left(\frac{s}{s-m_h^2} + \frac{t}{t-m_h^2} \right). \quad (\text{A.37})$$

In the last step we have used the following identity:

$$-(s+t) = u = -2p^2(1+\cos\theta) \approx -2E^2(1+\cos\theta) = -\frac{s}{2}(1+\cos\theta). \quad (\text{A.38})$$

A.3 Total amplitude and Lee-Quigg-Thacker limit

Adding Eqs. (A.31) and (A.37) together, we can easily see that the remnant quadratic energy growth in the gauge part of the amplitude is exactly canceled by the corresponding growth in the Higgs part of the amplitude. After the cancellation of the bad energy growth, the total amplitude reads

$$\mathcal{M}(\theta) = \mathcal{M}^{\gamma+Z} + \mathcal{M}^h = -\frac{g^2 m_h^2}{4M_W^2} \left(\frac{s}{s-m_h^2} + \frac{t}{t-m_h^2} \right), \quad (\text{A.39})$$

$$\Rightarrow \mathcal{M}(\theta) = -\frac{g^2 m_h^2}{4M_W^2} \left[\frac{s}{s-m_h^2} + \frac{\frac{s}{2}(1-\cos\theta)}{\frac{s}{2}(1-\cos\theta) + m_h^2} \right], \quad (\text{A.40})$$

$$= -\frac{g^2 m_h^2}{4M_W^2} [\mathcal{M}_1(\theta) + \mathcal{M}_2(\theta)] \quad (\text{say}). \quad (\text{A.41})$$

Now, let us define the following:

$$\mathcal{I}_1 = \int_{-1}^{+1} \mathcal{M}_1(\theta) d(\cos\theta) = \frac{2s}{s-m_h^2}, \quad (\text{A.42})$$

$$\begin{aligned} \mathcal{I}_2 &= \int_{-1}^{+1} \mathcal{M}_2(\theta) d(\cos\theta) = \int_{-1}^{+1} \frac{\frac{s}{2}(1-\cos\theta)}{\frac{s}{2}(1-\cos\theta) + m_h^2} d(\cos\theta) \\ &= \left[2 - \frac{2m_h^2}{s} \ln \left(1 + \frac{s}{m_h^2} \right) \right]. \end{aligned} \quad (\text{A.43})$$

One may recall from Eq. (1.44)

$$\begin{aligned} a_0 &= \frac{1}{32\pi} \int_{-1}^{+1} \mathcal{M}(\theta) d(\cos\theta) \\ &= \frac{1}{32\pi} \left(-\frac{g^2 m_h^2}{4M_W^2} \right) (\mathcal{I}_1 + \mathcal{I}_2) \end{aligned} \quad (\text{A.44})$$

$$= -\frac{G_F m_h^2}{8\pi\sqrt{2}} \left[2 + \frac{m_h^2}{s-m_h^2} - \frac{m_h^2}{s} \ln \left(1 + \frac{s}{M_H^2} \right) \right]. \quad (\text{A.45})$$

At the limit $s \gg m_h^2$, the above equation can be approximated as:

$$a_0 \approx -\frac{G_F m_h^2}{4\pi\sqrt{2}}. \quad (\text{A.46})$$

Now, if we apply the unitarity condition of Eq. (1.2), we can get an upper limit on the Higgs mass as:

$$m_h^2 \leq \frac{4\pi\sqrt{2}}{G_F} = 1.26 \text{ TeV}, \quad (\text{A.47})$$

where, in the last step, we have used $G_F = 1.12 \times 10^{-5} \text{ GeV}^{-2}$.

B

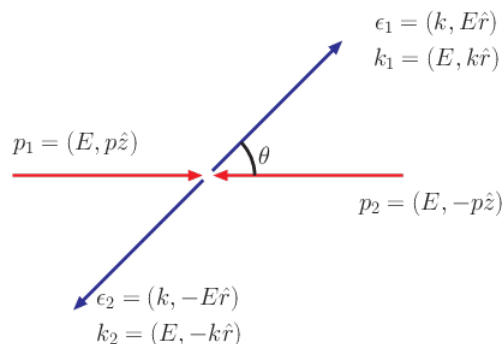
Calculation of the $e^-e^+ \rightarrow WW$ scattering amplitude

Consider the following elastic scattering process in the CM frame:

$$e^+(p_1) + e^-(p_2) \rightarrow W_L^-(k_1) + W_L^+(k_2).$$

Although we display the calculation for e^+e^- pair, it can be easily generalized for any fermion-antifermion pairs in the SM. As in Appendix A, here also we abbreviate $\epsilon_L(k_1) = \epsilon_1/M_W$ and

$\epsilon_L(k_2) = \epsilon_2/M_W$. Since $k \cdot \epsilon_L(k) = 0$ and $\epsilon_L(k) \cdot \epsilon_L(k) = -1$, we may take, in the CM frame, the momentum and polarization vectors as shown in the adjacent figure. For our calculation, we shall need the following expressions which follow from the kinematics in the CM frame:



$$\epsilon_1^\mu = k_1^\mu + \frac{M_W^2}{2E} X_1^\mu \quad \text{with } X_1^\mu = (-1, \hat{r}), \quad (\text{B.1a})$$

$$\epsilon_2^\mu = k_2^\mu + \frac{M_W^2}{2E} X_2^\mu \quad \text{with } X_2^\mu = (-1, -\hat{r}), \quad (\text{B.1b})$$

$$(\epsilon_1 - \epsilon_2)^\mu = (k_1 - k_2)^\mu + \frac{M_W^2}{E} X^\mu \quad \text{with } X^\mu = (0, \hat{r}), \quad (\text{B.1c})$$

$$k_1 \cdot k_2 = \epsilon_1 \cdot \epsilon_2 = E^2 + k^2 = \frac{s}{2} - M_W^2, \quad (\text{B.1d})$$

$$k_2 \cdot \epsilon_1 = k_1 \cdot \epsilon_2 = 2Ek = \frac{s}{2} - M_W^2 + \mathcal{O}\left(\frac{M_W^4}{E^2}\right). \quad (\text{B.1e})$$

Thus, in the high energy limit when $s \gg M_W^2$, we can approximate

$$k_1 \cdot k_2 = \epsilon_1 \cdot \epsilon_2 = k_2 \cdot \epsilon_1 = k_1 \cdot \epsilon_2 = \frac{s}{2} - M_W^2. \quad (\text{B.2})$$

The Feynman diagrams for the scattering process in consideration is displayed below.

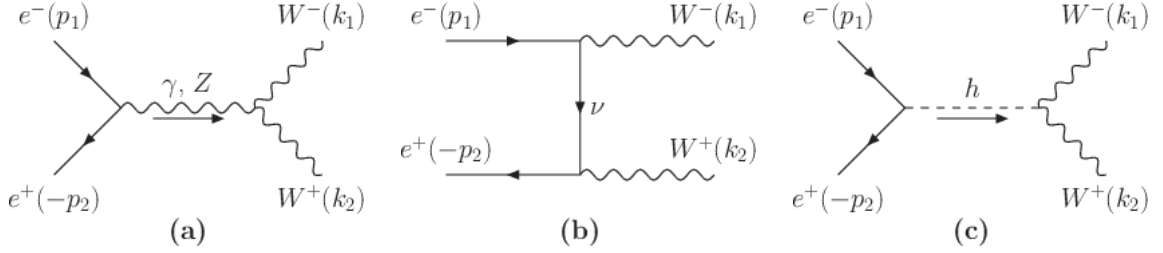


FIGURE B.1: Feynman diagrams for $e^-(p_1) + e^+(p_2) \rightarrow W_L^-(k_1) + W_L^+(k_2)$.

B.1 s-channel photon exchange

The amplitude for the relevant Feynman diagram can be written as

$$\begin{aligned} i\mathcal{M}_a^\gamma &= \bar{v}(p_2)(ie\gamma_\alpha)u(p_1) \times \left(-\frac{ig^{\alpha\beta}}{s}\right) \\ &\quad \times ie [(-k_1 + k_2)_\beta g_{\mu\nu} + (-k_2 - q)_\mu g_{\nu\beta} + (q + k_1)_\nu g_{\beta\mu}] \times \frac{\epsilon_1^\mu \epsilon_2^\nu}{M_W^2}, \end{aligned} \quad (\text{B.3})$$

where, $q = p_1 + p_2$ is the four momentum of the intermediate particle. After some simplification we obtain

$$\mathcal{M}_a^\gamma = \frac{e^2}{M_W^2 s} \bar{v}(p_2)\gamma^\beta u(p_1) [(k_2 - k_1)_\beta (\epsilon_1 \cdot \epsilon_2) - 2(k_2 \cdot \epsilon_1)\epsilon_{2\beta} + 2(k_1 \cdot \epsilon_2)\epsilon_{1\beta}] \quad (\text{B.4a})$$

$$= \frac{e^2}{M_W^2 s} \bar{v}(p_2)\gamma^\beta u(p_1) [(k_2 - k_1)_\beta - 2(\epsilon_2 - \epsilon_1)_\beta] \left\{ \left(\frac{s}{2} - M_W^2\right) + \mathcal{O}\left(\frac{M_W^4}{E^2}\right) \right\} \quad (\text{B.4b})$$

$$= \frac{e^2}{M_W^2 s} \bar{v}(p_2)\gamma^\beta u(p_1) \left[-(k_2 - k_1)_\beta + \frac{M_W^2}{E} X_\beta \right] \left\{ \left(\frac{s}{2} - M_W^2\right) + \mathcal{O}\left(\frac{M_W^4}{E^2}\right) \right\} \quad (\text{B.4c})$$

$$= \frac{e^2}{M_W^2 s} \bar{v}(p_2) \left[(\not{k}_1 - \not{k}_2) + \frac{M_W^2}{E} \not{X} \right] u(p_1) \times \left(\frac{s}{2} - M_W^2\right). \quad (\text{B.4d})$$

Now, using the conservation of four momentum we get $k_1 - k_2 = 2k_1 - (p_1 + p_2)$ and Dirac equation implies $\bar{v}(p_2)(\not{p}_1 + \not{p}_2)u(p_1) = 0$. Hence we may write

$$\bar{v}(p_2)(\not{k}_1 - \not{k}_2)u(p_1) = 2 \bar{v}(p_2) \not{k}_1 u(p_1). \quad (\text{B.5})$$

Using this, we get the final expression as

$$\mathcal{M}_a^\gamma = \frac{e^2}{M_W^2 s} \bar{v}(p_2) \left[2 \not{k}_1 + \frac{M_W^2}{E} \not{X} \right] u(p_1) \times \left(\frac{s}{2} - M_W^2 \right) \quad (\text{B.6a})$$

$$= \underbrace{\frac{e^2}{M_W^2} \bar{v}(p_2) \not{k}_1 u(p_1)}_{\mathcal{O}(E^2)} - \underbrace{\frac{2e^2}{s} \bar{v}(p_2) \not{k}_1 u(p_1) + \frac{e^2}{2E} \bar{v}(p_2) \not{X} u(p_1)}_{\mathcal{O}(1)}. \quad (\text{B.6b})$$

We have learned that the term involving X_β in Eq. (B.4c) contributes to $\mathcal{O}(1)$ terms in the amplitude and therefore will not be significant for the high energy behavior. We shall drop such terms hereafter.

B.2 s -channel Z exchange

To begin with, we will assume a general coupling of the following form:

$$\bar{e} \gamma^\mu (g_L P_L + g_R P_R) e Z_\mu \equiv \frac{1}{2} \bar{e} \gamma^\mu \{ (g_R + g_L) + (g_R - g_L) \gamma_5 \} e Z_\mu. \quad (\text{B.7})$$

Next let us be convinced that the $q^\alpha q^\beta$ term in the Z -boson propagator does not contribute to the amplitude. For this, we note the following:

$$q^\alpha q^\beta [(-k_1 + k_2)_\beta g_{\mu\nu} + (-k_2 - q)_\mu g_{\nu\beta} + (q + k_1)_\nu g_{\beta\mu}] \times \epsilon_1^\mu \epsilon_2^\nu \quad (\text{B.8a})$$

$$= q^\alpha q^\beta [(k_2 - k_1)_\beta (\epsilon_1 \cdot \epsilon_2) - 2(k_1 \cdot \epsilon_2)(\epsilon_2 - \epsilon_1)_\beta] = 0. \quad (\text{B.8b})$$

The last step follows if we substitute $q = k_1 + k_2$ and remember that $k_1^2 = k_2^2 = M_W^2$ because the external W^\pm s are on-shell and $k_1 \cdot \epsilon_1 = k_2 \cdot \epsilon_2 = 0$ due to gauge invariance.

Now denoting the WWZ coupling strength by g_{WWZ} , we can write the relevant amplitude by slightly modifying Eq. (B.4c) as:

$$\begin{aligned} \mathcal{M}_a^Z &= \frac{g_{WWZ}}{2M_W^2(s - M_Z^2)} \bar{v}(p_2) \gamma^\beta [(g_R + g_L) + (g_R - g_L) \gamma_5] u(p_1) [-(k_2 - k_1)_\beta] \\ &\quad \times \left\{ \left(\frac{s}{2} - M_W^2 \right) + \mathcal{O} \left(\frac{M_W^4}{E^2} \right) \right\} \end{aligned} \quad (\text{B.9a})$$

$$\begin{aligned} &= \frac{g_{WWZ}}{2M_W^2(s - M_Z^2)} \bar{v}(p_2) (\not{k}_1 - \not{k}_2) [(g_R + g_L) + (g_R - g_L) \gamma_5] u(p_1) \\ &\quad \times \left\{ \left(\frac{s}{2} - M_W^2 \right) + \mathcal{O} \left(\frac{M_W^4}{E^2} \right) \right\}. \end{aligned} \quad (\text{B.9b})$$

As has been calculated previously, here we have the following:

$$\bar{v}_2 (\not{k}_1 - \not{k}_2) u_1 = 2 \bar{v}_2 \not{k}_1 u_1, \quad (\text{B.10a})$$

$$\begin{aligned} \text{and, } \bar{v}_2(\not{k}_1 - \not{k}_2)\gamma^5 u_1 &= \bar{v}_2 \{2\not{k}_1 - (\not{p}_1 + \not{p}_2)\} \gamma^5 u_1 \\ &= 2\bar{v}_2 \not{k}_1 \gamma^5 u_1 - \bar{v}_2(\not{p}_1 + \not{p}_2)\gamma^5 u_1 \end{aligned} \quad (\text{B.10b})$$

$$= 2\bar{v}_2 \not{k}_1 \gamma^5 u_1 + m_e \bar{v}_2 \gamma^5 u_1 + \bar{v}_2 \gamma^5 \not{p}_1 u_1 \quad (\text{B.10c})$$

$$= 2\bar{v}_2 \not{k}_1 \gamma^5 u_1 + 2m_e \bar{v}_2 \gamma^5 u_1 = 2\bar{v}_2(\not{k}_1 + m_e)\gamma^5 u_1, \quad (\text{B.10d})$$

where we have introduced the shorthands \bar{v}_2 and u_1 for $\bar{v}(p_2)$ and $u(p_1)$ respectively. Now we rewrite Eq. (B.9b) as follows:

$$\begin{aligned} \mathcal{M}_a^Z &= \frac{g_{WWZ}}{2M_W^2 s} \times \left(1 + \frac{M_Z^2}{s} + \dots \right) \\ &\times \bar{v}_2(\not{k}_1 - \not{k}_2) \{ (g_R + g_L) + (g_R - g_L)\gamma^5 \} u_1 \times \left(\frac{s}{2} - M_W^2 \right) + \mathcal{O}(1) \end{aligned} \quad (\text{B.11a})$$

$$\approx \frac{g_{WWZ}}{2M_W^2 s} \times \bar{v}_2(\not{k}_1 - \not{k}_2) \{ (g_R + g_L) + (g_R - g_L)\gamma^5 \} u_1 \times \frac{s}{2} + \mathcal{O}(1) \quad (\text{B.11b})$$

$$= \frac{g_{WWZ}}{4M_W^2} \bar{v}_2(\not{k}_1 - \not{k}_2) \{ (g_R + g_L) + (g_R - g_L)\gamma^5 \} u_1 + \mathcal{O}(1) \quad (\text{B.11c})$$

$$= \frac{g_{WWZ}}{2M_W^2} \bar{v}_2 \{ (g_R + g_L)\not{k}_1 + (g_R - g_L)(\not{k}_1 + m_e)\gamma^5 \} u_1 + \mathcal{O}(1). \quad (\text{B.11d})$$

In the last step we have used the results of Eq. (B.10). The final expression for the Z mediated amplitude is given below:

$$\begin{aligned} \mathcal{M}_a^Z &= \underbrace{\frac{g_{WWZ}}{2M_W^2} (g_R + g_L) \bar{v}_2 \not{k}_1 u_1 + \frac{g_{WWZ}}{2M_W^2} (g_R - g_L) \bar{v}_2 \not{k}_1 \gamma^5 u_1}_{\mathcal{O}(E^2)} \\ &+ \underbrace{\frac{g_{WWZ} m_e}{2M_W^2} (g_R - g_L) \bar{v}_2 \gamma^5 u_1}_{\mathcal{O}(E)} + \mathcal{O}(1). \end{aligned} \quad (\text{B.12})$$

B.3 t -channel ν exchange

We assume the W -boson coupling with the fermions to be of the following form

$$-\frac{g}{\sqrt{2}} \bar{\nu} \gamma^\mu P_L e W_\mu^+ + \text{h.c.}$$

We now write the Feynman amplitude for the diagram B.1b as follows:

$$i\mathcal{M}_b^\nu = \bar{v}_2 \left\{ -\frac{ig}{2\sqrt{2}} \gamma_\nu (1 - \gamma^5) \right\} \frac{i(\not{q} + m_\nu)}{q^2 - m_\nu^2} \left\{ -\frac{ig}{2\sqrt{2}} \gamma_\mu (1 - \gamma^5) \right\} u_1 \times \frac{\epsilon_1^\mu \epsilon_2^\nu}{M_W^2} \quad (\text{B.13a})$$

$$\Rightarrow \mathcal{M}_b^\nu = -\frac{g^2}{8M_W^2(t - m_\nu^2)} \bar{v}_2 \gamma_\nu (1 - \gamma^5) (\not{q} + m_\nu) \gamma_\mu (1 - \gamma^5) u_1 \times \epsilon_1^\mu \epsilon_2^\nu, \quad (\text{B.13b})$$

where, $q = p_1 - k_1 = k_2 - p_2$ is the four momentum of the intermediate fermion. Note that the term proportional to m_ν at the numerator of Eq. (B.13b) do not contribute because $(1 -$

$\gamma^5)\gamma_\mu(1 - \gamma^5) = 0$. Using $(1 - \gamma^5)^2 = 2(1 - \gamma^5)$ we now rewrite Eq. (B.13b) as

$$\mathcal{M}_b^\nu = -\frac{g^2}{4M_W^2(t - m_\nu^2)} \bar{v}_2 \gamma_\nu \not{q} \gamma_\mu (1 - \gamma^5) u_1 \times \epsilon_1^\mu \epsilon_2^\nu. \quad (\text{B.13c})$$

It is worth noting at this point that any modification of $\mathcal{O}(M_W^2/E)$ in ϵ_1 or ϵ_2 will lead to $\mathcal{O}(1)$ contribution to the amplitude. Hence, using $\epsilon_1^\mu \approx k_1^\mu$ and $\epsilon_2^\mu \approx k_2^\mu$ in Eq. (B.13c), we obtain

$$\mathcal{M}_b^\nu = -\frac{g^2}{4M_W^2(t - m_\nu^2)} [\bar{v}_2 \not{k}_2 (\not{p}_1 - \not{k}_1) \not{k}_1 (1 - \gamma^5) u_1] + \mathcal{O}(1). \quad (\text{B.13d})$$

Now note that

$$\begin{aligned} (p_1 - k_1)k_1 u_1 &= (p_1 k_1 - k_1^2)u_1 = (2p_1 \cdot k_1 - k_1 p_1 - k_1^2)u_1 \\ &= (2p_1 \cdot k_1 - k_1^2)u_1 - m_e k_1 u_1 = (-t + m_e^2)u_1 - m_e k_1 u_1. \end{aligned} \quad (\text{B.14a})$$

Similarly, one can easily obtain

$$(p_1 - k_1)k_1(1 - \gamma^5)u_1 = (-t + m_e^2)(1 - \gamma^5)u_1 - m_e k_1(1 + \gamma^5)u_1. \quad (\text{B.14b})$$

Let us now proceed to simplify the expression that appears inside the square bracket in Eq. (B.13d):

$$\bar{v}_2 k_2 (p_1 - k_1)k_1(1 - \gamma^5)u_1 = \underbrace{-(t - m_e^2)\bar{v}_2 k_2(1 - \gamma^5)u_1}_{T_1} - \underbrace{m_e \bar{v}_2 k_2 k_1(1 + \gamma^5)u_1}_{T_2}. \quad (\text{B.14c})$$

■ **Evaluation of T_1 :**

$$\begin{aligned} T_1 &= -(t - m_e^2)\bar{v}_2 k_2(1 - \gamma^5)u_1 = -(t - m_e^2)\bar{v}_2(p_1 + p_2 - k_1)(1 - \gamma^5)u_1 \\ &= (t - m_e^2)\bar{v}_2 k_1(1 - \gamma^5)u_1 - (t - m_e^2)\bar{v}_2(p_1 + p_2)(1 - \gamma^5)u_1 \\ &= (t - m_e^2)\bar{v}_2 k_1(1 - \gamma^5)u_1 - 2m_e(t - m_e^2)\bar{v}_2 \gamma^5 u_1, \end{aligned} \quad (\text{B.14d})$$

where, in the last step, we have used the following identity:

$$\begin{aligned} \bar{v}_2(p_1 + p_2)(1 - \gamma^5)u_1 &= \bar{v}_2 p_2(1 - \gamma^5)u_1 + \bar{v}_2(1 + \gamma^5)p_1 u_1 \\ &= -m_e \bar{v}_2(1 - \gamma^5)u_1 + m_e \bar{v}_2(1 + \gamma^5)u_1 \\ &= 2m_e \bar{v}_2 \gamma^5 u_1. \end{aligned} \quad (\text{B.14e})$$

■ **Evaluation of T_2 :** For this, let us first note the following:

$$k_2 k_1 = (p_1 + p_2 - k_1)k_1 = p_1 k_1 + p_2 k_1 - k_1^2$$

$$= 2(p_1 \cdot k_1) - k_1 p_1 + p_2 k_1 - k_1^2 = -(t - m_e^2) - k_1 p_1 + p_2 k_1. \quad (\text{B.14f})$$

Now we can write

$$\begin{aligned} T_2 &= -m_e \bar{v}_2 k_2 k_1 (1 + \gamma^5) u_1 \\ &= m_e (t - m_e^2) \bar{v}_2 (1 + \gamma^5) u_1 + m_e \bar{v}_2 k_1 p_1 (1 + \gamma^5) u_1 - m_e \bar{v}_2 p_2 k_1 (1 + \gamma^5) u_1 \\ &= m_e (t - m_e^2) \bar{v}_2 (1 + \gamma^5) u_1 + m_e^2 \bar{v}_2 k_1 (1 - \gamma^5) u_1 + m_e^2 \bar{v}_2 k_1 (1 + \gamma^5) u_1. \end{aligned} \quad (\text{B.14g})$$

Therefore, adding Eqs. (B.14d) and (B.14g) together, we obtain

$$\begin{aligned} T_1 + T_2 &= t \bar{v}_2 k_1 (1 - \gamma^5) u_1 + m_e (t - m_e^2) \bar{v}_2 (1 - \gamma^5) u_1 + m_e^2 \bar{v}_2 k_1 (1 + \gamma^5) u_1 \\ &= \underbrace{t \bar{v}_2 k_1 (1 - \gamma^5) u_1}_{\text{leads to } \mathcal{O}(E^2)} + \underbrace{m_e t \bar{v}_2 (1 - \gamma^5) u_1}_{\text{leads to } \mathcal{O}(E)} \\ &\quad + \underbrace{m_e^2 \bar{v}_2 k_1 (1 + \gamma^5) u_1}_{\text{leads to } \mathcal{O}(1)} - \underbrace{m_e^3 \bar{v}_2 (1 - \gamma^5) u_1}_{\text{leads to } \mathcal{O}(1/E)}. \end{aligned} \quad (\text{B.14h})$$

Now we recast Eq. (B.13d) as follows:

$$\begin{aligned} \mathcal{M}_b^\nu &= -\frac{g^2}{4M_W^2 t} \left(1 + \frac{m_\nu^2}{t} + \dots \right) [T_1 + T_2] + \mathcal{O}(1) \\ &= -\frac{g^2}{4M_W^2} \bar{v}_2 k_1 (1 - \gamma^5) u_1 - \frac{g^2 m_e}{4M_W^2} \bar{v}_2 (1 - \gamma^5) u_1 + \mathcal{O}(1), \end{aligned} \quad (\text{B.15})$$

where we have used the result of Eq. (B.14h). One interesting thing to note from Eq. (B.15) is that the mass of the intermediate fermion (m_ν in this case) does not appear in the coefficients of the terms that grow with energy.

B.4 Amplitude without the Higgs

We now add Eqs. (B.6b), (B.12) and (B.15) together to obtain

$$\begin{aligned} \mathcal{M}_{a+b} &= \left[\frac{e^2}{M_W^2} + \frac{g_{WWZ}}{2M_W^2} (g_R + g_L) - \frac{g^2}{4M_W^2} \right] \underbrace{\bar{v}_2 k_1 u_1}_{\mathcal{O}(E^2)} + \left[\frac{g_{WWZ}}{2M_W^2} (g_R - g_L) + \frac{g^2}{4M_W^2} \right] \underbrace{\bar{v}_2 k_1 \gamma^5 u_1}_{\mathcal{O}(E^2)} \\ &\quad + m_e \left[\frac{g_{WWZ}}{2M_W^2} (g_R - g_L) + \frac{g^2}{4M_W^2} \right] \underbrace{\bar{v}_2 \gamma^5 u_1}_{\mathcal{O}(E)} - \frac{g^2 m_e}{4M_W^2} \underbrace{\bar{v}_2 u_1}_{\mathcal{O}(E)} + \mathcal{O}(1). \end{aligned} \quad (\text{B.16})$$

Clearly, the cancellation of $\mathcal{O}(E^2)$ growth requires

$$e^2 + \frac{g_{WWZ}}{2} (g_R + g_L) - \frac{g^2}{4} = 0, \quad (\text{B.17a})$$

$$\frac{g_{WWZ}}{2}(g_R - g_L) + \frac{g^2}{4} = 0. \quad (\text{B.17b})$$

Note that the condition (B.17b) also guarantees the cancellation of $\bar{v}_2\gamma^5 u_1$ term in Eq. (B.16). Thus no additional new physics contribution is required to cancel the $\mathcal{O}(E)$ growth carried by the $\bar{v}_2\gamma^5 u_1$ term. Remember that in the case of SM

$$g_L + g_R = \frac{g}{\cos\theta_w} \left(\frac{1}{2} - 2\sin^2\theta_w \right), \quad g_L - g_R = \frac{g}{2\cos\theta_w}, \quad (\text{B.18a})$$

$$e = g \sin\theta_w, \quad \text{and} \quad g_{WWZ} = g \cos\theta_w, \quad (\text{B.18b})$$

so that the conditions (B.17) are trivially satisfied. Thus only the $\mathcal{O}(E)$ growth carried by the term proportional to $\bar{v}_2 u_1$ remains to be canceled in Eq. (B.16). This necessitates the introduction of a new scalar particle with suitable interactions.

B.5 s -channel Higgs exchange

We assume the relevant couplings to be of the form

$$g_{eeh}\bar{e}(\cos\delta + i\sin\delta\gamma^5)eh + g_{WWh}W_\mu^+W^{\mu-}h. \quad (\text{B.19})$$

With this, one can write the Feynman amplitude for the diagram B.1c as follows:

$$i\mathcal{M}_c^h = \bar{v}_2 \{ig_{eeh}(\cos\delta + i\sin\delta\gamma^5)\} u_1 \frac{i}{s - m_h^2} (ig_{WWh}g_{\mu\nu}) \frac{\epsilon_1^\mu \epsilon_2^\nu}{M_W^2} \quad (\text{B.20a})$$

$$\Rightarrow \mathcal{M}_c^h = -\frac{g_{eeh}g_{WWh}}{M_W^2(s - m_h^2)} \bar{v}_2(\cos\delta + i\sin\delta\gamma^5)u_1(\epsilon_1 \cdot \epsilon_2) \quad (\text{B.20b})$$

$$= -\frac{g_{eeh}g_{WWh}}{M_W^2 s} \left(1 + \frac{m_h^2}{s} + \dots \right) \left(\frac{s}{2} - M_W^2 \right) \times \bar{v}_2(\cos\delta + i\sin\delta\gamma^5)u_1 \quad (\text{B.20c})$$

$$\approx -\frac{g_{eeh}g_{WWh}}{2M_W^2} \cos\delta \bar{v}_2 u_1 - \frac{ig_{eeh}g_{WWh}}{2M_W^2} \sin\delta \bar{v}_2\gamma^5 u_1 + \mathcal{O}\left(\frac{1}{E}\right). \quad (\text{B.20d})$$

In the case of SM

$$g_{eeh} = -\frac{gm_e}{2M_W}, \quad \delta = 0, \quad \text{and} \quad g_{WWh} = gM_W. \quad (\text{B.21})$$

Hence,

$$\left(\mathcal{M}_c^h\right)^{\text{SM}} = \frac{g^2 m_e}{4M_W^2} \bar{v}_2 u_1 + \mathcal{O}\left(\frac{1}{E}\right), \quad (\text{B.22})$$

which is exactly opposite to the residual $\mathcal{O}(E)$ growth in Eq. (B.16).

B.6 Explicit evaluation of the energy growths

To begin with, we write down the Dirac spinors for free fermions as

$$u^r(\vec{p}) = \sqrt{E+m} \begin{pmatrix} \chi^r \\ \frac{\vec{\sigma} \cdot \vec{p}}{E+m} \chi^r \end{pmatrix}, \quad v^r(\vec{p}) = -\sqrt{E+m} \begin{pmatrix} \frac{\vec{\sigma} \cdot \vec{p}}{E+m} \chi^r \\ \chi^r \end{pmatrix}, \quad (\text{B.23})$$

where the superscript r ($= 1, 2$) represents the helicity of the fermion. The column matrices, χ^r , are given by

$$\chi^1 = \begin{pmatrix} 1 \\ 0 \end{pmatrix}, \quad \chi^2 = \begin{pmatrix} 0 \\ 1 \end{pmatrix}. \quad (\text{B.24})$$

The orthonormality conditions satisfied by the spinors u and v are given below:

$$u^{r\dagger}(\vec{p})u^s(\vec{p}) = 2E\delta^{rs} \quad \text{or,} \quad \bar{u}^r(\vec{p})u^s(\vec{p}) = 2m\delta^{rs}, \quad (\text{B.25a})$$

$$v^{r\dagger}(\vec{p})v^s(\vec{p}) = 2E\delta^{rs} \quad \text{or,} \quad \bar{v}^r(\vec{p})v^s(\vec{p}) = -2m\delta^{rs}, \quad (\text{B.25b})$$

$$\bar{u}^r(\vec{p})v^s(\vec{p}) = \bar{v}^r(\vec{p})u^s(\vec{p}) = 0. \quad (\text{B.25c})$$

But note that,

$$u^{r\dagger}(\vec{p})v^s(\vec{p}) \neq 0 \quad \text{and} \quad v^{r\dagger}(\vec{p})u^s(\vec{p}) \neq 0, \quad (\text{B.25d})$$

$$\text{however,} \quad u^{r\dagger}(\vec{p})v^s(-\vec{p}) = 0 \quad \text{and} \quad v^{r\dagger}(-\vec{p})u^s(\vec{p}) \neq 0. \quad (\text{B.25e})$$

Taking the direction of \vec{p}_1 to be the positive z -axis and assuming that the scattering takes place in the x - z plane, we may take the different momentum four vectors as follows:

$$p_1^\mu = (E, 0, 0, p), \quad p_2^\mu = (E, 0, 0, -p), \quad (\text{B.26a})$$

$$k_1^\mu = (E, k \sin \theta, 0, k \cos \theta), \quad k_2^\mu = (E, -k \sin \theta, 0, -k \cos \theta). \quad (\text{B.26b})$$

In the Dirac-Pauli representation, different gamma matrices take the following form:

$$\gamma^0 = \gamma_0 = \begin{pmatrix} 1 & 0 \\ 0 & -1 \end{pmatrix}, \quad \gamma^i = -\gamma_i = \begin{pmatrix} 0 & \sigma_i \\ -\sigma_i & 0 \end{pmatrix}, \quad \gamma^5 = \gamma_5 = \begin{pmatrix} 0 & 1 \\ 1 & 0 \end{pmatrix}. \quad (\text{B.27})$$

Using these one may easily obtain

$$k_1^\mu = k_1^0 \gamma_0 + k_1^i \gamma_i = \begin{pmatrix} E & -k\vec{\sigma} \cdot \hat{e} \\ k\vec{\sigma} \cdot \hat{e} & -E \end{pmatrix}, \quad (\text{B.28})$$

where $\hat{e} = (\sin \theta, 0, \cos \theta)$ is the unit vector in the direction of \vec{k}_1 . Similarly, one can also get

$$\not{k}_1 \gamma^5 = \begin{pmatrix} -k\vec{\sigma} \cdot \hat{e} & E \\ -E & k\vec{\sigma} \cdot \hat{e} \end{pmatrix}. \quad (\text{B.29})$$

Then clearly,

$$\gamma^0 \not{k}_1 = \begin{pmatrix} E & -k\vec{\sigma} \cdot \hat{e} \\ -k\vec{\sigma} \cdot \hat{e} & E \end{pmatrix}, \quad \gamma^0 \not{k}_1 \gamma^5 = \begin{pmatrix} -k\vec{\sigma} \cdot \hat{e} & E \\ E & -k\vec{\sigma} \cdot \hat{e} \end{pmatrix}. \quad (\text{B.30})$$

Again note that,

$$\frac{\vec{\sigma} \cdot \vec{p}_1}{E+m} \approx \sigma_z + \mathcal{O}\left(\frac{1}{E}\right), \quad \frac{\vec{\sigma} \cdot \vec{p}_2}{E+m} \approx -\sigma_z + \mathcal{O}\left(\frac{1}{E}\right). \quad (\text{B.31})$$

Now using $\sigma_z \chi^1 = \chi^1$ and $\sigma_z \chi^2 = -\chi^2$ one may easily show the following:

$$u^1(\vec{p}_1) = \sqrt{E} \begin{pmatrix} 1 \\ 1 \end{pmatrix} \chi^1 + \mathcal{O}\left(\frac{1}{\sqrt{E}}\right), \quad u^2(\vec{p}_1) = \sqrt{E} \begin{pmatrix} 1 \\ -1 \end{pmatrix} \chi^2 + \mathcal{O}\left(\frac{1}{\sqrt{E}}\right) \quad (\text{B.32a})$$

$$v^1(\vec{p}_2) = \sqrt{E} \begin{pmatrix} 1 \\ -1 \end{pmatrix} \chi^1 + \mathcal{O}\left(\frac{1}{\sqrt{E}}\right), \quad v^2(\vec{p}_1) = -\sqrt{E} \begin{pmatrix} 1 \\ 1 \end{pmatrix} \chi^2 + \mathcal{O}\left(\frac{1}{\sqrt{E}}\right) \quad (\text{B.32b})$$

$$\Rightarrow \bar{v}^1(\vec{p}_2) = v^{1\dagger}(\vec{p}_2) \gamma^0 = \sqrt{E} \chi^{1\dagger} \begin{pmatrix} 1 & 1 \end{pmatrix}, \quad \bar{v}^2(\vec{p}_1) = -\sqrt{E} \chi^{2\dagger} \begin{pmatrix} 1 & -1 \end{pmatrix}. \quad (\text{B.32c})$$

B.6.1 The same helicity case

■ **Case-I** ($r_1 = r_2 = 1$):

$$\bar{v}^1(\vec{p}_2) u^1(\vec{p}_1) = E \chi^{1\dagger} \begin{pmatrix} 1 & 1 \end{pmatrix} \begin{pmatrix} 1 \\ 1 \end{pmatrix} \chi^1 = 2E. \quad (\text{B.33a})$$

$$\bar{v}^1(\vec{p}_2) \gamma^5 u^1(\vec{p}_1) = E \chi^{1\dagger} \begin{pmatrix} 1 & 1 \end{pmatrix} \begin{pmatrix} 0 & 1 \\ 1 & 0 \end{pmatrix} \begin{pmatrix} 1 \\ 1 \end{pmatrix} \chi^1 = 2E. \quad (\text{B.33b})$$

$$\bar{v}^1(\vec{p}_2) \not{k}_1 u^1(\vec{p}_1) = E \chi^{1\dagger} \begin{pmatrix} 1 & 1 \end{pmatrix} \begin{pmatrix} E & -k\vec{\sigma} \cdot \hat{e} \\ k\vec{\sigma} \cdot \hat{e} & -E \end{pmatrix} \begin{pmatrix} 1 \\ 1 \end{pmatrix} \chi^1 = 0. \quad (\text{B.33c})$$

$$\bar{v}^1(\vec{p}_2) \not{k}_1 \gamma^5 u^1(\vec{p}_1) = E \chi^{1\dagger} \begin{pmatrix} 1 & 1 \end{pmatrix} \begin{pmatrix} -k\vec{\sigma} \cdot \hat{e} & E \\ -E & k\vec{\sigma} \cdot \hat{e} \end{pmatrix} \begin{pmatrix} 1 \\ 1 \end{pmatrix} \chi^1 = 0. \quad (\text{B.33d})$$

■ **Case-I** ($r_1 = r_2 = 2$):

$$\bar{v}^2(\vec{p}_2) u^2(\vec{p}_1) = E \chi^{2\dagger} \begin{pmatrix} 1 & -1 \end{pmatrix} \begin{pmatrix} 1 \\ -1 \end{pmatrix} \chi^2 = 2E. \quad (\text{B.34a})$$

$$\bar{v}^2(\vec{p}_2)\gamma^5 u^2(\vec{p}_1) = E\chi^{2\dagger} \begin{pmatrix} 1 & -1 \end{pmatrix} \begin{pmatrix} 0 & 1 \\ 1 & 0 \end{pmatrix} \begin{pmatrix} 1 \\ -1 \end{pmatrix} \chi^2 = -2E. \quad (\text{B.34b})$$

$$\bar{v}^2(\vec{p}_2)k'_1 u^2(\vec{p}_1) = E\chi^{2\dagger} \begin{pmatrix} 1 & -1 \end{pmatrix} \begin{pmatrix} E & -k\vec{\sigma} \cdot \hat{e} \\ k\vec{\sigma} \cdot \hat{e} & -E \end{pmatrix} \begin{pmatrix} 1 \\ -1 \end{pmatrix} \chi^2 = 0. \quad (\text{B.34c})$$

$$\bar{v}^2(\vec{p}_2)k'_1\gamma^5 u^2(\vec{p}_1) = E\chi^{2\dagger} \begin{pmatrix} 1 & -1 \end{pmatrix} \begin{pmatrix} -k\vec{\sigma} \cdot \hat{e} & E \\ -E & k\vec{\sigma} \cdot \hat{e} \end{pmatrix} \begin{pmatrix} 1 \\ -1 \end{pmatrix} \chi^2 = 0. \quad (\text{B.34d})$$

B.6.2 The opposite helicity case

■ **Case-I** ($r_1 = 1, r_2 = 2$):

$$\bar{v}^2(\vec{p}_2)u^1(\vec{p}_1) = -E\chi^{2\dagger} \begin{pmatrix} 1 & -1 \end{pmatrix} \begin{pmatrix} 1 \\ 1 \end{pmatrix} \chi^1 = 0. \quad (\text{B.35a})$$

$$\bar{v}^2(\vec{p}_2)\gamma^5 u^1(\vec{p}_1) = -E\chi^{1\dagger} \begin{pmatrix} 1 & -1 \end{pmatrix} \begin{pmatrix} 0 & 1 \\ 1 & 0 \end{pmatrix} \begin{pmatrix} 1 \\ 1 \end{pmatrix} \chi^1 = 0. \quad (\text{B.35b})$$

$$\begin{aligned} \bar{v}^2(\vec{p}_2)k'_1 u^1(\vec{p}_1) &= -E\chi^{2\dagger} \begin{pmatrix} 1 & -1 \end{pmatrix} \begin{pmatrix} E & -k\vec{\sigma} \cdot \hat{e} \\ k\vec{\sigma} \cdot \hat{e} & -E \end{pmatrix} \begin{pmatrix} 1 \\ 1 \end{pmatrix} \chi^1 \\ &= -2E \chi^{2\dagger} \{E - k\vec{\sigma} \cdot \hat{e}\} \chi^1 = 2Ek \sin \theta. \end{aligned} \quad (\text{B.35c})$$

$$\begin{aligned} \bar{v}^2(\vec{p}_2)k'_1\gamma^5 u^1(\vec{p}_1) &= -E\chi^{2\dagger} \begin{pmatrix} 1 & -1 \end{pmatrix} \begin{pmatrix} -k\vec{\sigma} \cdot \hat{e} & E \\ -E & k\vec{\sigma} \cdot \hat{e} \end{pmatrix} \begin{pmatrix} 1 \\ 1 \end{pmatrix} \chi^1 \\ &= -2E \chi^{2\dagger} \{E - k\vec{\sigma} \cdot \hat{e}\} \chi^1 = 2Ek \sin \theta. \end{aligned} \quad (\text{B.35d})$$

In the last two steps we have used the following:

$$E - k\vec{\sigma} \cdot \hat{e} = E \mathbf{I}_2 - k\sigma_x \sin \theta - k\sigma_z \cos \theta, \quad (\text{B.36a})$$

$$\mathbf{I}_2 \chi^1 = \chi^1, \quad \sigma_z \chi^1 = \chi^1, \quad \sigma_x \chi^1 = \chi^2, \quad \chi^{2\dagger} \chi^1 = 0. \quad (\text{B.36b})$$

C

Flavor observables and 2HDM

C.1 Neutral meson mixing

The dominant one-loop effective Lagrangian for $\Delta F = 2$ is

$$\mathcal{L}_{\text{eff}}^{\Delta F=2} = \frac{G_F^2 M_W^2}{16\pi^2} \sum_{a,b=u,c,t} \lambda_a \lambda_b w_a w_b [S(w_a, w_b) + X_a X_b \{2I_1(w_a, w_b, w_{1+}) + X_a X_b I_2(w_a, w_b, w_{1+})\}] O_F. \quad (\text{C.1})$$

Here, the $S(w_a, w_b)$ part is the SM contribution and the rest is due to the charged Higgs box diagrams. For i -type BGL model, $X_q = -\cot \beta$ if $q = i$ and $X_q = \tan \beta$ otherwise. Since we have assumed the external particles to have zero (four) momenta, the down-type quark masses have been set to zero. Under this approximation, the charged Higgs part of the Yukawa interaction for Type I and II models are identical and scaled by a $\cot \beta$ factor for all three generations. This means, for Type I and II models, $X_q = \cot \beta$ for $q = u, c, t$. The dimension-6 operator for $K^0-\bar{K}^0$ mixing is

$$O_F = (\bar{s}\gamma^\mu P_L d)^2. \quad (\text{C.2})$$

Similar expressions can be obtained for B systems. The relevant parameters and functions are defined as follows:

$$\begin{aligned}
\lambda_a = V_{ad}^* V_{as}, \quad w_a &= \frac{m_a^2}{M_W^2}, \quad f(x) = \frac{(x^2 - 8x + 4) \ln x + 3(x - 1)}{(x - 1)^2}, \\
S(w_a, w_b) &= \frac{f(w_a) - f(w_b)}{w_a - w_b}, \quad g(x, y, z) = \frac{x(x - 4) \ln x}{(x - 1)(x - y)(x - z)}, \\
I_1(w_a, w_b, w_c) &= [g(w_a, w_b, w_c) + g(w_b, w_c, w_a) + g(w_c, w_a, w_b)], \\
I_2(w_a, w_b, w_c) &= \frac{1}{w_a - w_b} \left[\frac{w_a^2 \ln w_a}{(w_c - w_a)^2} - \frac{w_b^2 \ln w_b}{(w_c - w_b)^2} \right] \\
&\quad + \frac{w_c [(w_c - w_a)(w_c - w_b) + \{2w_a w_b - w_c(w_a + w_b)\} \ln w_c]}{(w_c - w_a)^2 (w_c - w_b)^2}. \quad (\text{C.3})
\end{aligned}$$

Obtaining M_{12} from the effective Lagrangian is straightforward. As an example, for K -meson system (with B_K as bag parameter),

$$M_{12}^K = -\frac{1}{2m_K} \langle K^0 | \mathcal{L}_{\text{eff}}^{\Delta F=2} | \bar{K}^0 \rangle, \quad (\text{C.4})$$

$$\langle K^0 | O_F | \bar{K}^0 \rangle = \frac{2}{3} f_K^2 m_K^2 B_K. \quad (\text{C.5})$$

C.2 Expressions for $b \rightarrow s\gamma$

The effective Lagrangian for $b \rightarrow s\gamma$ can be written as

$$\begin{aligned}
\mathcal{L}_{\text{eff}} &= \sqrt{\frac{G_F^2}{8\pi^3}} V_{ts}^* V_{tb} m_b [\sqrt{\alpha} \{C_{7L} \bar{s}_L \sigma^{\mu\nu} b_R + C_{7R} \bar{s}_R \sigma^{\mu\nu} b_L\} F_{\mu\nu} \\
&\quad \sqrt{\alpha_s} \{C_{8L} \bar{s}_L T_a \sigma^{\mu\nu} b_R + C_{8R} \bar{s}_R T_a \sigma^{\mu\nu} b_L\} G_{\mu\nu}^a] + \text{h.c.}, \quad (\text{C.6})
\end{aligned}$$

where $F_{\mu\nu}$ and $G_{\mu\nu}^a$ are field strength tensors for photon and gluon, respectively, and T^a s are the SU(3) generators. The branching ratio $\text{Br}(b \rightarrow s\gamma)$ is given by

$$\frac{\text{Br}(b \rightarrow s\gamma)}{\text{Br}(b \rightarrow ce\bar{\nu})} = \frac{6\alpha}{\pi B} \left| \frac{V_{ts}^* V_{tb}}{V_{cb}} \right|^2 \left[|C_{7L}^{\text{eff}}|^2 + |C_{7R}^{\text{eff}}|^2 \right], \quad (\text{C.7})$$

where, we have taken $B = 0.546$ [62]. The effective Wilson coefficients are

$$C_{7L}^{\text{eff}} = \eta^{16/23} C_{7L} + \frac{8}{3} \left(\eta^{14/23} - \eta^{16/23} \right) C_{8L} + \mathcal{C}, \quad (\text{C.8a})$$

$$C_{7R}^{\text{eff}} = \eta^{16/23} C_{7R} + \frac{8}{3} \left(\eta^{14/23} - \eta^{16/23} \right) C_{8R}. \quad (\text{C.8b})$$

In the above equations, $\eta = \alpha_s(M_Z)/\alpha_s(\mu)$, where μ is the QCD renormalization scale; \mathcal{C} corresponds to the leading log QCD corrections in SM. In the expression for the effective Wilson

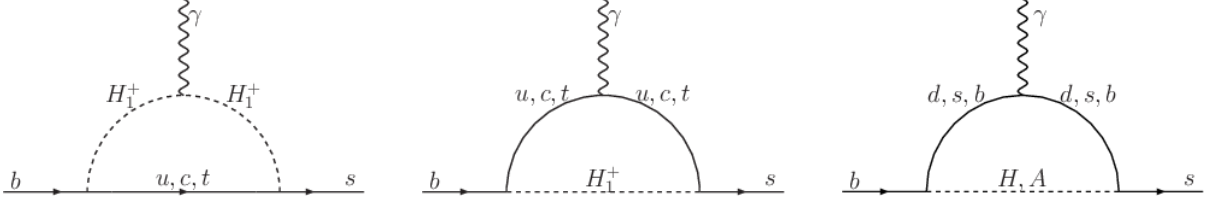


FIGURE C.1: Feynman diagrams involving nonstandard scalars contributing to $b \rightarrow s\gamma$ amplitude.

co-efficients (Eq. (C.8)), the correction term is given by

$$\mathcal{C} = \sum_{i=1}^8 h_i \eta^{a_i}, \quad (\text{C.9})$$

where,

$$a_i = \left(\frac{14}{23}, \frac{16}{23}, \frac{6}{23}, -\frac{12}{23}, 0.4086, -0.4230, -0.8994, 0.1456 \right), \quad (\text{C.10a})$$

$$h_i = \left(\frac{626126}{272277}, -\frac{56281}{51730}, -\frac{3}{7}, -\frac{1}{14}, \right. \\ \left. -0.6494, -0.0380, -0.0186, -0.0057 \right). \quad (\text{C.10b})$$

These values of h_i and a_i can be found in [70] [see Eq. (2.3) and Table 1 of Ref. [70]].

To understand the above expressions, we first define the following functions:

$$\mathcal{F}_0(t) = \int_0^1 dx \frac{1-x}{x+(1-x)t} = -\frac{1}{1-t} - \frac{\ln t}{(1-t)^2}, \quad (\text{C.11a})$$

$$\mathcal{F}_1(t) = \int_0^1 dx \frac{(1-x)^2}{x+(1-x)t} = \frac{-3+4t-t^2}{2(1-t)^3} - \frac{\ln t}{(1-t)^3}, \quad (\text{C.11b})$$

$$\mathcal{F}_2(t) = \int_0^1 dx \frac{(1-x)^3}{x+(1-x)t} = \frac{-11+18t-9t^2+2t^3-6\ln t}{6(1-t)^4}, \quad (\text{C.11c})$$

$$\overline{\mathcal{F}}_0(t) = \int_0^1 dx \frac{x}{x+(1-x)t} = \frac{1-t+t\ln t}{(1-t)^2}, \quad (\text{C.11d})$$

$$\overline{\mathcal{F}}_1(t) = \int_0^1 dx \frac{x^2}{x+(1-x)t} = \frac{1-4t+3t^2-2t^2\ln t}{2(1-t)^3}, \quad (\text{C.11e})$$

$$\overline{\mathcal{F}}_2(t) = \int_0^1 dx \frac{x^3}{x + (1-x)t} = \frac{2 - 9t + 18t^2 - 11t^3 + 6t^3 \ln t}{6(1-t)^4}. \quad (\text{C.11f})$$

Let us further define $x_t = m_t^2/m_W^2$, $y_q = m_q^2/m_{1+}^2$, $z_q = m_q^2/m_H^2$, $z'_q = m_q^2/m_A^2$. Now the expressions for C_{7L} , C_{7R} , C_{8L} , C_{8R} read

$$C_{7L} = A_\gamma^{\text{SM}} + A_{\gamma L}^+ + \frac{Q_b}{V_{ts}^* V_{tb}} \sum_{q=b,s} [A_L^H(z_q) + A_L^A(z'_q)], \quad (\text{C.12a})$$

$$C_{7R} = \frac{m_s}{m_b} A_\gamma^{\text{SM}} + A_{\gamma R}^+ + \frac{Q_b}{V_{ts}^* V_{tb}} \sum_{q=b,s} [A_R^H(z_q) + A_R^A(z'_q)], \quad (\text{C.12b})$$

$$C_{8L} = A_g^{\text{SM}} + A_{gL}^+ + \frac{1}{V_{ts}^* V_{tb}} \sum_{q=b,s} [A_L^H(z_q) + A_L^A(z'_q)], \quad (\text{C.12c})$$

$$C_{8R} = \frac{m_s}{m_b} A_g^{\text{SM}} + A_{gR}^+ + \frac{1}{V_{ts}^* V_{tb}} \sum_{q=b,s} [A_R^H(z_q) + A_R^A(z'_q)]. \quad (\text{C.12d})$$

In the above expressions, A^+ and $A^{H,A}$ represent the (nonstandard) charged and neutral scalar contributions respectively (See Fig. C.1). Note that $A^{H,A} = 0$ for Type I and II 2HDMs because of the absence of tree-level FCNC in these models. They only become relevant in case of BGL models.

The SM and the new physics contributions are given below:

■ SM:

$$A_\gamma^{\text{SM}} = \frac{1}{2} \left[\overline{\mathcal{F}}_1(x_t) + \overline{\mathcal{F}}_2(x_t) + \frac{1}{2} x_t \overline{\mathcal{F}}_2(x_t) - \frac{3}{2} x_t \overline{\mathcal{F}}_1(x_t) + x_t \overline{\mathcal{F}}_0(x_t) + \frac{4}{3} \mathcal{F}_0(x_t) - 2\mathcal{F}_1(x_t) + \frac{2}{3} \mathcal{F}_2(x_t) + \frac{1}{3} x_t \mathcal{F}_1(x_t) + \frac{1}{3} x_t \mathcal{F}_2(x_t) \right] - \frac{23}{36}, \quad (\text{C.13a})$$

$$A_g^{\text{SM}} = \frac{1}{2} \left[2\mathcal{F}_0(x_t) - 3\mathcal{F}_1(x_t) + \mathcal{F}_2(x_t) + \frac{1}{2} x_t \mathcal{F}_1(x_t) + \frac{1}{2} x_t \mathcal{F}_2(x_t) \right] - \frac{1}{3}, \quad (\text{C.13b})$$

■ Charged Higgs:

BGL Models:

$$A_{gL}^+ = \frac{1}{4V_{ts}^* V_{tb}} \sum_{q=u,c,t} V_{qs}^* V_{qb} X_q^2 [y_q \mathcal{F}_1(y_q) + y_q \mathcal{F}_2(y_q)], \quad (\text{C.14a})$$

$$A_{\gamma L}^+ = \frac{1}{V_{ts}^* V_{tb}} \sum_{q=u,c,t} V_{qs}^* V_{qb} X_q^2 C(y_q), \quad (\text{C.14b})$$

$$A_{gR}^+ = \frac{m_s}{m_b} A_{gL}^+, \quad A_{\gamma R}^+ = \frac{m_s}{m_b} A_{\gamma L}^+, \quad (\text{C.14c})$$

with

$$C(y) = \frac{1}{2} \left[\frac{1}{2} y \overline{\mathcal{F}}_2(y) - \frac{3}{2} y \overline{\mathcal{F}}_1(y) + y \overline{\mathcal{F}}_0(y) + \frac{1}{3} y \mathcal{F}_1(y) + \frac{1}{3} y \mathcal{F}_2(y) \right], \quad (\text{C.15})$$

and for i -type model, $X_q = -\cot \beta$ if $q = i$ and $X_q = \tan \beta$ otherwise (e.g. for t -type model, $X_u = X_c = \tan \beta$, $X_t = -\cot \beta$).

Type I and II Models:

$$A_{\gamma L}^+ = \frac{1}{V_{ts}^* V_{tb}} \sum_{q=u,c,t} V_{qs}^* V_{qb} \left[C_{1L}(y_q) + \frac{2}{3} C_{2L}(y_q) \right], \quad (\text{C.16a})$$

$$A_{\gamma R}^+ = \frac{1}{V_{ts}^* V_{tb}} \sum_{q=u,c,t} V_{qs}^* V_{qb} \left[C_{1R}(y_q) + \frac{2}{3} C_{2R}(y_q) \right], \quad (\text{C.16b})$$

$$A_{gL}^+ = \frac{1}{V_{ts}^* V_{tb}} \sum_{q=u,c,t} V_{qs}^* V_{qb} C_{2L}(y_q), \quad (\text{C.16c})$$

$$A_{gR}^+ = \frac{1}{V_{ts}^* V_{tb}} \sum_{q=u,c,t} V_{qs}^* V_{qb} C_{2R}(y_q), \quad (\text{C.16d})$$

with,

$$C_{1L}(y_q) = \frac{y_q}{2} \left[\frac{1}{2} \{ \overline{\mathcal{F}}_2(y_q) - \overline{\mathcal{F}}_1(y_q) \} \left(\frac{m_s^2}{m_q^2} Y^2 + X^2 \right) + XY \{ \overline{\mathcal{F}}_1(y_q) - \overline{\mathcal{F}}_0(y_q) \} \right], \quad (\text{C.17a})$$

$$C_{1R}(y_q) = \frac{y_q}{2} \left[\frac{1}{2} \{ \overline{\mathcal{F}}_2(y_q) - \overline{\mathcal{F}}_1(y_q) \} \left(\frac{m_b^2}{m_q^2} Y^2 + X^2 \right) + XY \{ \overline{\mathcal{F}}_1(y_q) - \overline{\mathcal{F}}_0(y_q) \} \right], \quad (\text{C.17b})$$

$$C_{2L}(y_q) = \frac{y_q}{2} \left[\frac{1}{2} \{ \mathcal{F}_2(y_q) - \mathcal{F}_1(y_q) \} \left(\frac{m_s^2}{m_q^2} Y^2 + X^2 \right) - XY \mathcal{F}_1(y_q) \right], \quad (\text{C.17c})$$

$$C_{2R}(y_q) = \frac{y_q}{2} \left[\frac{1}{2} \{ \mathcal{F}_2(y_q) - \mathcal{F}_1(y_q) \} \left(\frac{m_b^2}{m_q^2} Y^2 + X^2 \right) - XY \mathcal{F}_1(y_q) \right]. \quad (\text{C.17d})$$

In Eq. (C.17), we have to substitute $X = \cot \beta$, $Y = -\cot \beta$ for Type I model and $X = \cot \beta$, $Y = \tan \beta$ for Type II model.

■ CP-even Higgs (BGL Models):

$$A_L^H(z_b) = -\frac{1}{8} \left[\{ z_b \mathcal{F}_1(z_b) - z_b \mathcal{F}_2(z_b) \} \left(\frac{AD}{m_b^2} + \frac{BC}{m_b^2} \frac{m_s}{m_b} \right) + 2z_b \mathcal{F}_1(z_b) \frac{AC}{m_b^2} \right], \quad (\text{C.18a})$$

$$A_R^H(z_b) = -\frac{1}{8} \left[\{ z_b \mathcal{F}_1(z_b) - z_b \mathcal{F}_2(z_b) \} \left(\frac{AD}{m_b^2} \frac{m_s}{m_b} + \frac{BC}{m_b^2} \right) + 2z_b \mathcal{F}_1(z_b) \frac{BD}{m_b^2} \right], \quad (\text{C.18b})$$

with $A = (N_d)_{sb}$, $B = (N_d)_{bs}^*$, $C = (N_d)_{bb}$, $D = (N_d)_{bb}^*$.

$$A_L^H(z_s) = -\frac{1}{8} \left[\{ z_s \mathcal{F}_1(z_s) - z_s \mathcal{F}_2(z_s) \} \left(\frac{AD}{m_s^2} + \frac{BC}{m_s^2} \frac{m_s}{m_b} \right) + 2z_s \mathcal{F}_1(z_s) \frac{AC}{m_s^2} \frac{m_s}{m_b} \right] \quad (\text{C.19a})$$

$$A_R^H(z_s) = -\frac{1}{8} \left[\{z_s \mathcal{F}_1(z_s) - z_s \mathcal{F}_2(z_s)\} \left(\frac{AD}{m_s^2} \frac{m_s}{m_b} + \frac{BC}{m_s^2} \right) + 2z_s \mathcal{F}_1(z_s) \frac{BD}{m_s^2} \frac{m_s}{m_b} \right] \quad (\text{C.19b})$$

with $A = (N_d)_{ss}$, $B = (N_d)_{ss}^*$, $C = (N_d)_{sb}$, $D = (N_d)_{bs}^*$.

■ CP-odd Higgs (BGL Models):

$$A_L^A(z'_b) = \frac{1}{8} \left[\{z'_b \mathcal{F}_1(z'_b) - z'_b \mathcal{F}_2(z'_b)\} \left(\frac{AD}{m_b^2} + \frac{BC}{m_b^2} \frac{m_s}{m_b} \right) + 2z'_b \mathcal{F}_1(z'_b) \frac{AC}{m_b^2} \right], \quad (\text{C.20a})$$

$$A_R^A(z'_b) = \frac{1}{8} \left[\{z'_b \mathcal{F}_1(z'_b) - z'_b \mathcal{F}_2(z'_b)\} \left(\frac{AD}{m_b^2} \frac{m_s}{m_b} + \frac{BC}{m_b^2} \right) + 2z'_b \mathcal{F}_1(z'_b) \frac{BD}{m_b^2} \right], \quad (\text{C.20b})$$

with $A = (N_d)_{sb}$, $B = -(N_d)_{bs}^*$, $C = (N_d)_{bb}$, $D = -(N_d)_{bb}^*$.

$$A_L^A(z'_s) = \frac{1}{8} \left[\{z'_s \mathcal{F}_1(z'_s) - z'_s \mathcal{F}_2(z'_s)\} \left(\frac{AD}{m_s^2} + \frac{BC}{m_s^2} \frac{m_s}{m_b} \right) + 2z'_s \mathcal{F}_1(z'_s) \frac{AC}{m_s^2} \frac{m_s}{m_b} \right] \quad (\text{C.21a})$$

$$A_R^A(z'_s) = \frac{1}{8} \left[\{z'_s \mathcal{F}_1(z'_s) - z'_s \mathcal{F}_2(z'_s)\} \left(\frac{AD}{m_s^2} \frac{m_s}{m_b} + \frac{BC}{m_s^2} \right) + 2z'_s \mathcal{F}_1(z'_s) \frac{BD}{m_s^2} \frac{m_s}{m_b} \right] \quad (\text{C.21b})$$

with $A = (N_d)_{ss}$, $B = -(N_d)_{ss}^*$, $C = (N_d)_{sb}$, $D = -(N_d)_{bs}^*$.

C.3 Leptonic and semileptonic B decays

We shall quote the formula used in [124]. The effective Hamiltonian is written as

$$\mathcal{H}_{\text{eff}} = C_{\text{SM}}^{qb} O_{\text{SM}}^{qb} + C_R^{qb} O_R^{qb} + C_L^{qb} O_L^{qb}, \quad (\text{C.22})$$

with

$$O_{\text{SM}}^{qb} = (\bar{q} \gamma_\mu P_L b) (\bar{\tau} \gamma^\mu P_L \nu_\tau), \quad (\text{C.23})$$

$$O_R^{qb} = (\bar{q} P_R b) (\bar{\tau} P_L \nu_\tau), \quad (\text{C.24})$$

$$O_L^{qb} = (\bar{q} P_L b) (\bar{\tau} P_L \nu_\tau), \quad (\text{C.25})$$

In the above equations, $q = u$ for $B \rightarrow \tau \nu$ and $q = c$ for $B \rightarrow D^{(*)} \tau \nu$.

$$\frac{R(D)}{R_{\text{SM}}(D)} = 1 + 1.5 \operatorname{Re} \left(\frac{C_R^{cb} + C_L^{cb}}{C_{\text{SM}}^{cb}} \right) + 1.0 \left| \frac{C_R^{cb} + C_L^{cb}}{C_{\text{SM}}^{cb}} \right|^2, \quad (\text{C.26})$$

$$\frac{R(D^*)}{R_{\text{SM}}(D^*)} = 1 + 0.12 \operatorname{Re} \left(\frac{C_R^{cb} - C_L^{cb}}{C_{\text{SM}}^{cb}} \right) + 0.05 \left| \frac{C_R^{cb} - C_L^{cb}}{C_{\text{SM}}^{cb}} \right|^2, \quad (\text{C.27})$$

$$\frac{\operatorname{Br}(B \rightarrow \tau \nu)}{\operatorname{Br}(B \rightarrow \tau \nu)_{\text{SM}}} = \left| 1 + \frac{m_B^2}{m_b m_\tau} \frac{(C_R^{ub} - C_L^{ub})}{C_{\text{SM}}^{ub}} \right|^2 \times \frac{\Gamma_B^{\text{SM}}}{\Gamma_B}. \quad (\text{C.28})$$

Γ_B is the total decay width of the B meson. If the NP only affects the rare decay modes, then we can take $\Gamma_B \approx \Gamma_B^{\text{SM}}$. Now, let us proceed to find the Wilson coefficients. For the SM part, the relevant Lagrangian should be

$$\mathcal{L}_{\text{SM}} = \frac{g}{\sqrt{2}} V_{qb} (\bar{q} \gamma^\mu P_L b) W_\mu^+ + \frac{g}{\sqrt{2}} (\bar{\tau} \gamma^\mu P_L \nu_\tau) W_\mu^- . \quad (\text{C.29})$$

Hence at low energy, we may write

$$C_{\text{SM}}^{qb} = \frac{g^2}{2M_W^2} V_{qb} = \frac{2}{v^2} V_{qb} = 2\sqrt{2} G_F V_{qb} . \quad (\text{C.30})$$

For the NP contributions, C_L and C_R , we need to look at

$$\mathcal{L} = \frac{\sqrt{2}}{v} \left[\bar{u} (V N_d) P_R d - \bar{u} (N_u^\dagger V) P_L d \right] H_1^+ + \frac{\sqrt{2}}{v} \bar{e} N_e^\dagger P_L \nu H_1^- . \quad (\text{C.31})$$

According to the definition, we may write

$$-C_R^{qb} = \frac{2}{v^2 m_\xi^2} (V N_d)_{qb} (N_e^\dagger)_{\tau\tau} , \quad (\text{C.32})$$

$$-C_L^{qb} = -\frac{2}{v^2 m_\xi^2} (N_u^\dagger V)_{qb} (N_e^\dagger)_{\tau\tau} . \quad (\text{C.33})$$

Note the occurrence of an extra negative sign compared to C_{SM}^{qb} . This is because the spin-1 propagator differs from a spin-0 one by a relative negative sign ($-ig^{\mu\nu}/(k^2 - M_W^2)$ compared to $i/(k^2 - m_{1+}^2)$). Since N_u is diagonal with real entries, we have

$$(N_u^\dagger V)_{qb} = (N_u)_{qq} V_{qb} . \quad (\text{C.34})$$

and,

$$\begin{aligned} (V N_d)_{qb} &= \sum_a V_{qa} (N_d)_{ab} \\ &= \tan \beta \sum_a V_{qa} \delta_{ab} m_a^d - m_b (\tan \beta + \cot \beta) \left(\sum_a V_{qa} V_{ia}^* \right) V_{ib} \end{aligned} \quad (\text{C.35})$$

$$= \tan \beta m_b V_{qb} - (\tan \beta + \cot \beta) m_b V_{ib} \delta_{iq} . \quad (\text{C.36})$$

Now, the question is, what should we use for the matrix N_e in the leptonic sector? According to our assumption, the leptonic sector will be the exact replica of the quark sector except that neutrinos are massless. This allows us to choose same rotation matrices for e_L and ν_L which will make the PMNS matrix, $V = I_{3 \times 3}$ in the leptonic sector. So the quark sector couplings will apply also to the leptonic sector with $V = I_{3 \times 3}$ which means that there will be no flavor

violating processes in the leptonic sector. Thus, for the leptonic sector we may write

$$(N_e)_{ab} = \tan \beta m_a^e \delta_{ab} - (\tan \beta + \cot \beta) \delta_{ia} \delta_{ib} m_b^e, \quad (\text{C.37a})$$

$$= \tan \beta \text{diag}\{0, m_\mu, m_\tau\} - \cot \beta \text{diag}\{m_e, 0, 0\} \quad \text{for } i = u, \quad (\text{C.37b})$$

$$= \tan \beta \text{diag}\{m_e, 0, m_\tau\} - \cot \beta \text{diag}\{0, m_\mu, 0\} \quad \text{for } i = c, \quad (\text{C.37c})$$

$$= \tan \beta \text{diag}\{m_e, m_\mu, 0\} - \cot \beta \text{diag}\{0, 0, m_\tau\} \quad \text{for } i = t, \quad (\text{C.37d})$$

$$N_\nu = 0, \quad (\text{C.37e})$$

where the change of notation is obvious.

Now it is straightforward to evaluate the matrix elements for specific models:

u-model:

$$(N_e)_{\tau\tau} = m_\tau \tan \beta, \quad (\text{C.38a})$$

$$(N_u^\dagger V)_{ub} = -m_u \cot \beta V_{ub}; \quad (N_u^\dagger V)_{cb} = m_c \tan \beta V_{cb}, \quad (\text{C.38b})$$

$$(VN_d)_{ub} = -m_b \cot \beta V_{ub}; \quad (VN_d)_{cb} = m_b \tan \beta V_{cb}. \quad (\text{C.38c})$$

c-model:

$$(N_e)_{\tau\tau} = m_\tau \tan \beta, \quad (\text{C.39a})$$

$$(N_u^\dagger V)_{ub} = m_u \tan \beta V_{ub}; \quad (N_u^\dagger V)_{cb} = -m_c \cot \beta V_{cb}, \quad (\text{C.39b})$$

$$(VN_d)_{ub} = m_b \tan \beta V_{ub}; \quad (VN_d)_{cb} = -m_b \cot \beta V_{cb}. \quad (\text{C.39c})$$

t-model:

$$(N_e)_{\tau\tau} = -m_\tau \cot \beta, \quad (\text{C.40a})$$

$$(N_u^\dagger V)_{ub} = m_u \tan \beta V_{ub}; \quad (N_u^\dagger V)_{cb} = m_c \tan \beta V_{cb}, \quad (\text{C.40b})$$

$$(VN_d)_{ub} = m_b \tan \beta V_{ub}; \quad (VN_d)_{cb} = m_b \tan \beta V_{cb}. \quad (\text{C.40c})$$

Note that, for t-models neither of the above mentioned decay widths will depend on $\tan \beta$.

C.4 $B_s \rightarrow \mu^+ \mu^-$

The effective Hamiltonian is

$$\mathcal{H}_{\text{eff}} = C_A^{bs} O_A^{bs} + C_S^{bs} O_S^{bs} + C_P^{bs} O_P^{bs}, \quad (\text{C.41})$$

with

$$O_A^{bs} = (\bar{b}\gamma_\alpha P_L s)(\bar{\mu}\gamma^\alpha\gamma_5\mu), \quad O_S^{bs} = m_b(\bar{b}P_L s)(\bar{\mu}\mu), \quad O_P^{bs} = m_b(\bar{b}P_L s)(\bar{\mu}\gamma_5\mu). \quad (\text{C.42})$$

Note that in addition to the above operators, there will be operators of the form $(\bar{b}P_R s)(\bar{\mu}\mu)$ and $(\bar{b}P_R s)(\bar{\mu}\gamma_5\mu)$. But the Wilson coefficients corresponding to these operators will be proportional to m_s (instead of m_b) and their contribution can be neglected ($m_b \gg m_s$) as argued in [125]. With this assumption we can write

$$\frac{\text{Br}(B_s \rightarrow \mu^+\mu^-)}{\text{Br}(B_s \rightarrow \mu^+\mu^-)_{\text{SM}}} = \left\{ \left| 1 - m_{B_s}^2 \frac{C_P^{bs}}{2m_\mu C_A^{bs}} \right|^2 + m_{B_s}^4 \left(1 - \frac{4m_\mu^2}{m_{B_s}^2} \right) \left| \frac{C_S^{bs}}{2m_\mu C_A^{bs}} \right|^2 \right\} \frac{\Gamma_B^{\text{SM}}}{\Gamma_B}. \quad (\text{C.43})$$

The relevant part of the Lagrangian (for BGL models) to evaluate C_S^{bs} and C_P^{bs} is

$$\begin{aligned} \mathcal{L}_{\text{quark}} &= \frac{R}{v} \bar{d}(N_d P_R + N_d^\dagger P_L)d + i \frac{A}{v} \bar{d}(N_d P_R - N_d^\dagger P_L)d \\ &= (N_d^\dagger)_{bs} \frac{R}{v} \bar{b}P_L s - i(N_d^\dagger)_{bs} \frac{A}{v} \bar{b}P_L s \\ &= (N_d^\dagger)_{bs} \frac{h}{v} \cos(\beta - \alpha) \bar{b}P_L s - (N_d^\dagger)_{bs} \frac{H}{v} \sin(\beta - \alpha) \bar{b}P_L s - i(N_d^\dagger)_{bs} \frac{A}{v} \bar{b}P_L s, \quad (\text{C.44}) \\ \mathcal{L}_{\text{lepton}} &= -\frac{H^0}{v} \bar{e}D_e e + \frac{R}{v} \bar{e}(N_e P_R + N_e^\dagger P_L)e + i \frac{A}{v} \bar{e}(N_e P_R - N_e^\dagger P_L)e \\ &= -\frac{m_\mu}{v} \bar{\mu}\mu H^0 + \frac{(N_e)_{\mu\mu}}{v} \bar{\mu}\mu R + \frac{i(N_e)_{\mu\mu}}{v} \bar{\mu}\gamma_5\mu A \\ &= \left[\frac{h}{v} \{-\sin(\beta - \alpha)m_\mu + \cos(\beta - \alpha)(N_e)_{\mu\mu}\} \right. \\ &\quad \left. + \frac{H}{v} \{-\cos(\beta - \alpha)m_\mu - \sin(\beta - \alpha)(N_e)_{\mu\mu}\} \right] \bar{\mu}\mu + i \frac{A}{v} (N_e)_{\mu\mu} \bar{\mu}\gamma_5\mu. \quad (\text{C.45}) \end{aligned}$$

Note that terms involving $\bar{b}P_R s$ have not been displayed. Their coefficients are proportional to $(N_d)_{bs}$, which is proportional to m_s , and are therefore neglected.

$$(N_d)_{bs} = -(\tan\beta + \cot\beta) V_{ib}^* V_{is} m_s, \quad (\text{C.46a})$$

$$(N_d^\dagger)_{bs} = (N_d)_{sb}^* = -(\tan\beta + \cot\beta) V_{ib}^* V_{is} m_b. \quad (\text{C.46b})$$

The Wilson coefficients are

$$\begin{aligned} C_S^{bs} &= (\tan\beta + \cot\beta) \frac{V_{ib}^* V_{is}}{v^2} \left\{ \frac{\cos(\beta - \alpha)}{m_h^2} [-\sin(\beta - \alpha)m_\mu + \cos(\beta - \alpha)(N_e)_{\mu\mu}] \right. \\ &\quad \left. + \frac{\sin(\beta - \alpha)}{m_H^2} [\cos(\beta - \alpha)m_\mu + \sin(\beta - \alpha)(N_e)_{\mu\mu}] \right\}, \quad (\text{C.47}) \end{aligned}$$

and

$$C_P^{bs} = (\tan \beta + \cot \beta) \frac{V_{ib}^* V_{is}}{v^2} \frac{(N_e)_{\mu\mu}}{m_A^2}. \quad (\text{C.48})$$

The SM Wilson coefficient is [125]

$$C_A^{bs} = \frac{\alpha G_F}{2\sqrt{2}\pi \sin^2 \theta_w} V_{tb}^* V_{ts} 2Y(x_t), \quad Y(x_t) = 0.997 \left[\frac{m_t(m_t)}{166 \text{ GeV}} \right]^{1.55} \approx 1.0. \quad (\text{C.49})$$

C.5 Current experimental numbers

1. $b \rightarrow s\gamma$: SM = $(3.15 \pm 0.23) \times 10^{-4}$ [70–72], EXP = $(3.55 \pm 0.26) \times 10^{-4}$ [59], $\text{Br}(b \rightarrow ce\nu)_{\text{exp}} = (10.51 \pm 0.13)\%$ [126]. Note that we have taken $\text{Br}(b \rightarrow ce\nu) \approx \text{Br}(b \rightarrow cl\nu)$.
2. $R(D), R(D^*)$: The experimental numbers are [127]:

$$R(D) \equiv \frac{\text{Br}(B \rightarrow D\tau\nu)}{\text{Br}(B \rightarrow D\ell\nu)} = 0.440 \pm 0.072, \quad (\text{C.50})$$

$$R(D^*) \equiv \frac{\text{Br}(B \rightarrow D^*\tau\nu)}{\text{Br}(B \rightarrow D^*\ell\nu)} = 0.332 \pm 0.030, \quad (\text{C.51})$$

$$R \equiv \frac{\tau(B^0)}{\tau(B^-)} \frac{\text{Br}(B^- \rightarrow \tau^- \bar{\nu})}{\text{Br}(\bar{B}^0 \rightarrow \pi^+ \ell^- \bar{\nu})} = 0.73 \pm 0.15. \quad (\text{C.52})$$

But, for analysis purpose, the following numbers will be directly usable [127]:

$$\frac{R(D)_{\text{exp}}}{R(D)_{\text{SM}}} = 1.49 \pm 0.26, \quad (\text{C.53})$$

$$\frac{R(D^*)_{\text{exp}}}{R(D^*)_{\text{SM}}} = 1.32 \pm 0.12, \quad (\text{C.54})$$

$$\frac{R_{\text{exp}}}{R_{\text{SM}}} = 2.38 \pm 0.66. \quad (\text{C.55})$$

3. $B_s \rightarrow \mu^+ \mu^-$: SM = $(3.65 \pm 0.30) \times 10^{-9}$ [128, 129], SM(updated) = $(3.54 \pm 0.23) \times 10^{-9}$ [73], EXP = $(3.2 \pm 1.0) \times 10^{-9}$ [74].
4. For $\Delta M_K, \Delta M_d$ and ΔM_s , we have used the central values given in PDG because the errors are very small.

Bibliography

- [1] S. Weinberg, *A Model of Leptons*, *Phys.Rev.Lett.* **19** (1967) 1264–1266.
- [2] S. D. Joglekar, *S matrix derivation of the Weinberg model*, *Annals Phys.* **83** (1974) 427.
- [3] J. Horejsi, *Introduction to electroweak unification: Standard model from tree unitarity*, *PRA-HEP-93-8* (1993).
- [4] G. Bhattacharyya, *A Pedagogical Review of Electroweak Symmetry Breaking Scenarios*, *Rept.Prog.Phys.* **74** (2011) 026201, [[arXiv:0910.5095](https://arxiv.org/abs/0910.5095)].
- [5] M. S. Chanowitz, M. Furman, and I. Hinchliffe, *Weak Interactions of Ultraheavy Fermions. 2.*, *Nucl.Phys.* **B153** (1979) 402.
- [6] L. Michel, *Interaction between four half spin particles and the decay of the mu meson*, *Proc.Phys.Soc.* **A63** (1950) 514–531.
- [7] T. P. Cheng and L. F. Li, *Gauge Theory of Elementary Particle Physics*, *ISBN-9780198519614* (1984).
- [8] H. Georgi and S. L. Glashow, *Unified weak and electromagnetic interactions without neutral currents*, *Phys.Rev.Lett.* **28** (1972) 1494.
- [9] C. H. Llewellyn Smith, *High-Energy Behavior and Gauge Symmetry*, *Phys.Lett.* **B46** (1973) 233–236.
- [10] C. Llewellyn Smith, *On the Determination of $\sin^2\theta_w$ in Semileptonic Neutrino Interactions*, *Nucl.Phys.* **B228** (1983) 205.
- [11] J. M. Cornwall, D. N. Levin, and G. Tiktopoulos, *Derivation of Gauge Invariance from High-Energy Unitarity Bounds on the s Matrix*, *Phys.Rev.* **D10** (1974) 1145.
- [12] B. W. Lee, C. Quigg, and H. Thacker, *Weak Interactions at Very High-Energies: The Role of the Higgs Boson Mass*, *Phys.Rev.* **D16** (1977) 1519.
- [13] J. Gunion, H. Haber, and J. Wudka, *Sum rules for Higgs bosons*, *Phys.Rev.* **D43** (1991) 904–912.

- [14] C. Csaki, C. Grojean, H. Murayama, L. Pilo, and J. Terning, *Gauge theories on an interval: Unitarity without a Higgs*, *Phys.Rev.* **D69** (2004) 055006, [[hep-ph/0305237](#)].
- [15] A. Lahiri and D. Mukhopadhyay, *Unitarity in $WW \rightarrow WW$ elastic scattering without a Higgs boson*, [arXiv:1107.1501](#).
- [16] **ATLAS** Collaboration, G. Aad et al., *Observation of a new particle in the search for the Standard Model Higgs boson with the ATLAS detector at the LHC*, *Phys.Lett.* **B716** (2012) 1–29, [[arXiv:1207.7214](#)].
- [17] **CMS** Collaboration, S. Chatrchyan et al., *Observation of a new boson at a mass of 125 GeV with the CMS experiment at the LHC*, *Phys.Lett.* **B716** (2012) 30–61, [[arXiv:1207.7235](#)].
- [18] G. Bhattacharyya, D. Das, and P. B. Pal, *Modified Higgs couplings and unitarity violation*, *Phys.Rev.* **D87** (2013), no. 1 011702, [[arXiv:1212.4651](#)].
- [19] M. Carena, I. Low, and C. E. Wagner, *Implications of a Modified Higgs to Diphoton Decay Width*, *JHEP* **1208** (2012) 060, [[arXiv:1206.1082](#)].
- [20] K. Cheung, C.-W. Chiang, and T.-C. Yuan, *Partially Strong WW Scattering*, *Phys.Rev.* **D78** (2008) 051701, [[arXiv:0803.2661](#)].
- [21] A. Azatov, R. Contino, and J. Galloway, *Model-Independent Bounds on a Light Higgs*, *JHEP* **1204** (2012) 127, [[arXiv:1202.3415](#)].
- [22] T. Plehn and M. Rauch, *Higgs Couplings after the Discovery*, *Europhys.Lett.* **100** (2012) 11002, [[arXiv:1207.6108](#)].
- [23] P. P. Giardino, K. Kannike, M. Raidal, and A. Strumia, *Is the resonance at 125 GeV the Higgs boson?*, *Phys.Lett.* **B718** (2012) 469–474, [[arXiv:1207.1347](#)].
- [24] J. Espinosa, C. Grojean, M. Muhlleitner, and M. Trott, *First Glimpses at Higgs' face*, *JHEP* **1212** (2012) 045, [[arXiv:1207.1717](#)].
- [25] S. Banerjee, S. Mukhopadhyay, and B. Mukhopadhyaya, *New Higgs interactions and recent data from the LHC and the Tevatron*, *JHEP* **1210** (2012) 062, [[arXiv:1207.3588](#)].
- [26] K. Whisnant, B.-L. Young, and X. Zhang, *Unitarity and anomalous top quark Yukawa couplings*, *Phys.Rev.* **D52** (1995) 3115–3118, [[hep-ph/9410369](#)].
- [27] A. Djouadi, *The Anatomy of electro-weak symmetry breaking. I: The Higgs boson in the standard model*, *Phys.Rept.* **457** (2008) 1–216, [[hep-ph/0503172](#)].
- [28] B. Bellazzini, C. Csaki, J. Hubisz, J. Serra, and J. Terning, *Composite Higgs Sketch*, *JHEP* **1211** (2012) 003, [[arXiv:1205.4032](#)].

- [29] G. Branco, P. Ferreira, L. Lavoura, M. Rebelo, M. Sher, et al., *Theory and phenomenology of two-Higgs-doublet models*, *Phys.Rept.* **516** (2012) 1–102, [[arXiv:1106.0034](#)].
- [30] S. L. Glashow and S. Weinberg, *Natural Conservation Laws for Neutral Currents*, *Phys.Rev.* **D15** (1977) 1958.
- [31] E. Paschos, *Diagonal Neutral Currents*, *Phys.Rev.* **D15** (1977) 1966.
- [32] G. Branco, W. Grimus, and L. Lavoura, *Relating the scalar flavor changing neutral couplings to the CKM matrix*, *Phys.Lett.* **B380** (1996) 119–126, [[hep-ph/9601383](#)].
- [33] J. F. Gunion and H. E. Haber, *The CP conserving two Higgs doublet model: The Approach to the decoupling limit*, *Phys.Rev.* **D67** (2003) 075019, [[hep-ph/0207010](#)].
- [34] J. Bernon, B. Dumont, and S. Kraml, *Status of Higgs couplings after run 1 of the LHC*, *Phys.Rev.* **D90** (2014), no. 7 071301, [[arXiv:1409.1588](#)].
- [35] O. Eberhardt, U. Nierste, and M. Wiebusch, *Status of the two-Higgs-doublet model of type II*, *JHEP* **1307** (2013) 118, [[arXiv:1305.1649](#)].
- [36] B. Coleppa, F. Kling, and S. Su, *Constraining Type II 2HDM in Light of LHC Higgs Searches*, *JHEP* **1401** (2014) 161, [[arXiv:1305.0002](#)].
- [37] C.-Y. Chen, S. Dawson, and M. Sher, *Heavy Higgs Searches and Constraints on Two Higgs Doublet Models*, *Phys.Rev.* **D88** (2013), no. 3 015018, [[arXiv:1305.1624](#)].
- [38] N. Craig, J. Galloway, and S. Thomas, *Searching for Signs of the Second Higgs Doublet*, [arXiv:1305.2424](#).
- [39] B. Dumont, J. F. Gunion, Y. Jiang, and S. Kraml, *Constraints on and future prospects for Two-Higgs-Doublet Models in light of the LHC Higgs signal*, *Phys.Rev.* **D90** (2014), no. 3 035021, [[arXiv:1405.3584](#)].
- [40] **ATLAS** Collaboration.
<https://atlas.web.cern.ch/Atlas/GROUPS/PHYSICS/CombinedSummaryPlots/HIGGS/>.
- [41] **CMS** Collaboration, *CMS-PAS-HIG-14-009*,
<http://cds.cern.ch/record/1728249?ln=en>.
- [42] K. Klimenko, *On Necessary and Sufficient Conditions for Some Higgs Potentials to Be Bounded From Below*, *Theor.Math.Phys.* **62** (1985) 58–65.
- [43] M. Maniatis, A. von Manteuffel, O. Nachtmann, and F. Nagel, *Stability and symmetry breaking in the general two-Higgs-doublet model*, *Eur.Phys.J.* **C48** (2006) 805–823, [[hep-ph/0605184](#)].

- [44] J. Maalampi, J. Sirkka, and I. Vilja, *Tree level unitarity and triviality bounds for two Higgs models*, *Phys.Lett.* **B265** (1991) 371–376.
- [45] S. Kanemura, T. Kubota, and E. Takasugi, *Lee-Quigg-Thacker bounds for Higgs boson masses in a two doublet model*, *Phys.Lett.* **B313** (1993) 155–160, [[hep-ph/9303263](#)].
- [46] A. G. Akeroyd, A. Arhrib, and E.-M. Naimi, *Note on tree level unitarity in the general two Higgs doublet model*, *Phys.Lett.* **B490** (2000) 119–124, [[hep-ph/0006035](#)].
- [47] J. Horejsi and M. Kladiva, *Tree-unitarity bounds for THDM Higgs masses revisited*, *Eur.Phys.J.* **C46** (2006) 81–91, [[hep-ph/0510154](#)].
- [48] P. B. Pal, *What is the equivalence theorem really?*, [hep-ph/9405362](#).
- [49] J. Horejsi, *Electroweak interactions and high-energy limit: An Introduction to equivalence theorem*, *Czech.J.Phys.* **47** (1997) 951–977, [[hep-ph/9603321](#)].
- [50] D. Das, *New limits on $\tan\beta$ for 2HDMs with \mathbf{Z}_2 symmetry*, [arXiv:1501.02610](#).
- [51] G. Bhattacharyya and D. Das, *Nondecoupling of charged scalars in Higgs decay to two photons and symmetries of the scalar potential*, *Phys.Rev.* **D91** (2015), no. 1 015005, [[arXiv:1408.6133](#)].
- [52] CMS Collaboration, V. Khachatryan et al., *Observation of the diphoton decay of the Higgs boson and measurement of its properties*, *Eur.Phys.J.* **C74** (2014), no. 10 3076, [[arXiv:1407.0558](#)].
- [53] ATLAS Collaboration, G. Aad et al., *Measurement of Higgs boson production in the diphoton decay channel in pp collisions at center-of-mass energies of 7 and 8 TeV with the ATLAS detector*, [arXiv:1408.7084](#).
- [54] LEP Higgs Working Group for Higgs boson searches, ALEPH Collaboration, DELPHI Collaboration, L3 Collaboration, OPAL Collaboration Collaboration, *Search for charged Higgs bosons: Preliminary combined results using LEP data collected at energies up to 209-GeV*, [hep-ex/0107031](#).
- [55] G. Bhattacharyya, D. Das, P. B. Pal, and M. Rebelo, *Scalar sector properties of two-Higgs-doublet models with a global $U(1)$ symmetry*, *JHEP* **1310** (2013) 081, [[arXiv:1308.4297](#)].
- [56] H.-J. He, N. Polonsky, and S.-f. Su, *Extra families, Higgs spectrum and oblique corrections*, *Phys.Rev.* **D64** (2001) 053004, [[hep-ph/0102144](#)].
- [57] W. Grimus, L. Lavoura, O. Ogreid, and P. Osland, *A Precision constraint on multi-Higgs-doublet models*, *J.Phys.* **G35** (2008) 075001, [[arXiv:0711.4022](#)].

- [58] M. Baak and R. Kogler, *The global electroweak Standard Model fit after the Higgs discovery*, [arXiv:1306.0571](#).
- [59] **Heavy Flavor Averaging Group** Collaboration, Y. Amhis et al., *Averages of B-Hadron, C-Hadron, and tau-lepton properties as of early 2012*, [arXiv:1207.1158](#).
- [60] **Particle Data Group** Collaboration, K. Olive et al., *Review of Particle Physics*, *Chin.Phys.* **C38** (2014) 090001.
- [61] F. Mahmoudi and O. Stal, *Flavor constraints on the two-Higgs-doublet model with general Yukawa couplings*, *Phys.Rev.* **D81** (2010) 035016, [[arXiv:0907.1791](#)].
- [62] O. Deschamps, S. Descotes-Genon, S. Monteil, V. Niess, S. T’Jampens, et al., *The Two Higgs Doublet of Type II facing flavour physics data*, *Phys.Rev.* **D82** (2010) 073012, [[arXiv:0907.5135](#)].
- [63] A. Crivellin, A. Kokulu, and C. Greub, *Flavor-phenomenology of two-Higgs-doublet models with generic Yukawa structure*, *Phys.Rev.* **D87** (2013), no. 9 094031, [[arXiv:1303.5877](#)].
- [64] D. Atwood, L. Reina, and A. Soni, *Phenomenology of two Higgs doublet models with flavor changing neutral currents*, *Phys.Rev.* **D55** (1997) 3156–3176, [[hep-ph/9609279](#)].
- [65] **Particle Data Group** Collaboration, J. Beringer et al., *Review of Particle Physics (RPP)*, *Phys.Rev.* **D86** (2012) 010001.
- [66] G. Bhattacharyya, D. Das, and A. Kundu, *Feasibility of light scalars in a class of two-Higgs-doublet models and their decay signatures*, *Phys.Rev.* **D89** (2014), no. 9 095029, [[arXiv:1402.0364](#)].
- [67] B. Grinstein and M. B. Wise, *Weak Radiative B Meson Decay as a Probe of the Higgs Sector*, *Phys.Lett.* **B201** (1988) 274.
- [68] F. Borzumati and C. Greub, *2HDMs predictions for anti-B \rightarrow X(s) gamma in NLO QCD*, *Phys.Rev.* **D58** (1998) 074004, [[hep-ph/9802391](#)].
- [69] X.-D. Cheng, Y.-D. Yang, and X.-B. Yuan, *Phenomenological discriminations of the Yukawa interactions in two-Higgs doublet models with Z_2 symmetry*, *Eur.Phys.J.* **C74** (2014), no. 10 3081, [[arXiv:1401.6657](#)].
- [70] P. Gambino and M. Misiak, *Quark mass effects in anti-B \rightarrow X(s gamma)*, *Nucl.Phys.* **B611** (2001) 338–366, [[hep-ph/0104034](#)].
- [71] M. Misiak, H. Asatrian, K. Bieri, M. Czakon, A. Czarnecki, et al., *Estimate of B(anti-B \rightarrow X(s) gamma) at $O(\alpha(s)^{**2})$* , *Phys.Rev.Lett.* **98** (2007) 022002, [[hep-ph/0609232](#)].

- [72] M. Misiak and M. Steinhauser, *NNLO QCD corrections to the anti- $B \rightarrow X(s)$ gamma matrix elements using interpolation in $m(c)$* , *Nucl.Phys.* **B764** (2007) 62–82, [[hep-ph/0609241](#)].
- [73] C. Bobeth, M. Gorbahn, T. Hermann, M. Misiak, E. Stamou, et al., *$B_{s,d} \rightarrow \ell^+ \ell^-$ in the Standard Model with Reduced Theoretical Uncertainty*, *Phys.Rev.Lett.* **112** (2014) 101801, [[arXiv:1311.0903](#)].
- [74] <http://www.slac.stanford.edu/xorg/hfag/rare/2013/bs/OUTPUT/TABLES/bs.pdf> , *HFAG Website* (2013).
- [75] M. Aoki, S. Kanemura, K. Tsumura, and K. Yagyu, *Models of Yukawa interaction in the two Higgs doublet model, and their collider phenomenology*, *Phys.Rev.* **D80** (2009) 015017, [[arXiv:0902.4665](#)].
- [76] M. Aoki, R. Guedes, S. Kanemura, S. Moretti, R. Santos, et al., *Light Charged Higgs bosons at the LHC in 2HDMs*, *Phys.Rev.* **D84** (2011) 055028, [[arXiv:1104.3178](#)].
- [77] **CMS** Collaboration, <http://cms-physics.web.cern.ch/cms-physics/public/HIG-13-007-pas.pdf> , .
- [78] **ATLAS** Collaboration, <https://cds.cern.ch/record/1523695/files/ATLAS-CONF-2013-010.pdf> , .
- [79] <https://twiki.cern.ch/twiki/bin/view/LHCPhysics/CERNYellowReportPageAt14TeV>, *CERN Yellow Reports*.
- [80] A. Djouadi, *The Anatomy of electro-weak symmetry breaking. II. The Higgs bosons in the minimal supersymmetric model*, *Phys.Rept.* **459** (2008) 1–241, [[hep-ph/0503173](#)].
- [81] J. F. Gunion, H. E. Haber, G. L. Kane, and S. Dawson, *The Higgs Hunter’s Guide*, *Front.Phys.* **80** (2000) 1–448.
- [82] A. Djouadi, V. Driesen, W. Hollik, and A. Kraft, *The Higgs photon - Z boson coupling revisited*, *Eur.Phys.J.* **C1** (1998) 163–175, [[hep-ph/9701342](#)].
- [83] J. Kubo, *Majorana phase in minimal $S(3)$ invariant extension of the standard model*, *Phys.Lett.* **B578** (2004) 156–164, [[hep-ph/0309167](#)].
- [84] Y. Koide, *Universal seesaw mass matrix model with an $S(3)$ symmetry*, *Phys.Rev.* **D60** (1999) 077301, [[hep-ph/9905416](#)].
- [85] P. Harrison and W. Scott, *Permutation symmetry, tri - bimaximal neutrino mixing and the $S3$ group characters*, *Phys.Lett.* **B557** (2003) 76, [[hep-ph/0302025](#)].

- [86] J. Kubo, A. Mondragon, M. Mondragon, and E. Rodriguez-Jauregui, *The Flavor symmetry*, *Prog.Theor.Phys.* **109** (2003) 795–807, [[hep-ph/0302196](#)].
- [87] T. Teshima, *Flavor mass and mixing and $S(3)$ symmetry: An $S(3)$ invariant model reasonable to all*, *Phys.Rev.* **D73** (2006) 045019, [[hep-ph/0509094](#)].
- [88] Y. Koide, *$S(3)$ symmetry and neutrino masses and mixings*, *Eur.Phys.J.* **C50** (2007) 809–816, [[hep-ph/0612058](#)].
- [89] C.-Y. Chen and L. Wolfenstein, *Consequences of approximate $S(3)$ symmetry of the neutrino mass matrix*, *Phys.Rev.* **D77** (2008) 093009, [[arXiv:0709.3767](#)].
- [90] A. Mondragon, M. Mondragon, and E. Peinado, *Lepton masses, mixings and FCNC in a minimal $S(3)$ -invariant extension of the Standard Model*, *Phys.Rev.* **D76** (2007) 076003, [[arXiv:0706.0354](#)].
- [91] R. Jora, J. Schechter, and M. Naeem Shahid, *Perturbed $S(3)$ neutrinos*, *Phys.Rev.* **D80** (2009) 093007, [[arXiv:0909.4414](#)].
- [92] Z.-z. Xing, D. Yang, and S. Zhou, *Broken S_3 Flavor Symmetry of Leptons and Quarks: Mass Spectra and Flavor Mixing Patterns*, *Phys.Lett.* **B690** (2010) 304–310, [[arXiv:1004.4234](#)].
- [93] T. Kaneko and H. Sugawara, *Broken S_3 Symmetry in Flavor Physics*, *Phys.Lett.* **B697** (2011) 329–332, [[arXiv:1011.5748](#)].
- [94] S. Zhou, *Relatively large θ_{13} and nearly maximal θ_{23} from the approximate S_3 symmetry of lepton mass matrices*, *Phys.Lett.* **B704** (2011) 291–295, [[arXiv:1106.4808](#)].
- [95] T. Teshima and Y. Okumura, *Quark/lepton mass and mixing in S_3 invariant model and CP-violation of neutrino*, *Phys.Rev.* **D84** (2011) 016003, [[arXiv:1103.6127](#)].
- [96] S. Dev, S. Gupta, and R. R. Gautam, *Broken S_3 Symmetry in the Neutrino Mass Matrix*, *Phys.Lett.* **B702** (2011) 28–33, [[arXiv:1106.3873](#)].
- [97] S. Dev, R. R. Gautam, and L. Singh, *Broken S_3 Symmetry in the Neutrino Mass Matrix and Non-Zero θ_{13}* , *Phys.Lett.* **B708** (2012) 284–289, [[arXiv:1201.3755](#)].
- [98] D. Meloni, *S_3 as a flavour symmetry for quarks and leptons after the Daya Bay result on θ_{13}* , *JHEP* **1205** (2012) 124, [[arXiv:1203.3126](#)].
- [99] A. Dias, A. Machado, and C. Nishi, *An S_3 Model for Lepton Mass Matrices with Nearly Minimal Texture*, *Phys.Rev.* **D86** (2012) 093005, [[arXiv:1206.6362](#)].
- [100] K. Siyeon, *Non-vanishing U_{e3} under S_3 symmetry*, *Eur.Phys.J.* **72** (2012) 2081, [[arXiv:1203.1593](#)].

- [101] F. Gonzalez Canales, A. Mondragon, and M. Mondragon, *The S_3 Flavour Symmetry: Neutrino Masses and Mixings*, *Fortsch.Phys.* **61** (2013) 546–570, [[arXiv:1205.4755](#)].
- [102] F. González Canales, A. Mondragón, M. Mondragón, U. J. Saldaña Salazar, and L. Velasco-Sevilla, *Quark sector of S_3 models: classification and comparison with experimental data*, *Phys.Rev.* **D88** (2013) 096004, [[arXiv:1304.6644](#)].
- [103] H. Benaoum, *Broken S_3 Neutrinos*, *Phys.Rev.* **D87** (2013) 073010, [[arXiv:1302.0950](#)].
- [104] A. E. C. Hernández, R. Martinez, and J. Nisperuza, *S_3 flavour symmetry breaking scheme for understanding the quark mass and mixing pattern in $SU(3)_C \otimes SU(3)_L \otimes U(1)_X$ models*, [arXiv:1401.0937](#).
- [105] E. Ma and B. Melic, *Updated S_3 model of quarks*, *Phys.Lett.* **B725** (2013) 402–406, [[arXiv:1303.6928](#)].
- [106] S. Pakvasa and H. Sugawara, *Discrete Symmetry and Cabibbo Angle*, *Phys.Lett.* **B73** (1978) 61.
- [107] J. Kubo, H. Okada, and F. Sakamaki, *Higgs potential in minimal $S(3)$ invariant extension of the standard model*, *Phys.Rev.* **D70** (2004) 036007, [[hep-ph/0402089](#)].
- [108] Y. Koide, *Permutation symmetry $S(3)$ and VEV structure of flavor-triplet Higgs scalars*, *Phys.Rev.* **D73** (2006) 057901, [[hep-ph/0509214](#)].
- [109] T. Teshima, *Higgs potential in S_3 invariant model for quark/lepton mass and mixing*, *Phys.Rev.* **D85** (2012) 105013, [[arXiv:1202.4528](#)].
- [110] A. Machado and V. Pleitez, *Natural Flavour Conservation in a three Higgs-doublet Model*, [arXiv:1205.0995](#).
- [111] G. Bhattacharyya, P. Leser, and H. Pas, *Exotic Higgs boson decay modes as a harbinger of S_3 flavor symmetry*, *Phys.Rev.* **D83** (2011) 011701, [[arXiv:1006.5597](#)].
- [112] G. Bhattacharyya, P. Leser, and H. Pas, *Novel signatures of the Higgs sector from S_3 flavor symmetry*, *Phys.Rev.* **D86** (2012) 036009, [[arXiv:1206.4202](#)].
- [113] S.-L. Chen, M. Frigerio, and E. Ma, *Large neutrino mixing and normal mass hierarchy: A Discrete understanding*, *Phys.Rev.* **D70** (2004) 073008, [[hep-ph/0404084](#)].
- [114] O. F. Beltran, M. Mondragon, and E. Rodriguez-Jauregui, *Conditions for vacuum stability in an $S(3)$ extension of the standard model*, *J.Phys.Conf.Ser.* **171** (2009) 012028.
- [115] E. Barradas-Guevara, O. Felix-Beltran, and E. R. Jauregui, *$S(3)$ flavoured Higgs model trilinear self-couplings*, [arXiv:1402.2244](#).

- [116] A. Arhrib, M. Capdequi Peyranere, W. Hollik, and S. Penaranda, *Higgs decays in the two Higgs doublet model: Large quantum effects in the decoupling regime*, *Phys.Lett.* **B579** (2004) 361–370, [[hep-ph/0307391](#)].
- [117] P. Ferreira, J. F. Gunion, H. E. Haber, and R. Santos, *Probing wrong-sign Yukawa couplings at the LHC and a future linear collider*, *Phys.Rev.* **D89** (2014), no. 11 115003, [[arXiv:1403.4736](#)].
- [118] W.-F. Chang, J. N. Ng, and J. M. Wu, *Constraints on New Scalars from the LHC 125 GeV Higgs Signal*, *Phys.Rev.* **D86** (2012) 033003, [[arXiv:1206.5047](#)].
- [119] D. Fontes, J. Romao, and J. P. Silva, *A reappraisal of the wrong-sign $hb\bar{b}$ coupling and the study of $h \rightarrow Z\gamma$* , *Phys.Rev.* **D90** (2014) 015021, [[arXiv:1406.6080](#)].
- [120] B. Swiezewska and M. Krawczyk, *Diphoton rate in the inert doublet model with a 125 GeV Higgs boson*, *Phys.Rev.* **D88** (2013) 035019, [[arXiv:1212.4100](#)].
- [121] D. Das and U. K. Dey, *Analysis of an extended scalar sector with S_3 symmetry*, *Phys.Rev.* **D89** (2014) 095025, [[arXiv:1404.2491](#)].
- [122] E. Ma and G. Rajasekaran, *Softly broken $A(4)$ symmetry for nearly degenerate neutrino masses*, *Phys.Rev.* **D64** (2001) 113012, [[hep-ph/0106291](#)].
- [123] R. de Adelhart Toorop, F. Bazzocchi, L. Merlo, and A. Paris, *Constraining Flavour Symmetries At The EW Scale I: The A_4 Higgs Potential*, *JHEP* **1103** (2011) 035, [[arXiv:1012.1791](#)].
- [124] A. Crivellin, C. Greub, and A. Kokulu, *Explaining $B \rightarrow D\tau\nu$, $B \rightarrow D^*\tau\nu$ and $B \rightarrow \tau\nu$ in a 2HDM of type III*, *Phys.Rev.* **D86** (2012) 054014, [[arXiv:1206.2634](#)].
- [125] H. E. Logan and U. Nierste, *$B(s, d) \rightarrow \ell^+\ell^-$ in a two Higgs doublet model*, *Nucl.Phys.* **B586** (2000) 39–55, [[hep-ph/0004139](#)].
- [126] <http://pdg.lbl.gov/2013/tables/rpp2013-tab-mesons-bottom.pdf>. See under the section B^\pm/B^0 admixture and subsection semileptonic and leptonic modes.
- [127] S. Fajfer, J. F. Kamenik, I. Nisandzic, and J. Zupan, *Implications of Lepton Flavor Universality Violations in B Decays*, *Phys.Rev.Lett.* **109** (2012) 161801, [[arXiv:1206.1872](#)].
- [128] K. De Bruyn, R. Fleischer, R. Knegjens, P. Koppenburg, M. Merk, et al., *Branching Ratio Measurements of B_s Decays*, *Phys.Rev.* **D86** (2012) 014027, [[arXiv:1204.1735](#)].
- [129] R. Fleischer, *Theory News on $B_{s(d)} \rightarrow \mu^+\mu^-$ Decays*, [arXiv:1212.4967](#).